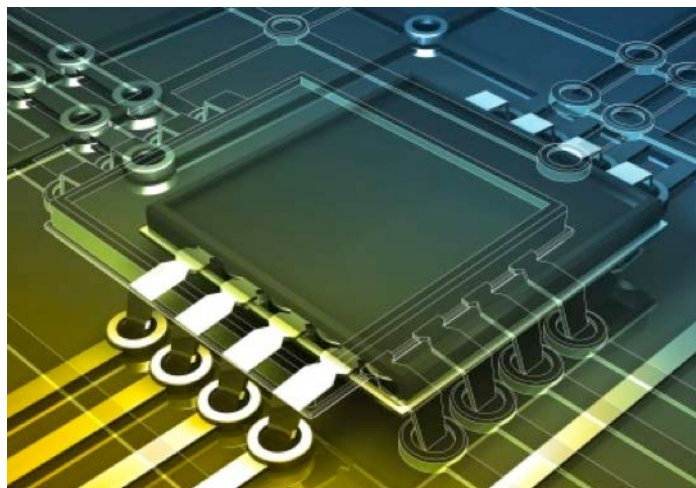
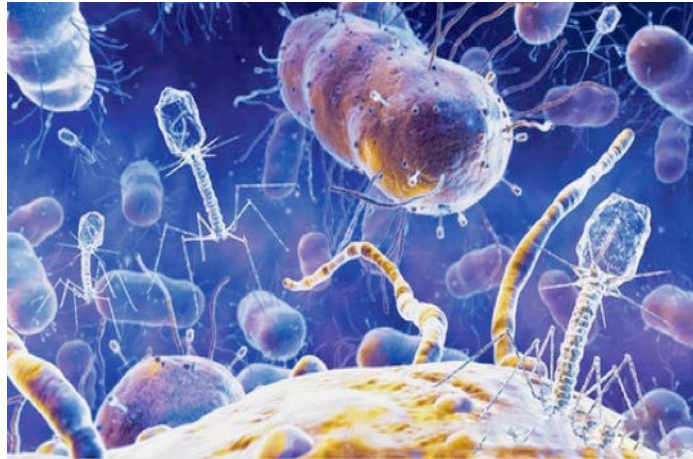


Proceedings Book

Humboldt Kolleg



Nanoscale Science and Technology (NS&T'12)

Edited by

Prof. Dr. Michael J. Schöning

Prof. Dr. Adnane Abdelghani

Tunisia, 17-19 March, 2012

Welcome Address

Dear Participants,

Welcome to the 2nd Humboldt Kolleg in "Nanoscale Science and Technology" (NS&T'12) in Tunisia, sponsored by the "Alexander von Humboldt" foundation. The NS&T'12 multi-disciplinary scientific program includes seven "hot" topics dealing with "Nanoscale Science and Technology" covering basic and application-oriented research as well as industrial (market) aspects:

- Molecular Biophysics, Spectroscopy Techniques, Imaging Microscopy
- Nanomaterials Synthesis for Medicine and Bio-chemical Sensors
- Nanostructures, Semiconductors, Photonics and Nanodevices
- New Technologies in Market Industry
- Environment, Electro-chemistry, Bio-polymers and Fuel Cells
- Nanomaterials, Photovoltaic, Modelling, Quantum Physics
- Microelectronics, Sensors Networks and Embedded Systems

We are deeply indebted to all members of the Scientific Committee and General Chairs for joint Sessions and to all speakers and chairmen, who have dedicated invaluable time and efforts for the realization of this event.

On behalf of the Organizing Committee, we are cordially inviting you to join the conference and hope that your stay will be fruitful, rewarding and enjoyable.

Prof. Dr. Michael J. Schöning

Prof. Dr. Adnane Abdelghani

Preface

The themes of the conference are based on nanoscale studies of materials for different applications. The multidisciplinary nature of the conference will provide large spectra of lectures in all fields of science including quantum physics, semiconductors, lasers, chemistry, biophysics, biochemistry, energy, microsystems, sensing, biomedicine, metrology, imaging and spectroscopic techniques, microelectronics and embedded systems. The participants will have the possibilities to learn how we can manipulate nano-objects with different techniques to produce different phenomena.

The Humboldt Kolleg'12 sponsored by the Alexander von Humboldt Foundation (Germany) on “Nanoscale Science & Technology” and organized by Tunisian Humboltianers will motivate scientists to acquire a deep knowledge of matter in nanoscale size. The success of the multidisciplinary conference lies not only in promising presentations but also in the active interaction of all the participants. The main objectives of the Humboldt Kolleg are:

- To encourage students to listen and discuss with pioneering scientists on nanoscale science and technology.
- To strengthen the high interdisciplinarity between physicists, engineers, chemists and (micro-)biologists for modern research aspects.
- To intensify the network between junior Tunisian researchers and the Alexander von Humboldt programs.
- To encourage junior researchers and young scientists to apply for post-doc positions with the Alexander von Humboldt foundation.
- To form a collaborative network within the developing countries.
- To show the impact of nanoscale science and technology for industrial requests (start-up and spin-off).



Unterstützt von / Supported by



Alexander von Humboldt
Stiftung / Foundation

Humboldt Kolleg '12

«Nanoscale Science and Technology»

17-19 March, 2012, Hammamet, Tunisia

Program

March 17, 2012

07:45 – 08:45: Registration

08:50 – 09:00: Opening Session

Prof. Slim Ben Saoud, Director of INSAT, Tunisia

Prof. Adnane Abdelghani (Humboltianer), INSAT, Tunisia

09:05 – 09:10: Welcome Address on behalf of the President of the Alexander von Humboldt Foundation, held by Dr. Christina Schuh, AvH, Bonn, Germany

09:15 – 09:20: Alexander von Humboldt: Network for the future

Chairman: Prof. Hermann Gaub

09:25 – 09:50: Biomimetic engineering: Nature as material designer and engineer, Prof. Erich Sackmann, Ludwig-Maximilians-Universität, München, Germany (**Keynote**)

09:55 – 10:20: Nanobiosensors: A bottom-up approach to integrated biosensor design, Prof. Anthony Turner, Editor of Biosensors and Bioelectronics, Linköping University, Sweden (**Keynote**)

10:25 - 11:05: Coffee Break / Group Photo

Session 1: “Molecular Biophysics / Spectroscopy Techniques / Imaging Microscopy“

Chairman: Prof. Michael J. Schöning

11:10 – 11:35: Force and function: Mechanoenzymatics investigated by single molecule force spectroscopy, Prof. Hermann Gaub, Ludwig-Maximilians-Universität, München, Germany (**Keynote**)

11:40 – 12:05: Study by Atomic force microscopy (AFM) of supported lipidic monolayers in interaction with nanoparticles, Dr. Christine Grauby Heywang, University of Bordeaux, France (**Keynote**)

12:10 – 12:30: Controlling molecular environment to tune binding kinetics at surfaces, Dr. Laurent Limozin, Laboratoire Adhésion et Inflammation, CNRS-INSERM, Marseille, France

12:35 – 12:55: Specific ligand/receptor mediated adhesion in model cells, Dr. Kheya Sengupta, Centre Interdisciplinaire des Nanosciences de Marseille, CNRS, Marseille, France

13:00 – 13:20: Cohesive and adhesive test for micro and nanoparticle-based coatings using sonication, Dr. Laurent Vonna, ICS- Mulhouse, France

13:25 – 14:45: Lunch

Session 2: “Nanomaterials Synthesis for Medicine and Bio-chemical Sensors “

Chairman: Dr. Mouna Marrakchi

14:50 – 15:15: (Bio-)chemical sensor array based on nanoplate SOI capacitors, Prof. Michael J. Schöning, Aachen University of Applied Sciences, Germany (**Keynote**).

15:20 – 15:45: Synthesis and characterization well-defined nanomaterials and their biological and environmental applications, Prof. Sherine Obare, Western Michigan University, USA (**Keynote**)

15:50 – 16:20: Coffee Break / Poster Session

Chairman: Dr. Saber Chatti (Humboltianer)

16:25 – 16:45: Gas sensing properties of metal decorated tungsten or tin oxide nano-needles grown by aerosol-assisted chemical vapour deposition, Prof. Eduard Llobet, University of Tarragona, Spain

16:50 – 17:10: Towards a paradigm change – mammalian cells as sensitive biosensor layers for the detection of unexpected toxic substances in air, Ulrich Bohrn, Siemens AG, Germany

17:15 – 17:35: Characterisation of aseptic sterilisation processes using an electronic nose, Steffen Reisert, Aachen University of Applied Sciences, Germany

17:40 – 18:00: Microfluidic detection based on impedimetric bacteriophage biosensor, Moataz Bellah Mejri, INSAT, Tunisia

18:05 – 18:25: Biopolymer-degradation monitoring by chip-based impedance spectroscopy technique, Sebastian Schusser, Aachen University of Applied Sciences, Germany

18:30 – 18:40: Improvement of a pesticide interdigitated microelectrodes immunosensor performance using oriented antibody immobilization, Dr. Mouna Marrakchi, INSAT, Tunisia

18:45 – 19:15: Poster Session

19:30: Dinner

March 18, 2012

Chairman: Dr. Christine-Grauby Heywang (Humboltianer)

08:45 – 09:10: Nanomechanical resonators – Improving coherence and transduction, Prof. Jörg P. Kotthaus, Ludwig-Maximilians-Universität, München, Germany (**Keynote**)

09:15 – 09:40: Semiconductor nanowires for third generation photovoltaics, Prof. A. Fontcuberta i Morral, EPFL, Switzerland (**Keynote**)

09:45 – 10:10: Raman spectroscopy of graphene in high magnetic fields, Prof. Khaled Karrai, (Humboltianer), Attocube, Germany (**Keynote**)

10:15 – 10:45: Coffee Break / Poster Session

Session 3: “Nanostructures / Semiconductors / Photonics / Nanodevices”

Chairman: Dr. Laurent Vonna (Humboltianer)

10:50 – 11:15: 3D integration of low power nanoelectronic devices above CMOS circuits, Prof. Abdelkader Souifi, INSA-Lyon, France (**Keynote**)

11:25 – 11:45: Photovoltaic response of InAs/InGaAs/GaAs quantum dots heterostructures intermediate-band solar cell, Maher Ezzzdini, FSM, Tunisia

11:50 – 12:10: Optical properties of exciton and acceptor-exicton complexes to explain the origin of ultraviolet photoluminescence in ZnO quantum dots embedded SiO₂ matrix, Dallali Lobna, FSB, Tunisia Tunisia

12:15 – 12:35: Relationship between the electronic and structural properties of n-GaAs layer grown on rough Si substrate by molecular beam epitaxy, Bilel Azeza, FSM, Tunisia

12:40 – 13:00: Design of optical devices based on hybrid periodic/Fibonacci photonic crystal in the visible and the near infrared domains, Mouldi Abir, ENIT, Tunisia

13:05 – 14:45: Lunch

Session 4: “New Technologies in Market Industry”

Chairman: Dr. Laurent Limozin (Humboltianer)

14:50 – 15:10: Perform SPRi binding measurement and MS identification on a single biochip: biological model of the ligand fishing in human plasma, Dr. Chiraz Frydman, HORIBA Scientific, France

15:15 – 15:35: Scanning electrochemical microscopy, Rob Sides, Ametek Princeton Applied Research, USA

15:40 – 16:00: Optical characterization of nanomaterials using spectroscopic ellipsometry, Jean-Paul Gaston, HORIBA Scientific, France

16:05 – 16:25: Design and prototyping of an electric city car in Tunisia, Dr. Ridha Rejeb, Tunisia

16:30 – 16:40: Techno-Park of Sousse: State of the art and perspectives, Hichem Turki, Techno-Park Sousse, Tunisia

16:45- 17:15: Coffee Break / Poster Session

Session 5: “Environment / Chemistry / Bio-polymers / Fuel Cells“

Chairman: Prof. Belkhiss Bouhaouala

17:20 – 17:40: Synthesis, structural and electrical characterization of doped apatite-like silicates for fuel cell electrolyte, Dr. Adel Madani, FSB, Tunisia

17:45 – 18:05: Electrochemical behavior of Pt-Sn/C heat treated electrocatalysts for oxygen reduction reaction in direct methanol fuel cells, Sarra Knani, FST, Tunisia

18: 10 – 18:20: New biomaterials (PEK) from starch: Characterization by MALDI-ToF and NMR, Dr. Saber Chatti, INRAP, Tunisia

18:25 – 18:45: New insights into organocatalysis, Dr. Sami Lakhdar (Humboltianer), Ludwig-Maximilians-Universität, München, Germany

18:50 – 19:30: Poster Session

20:00: Conference Dinner

March 19, 2012

Chairman: Prof. Ridha Mghaieth

08:30 – 08:55: Nanomaterials applied in medicine, cultural heritage and chemical sensor technology, Prof. Giuseppe Palleschi, Dipartimento di Scienze e Tecnologie Chimiche, Italy.

(Keynote)

09:00 – 09:25: New challenges of protein bioencapsulation in transparent sol-gel glasses and their applications, Dr. Bouzid Menaâ, Fluorotronics, INC, CA, USA **(Keynote)**

09:30 – 09:55: Nanoparticle characterization using light scattering techniques, Michael Kaszuba, Malvern Instruments, UK **(Keynote)**

10:00 – 10:30: Coffee Break

Session 6: “Nanomaterials / Photovoltaic / Modelling/ Quantum Physics“

Chairman: Prof. Larbi Sfaxi

10:35 – 10:55: Organic nanocomposites for OPV applications, Dr. Adnen Ltaief, FSM, Tunisia

11:00 – 11:20: Hydrothermal growth of ZnO nanorods by TiO₂ nanotubes template, Benkara Salima, Algeria

11:25 – 11:45: Hybrid nanocomposites based on silicon nanowires and conducting polymer for photovoltaic application, Chehata Nadia, FSM, Tunisia

11:50 – 12:10: Effect of substrate type on CuInS₂ thin films properties sputtered from nanoparticles synthesised by solvothermal route, Faouzi Ghribi, FSG, Tunisia

12:15 – 12:35: Structural and optical properties of FeTe₂ synthesized by heat treatment under tellurium pressure of amorphous iron oxide nano-films, Khaled Ben Messaoud, FST, Tunisia

12:40 – 13:00: Scattering elastic wave by integrated nanostructure on mesoscopic System 2D, Dr. Rachid Tigrine, University of Mouloud Mammeri, Algeria

13:05 – 13:25: AgInSe₂ ternary material synthesized by selenisation of nano-films of Ag and In elements obtained by thermal evaporation for photovoltaic application, Aymen Gantassi, FST, Tunisia

13:30 – 14:45: Lunch

Session 7: “Microelectronics / Sensors Networks / Embedded Systems“

Chairman: Dr. Kheya Gupta (Humboltianer)

14:50 – 15:10: Skills requirements for today’s embedded system’s design, Dr. Imed Bennour, FSM, Tunisia

15:15 – 15:35: On the coordinated path following control and trajectory tracking of multiple autonomous systems, Dr. Jawher Ghommam, INSAT, Tunisia

15:40 – 16:00: Evaluation of medical wireless sensors networks at emergency cases, Jihed Khaskhoussi, ENIM, Tunisia

16:05 – 16:25: Reinforcement learning based hierarchical dynamic power management, Maryam Triki, INSAT, Tunisia.

16:30 – 17:00: Coffee Break

Chairman: Dr. Ismail Trabelsi (Humboltianer)

17:05 – 17:20: The Maghreb-AvH Alumni Association: a network of Excellence that promotes science in the MENA region, Prof. Abdelhadi Soudi, Marocco

17:20 – 17:25: Selection of “Best Poster Presentation”

17:30: Closing Session

19:30: Dinner

General Chairs

S. Ben Saoud-INSAT, TN
E. Sackmann-LMU, GER
J.P. Kotthaus-LMU, GER

Scientific Committee

A. Turner, LIU-IFM, SE
A. Bouazizi, FSM, TN
A. F. I Morral, EPFL, CH
A. Ltaief, FSM, TN
B. Mena, Fluorotronics, USA
B. Bouhaouala, IPT, TN
C. Zerrouki, CNAM, FR
C. Heywang, LOMA, FR
C. Frydmann, Horiba, FR
F. Ben Ammar, INSAT, TN
F. Ben Hatira, INSAT, TN
G. Palleschi, UNI2, IT
H. Gaub, LMU, GER
H. Mattoussi, FL-Univ, USA
L. Vonna, IS2M, FR
L. Sfaxi, ESSTHS, TN
L. Lechuga, CIN2-CSIC, SP
M. Bawendi, MIT, USA
M. A.Maaref, INSAT, TN
M. Marrackchi, ISSBAT, TN
M. Amlouk, FSB, TN
M. Ben Ali, IPEIN, TN
N. De Rooij, Samlab, CH
N. Fourati, CNAM, FR
R. Mghaieth, FSM, TN
R. Ajjal, ESSTHS, TN
S. Jaziri, FSB, TN
S. Lakhdar, LMU, GER
S. Ameer, ISAC, TN
S. Helali, Borj-Cedria, TN
S. Chatti, INRAP, TN
T. Ktari, INSAT, TN
W. Touayar, INSAT, TN

Local Organizing Committee

A. Abdelghani, INSAT, TN
M. Said, FSM, TN
I. Trabelsi, Borj-Cedria, TN
M. Ellouze, FSS, TN

Program Chairs

K. Karrai-Attocube, GER
M.J. Schöning-AcUAS, GER
A. Abdelghani-INSAT, TN

Main Topics

The topics of the conference will include, but will not be limited to, the followings:

- Quantum dots, Quantum Wells and Quantum wires
- Photonics and Nano-Biophotonics
- Biosensors and Bioelectronics
- Conducting Polymers for Microelectronic Devices
- Biophysics, Biochemistry
- Electrochemistry, Fuel Cells
- Microsensors and Microsystems
- Renewal Energy and Photovoltaic cells
- Micro- and Nanoparticles for Drug Delivery
- Proteomics, Single-Cell Analysis and Electronic Noses
- Scanning Near-field Optical Microscopy Techniques (AFM, MFM, STM, SNOM)
- Nanometrology, Embedded Systems
- Wireless Sensors, Robotics

Table of Contents

Keynote Speakers

Keynote 1 : Pr. E. Sackmann

Biomimetic engineering: Nature as material designer and engineer

Keynote 2 : Pr. A. P. F. Turner

Nanobiosensors: A bottom-up approach to integrated biosensor design

Keynote 3 : Pr. H. Gaub

Force and function: Mechanoenzymatics investigated by single molecule force spectroscopy

Keynote 4 : Dr. C. Grauby - Heywang

Study by Atomic Force Microscopy (AFM) of supported lipidic monolayers in interaction with nanoparticles

Keynote 5 : Pr. M. J. Schöning

(Bio-)chemical sensor array based on nanoplate SOI capacitors

Keynote 6 : Pr. S. O. Obare

Synthesis and characterization well-defined nanomaterials and their biological and environmental applications

Keynote 7 : Pr. J. P. Kotthaus

Nanomechanical resonators - Improving coherence and transduction

Keynote 8 : Pr. A. Fontcuberta i Morral

Self-catalyzed III-V nanowires and heterostructures for photovoltaic applications

Keynote 9 : Pr. K. Karrai

Raman spectroscopy of graphene in high magnetic fields

Keynote 10 : Pr. A. Souifi

3D integration of low power nanoelectronic devices above CMOS circuits

Keynote 11 : Pr. G. Palleschi

Nanomaterials applied in medicine, cultural heritage, and chemical sensor technology

Keynote 12 : Dr. B. Mena

Challenges on protein bioencapsulation in transparent nanoporous sol-gel glasses and their applications

Keynote 13 : Mr. M. Kaszuba

Nanoparticle characterization using light scattering techniques

Orals Communications

OC1 : Dr. L. Limozin

Controlling molecular environment to tune binding kinetics at surfaces

OC2 : Dr. K. Sengupta

Novel strategies for micro and nano patterning

OC3 : Dr. L. Vonna

Cohesive and adhesive test for micro and nanoparticle-based coatings using sonication

OC4 : Pr. E. Llobet

Gas sensing properties of metal decorated tungsten or tin oxide nano-needles grown by aerosol-assisted chemical vapour deposition

OC5 : U. Bohrn

Towards a paradigm change – mammalian cells as sensitive biosensor layers for the detection of unexpected toxic substances in air

OC6 : S. Reisert

Characterisation of aseptic sterilisation processes using an electronic nose

OC7 : M. B. Mejri

Microfluidic detection based on impedimetric bacteriophage biosensor

OC8 : S. Schusser

Biopolymer-degradation monitoring by chip-based impedance spectroscopy technique

OC9 : Dr. M. Marrakchi

Improvement of a pesticide interdigitated microelectrodes immunosensor performance using oriented antibody immobilization

OC10 : M. Ezzdini

Photovoltaic response of InAs/InGaAs/GaAs quantum dots heterostructures intermediate-band solar Cell

OC11 : L. Dallali

Energy of excitons and acceptor-exciton complexes to explain the origin of ultraviolet photoluminescence in ZnO Quantum dots embedded SiO₂ matrix

OC12 : B. Azeza

Relationship between the electronic and structural properties of n-GaAs layer grown on rough Si substrate by molecular beam epitaxy

OC13 : A. Mouldi

Design of optical devices based on hybrid periodic/fibonacci photonic crystal in the visible and the near infrared domains

OC14 : Dr. C. Frydman

Perform SPRi binding measurement and MS identification on a single biochip: "biological model of the ligand fishing in human plasma"

OC15 : R. Sides

Scanning electrochemical microscopy

OC16 : J. P. Gaston

Optical characterization of nanomaterials using spectroscopic ellipsometry

OC17 : Dr. R. Rejeb

Design and prototyping of an electric city car in Tunisia

OC18 : H. Turki

Techno-Park of Sousse: state of the art and perspectives

OC19 : Dr. A. Madani

Synthesis, structural and electrical characterization of doped apatite-like silicates for fuel cell electrolyte

OC20 : S. Knani

Electrochemical behavior of Pt-Sn/C heat treated electrocatalysts for oxygen reduction reaction in direct methanol fuel cells

OC21 : Dr. S. Chatti

New biomaterials (PEK) from starch: Characterization by MALDI-ToF and NMR

OC22 :Dr. S. Lakhdar

New insights into organocatalysis

OC23 : Dr. A. Ltaief

Organic nanocomposites for OPV applications

OC24 : S. Benkara

Hydrothermal growth of ZnO nanorods by TiO₂ nanotubes template

OC25: N. Chahata

Hybrid nanocomposites based on silicon nanowires and conducting polymer for photovoltaic application

OC26 : F. Ghribi

Effect of substrate type on CuInS₂ thin films properties sputtered from nanoparticles synthesised by solvothermal route

OC27 : K. Ben Messaoud

Structural and optical properties of FeTe₂ synthesized by heat treatment under tellurium pressure of amorphous iron oxide nano-films

OC28 : Dr. R. Tigrine

Scattering elastic wave by integrated nanostructure on mesoscopic system 2D

OC29 : A. Gantassi

AgInSe₂ ternary material synthesized by selenisation of nano-films of Ag and In elements obtained by thermal evaporation for photovoltaic application

OC30 : Dr. I. Bennour

Skills requirements for today's embedded systems designs

OC31 : Dr. J. Ghommam

On the coordinated path following control and trajectory tracking of multiple autonomous systems

OC32 : J. Khaskhoussi

Evaluation of a medical wireless sensors network at emergency cases

OC33 : M. Triki

Reinforcement learning based hierarchical dynamic power management

OC34 : Pr. A. Souidi

The Maghreb-AvH Alumni Association: a network of excellence that promotes science in the MENA region

Posters Communications

P1 : A. Bensmain, H. Tayoub, B. Zebentout, Z. Benamara, Investigation of the band discontinuities effect in single and double a-Si:H/c-Si heterojunction solar cells using AMPS-1D simulations

P2 : A. Benzina, M. Hadjab, R. Naoum, H. Abid, Conception of an WDM optical transmission link at 4*10 Gbit/s

P3 : A. Bouafsoun, L. Mora, Studying of endothelial cells adhesion onto fonctionalized substrates using surface plasmon resonance

P4 : A. Bougharouat, A. Bellel, S. Sahli, Y. Segui, P. Raynaud, QCM coated with plasma polymerized TEOS/O₂ for the detection of volatile organic compounds

P5 : A. Bouhadiba, N. Leila, H. Sakina, I. Djilani, F. Djebroune, Theoretical study on interactions of β -Cyclodextrin with dimethylamino-4-benzal para-nitroaniline

P6 : A. Boukezzata, A. Keffous, N. Gabouze, G. Nezzal, M. Kechouane, H. Menari, Formation of porous amorphous silicon carbide thin films by electrochemical etching

P7 : A. Boukhachem, B. Ouni, K. Boubaker, A. Amlouk, M. Amlouk, Comparative study of optical properties of ZnO:In and ZnO:Yb sprayed thin films

P8 : A. Boumeddiene, F. Bouamra, H. Belkhir, First principle study of electronics properties of Sb-doped SnO₂(110) surfaces

P9 : A. Bouzidi, H. Smaoui, H Guerhazi, L. El Mir, Electrical properties of epoxy based nanocomposites

P10 : A. Djedouani, L. Hasniou, W. Merouani, H. Boulemche, S. Chafaa, Novel zwitterionic schiff base compound as corrosion inhibitor for mild steel in acidic media

P11 : A. Fargi, N. Hizem, A.Kalboussi, A. Souifi, Investigation of kink effect in indium doped silicon for sub 100 nm N channel MOSFET technology

P12 : A. Hassini, A.H. Belbachir, AVHRR-NOAA and MODIS-Aqua/Terra data receiving and processing system

P13 : A. Kermad, S. Sam, N. Ghellai, N.E. Gabouze, Hydrogen peroxide biosensor based on horseradish peroxidase immobilized on functionalized porous silicon

P14 : A. Labidi, A. Bejaoui, J. Guérin, M. Maaref, K. Aguir, Spectroscopic ellipsometry and X-ray diffraction characterizations of the reactive sputtering powers effects on the physical properties of CuO thin film

P15 : A. Mhamdi, A. Boukhachem, M. Madani, A. Amlouk, M. Amlouk, Study of vanadium doping effects on structural and optical properties of sprayed ZnO thin films

P16 : A. M. Krarroubi, L. Barkat, F. Z. Dahou, J. C. Bernede, A. Khelil, Optimization of the interface anode / organic materials in organic solar cells

P17 : A.Said, Y. Oussaifi, D. Ceresoli, M. Said, Theoretical investigation of the electronic properties of wurtzite $\text{In}_x\text{Ga}_{1-x}\text{N}$ alloys

P18 : A. Saouli, F. Mansour, K.Mansour, Application of the near infra-red radiation in medical imaging

P19 : A. Soussou, S. Chatbouri, M. Troudi, N. Sghaïer, A. Kalboussi, Conception of single-electron memory with silicon nanowire using PSpice and Simon

P20 : A. Touhami, H. Hrichi, N. Jaballah, R. Ben Chaâbane, H. Ben Ouada, M. Majdoub, Effects of chemical modifications on optical, morphological, and electrical properties of three spin-coated PPV derivatives films

P21 : B. Bourahla, R. Rabhi, O. Nafa, A. Khater, R. Tigrine, Magnon scattering in ferromagnetic surface with atomic steps

P22 : B. Abida, L. Chirchi, S. Baranton, T. W. Napporn, J. M. Léger, A. Ghorbel, Electrocatalytic activity of Pt nanoparticles deposited on TiO₂ anatase supports toward methanol oxidation

P23 : D. Dergham, C. Nouveau, L. Chekour, N. Tamacha, A. Khelil, The annealing effect on the nitride coatings properties obtained by magnetron sputtering

P24 : D. Imene, N. Leila, H. Sakina, B. Abdelaziz, M. Fatiha, K. Djameleddine, Theoretical study of inclusion complex ortho-anisidine with β - cyclodextrin

P25 : E. Akkari, W. Touayar, F. J. del Campo, J. Montserrat, Improved electrical characteristics of porous germanium photodiode obtained by phosphorus ion implantation

P26 : E. Boudjennad, N. Keghouche, C. Minot, DFT study of the Ni – (m-ZrO₂) interaction

P27 : F. Benmaamar, M. F. Mosbah, N. Kalkoul, S. Mahdjoub, F. Bouaïcha, Effects of Ce doping in (Bi,Pb)2212 phase

P28 : F. Bouaïcha, M. F. Mosbah, N. Boussof, A. Amira, Effects of doping by Ti on structural and electrical properties of Bi(Pb)-2212 superconducting ceramics

P29 : F. Bouamra, A. Boumeddiene, H. Belkhir, First-principle study of magnetic behavior of nano-clusters of Rh-doped SnO₂(110) surfaces

P30 : H. Sakina, B. Azize, N. Leila, Host–guest inclusion complex between β -cyclodextrin and paeonol: Computational studies Based on PM3 and ONIOM methods

P31 : H. Baccar, E. Llobelt, A. Abdelghani, Multiwall carbon nanotubes for chemical vapour sensor

P32 : H. Belaid, M. Nouri, A. Alaya, Z. Ben Ayady, K. Djessas, L. El Mir, Effect of silicon type on Si/PS/ZnO:In solar cell structure based on nanopowder synthesized by sol-gel method

P33 : H. Bouazizi, N. Chaaben, A. Bchetnia, T. Boufaden, B. El Jani, Thermal decomposition study of AlGaN

P34 : H. Khemir, W. Dimassi, M. Jbali, H. Ezzaouia, Effect of acid treatment in silicon grain boundaries polycrystalline: Improving the performance of solar cells

P35 : H. Khmissi, M. H. Hadj Alouane, K. Naji, N. Chauvin, C. Bru-Chevallier, B. Ilahi, H. Maaref, G. Patriarche, M. Gendry, InP nanowires with InAs insertion grown by catalyst assisted molecular beam epitaxy on silicon substrates

P36 : H. M. Gafour, M. S. Rahal, K. Sail, A. Sayede, M. Springborg, A combined HF and DFT study of the effects of implicit and explicit solvents on the conformations of lactulose and turanose molecules

P37 : H. Rahene, A. Zouaoui, A study on the photoluminescence properties of spray pyrolysis deposited crystalline nanostructured ZnO thin films

P38 : H. Tayoub, A. Bensmain, B. Zebentout, Z. Benamara, Impact of the inhomogeneous structure of the active layer on the transfer Characteristic of polysilicon TFT's

P39 : I. Fezai, S. Jaziri, Thermodynamic properties of Landau levels in semiconductor two-dimensional systems

P40 : I. Hafaiedh, H. Baccar, T. Ktari, A. Abdelghani, Streptavidin-HRP immobilized on multiwall carbon nanotubes for biosensor application

P41 : I. Nouicer, S. Sahli, Z. Ziari, Improvement of the polyimide films hydrophobic character by plasma deposited organosilicon nanolayers coating

P42 : I. Boudraa, H. Allal, C. Benhamideche, S. E. Bouaoud, M. Poulain, Influence of alkali substitution on the physical characteristics of alypbmg glass

P43 : I. Zgaren, S. Jaziri, Carrier relaxation mechanisms in CdS/ZnS core-shell quantum dots: Auger relaxation

- P44** : J. Chermiti, M. Ben Ali, C. Dridi, Y. Korpan, N. Jaffrezic-Renault, Modelling of biosensors for cancer monitoring
- P45** : K. Brik, F. Ben Ammar, A. Djerdir, A. Miraoui, Reliability study of proton exchange membrane fuel cell by causal tree analysis
- P46** : K. charradi, Z. Beji, Z. Ahmed, R. Chtourou, Performance of modified SPEEK membrane by inorganic nanocomposite for Fuel Cell
- P47** : K. Farah, F. Hosni, A. Mejri, B. Boizot, A. H. Hamzaoui, Effect of gamma irradiation and thermal annealing on the nanosize particles formation in silver ion-exchanged silicate glass
- P48** : K. Marzougui, K. Farah, A. H. Hamzaoui, H. Ben Ouada, Elaboration and characterization of sol-gel silica EPR dosimeters for high dose dosimetry
- P49** : K. Omri, H. Dahman, C. Barthou, L. El Mir, Yellow emission in $\text{SiO}_2/\text{Zn}_2\text{SiO}_4:\text{Mn}$ nanocomposite synthesized by sol-gel method combined with a furnace firing
- P50** : K. Rida, L. Merabet, I. Kehal, Electrochemical properties of spinel-type ZnM_2O_4 (M = Cr and Mn) electrodes for oxygen evolution in alkaline solutions
- P51** : K. Sail, M. H. Gafour, G. Bassou, M. R. Sekkal, A. Kadoun, Optimization of the Detection in Microanalysis X by Sample Treatment
- P52** : L. Barkat, A. Mohammed-Krarroubi, F. Z. Dahou, J. C. Bernede, A. Khelil, Transparent conductive layers based multilayer $\text{MoO}_3/\text{Ag}/\text{MoO}_3$, application as an anode in organic optoelectronic devices
- P53** : L. Benterrouche, S. Sahli, F. Sebihi, A. Benhamouda, Inactivation of E-coli bacteria by atmospheric dielectric barrier discharge
- P54** : L. Chirchi, S. Knani, S. Baranton, T. W. Napperon, J. M. Léger, A. Ghorbel, Synthesis of carbon vulcan XC72 supported platinum/TIN electrocatalyst and evaluation of its methanol tolerance for Direct Methanol Fuel Cells (DMFC)

P55 : L. Djellal, M. Trari, Photo-electrochemical cell from chalcopyrite $\text{Cu}(\text{In}_{0.6}\text{Ga}_{0.4})_3\text{Se}_5$ semiconductor

P56 : L. A. Wajira Ariyadasa, N. O. Masika, S. O. Obare, Electrochemical properties of metallic clusters nanoclusters

P57 : L. Messad, T. Bouzar, C. Goyhenex, H. Bouzar, V. Pierron-Bohnes, Molecular dynamics calculations of elastic constants in CoPt-L10 single crystal

P58 : M. Bennour, F. Saidi, L. Bouzaïene, L. Sfaxi, H. Maaref, Effect of the $\text{In}_x\text{Ga}_{(1-x)}$ As surrounding thickness and In compositions on electronic transitions of InAs DWELL structure grown on GaAs high index substrates

P59 : M. Bouzidi, M. Souissi, A. Bchetnia, Z. Chine, B. El Jani, Thermal annealing effects on structural and optical property of V-doped GaN films

P60 : M. Charfeddine, M. Gassoumi, H. Belmabrouk, M. A. Zaidi, H. Maaref, Theoretical investigation of kink effect and dependence between deep defects and temperature in AlGaIn/GaN HEMT's

P61 : M. Hajiri, F. Ghribi, L. El Mir, Influence of heat treatment and indium concentration on structural and optical properties of ZnO thin films prepared spin-coating technique

P62 : M. Karyaoui, J. Ben Naceur, M. Ben Rabha, R. Chtourou, M. Amlouk, Effect of specific surface of Si substrates on TiO_2 nano-films on structural, optical and photocatalytic activity

P63 : M. Kihel, R. Clergereaux, M. Calafat, S. Sahli, P. Raynaud, Y. Segui, I. Nouicer, Relaxation effect in the nano-composites films deposited by plasma microwave from acetylene

P64 : M. Sahraoui, A. Abderrahmen, R. Ben Chaabane, H. Ben Ouada, A. Gharbi, Surface treatment of liquid crystal alignment: effect on electrical properties of nematic liquid crystal cell

P65 : M. S. Rabia, Phonon scattering in a quantum nanowire: Application to substitution bulk defect

P66 : N. Bachtouli, S. Aouida, B. Bessais, Investigation of surface morphology and optoelectronic properties of monocrystalline silicon

P67 : N. Ben Mansour, S. Gouadria, I. Najeh, M. Hajiri, H. Dahman, L. El Mir, Electrical characterization of carbon-nickel nanocomposites prepared by sol-gel method

P68 : N. B. B. Bestaoui, M. S. Rahal, A. Sayede, N. Yousfi, Relaxed energetic maps of -2-O-sulphated 3,6 anhydro- α -D-galactose and ι -carrabiose : A DFT study

P69 : N. Boussouf, M. F. Mosbah, F. Bouaicha, Amira, The effect of SiO₂ addition on the microstructure and superconducting properties of Bi2212

P70 : N. Boutabia, B. Bouzabata, Induced phases transformation by mechanical alloying of the haematite/magnesium mixture

P71 : N. Chehata, A. Ltaief, A. Farzi, A. Bouazi, Optimization of properties of MEH-PPV/CNTs films for organic solar cells:effects of CNTs concentrations and thermal treatments

P72 : N. Chiboub, K. Khaldi, N. Gabouze, R. Boukherroub, S. Ghodbane, S. Sam, Nanocomposites based on boron-doped diamond for ammonia sensing

P73 : N. Hanene, T. Abdelhafid, Study kinetics of recrystallization, precipitation and texture development in cold rolled and annealed aluminium alloys

P74 : N. Hamdaoui, R. Ajjel, B. Salem, M. Gendry, Capture of electrons in self-assembled InAs quantum dots

P75 : N. Kalkoul, M. F. Mosbah, F. Benmaamar, F. Bouaïcha, Effect of AlO₂ addition on the superconducting properties of Bi2212 superconductor

P76 : N. Yahyaoui, N. Sfina, J. L. Lazzari, M. Said, Band structure calculations of $\text{Ge}_{1-x}\text{Sn}_x$ / $\text{Si}_{1-x}\text{Sn}_x$ and $\text{Ge}_{1-x-y}\text{Si}_x\text{Sn}_y$ / $\text{Ge}_{1-z}\text{Sn}_z$ alloys: achieving direct band gap materials

P77 : N. Zeiri, N. Safina, S. Abdi-ben Nasrallah, M. Said, Optical nonlinearities in asymmetric (CdS/ZnSe/BeTe)(ZnSe/ BeTe) quantum well

P78 : O. Benamara, A. Boufelfel, First- principles calculation of magnetic properties of tetragonal $\text{BaTi}_{1-x}\text{TM}_x\text{O}_{3-\delta}$; TM=[Fe, Co, Cr, Mn,]

P79 : O. Dhibi, S. Zghal, A. Lateif, S. Jomni, L. Beji, A. Bouazizi, Optimization of electrical and dielectrical properties of ITO/MEH-PPV/Al structures by inserting of a thin gold interlayer

P80 : O. Msehli, I. Hmila, A. Mezni, I. Hafaiedh, M. El Ayeb, L. Smiri, A. Mlayah, A. Abdelghani, B. Bouhaouala-Zahar, Gold nanoparticle-nanobody complex: A comprehensive understanding of bio-functionalization

P81 : O. Nafa, B. Bourahla, A. Khater, Spin waves propagation through sandwich layers in ultrathin films

P82 : O. Ould Fella, M. Tamine, N. Randrianantoandro, J. M. Grenèche, Annealing effect on the magnetic and structural properties of milled zinc ferrites ZnFe_2O_4

P83 : R. Ayache, A. Bouabellou, Study of ion beam synthesized cobalt silicide layers in Si(111)

P84 : R. Ben Abderrazek, I. Hmila, M. El Ayeb, S. Muyldermans, B. Bouhaouala-Zahar, Determination of epitope complementation groups of AahII toxin binders by surface plasmon resonance

P85 : R. Ben Mahersia, L. Bouzaienne, H. Maaref, Effects of applied electric field, hydrostatic pressure and temperature on the second and the third harmonic generations in quantum dot

P86 : R. Chadli, A. Khater, R. Tigrine, Structural and vibrational properties of Au(100)-c(2x2)-Pd ordered metallic surface alloy

P87 : R. Hammami, J. Ben Naceur, K. Charradi, I. Ben Assaker, A. Carbone, B. Auvity, G. Squadrito, Z. Ahamed, R. Chtourou, Hybrid polymer electrolytes Nafion-TiO₂ for PEMFCs: synthesis and characterization

P88 : R. Hammami, J. Ben Naceur, K. Charradi, A. Carbone, B. Auvity, I. Ben Assaher, G. Squadrito, Z. Ahamed, R. Chtourou, Room temperature synthesis of hybrid polymer electrolytes nafion-TiO₂ for PEMFCs

P89 : R. Otmani, N. Benmoussa, Micro pressure sensor model validation by finite element method

P90 : S. Bellayouni, N. Mabrouk, H. Berriche, Vibrational-level spacings and evaluation of adiabatic correction for the six $^1\Sigma^+$ states of LiK molecule

P91 : S. Ben Taieb, A. Bardaoui, I. Ben Assaker, R. Chtourou, structural and optical characterization of CdSe/TiO₂ nanocomposite

P92 : S. Bouras, F. Gheldane, Y. Berriche, Study of the resistance to crack propagation in nano fine grained alumina by acoustic emission

P93 : S. Dabbous, A. Amlouk, K. Boubaker, M. Amlouk, WS₂ binary material synthesized by sulfuration of nano-films of WO₃ obtained by spray for photovoltaic application

P94 : S. Tahmasebi Nick, E. L. Bejcek, B. E. Bejcek, S. O.Obare, Controlling biological activity of coordination compounds at nanoparticle interfaces

P95 : S. Guadria, H. Dahman, K. Omri, L. El Mir, Negative differential resistance in carbon-silica nanocomposites

P96 : S. Hammani, N. Moulai-Mostefa, L. Benyahia, J. F. Tassin, Effect of carbon black nanoparticle on the morphology rheology and thermal properties of immiscible polymer blends

P97 : S. Merabet, A. Bounar, M. Boukezzata, D. Bielle-Daspét, G. Sarrabayrouse, Thermal oxidation of heavily boron-doped thin films of polycrystalline silicon

P98 : S. Merazga, A. Brighet, A. Keffous, K. Mirouh, M. Kechouane, Effect of hydrogen on the optical and structural properties of amorphous silicon carbide films

P99 : T. Bouzar, L. Messad, C. Goyhenex, H. Bouzar, V. Pierron-Bohnes, Molecular dynamics simulations of atomic migration in ordered CoPt L1₀ Alloys

P100 : W. Aloui, A. Ltaief, H. Majdoub, A. Farzi and A. Bouazizi, PET/CNTs flexible electrodes for organic solar cells devices

P101 : W. Ouerghi, R. Naouri, M. A. Maaref, C. Testelin, F. Bernadot, Excitonic behavior in self-assembled InGaAs/GaAs quantum rings in low magnetic fields

P102 : W. Zaghdoudi, A. Bardaoui, Y. Abid, H. Houichet, R. Chtourou, Preparations and characterizations of organic-inorganic hybrid perovskite multiple quantum well structure embedded in porous anodic alumina

P103 : Y. Braham, H. Barhoumi, A. Maaref, A. Bakhrouf, Modified gold electrode with proteus mirabilis bacteria for urea biosensor development

P104 : Y. Cheballah, A. Ziane, Optical properties of the compound FeN

P105 : Y. Hattab, N. Benharrats, Synthesis and characterisations of organophilic montmorillonite –copolymer (St-THF) nanocomposite

P106 : Y. Souilah, S. Boukhessaim, M. Draissia, M. Y. Debili, Electrochemical properties study of high-frequency magnetic induction melting Al- 4 to 50 wt.% Mg alloys

P107 : Z. Harrabi, A. Ltaief, L. Béji, A. Bouazizi, Electrical and dielectrical behaviours of CdS layers grown on GaAs and porous GaAs substrates

P108 : Z. Mazouz, A. Omezzine, R. Kalfat, A. Othmane, Detection of human apolipoprotein E genotypes by a DNA electrochemical biosensor

Keynote Speakers

Biomimetic engineering: Nature as material designer and engineer

Erich Sackmann

Technical University Munich, Physics Department E22, James Franck Str.1 D85747 Garching, Germany. Email: sackmann@ph.tum.de

Introduction:

Many concepts of modern material design and construction of highly sophisticated mechanical structures have been invented by mother nature several billion years ago. Based on the principle of hierarchical design and scaling laws of physics, modulated by interplay of genetics and physics, a sheer infinite manifold of living beings have been designed with an astonishing small number of molecules. In contrast to stepwise linear optimization used by engineers, nature uses the trick of mutations resulting in materials with stunning physical properties

Beautiful examples of nature as material designer are biomaterials with mechanical properties, unmatched by engineers. Examples are shell-string composites enabling cells to travel several hundred km through narrow capillaries or biominerals, designed by epitactic principle. The stratified shells combine unmatched strength with docility enabling sea animals to survive several thousand meters below sea level.

To enable life under the harsh conditions of the desert, nature was particularly inventive. Examples are the design of a unique navigating system of desert ants, the development of nanostructured surfaces to minimize friction of animals moving in sand. A decisive step towards the development of higher animals was the invention of the piezoelectric force transducer enlarging the dynamic range of hearing to the 100 kHz.

The purpose of my talk is to stimulate new interest in the field of bionics. Learning from nature is expected to open new strategies for solving challenging technical problems or strategies of survival under harsh conditions. Nature designs and optimizes materials and machines by Darwin principle which is infinitely slow compared to the lifetime of human beings. However, we can overcome this problem and accelerate the evolution of new materials through our understanding of the interplay of physics and genetics.

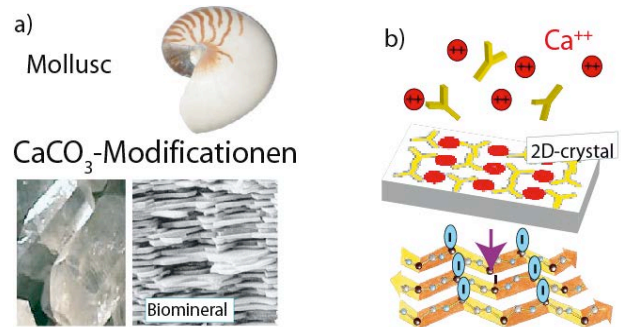


Fig.1 Self assembly of biomineral permut by epitactic growth controlled by charged proteins



Fig. 2. Lizzards and insects move on walls and ceilings by van der Waals forces

References:

- [1] E.Sackmann and R. Merkel Lehrbuch der Biphysik; Chapter I. Wiley 2009
- [2]E. Arzt, S. Gorb and R. Spolenak, PNAS 100; 10603-10606; 2003
- [3] P. Fratzl Von Knochen Holz und Zähnen Physik Journal;1.49-55; 2002

Nanobiosensors: A bottom-up approach to integrated biosensor design

Anthony P F Turner*

Biosensors and Bioelectronics Centre,

IFM, Linköping University, SE-581 83, Linköping, SWEDEN. www.ifm.liu.se/biosensors

*Corresponding author : E-mail address : anthony.turner@liu.se

The world market for biosensors is in excess of US\$13 billion, with nine tenths of that still accounted for by glucose measurement. This extraordinary dominance of the field by a single product type is driven by the extraordinary needs of people with diabetes combined with the success of biosensors in meeting their demands for an appropriate product. Now, the highly competitive and mature home-test, finger-stick market is driven by the need to reduce manufacturing cost and introduce additional convenience and utility. While personalised medicine is still in its infancy, the poor efficacy of many current pharmaceuticals is a strong driver for combining diagnostics with therapy. Molecular diagnostics to enable better administration of anticoagulant therapy, predict drug metabolism and detect mutations that identify patients likely to respond to cancer therapy, have already met with notable success. Moreover, the combination of diagnostics with pharmaceuticals not only furnishes immense clinical benefit, but provides a new financial model to drive forward the development of new sensors.

The creation of new materials is one of the fundamental driving forces of industry and lays the foundation for new products to enhance the wealth and well being of society. The recent extraordinary boom in the generation and use of new nanomaterials has been driven by advances in synthetic chemistry, often drawing inspiration from nature. Healthcare is one of the largest and most rapidly expanding needs in society today and smart nanomaterials are addressing diverse applications including drug screening, biocompatible materials, drug delivery, self-assembled scaffolds, medical imaging, regenerative medicine and diagnostics. Current products have been dominated by simple nanostructures with beneficial properties, such as the antimicrobial properties of silver nanoparticles. However, we are now witnessing the emergence of active nanostructures in the form of electronics, sensors, drug release technologies and adaptive structures. Bioelectronics embodies the exploitation of biological or biologically-inspired molecules as an integral part of an electronic devices and biosensors are the analytical embodiment of this art. The incorporation of nanomaterials such as hyperbranched polymers, nanowires, ordered arrays of CNTs and viral nanocages, has resulted in significantly improved sensitivity. Smart biocompatible polymer matrices open up new possibilities for hybrid organic electronic devices

and nanoreactors, while simplified self-assembly systems enable immobilisation for electrochemical, optical or piezoelectric detection. New semi-synthetic receptors such as aptamers and affibodies are delivering new possibilities for detection and computational design has proved a promising tool to enhance combinatorial selection methods. The combination of nanoparticle technology with synthetic receptor technology has proved particularly productive creating robust "plastic antibodies" that can potentially be used to sense, image or release specific components, and synthetic "enzyme electrodes", which can specifically catalyse the oxidation of an analyte to produce an amperometric response. These approaches lay the foundations for smart fabrics, wearable sensors and autonomous, self-powered sensing systems. The future continues to be rich in diagnostic challenges and new biosensor research is not only unveiling new commercial opportunities, but is advancing our knowledge in fundamental areas such as interactions at biointerfaces and mechanisms of infection.

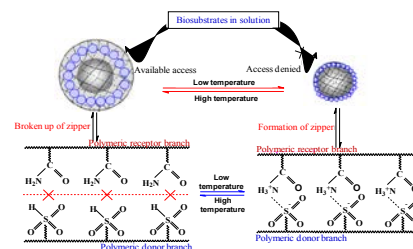


Figure 1: Zipper-like nanobioreactor for switchable molecular recognition

References:

- Berti, F. and Turner, A.P.F. (2011). New micro- and nano-technologies for electrochemical biosensor development. In: *Biosensor Nanomaterials* (Eds. S. Li, J. Singh, H. Li and I. A. Banerjee). Wiley. pp 1-35.
- Li, S., Ge, Y., Piletsky, S.A. and Turner, A.P.F. (2011). A zipper-like on/off-switchable molecularly imprinted polymer. *Advanced Functional Materials* 21, 3344-3349.
- Newman, J.D. and Turner, A.P.F. (2005). Home blood glucose biosensors: a commercial perspective. *Biosensors and Bioelectronics* 20, 2435-2453.
- Poma, A., Turner, A.P.F. and Piletsky, S. (2010). Advances in the manufacture of MIP nanoparticles. *Trends in Biotechnology* 28, 629-637.

Study by Atomic Force Microscopy (AFM) of supported lipidic monolayers in interaction with nanoparticles

N.R. Faye¹, F. Moroté¹, C. Grauby-Heywang^{1*}, T. Cohen-Bouhacina¹

¹Laboratoire Ondes et Matière d'Aquitaine, UMR CNRS 5798 Université Bordeaux 1, FRANCE

*Corresponding author : E-mail adress : ch.heywang@loma.u-bordeaux1.fr

Introduction: Nanoparticles (NPs) are currently used in many industrial or research applications (paints, cosmetics, drug delivery systems...). Recent papers demonstrate clearly their activity with biological membranes (nanoscale holes, membrane thinning, disruption). Different parameters seem to be particularly important, such as the NP size, their surface properties, or their aggregation state. Composition of biological membranes being complex, supported lipid monolayers can be used as simplified membrane model to study the NP-membrane interaction, these two-dimensional systems being moreover convenient for surface analysis techniques such as AFM or fluorescence microscopy (FM).

Material and method : Supported monolayers were made of oleoyl-palmitoyl-phosphatidylcholine (OPPC, lipid representative of the fluid phase of membranes) or sphingomyeline (SM, representative of the raft phase). Monolayers were transferred on mica by the Langmuir-Blodgett technique at a surface pressure of 30 mN/m. Mica was nude or previously recovered with silica beads (10 or 100 nm in diameter), in order to mimick the NP-membrane interaction. In the case of FM experiments, Langmuir monolayers contained 0.5 mol% of NBD-PC, a fluorescent probe localizing in fluid phases of monolayers.

Main results : AFM and FM images of samples were systematically compared in the absence or in the presence of NPs. Figure 1a shows for instance FM image of a SM monolayer, revealing the presence of separated condensed (dark) and fluid (fluorescent) phases in the monolayer. AFM confirms this phase separation, showing that condensed phase is slightly higher than the fluid one, of about 0.8 nm (data not shown). In the presence of NPs (Figure 1b), we observe mainly the localization of small aggregates of NPs at the edges of condensed phases, or if aggregates are bigger, their localization within condensed phase (data not shown). This colocalization is also observed in the case of other lipids characterized by a phase separation (data not shown).

At last, we also tested the stability in time of OPPC monolayers, this lipid being sensitive to oxidation because of the presence of a double bond on one hydrophobic chain. Figure 2 shows that the OPPC monolayer, initially homogenous (in

agreement with the fact that this lipid is in an expanded fluid phase), deteriorates with time, with the appearance of small domains (about 0.8 nm of height and of varying diameters).

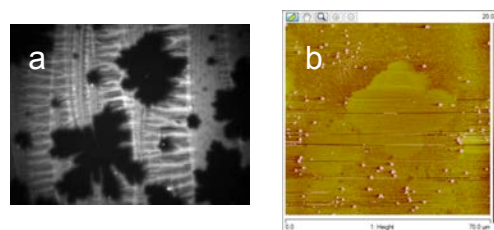


Figure 1: images of a SM monolayer on mica (a) by FM (100x140 μm) and (b) by AFM (70x70 μm) in the presence of silica NPs (light spots on the AFM image).

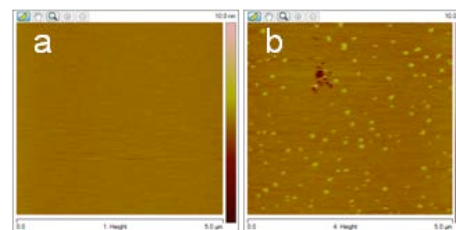


Figure 2: AFM images of an OPPC monolayer observed (a) just after the transfer (5x5 μm) and (b) 2 days later (5x5 μm).

Perspectives : first results enabled us in one hand to optimize our experimental protocol by taking into account some parameters such as the lifetime of lipid films (case of OPPC). In the other hand they suggest that NPs induce locally the presence of condensed lipid phases. This point has to be clarified by studying other lipids and the influence of cholesterol. We also plan to modify other parameters such as the size of NPs, or their nature. Other issues must be clarified, such as: are NPs recovered by the monolayer or not ? Are results similar in the case of a lipid bilayer ?

References:

Roiter, Y. et al. (2008) Interaction of nanoparticles with lipid membrane, *Nanoletters*, 8, 941-944.
 Leroueil P. et al. (2008) Wide varieties of cationic nanoparticles induce defects in supported lipid bilayers, *Nanoletters*, 8, 420-424.

(Bio-)chemical sensor array based on nanoplate SOI capacitors

A. Poghossian^{1,2}, M.H. Abouzar^{1,3}, M.J. Schöning^{1,2*}

¹Institute of Nano- and Biotechnologies, Aachen University of Applied Sciences, Campus Jülich, GERMANY

*Corresponding author : E-mail address : schoening@fh-aachen.de

² Peter Grünberg Institute (PGI-8, Bioelectronics), Research Centre Jülich GmbH, Jülich, GERMANY

³ Department of Informatics and Microsystem Technology, University of Applied Sciences Kaiserslautern, Campus Zweibrücken, GERMANY

Introduction: Due to the simplicity of layout and easy in fabrication, semiconductor field-effect capacitive electrolyte-insulator-semiconductor (EIS) single sensors are widely utilised for the detection of various (bio-)chemical parameters. However, one-chip integration of multiple capacitive EIS sensors is problematic due to difficulties in preparation of separate, electrically isolated individual EIS capacitors.

Results: In this work, an array of individually addressable nanoplate field-effect capacitive sensors based on an SOI (silicon-on-insulator) structure has been developed for multi-parameter (bio-)chemical sensing. The isolation of the individual capacitors was achieved by forming a trench in the top silicon layer with a thickness of about 350 nm. The realised sensor array allows addressable biasing and electrical readout of multiple nanoplate EISOI (electrolyte-insulator-silicon-on-insulator) capacitive biosensors on the same SOI chip as well as differential-mode measurements.

Conclusions: The feasibility of the proposed approach has been demonstrated by realising sensors for the detection of pH, penicillin concentration as well as for the electrical monitoring of a layer-by-layer adsorption of polyelectrolyte multi-layers. In addition, the possibility of label-free electrical detection of a consecutive DNA (deoxyribonucleic acid) hybridisation/denaturation event by means of nanoplate SOI capacitors modified with gold nanoparticles (Au-NP) is demonstrated. The proposed device detects charge changes on the Au-NP/DNA hybrids induced by the particular hybridisation or denaturation event. An electrostatic model for the capacitive field-effect sensor modified with the Au-NP/DNA hybrids will be presented. The presented examples demonstrate the potential of nanoplate SOI capacitors as a new basic structural element for the development of different types of field-effect type biosensors.

Synthesis and characterization well-defined nanomaterials and their biological and environmental applications

Sherine O. Obare *

¹Department of Chemistry, Western Michigan University,
Kalamazoo, MI 49008-5413, USA

*Corresponding author : E-mail address : sherine.obare@wmich.edu

Nanoscale metallic particles are of great interest due to their importance in advanced technological applications. Synthetic procedures that produce gram-scale, well defined and monodisperse metallic nanoparticles with controlled size and shape, especially within the 1-4 nm size range is a continuing challenge in nanoscale science (Lin 2010). We have developed new organic ligands that when used as stabilizers for metal nanoparticles, provide the ability to gain control of the particle size in one-step synthetic procedures. Monodisperse metallic nanoparticles were synthesized and characterized using spectroscopic, microscopic and x-ray techniques. We have further investigated the electrochemical quantized double-layer (QDL) charging differences of 1-4 nm metallic nanoparticles. Within this size range, the electronic properties transition from a bulk-like continuum of electronic states to molecule-like, discrete electronic orbital levels.

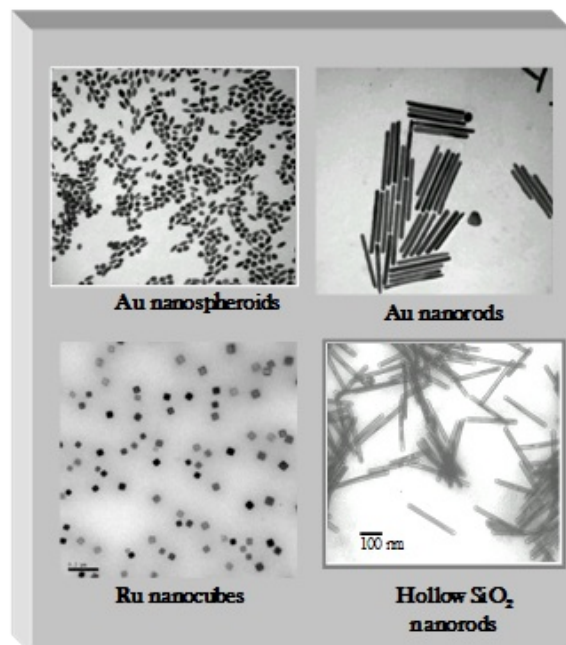


Figure 1. Nanomaterials can be made in a wide range of shapes and sizes and chemical compositions. This represents a major challenge in

understanding nanomaterials and their interactions with the environment and biological molecules and systems.

Such properties have led us to investigate their charging and discharging at large band-gap semiconductor interfaces. The results are paramount toward understanding and developing advanced materials for catalysis. We demonstrate the efficiency of the semiconductor/metal nanoparticle interfaces for the storage of solar energy and for using this energy as needed, specifically, in the degradation of common environmental pollutants as well as their interaction with microbial pathogens (Ciptadjaya 2009, Guo 2008, Obare 2010).

References:

- Ciptadjaya, C. G. E.; Guo, W.; Angeli, J. M.; Obare, S. O. 'Controlling the Reactivity of Chlorinated Ethylenes with FMNH₂,' *Environ. Sci. Technol.* **2009**, 43, 1591-1597.
- Guo, W.; Ciptadjaya, C. G. E.; Liu, M.; Simms, C. M.; Obare, S. O. 'Modulating the Reactivity of Nanocrystalline TiO₂ for the Degradation of Organophosphorus Pesticides,' *J. Adv. Oxid. Technol.* **2008**, 11, 459-462.
- Guo, W.; Obare, S. O. 'Tuning the reduction of 9,11,20,22-tetraaza-tetrapyridopentacene (TATPP),' *Tetrahedron Lett.* **2008**, 49, 4933-4936.
- Ganesan, M.; Freemantle, R.; Obare, S. O. 'Monodisperse Thioether Stabilized Palladium Nanoparticles: Synthesis, Characterization and Reactivity,' *Chem. Mater.* **2007**, 19, 3464-3471.
- Lin, R.; Freemantle, R. G.; Kelly, N.M.; Obare, S. O.; Ofoli, R. Y. In-situ immobilization of palladium nanoparticles in microfluidic reactors and assessment of their catalytic reactivity *Nanotechnology* **2010**, 21, 325605.
- Obare, S. O.; De, C.; Guo, W.; T. A.; Haywood, T. L.; Samuels, T. A.; Adams, C. P.; Masika, N. O.; Murray, D. H.; Anderson, G. A.; Campbell, K.; Fletcher, K. Fluorescent Chemosensors for Toxic Organophosphorus Pesticides: A Review," *Sensors* **2010**, 10, 7018 - 7043.

Nanomechanical resonators - Improving coherence and transduction -

Jörg P. Kotthaus*

Faculty of Physics and Center for NanoScience (CeNS), Ludwig-Maximilians University
Geschwister-Scholl-Platz 1, D 80539 Munich, Germany
* E-mail address : kotthaus@lmu.de

Nanomechanical resonators offer an outstanding potential in measuring masses down to the atomic scale [Ekinici 2005] and forces close to the standard quantum limit [Teufel 2009]. They also are increasingly explored regarding signal processing based on their controllable non-linear behavior in the classical regime [Mahboob 2011, Unterreithmeier 2010a] and their potential for quantum information processing [Stannigel 2010]. Here recent studies are summarized that contribute to a better understanding of relevant damping mechanisms [Unterreithmeier 2010b], thus allowing to improve coherence via optimizing resonators via best choice of materials and geometry as well as built-in strain. Since nanomechanical resonators with low damping and correspondingly high mechanical quality factors are mostly insulators or superconductors, thus avoiding the increased dissipation in most metallic systems, we continue to explore various

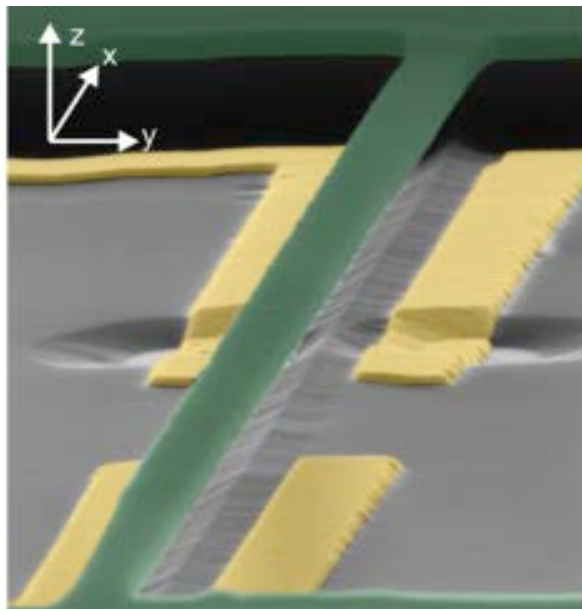


Figure 1: A doubly-clamped nanomechanical resonator with typical cross section of 200x100 nm etched out of a prestrained silicon nitride film (green) is fabricated above two pairs of gold electrodes on a silicon chip with a thin layer of SiO₂

(grey) serving as insulator. The electrodes serve to actuate the resonator via electric gradient fields and detect its motion.

routes to optimize transduction to insulating dielectric resonators via electrical and optical gradient fields [Unterreithmeier 2009, Anetsberger 2009, Unterreithmeier 2010c, Faust 2011].

The wide utilization of nanomechanical resonators for studies of fundamental physics in both, the classical and in the quantum regime, as well as their potential applications for extremely sensitive sensing will be discussed.

References:

- Anetsberger G. et al. (2009), Near-field cavity optomechanics with nanomechanical oscillators, *Nature Physics* **5**, 909
- Ekinici K. L. and Roukes M. L. (2005), Nanoelectromechanical systems, *Rev. Sci. Instrum.* **76**, 061101
- Faust, T. et al. (2011), Microwave cavity-enhanced transduction for plug and play nanomechanics at room temperature, arXiv 1109/1156
- Stannigel, K. et al. (2010), Optomechanical transducers for long-distance quantum communication, *Phys. Rev. Lett.* **105**, 220501
- Teufel, J. D. et al. (2009), Nanomechanical motion measured with an imprecision below that at the standard quantum limit, *Nature Nanotech.* **4**, 820
- Unterreithmeier, Q. P., Weig, E. M., and Kotthaus, J. P. (2009), Universal transduction scheme for nanomechanical systems based on dielectric forces, *Nature* **458**, 1001
- Unterreithmeier, Q. P., Faust, T., and Kotthaus, J. P. (2010a), Nonlinear switching dynamics in a nanomechanical resonator, *Phys. Rev. B* **81**, 241405(R)
- Unterreithmeier, Q. P., Faust, T., and Kotthaus, J. P. (2010b), Damping of nanomechanical resonators, *Phys. Rev. Lett.* **105**, 027205
- Unterreithmeier, Q. P., Faust, T., Manus, S., and Kotthaus, J. P. (2010c), On-chip interferometric detection of mechanical motion, *Nano Letters* **10**, 887

Self-catalyzed III-V nanowires and heterostructures for photovoltaic applications

A. Fontcuberta i Morral^{1*}

¹Intelligent Laboratoire des Matériaux Semiconducteurs, Ecole Polytechnique Federale de Lausanne, EPFL, 1015 Lausanne, SWITZERLAND

*Corresponding author : E-mail adress : anna.fontcuberta-morral@epfl.ch

Nanowires are filamentary crystals with a diameter of few to hundreds of nanometers. Thanks to their dimensions they are the perfect playground for fundamental studies. At the same time, their interesting properties and morphology have opened great expectatives for improving or providing new concepts in optoelectronic devices such as solar cells.

Nanowires are typically obtained by the vapor-liquid-solid method in which gold is used as a catalyst for the gathering of the precursor species and nanowire growth. It has been shown that gold can affect negatively the electronic and optical properties of semiconductors. In our group we avoid the use of gold in the synthesis process and fabricate ultra-high purity GaAs nanowires by additionally using of molecular beam epitaxy (MBE). MBE offers also the unique possibility of growing with epitaxial quality on the nanowire facets. Prismatic quantum wells and Stranski-Krastanov quantum dots are obtained with a very high quality, as demonstrated by the optical spectroscopy measurements realized on single nanowires.

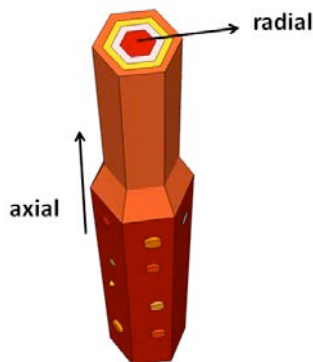


Figure 1: Schematical drawing of a nanowire containing heterostructures in the axial and radial directions.

Finally, we show how these nanowires are excellent candidates for the fabrication of third generation solar cells. Conversion efficiencies up to 10% in single nanowires have been achieved.

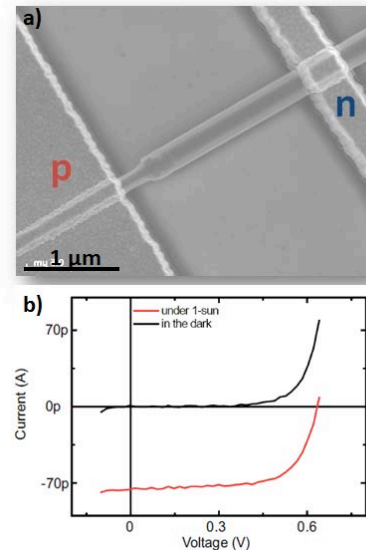


Figure 2: a) Scanning electron micrograph of a nanowire based radial pn junction with electrical contacts, b) current-voltage characteristics of the diode in the dark and under AM 1.5 illumination.

References:

- Colombo, C. et al., Growth mechanisms of Ga-assisted catalyst-free MBE GaAs nanowires, *Phys. Rev. B*, (2008) 77, 155326.
- Colombo, C. et al., Gallium arsenide p-i-n radial structures for photovoltaic applications, *Appl. Phys. Lett.* (2009) 94, 173108.
- Fontcuberta i Morral, A. et al., Prismatic Quantum Heterostructures Synthesized on Molecular-Beam Epitaxy GaAs Nanowires, *Small* (2008) 4, 899.
- Heigoldt, M. et al., Long Range Epitaxial Growth of Prismatic Heterostructures on the facets of Catalyst-Free GaAs Nanowires, *J. Mater. Chemistry* (2009) 19, 840
- Uccelli, E. et al., InAs quantum dot arrays decorating the facets of GaAs nanowires, *ACS Nano* (2010) 4, 5985.
- Uccelli, E. et al., Three-dimensional twinning of self-catalyzed GaAs nanowires on Si substrates, *Nano Lett.* (2011) 11, 3827.

Raman spectroscopy of graphene in high magnetic fields

C. dalSavio^{1*}, C. Faugeras², P. Kossacki², M. Potemski² and K. Karrai¹

¹attocube systems AG, Königinstr. 11a RGB, D-80539 München, Germany

²LNCMI-Grenoble, CNRS-UJF-UPS-INSA, France

*corresponding author : khaled.karrai@attocube.com

We report on sub-micro magneto-Raman scattering experiments performed on the surface of a freshly exfoliated single crystal of natural graphite (Faugeras 2011). Graphene flakes left on graphite are expected to be of very high electronic quality but are not easy to spot since they show no contrast in standard optical microscopy. In this work we image natural graphene flakes using high spatial resolution confocal Raman scattering microscopy in high magnetic fields (0-9 Tesla) at 4 K. Graphene flakes on graphite are revealed in the presence of a strong magnetic field, as first imaged in Faugeras 2011, when the E_{2g} phonon energy coincides with the electron-hole separation between the valence and conduction Landau levels $(-N,+M)$ of the Dirac cone. Resonant hybridization of the E_{2g} phonon and the Dirac magnetoexciton is a specific signature of graphene flakes (Faugeras 2009, Yan 2010) and display very rich Raman scattering spectra varying strongly as a function of magnetic field [1]. In the figures below the magnetic field evolution of Raman spectra are taken in region where the hybridization between the E_{2g} phonon and the $(-2,+1)$ and $(-1,+2)$ magneto-exciton takes place. We mapped the Raman scattering over $7 \times 7 \mu\text{m}$ with 600 nm spatial resolution on three different scattering bands namely i) centered, ii) blue-shifted and iii) red-shifted from the E_{2g} phonon peak and this at 4.3 T (lower three images) and 5.3 T (upper three images). These two magnetic fields are chosen to be just below and just above the resonant conditions for hybridization. As expected at 4.3 T the graphene flake appears bright in the blue shifted image (lower right), it appears bright in the red shifted image at 5.3 T while it is darker in the Raman scattering mapping centered on the E_{2g} (both center images). The upper right and lower left image have been shown here for completion with a much enhanced contrast. The weak structures are not understood but could be due to the sample surface inhomogeneities.

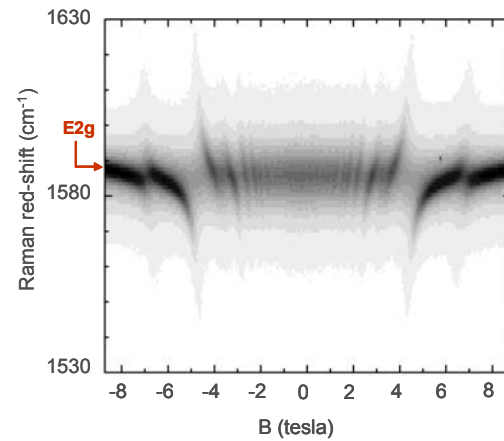


Figure 1: Magneto Raman spectra of exfoliated single crystal of natural graphite. The avoided crossings are identified as phonon and Dirac-Exciton coupling .

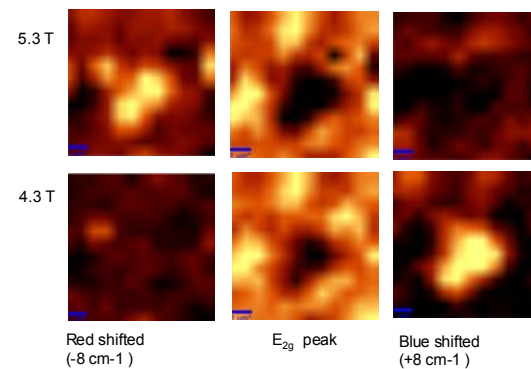


Figure 2: Magneto-Raman imaging of a flake of exfoliated single crystal of graphite deposited on graphite.

References:

- C. Faugeras et. al. Phys. Rev. Lett. **107**,036807 (2011).
 C. Faugeras et. al. Phys. Rev. Lett. **103**, 186803 (2009).
 J. Yan et. al. Phys. Rev. Lett. **105**, 227401 (2010)

3D integration of low power nanoelectronic devices above CMOS circuits

A. Souifi¹, N. Jouvet^{1,2}, S. Ecoffey¹, A. Beaumont², F. Calmon², S. Monfray³ and D. Drouin¹

¹Laboratoire International Nanotechnologies & Nanosystèmes – UMI-LN2 – CNRS 3463
3IT- Université de Sherbrooke, 2500 Boulevard Université, J1K 2R1 Sherbrooke, Canada.

²Institut des Nanotechnologies de Lyon, site INSA de Lyon - UMR 5270, Bât. Blaise Pascal, 7 Avenue Jean Capelle, 69621 Villeurbanne Cedex, France.

³ST Microelectronics, 850 Rue Jean Monnet
38920 Crolles, France

*Corresponding author : E-mail address : abdelkader.souifi@insa-lyon.fr

Introduction: Single Electron Devices (SEDs) for nanoelectronics are of great interest because of their ultra low power consumption and dissipation inherent to the fundamental basis of single electron memories and transistors where the information storage and the data processing use a reduced number of electric charges. For applications which do not require high speed, the SED-based circuits will more easily support a 3D design than stacked CMOS layers, at least from the thermal energy dissipation point of view. An example of what could be a 3D nanoelectronic SED-circuit is illustrated in fig.1.

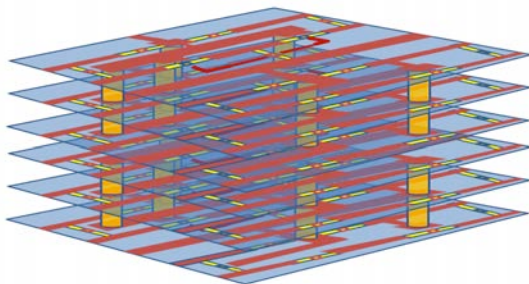


Figure 1: 3D stack metallic SET circuits.

Room Temperature CMOS compatible SETs: These last years, several research teams have explored various strategies for increasing the operation temperature of CMOS-compatible SETs. However, only two groups have really demonstrated high temperature CMOS compatible SETs with a reproducible process.

Very recently, a team from University of Chungbuk [Shin] as developed a SET fabrication process derivated from a standard FinFET technology. The principle is to reduce the size of the FinFET architecture with an oxidation step. The process allows obtaining sub-5nm isolated silicon islands perfectly aligned with source and drain access.

In 2007, the group of D. Drouin et al. from Univ. of Sherbrooke has published the first fabrication process of Titanium-based SETs operating up to 430K [Dubuc]. The “nanodamascene process” which has been used is based on the control of the Chemical Mechanical Polishing (CMP) of thin 10 nm-wide titanium lines.

Integration of SETs on CMOS : In this paper, we present the first integration of metallic SETs in the Back End Of Line (BEOL) of CMOS circuits using the nanodamascene process developed in Sherbrooke. Electrical characterization of these SETs will be also presented in this paper.

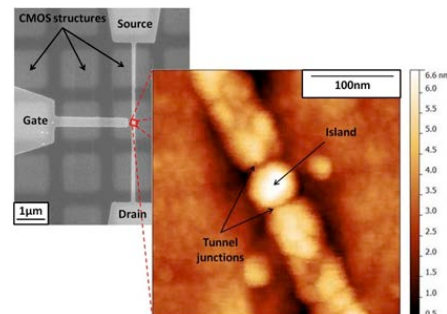


Figure 2: SEM image (left) of a SET on CMOS. AFM image (right) of the SET island.

References:

- Jouvet N. et al, Recent developments on 3D integration of metallic SET onto CMOS process for memory application, International Journal of Nanoscience, submitted (2012)
- Dubuc C. et al., Single-electron transistors with wide operating temperature range, Appl. Phys. Lett. 90, 113104 (2007)
- Shin S. J. et al., Si-based ultrasmall multiswitching single-electron transistor operating at room-temperature, Appl. Phys. Lett. 97, 103101 (2010)

Nanomaterials applied in medicine, cultural heritage, and chemical sensor technology

F. Valentini¹, M. Carbone¹, G. Palleschi^{1*}

¹Dipartimento di Scienze e Tecnologie Chimiche, Università di Roma Tor Vergata, Italy

*Corresponding author, Email: palleschi@uniroma2.it

Introduction: Herein, we report three different analytical applications of multi-layers of oxidized graphene nanoribbons (GNOs). The GNOs are synthesised by our method reported in literature [Cataldo, F. (2010)], characterized by high-resolution transmission electron microscope (HR-TEM), scanning tunneling microscopy/scanning tunneling spectroscopy (STM/STS), atomic force microscopy (AFM), Raman spectroscopy and X-ray photoelectron spectroscopy (XPS). In the applied Medicine, significant results were achieved by the study of the effect of GNOs on the proliferation of NIH3T3 murine fibroblasts. In these experiments, the cells are seeded at low density in 96-well plates in presence of both ground control (complete medium only or complete medium with the addition of 50 mg/ml BSA) and the different test materials (ranging from pristine, different functionalised single-wall carbon nanotubes-SWCNTs and carbon black-CB) at various concentrations in order to calculate the IC₅₀ (i.e. the concentration of a substance or material capable of inhibiting the growth of 50% of cells). Results show that GNOs represent the most biocompatible nanomaterials (see Figure 1) to be used as nano-carrier in nano-Medicine. In fact, GNO has been successfully used "in vitro", for the transfection of the viral genome, particularly that related to the hepatitis A virus (HAV normally is not able to replicate in some cell lines), in mammalian cells (BGM-Buffalo Green Monkey). The cell imaging is performed using the auto-fluorescence property of GNO one of many extraordinary optical features exhibited by this new nanomaterial, [Pulci, O. (2010)]. In the cultural heritage area, GNOs have been functionalised with ionic liquids (ILs) in order to obtain nano-composite materials with enhanced physical-chemical properties such as: the mechanical reinforcement features, the high Young's modulus (elasticity of the resulting material) and optical characteristics (such as transparency, [Chen, Y. (2010)]). All these properties made possible the use of nanocomposite materials (GO/ILs) for the restoration of modern tracing papers, obtained by refining forced (suffering from typical diseases due to poor preservation of Cultural Heritage, such as gaps, tears and belly flops, [Cook, P. (1994)]). After paper treatments the results show that the

tears and flaps "consolidated" by the created bridges of GO/ILs. The optical microscope images show encouraging results because papers do not show significant variations in the optical properties, after the specific treatment with the nanocomposite. Finally, in the third section of this paper, Ionic Liquids have been used to disperse GNO to obtain stable, uniform and homogeneous nanoemulsions, to be cast directly on the screen printed electrode (SPEs) surfaces. New chemical sensors for the selective electrochemical detection of: several neurotransmitters and NADH (for a new class of dehydrogenase based biosensors), have been also assembled.

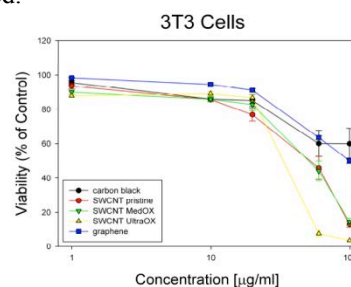


Figure 1: Dose-response curves obtained by colorimetric assays for all types of investigated nanomaterials: CB (as control), pristine and different functionalised SWCNTs; and the oxidized graphene nanoribbons (GNOs).

References:

- Cataldo, F. Valentini, F. Palleschi, G. (2010) Graphene nanoribbons produced by the oxidative unzipping of single-wall carbon nanotubes. *Carbon*, 48, 2596-2602, 2010.
- Chen, Y. P. Yu, Q. (2010) Nanomaterials: Graphene rolls off the press. *Nature Nanotechnology* 5, 559-560, 2010.
- Cook, P. Dennim, J. (1994) Ships Plans on Oil and Resin Impregnated Tracing Paper; a Pratical Repair Procedure, *The Paper Conservator. Journal of the Institute of Paper Conservation*, 18, 1119, 1994.
- Pulci, O. Gori, P. Marsili, M. Garbuio, V. Seitsonen, A. P. Bechstedt, F. Cricenti, A. and Del Sole, R. (2010) Electronic and optical properties of group IV two-dimensional materials. *Phys. Status Solidi A* 207(2), 291-299, 2010.

Challenges on protein bioencapsulation in transparent nanoporous sol-gel glasses and their applications

B. Mena, ^{1,2,*} F. Mena, ^{1,3} R. Djeribi²

¹Fluorotronics, Inc., Department of Nanobiotechnology, Cades Way, San Diego, USA

²University of Annaba, Laboratory of Biofilms and Biomaterials Contamination, Annaba, Algeria

³State University of Campinas, UNICAMP, (Hemocentro), São Paulo, Brazil

Abstract: Transparent organic-inorganic nanoporous silica glasses obtained via the sol-gel method constitute the ideal support for protein bioencapsulation and the study of the different factors influencing the protein folding process in a crowded environment (Mena *et al.*; 2010, 2011). Due to the facile silica surface modifications with the choice of Si-substituted organic groups, organically modified “wet-aged” based silica glasses can be used as host materials to mimic the crowded environment of the proteins and cells that can be found in the cytoplasm for instance. The transparent media allows spectroscopic studies such as the use of circular dichroism spectroscopy. We report the influence of different parameters (macromolecular crowding, porosity, hydrophobicity, surface hydration) on the protein conformation based on the design and the characterization of nanoporous silica-based materials bearing different functional groups favoring the protein folding (Figure 1). The enhancement of the protein folding owing the physical properties and microstructure of the host matrix induced by the nature of the functional groups and the siloxane network play a major role on the protein biological activity and therefore to the development efficient bionanodevices such as biocatalysts, sensors, drug delivery systems or implanted devices. In addition, we will introduce new challenges of using this type of host matrices in microbiology (Djeribi *et al.*, 2012). This study will also permit us to discuss a new surfactant-free micropatterning process on the porous glass surface that we have enlightened with potential optical applications.

Keywords: protein folding, nanoporous sol-gel glasses, silica-based biomaterials, circular dichroism spectroscopy, surface hydration, crowding effects, micropatterning, biomedical applications.

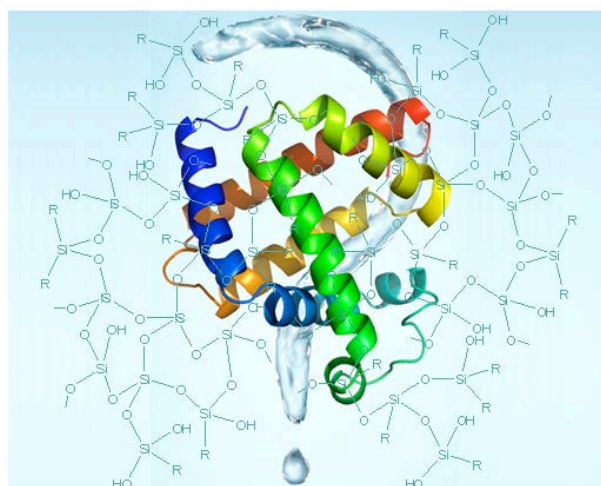


Figure 1: Figure illustrating the fundamental question that we are tempting to solve experimentally: what is the importance of silica surface modification nanoporous silica-based sol-gel glasses prepared from functionalized organosilane precursors on the parameters (such as crowding environment, surface hydration, hydrophobic effect) affecting the conformation, biological activity and functionality of encapsulated biomolecules?

References:

- Djeribi, R., Bouchloukh, W., Jouenne, T., Mena, B. (2012) Characterization of biofilms formation in urinary catheters, *Amer. J. Infect. Control.*, In Press.
- Mena, B., Montoneri, C., Mena, F., Montoneri, E., Boffa, V., Sharts, O. (2011), Protein helical structure enhancement in fluorinated-phosphonate nanoporous silica glasses characterized by circular dichroism spectroscopy, *Int. J. Nanotech.*, 8, 471-491.
- Mena, B., Mena, F., Aiolfi-Guimarães, C. Sharts, O. (2010), Silica-based nanoporous sol-gel glasses: from bioencapsulation to protein folding studies, *Int. J. Nanotech.*, 7,1-45.

Orals Communications

Controlling molecular environment to tune binding kinetics at surfaces

Laurent Limozin^{1*}

¹ Laboratory Adhesion and Inflammation

Inserm U600-CNRS U600, Aix-Marseille University, Luminy, Marseille, FRANCE

*E-mail address : laurent.limozin@inserm.fr

Abstract:

Cell adhesion is a fundamental process involved in many aspects of cell life cycle as well as in numerous pathologies and medical therapies. It is mediated by the specific interaction of membrane ligand-receptor pairs, many of which have been identified in the last twenty years. Their function is crucially dependent on details of individual bond association and dissociation, and of the nature of surface-bound molecules. During the last fifteen years, innovative techniques (Atomic Force Microscopy, Laminar Flow Chamber, Biomembrane Force Probe), disclosed a range of complex features on single bond dissociation, including multiple barriers in interaction energy landscape and catch bonds which strengthen under force.

However, new studies show that the resistance of a bond is also influenced by its age, emphasizing the role of the complete history of the bond in its adhesive properties, including its formation. Despite a few attempts to analyze association rate (k_{on}), the problem is more difficult to address than dissociation since the bond formation is more dependent on the length and flexibility of binding molecules, but also on the fine structure of adhering surfaces. Moreover, data analysis is more dependent on complex methodological features, for example the way adhering surfaces are brought into close contact. Additionally, study of association processes is complicated by the cooperative nature of assemblies of molecules and by the complex local environment surrounding adhesive units.

We setup the Colloid Surface Probe technique (CSP) which combines laminar flow chamber with RICM in order to measure the 3-dimensional motion of beads hovering above a surface. We found that the probability of bond formation was controlled by the thickness of a surface-grafted polymer repulsive layer (Fig. 1).

The systematic variation of the duration of interaction and the distance between ligand and receptor, combined with brownian dynamics simulations, suggested the existence of a minimal duration of the order of 6 ms necessary to form bonds detectable in the flow chamber.

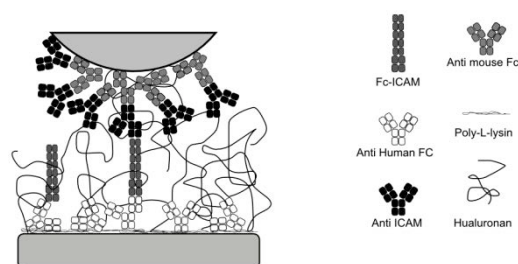


Figure 1: Adhesive-repulsive in-vitro construction for the study of a model glycoclayx and antibody-antigen kinetics association of Fc-ICAM / anti-ICAM ligand-receptor pair. Molecules are tethered on microbeads (top) and glass substrate (bottom). Each immunoglobulin domain (small squares) measures 4 nm. The distance between beads and surface is measured with Reflection Interference Contrast Microscopy (RICM).

In this context, the role of diffusion on bond formation was also studied by using ligands anchored on fluid supported lipid bilayers. Finally, effect of valency on bond stability is explored by comparing a monomeric and a dimeric ICAM constructions.

References:

- Robert P, Sengupta K, Puech PH, Bongrand P, Limozin L. (2008) Tuning the formation and rupture of single ligand-receptor bonds by hyaluronan-induced repulsion. *Biophys. J* 95: 3999-4012
- Robert P, Limozin L, Pierres A, Bongrand P (2009) Biomolecule Association Rates do not provide a complete description of bond formation *Biophys. J.* 96 : 4642-4650
- Robert P, Nicolas A, Aranda-Espinoza S, Bongrand P, Limozin L. (2011) Minimal Encounter Time and Separation Determine Ligand-Receptor Binding in Cell Adhesion. *Biophys. J.* 100: 2642-265.
- Lo Schiavo V., Robert P, Limozin L, Bongrand P Quantitative modeling reveals the contribution of bond strengthening, rebinding and force sharing to the avidity of adhesion receptors. Submitted

Novel strategies for micro and nano patterning

K. Sengupta

CNRS UMR 7325, Aix-Marseille University, CINaM - Centre Interdisciplinaire de Nanoscience de Marseille, Luminy, Marseille, France.

*Corresponding author : E-mail address : sengupta@cinam.univ-mrs.fr

Abstract:

As early as in 1997, it was shown that cells could be switched from growth to apoptosis by using micro-patterned substrates that contained extracellular matrix-coated adhesive islands of decreasing size to progressively restrict cell extension. In fact, cells also respond to nano-metric patterns (~100 nm). This is especially intriguing because the nano-scale is not only several orders of magnitude smaller than the cell size, but is also an order of magnitude smaller than the typical size of cellular adhesion domains (~ few μm). Cells have been shown to respond to both nano-topography and nano-biochemistry. Surfaces exhibiting ordered nano-features have a wide range of potential biomedical applications including scaffolding for tissue engineering, designer bandages for wound dressing, and anti-fouling surfaces for implants. Both for technological applications and in the context of fundamental cellular studies, the "perfect" fabrication technique is still missing.

Ideally, for cell studies, in addition to biocompatibility, there should be large coverage and compatibility with powerful modern optical microscopic techniques. The well known techniques are nano-imprint lithography (NIL) and self-assembly of colloids or phase separation of polymers. NIL usually depends on resource intensive techniques like e-beam lithography for fabrication of the initial stamp. Self assembly, though increasingly refined, has limited flexibility for the choice of motif. One example is di-block copolymer assisted gold nano-dot self-assembly [2].

We are developing alternative low cost strategies, which offers better compatibility with surface-sensitive optics as well as more flexible chemistry. Here I shall report different strategies being developed in our group. The first is based on exploitation of self-assembled porous anodic alumina which was used either as mould [1] to create plastic nano-pillars or as mask [2] to create bio-functional nano-islands. The second strategy is development of colloidal bead masks – that are both cheap and rapid to produce. Again, both topography and bio-chemical patterning can be achieved [3]. Finally we are also developing strategies based on pyramid shaped stamps for micro-contact printing which provide an alternative to expensive nano-contact printing [4].

References:

- [1] Sengupta K., Moyen E., Mace M., Benoliel A-M, Pierres A., Thibaudau F., Masson L., Limozin L., Bongrand P., and Hanbücken M. (2009) Large scale ordered plastic nano-pillars for quantitative live-cell imaging. *Small*, 5:449 (2009).
- [2] S. Massou, L. Masson, I. Ozerov, E. Moyen, K. Sengupta and M. Hanbücken, (2009) Large scale ordered topographical and chemical nano-features from anodic alumina templates, *Appl. Surf. Sci.*, 256:395-398 (2009).
- [3] Magiera-Millé L., Ozerov. I, Charrier A. and Sengupta K. Unpublished.
- [4] Charrier A., Bedu F., Durand H., Ozerov. I, and Sengupta K. Unpublished.

Cohesive and adhesive test for micro and nanoparticle-based coatings using sonication

L. Vonna*, W. Heni, H. Haidara

Institut de Science des Matériaux de Mulhouse (IS2M) – CNRS
15, rue Jean Starcky 68057 Mulhouse, France

*Corresponding author : E-mail adress : laurent.vonna@uha.fr

The application field for functional coatings is becoming extremely wide today. Depending on their uses, some of these coatings are made of crystalline grains, or assembled micro and nanoparticles. From a morphological point of view, the latter can be described as nanoporous coatings that are particularly fragile. Their stability thus appears to be of both fundamental and practical interest since the functional properties of these structures essentially arise from the organization of the particles or grains within the surface assembly. Moreover, in the case of nanoparticles-based coatings, the rupture of the coating can lead to the spreading of these nanoparticles in the environment. The qualitative and quantitative evaluation of the cohesive and/or adhesive performance of such coatings, as a function of the environment (fluid, temperature), is therefore of paramount importance for the development of such particle-based new materials. However, most of the existing testing methods appear to be not well designed, or simply not applicable for the study of the cohesion and adhesion of these particles-based coatings.

In this work we extend to particles-based coatings, a test using ultrasound vibrations (sonication) that was initially developed by our team to evaluate semi-qualitatively both adhesion and cohesion of thermally evaporated thin metal coatings on polymer films (Haidara, Papirer, Vallat, & Schultz, 1993; Haidara, Vallat, & Schultz, 1990).

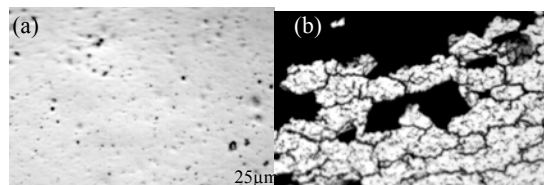


Figure 1 : Optical microscopy images of a thin copper film (100nm) deposited on a polyethylene théréphthalate film (a) before and (b) after sonication (40% of 600W during 15 seconds)

We present here the first experiments realized on gold and silica nanoparticles-based coatings and discuss their stability as a function of the strength of particle/particle and particle/substrate interactions. Similarly to previous results obtained on metal coatings (see Figure 1) composed of in-situ granular domains (M.-F. Vallat et al., 1996), the cohesion of the nanoparticles-based coatings is discussed as a function of the particles size that was shown to control at the mesoscale the thermo-mechanical stability of nanoparticles clusters and aggregates (Darwich, Mougin, & Haidara, 2010). Following these first results, we present the technical limitations and the potential of this sonication test to the qualitative and quantitative assessment of the mechanical and environment stability of nanoparticle-based coatings.

References:

Darwich, S., Mougin, K., and Haidara, H. (2010). Complex aggregation patterns in drying nanocolloidal suspensions: size matters when it comes to the thermomechanical stability of nanoparticle-based structures. *Journal of Surfaces and Colloids*, 26(22), 16928-16933.

Haidara, H., Papirer, Y., Vallat, M.-F., and Schultz, J. (1993). Relationships between structural properties of vapour deposit metallic films on to polymer and their relevant adhesive performance. *Journal of Materials Science*, 28, 3243-3246.

Haidara, H., Vallat, M., and Schultz, J. (1990). Films polymères métallisés: mesure de l'adhésion polymère/métal. *European polymer journal*, 26(8), 907-910.

Vallat, M.-F., Haidara, H., Ziegler, P., Rey, D., Papirer, Y., and Schultz, J. (1996). Adhesive behavior of aluminum layers evaporated on polyester films. The proceedings of the 53rd international meeting of physical chemistry: Organic coatings, 354, 14-22.

Gas sensing properties of metal decorated tungsten or tin oxide nano-needles grown by aerosol-assisted chemical vapour deposition

F.E. Annanouch¹, Stella Vallejos², C. Blackman², X. Correig¹, E. Llobet^{1*}

¹MINOS-EMaS, University Rovira i Virgili, Tarragona, SPAIN

*Corresponding author : E-mail address : eduard.llobet@urv.cat

² Department of Chemistry, University College London, UNITED KINGDOM

Introduction: Metal oxide gas sensors are still, more than two decades after their discovery, the subject of research. In the last few years semiconductor metal oxide nanowires have attracted interest as gas sensitive materials because they promise, on the one hand, highly increased surface area and dimensions close to the Debye length of the semiconductor (both related to increased sensitivity) and, on the other hand, an easier-to-understand chemistry since such structures are usually single-crystalline. In this work, tin or tungsten oxide single crystalline nanowires decorated with metal nanoparticles (i.e., gold, platinum, copper) have been grown by aerosol assisted chemical vapour co-deposition (AA-CVD) in a single step. This growth method is very flexible, affordable (e.g. it runs at atmospheric pressure) and can be easily scaled up for mass production of such nanostructured materials. The morphology, composition and the gas sensing properties of these materials will be discussed in depth.

Methodology: The metal decorated nanowires were grown by AA-CVD either on inert substrates (e.g. Oxidised silicon or alumina) or directly onto silicon-based gas sensor transducers (onto a thin dielectric silicon-based membrane comprising a Pt heating resistor and 50 μm gap Pt interdigitated electrodes). Additionally, sensor substrates having 3 μm gap interdigitated electrodes were employed to perform an ex-situ dielectrophoretic alignment of metal oxide nanowires. The morphology and composition of the different materials was studied by employing high-resolution transmission electron microscopy (HR-TEM) and X-ray photoelectron spectroscopy (XPS), respectively. The results of the dielectrophoretic alignment of nanowires were studied by scanning electron microscopy (SEM). Finally, the gas sensing properties were studied by employing a fully automated gas measurement rig, which allows for delivering reproducible gas mixtures to a gas sensor test chamber.

Main results: The growth of metal oxide nanowires decorated with metal nanoparticles was

successfully accomplished employing the AA-CVD method (see Figure 1).

The gas sensing properties of the different nano materials were investigated. Their response to humidity, benzene and ethanol vapours, nitrogen dioxide and carbon monoxide will be discussed in detail. Figure 2 shows the response of tungsten oxide nanowires to nitrogen dioxide.

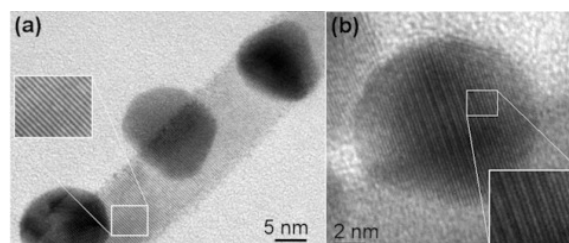


Figure 1: (a) HR-TEM image showing that tungsten oxide nanowires are single crystalline. (b) Au nanoparticle showing a crystalline arrangement.

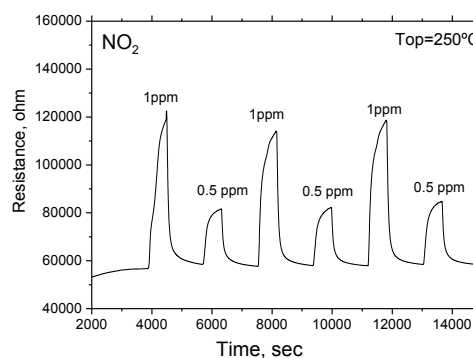


Figure 2: Repeated responses of a Au-decorated tungsten oxide nanowire sensor to nitrogen dioxide.

The sensors show an increased sensitivity to gases at lower operating temperatures (e.g., 6-fold increased response to ethanol). AA-CVD allows the bottom-up integration of nanostructures in functional devices.

References:

Blackman C., Llobet E., et al. (2011), Nanoparticle-functionalised WO₃ nanoneedles and their application in high sensitivity gas sensor devices, *Chemical Communications*, 47, 565-567.

Towards a paradigm change – mammalian cells as sensitive biosensor layers for the detection of unexpected toxic substances in air

U. Bohrn*^{1,2,3}, E. Stütz¹, M. Fleischer¹, M.J. Schöning², P. Wagner³

¹Corporate Research and Technologies, Siemens AG, GERMANY

²Institute of Nano- and Biotechnologies, Aachen University of Applied Sciences, GERMANY

³Institute for Materials Research (IMO/IMOMECE), Hasselt University, BELGIUM

* ulrichbohrn@hotmail.com

Introduction: Living mammalian cells respond highly sensitive and with multiple metabolic parameters to toxic substances – not only in liquids but also in gas phase. Standard *in vitro* technology is not able to get a continuous cell response in a label-free and non invasive way. Classical biosensors operate usually in the liquid phase and only to a minor degree in air [1]. In this study, we combined the benefits of *in vitro* technology with a modern real-time multiparametric sensor technology to develop a directly exposed cell-based gas biosensor (CBGB) for the detection of toxic substances in ambient air.

Experimental: The hereby used technology is the Bionas 2500 Analyzing System. This device incorporates 6 sensor chips. Each of them is able to simultaneously monitor the metabolic activity (acidification), the respiration (oxygen consumption) and the morphology (impedance) of mammalian cells. For the gas exposure, the nutrition medium was temporarily (few mins) removed and test gases were applied using a T-shaped device (see. Figure 1), plugged on the sensor chip [2].

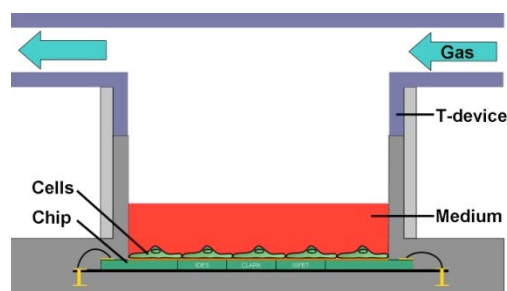


Figure 1: Scheme of a cross section of the sensor chip equipped with the gas exposure device.

Direct contact of the gas with the cell enables a straight uptake of gaseous pollutants which leads to alterations in the cellular metabolism or the cytoskeleton stability.

Results: Toxic carbon monoxide impairs the cellular respiration rates constantly at concentrations of 50 ppm [3]. Ammonia gas impairs the cell metabolism and leads to a decrease of the acidification rate at concentrations of only 20 ppm.

Conclusion: A novel cell-based gas biosensor system for the detection of unknown toxic gaseous substances has been realised. The here presented device has the possibility to be used for continuous environmental monitoring, toxicological screening and *in vitro* investigation of medical gases and aerosols.

References:

- [1] Sandström, K.J.M, Turner, A.P.F. (1999) Biosensors in air monitoring. J. Environ. Monit. 1:293–298.
- [2] Bohrn, U., Stütz, E., Fleischer, M., Schöning, M.J. and Wagner, P. (2010) Real-time detection of CO by eukaryotic cells. Procedia Engineering 5:17-20.
- [3] Bohrn, U., Stütz, E., Fleischer, M., Schöning, M.J. and Wagner, P. (2011) Eukaryotic cell lines as a sensitive layer for rapid monitoring of carbon monoxide. Physica Status Solidi (a) 208:1345-1350.

Characterisation of aseptic sterilisation processes using an electronic nose

S. Reisert^{1*}, H. Geissler², R. Flörke², C. Weiler², P. Wagner³, M.J. Schöning¹

¹Institute of Nano- and Biotechnologies, Aachen University of Applied Sciences, Campus Jülich, GERMANY

*Corresponding author : E-mail address : reisert@fh-aachen.de

²SIG Combibloc Systems GmbH, Linnich, GERMANY

³Institute for Materials Research, Hasselt University, BELGIUM

Introduction: The aseptic filling of pre-sterilised foodstuff has reached a high level of technical sophistication and is growing in importance. Hydrogen peroxide vapour is used as sterilising agent in aseptic processes. It has a high potential of bacterial and sporicidal inactivation and is at the same time friendly to the environment. An effective sterilisation of carton packages is necessary in order to avoid recontaminations by pathogenic microorganisms and to attain shelf-stable products. The effectiveness of aseptic sterilisation processes is thereto tested by means of so-called microbiological challenge tests.

Several attempts have been made to characterise sterilisation processes by monitoring the influence parameters, such as the hydrogen peroxide concentration or temperature. However, monitoring of one single parameter is often not sufficient for an accurate evaluation of a sterilisation process, since there is an interaction between the various influential parameters, like temperature, pressure, gas flow and humidity, which can have a decisive effect on the inactivation of microorganisms.

One promising approach for the evaluation of multi-component chemical media and dynamic processes relies on the use of multi-sensor systems. Concerning such multi-sensor systems, multi-component chemical media could be described not by a sum of the individual components (or corresponding response from the specific sensors) but by some abstract representation – a chemical image – a virtual fingerprint with a set of parameters intrinsic for a given multi-component medium.

Methods: In this work, six different gas sensors (four different metal oxide semiconductor gas sensors (MOX), a λ -probe and a calorimetric H_2O_2 sensor) have been used in order to obtain chemical images of the sterilising agent at different gas compositions. At the same time, microbiological tests with *Bacillus atrophaeus* spores have been carried out in order to determine the sterilisation efficacy.

Results & Discussion: The influencing factors of the microbial reduction of *Bacillus atrophaeus*

spores by hydrogen peroxide vapour, namely, the hydrogen peroxide concentration, humidity, gas temperature and flow rate, equally have an effect on the response of the gas sensors in test. It was possible to draw a correlation between the chemical images and the results of the microbiological tests (log-rate).

The collected data is used to calibrate the sensor system. In a further step, chemical image recognition techniques, like the Fuzzy Logic or an Artificial Neural Network (ANN) shall be implemented in order to determine the sterilisation efficacy of unknown gas compositions based on the correlation found during calibration. Such systems, combining an array of cross-sensitive gas sensors in combination with an chemical image recognition technique, have been named as “electronic nose”.

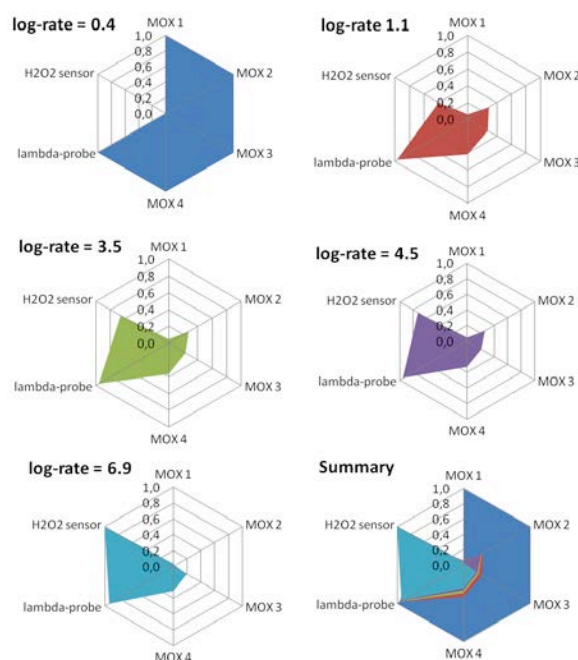


Figure 1: Resulting log-rates of *B. atrophaeus* and chemical images of the sterilisation medium at different gas compositions obtained by the sensor array, containing six gas sensors.

Microfluidic detection based on impedimetric bacteriophage biosensor

M.B.Mejri^{1,2}, H.Baccar¹, M Aouni²; A. Abdelghani^{1*}

¹ Nanotechnology Laboratory, Institut National des Sciences Appliquées et de Technologies, TUNISIA

*Corresponding author : aabdelghan@yahoo.fr

² Laboratoire des maladies transmissibles et des substances biologiquement actives (LR99ES27), faculté de pharmacie Monastir ; 5000 Monastir, Tunisia

Abstract :

Miniaturization is one of the strategies most commonly used to move forward with the performance of biosensors. Impedimetric Biosensors are imposing alternative for the detection of pathogens with be good levels of performance by undergoing this transformation. In this work, we report a approach to use alone chip integrated in microfluidic cell. The chip will be functionalized by T4-phages by simple physisorption. To improve the reproducibility of the measurements and facilitate sample handling, we have also designed and produced a dual flow cell where two chips can be simultaneously hosted. Phages are viruses able to identify specifically target bacterial species and interact with them inducing several biochemical process leading finally to bacterial lysis. Previous work confirmed the success of the based phages biodetection, but the optimization of our biosensing strategy requires miniaturization which can make easy the device handling, decrease the samples required volume and as commonly recognized increase the sensibility.

We develop new chips contain two interdigitated microelectrodes that can be used as working electrode. Another two electrodes can be used as reference and auxiliary electrodes.

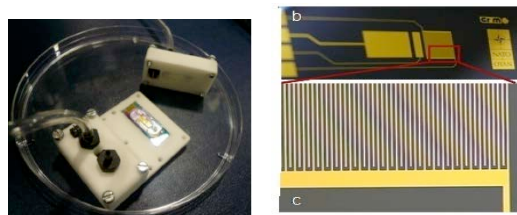


Figure 1

The new design does not require manual wire bonding and encapsulation, which makes chip production significantly easier, faster and cheaper, while it simplifies handling. and their connection pads match with industry-standard 0.05" connectors.

Figure2. shows the impedance spectroscopy of the interdigitated gold microelectrodes in microfluidic cells. It's show a stable behavior.

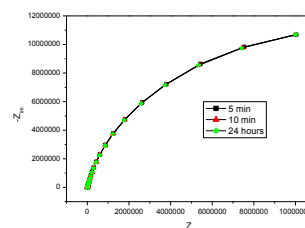


Figure2

The kinetic behavior was studied for E.coli detection using the new integrated interdigitated gold microelectrodes functionalized with T4-phages with the new microfluidic cell.

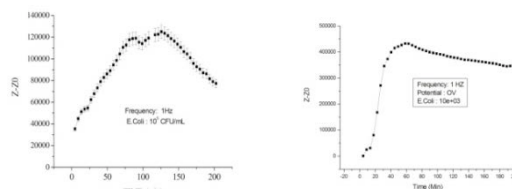


Figure 3

Figure.3 shows the absolute variation of impedance $|Z - Z_0|$ versus the time at fixed frequency (1 Hz), where Z is the impedance module of E.coli (105 CFU/mL) bacteria recognition with T4-phage, Z_0 is the impedance module of immobilized T4-phage. The use of new microfluidic cell allows us to detect lower detection limit of 103 CFU/mL (Figure.3).

References:

- [1] M. B. Mejri, M. Marrakchi, H. Baccar, S. Helali, M. Aouni, M. Hamdi, N. Jaffrezic-Renault, and A. Abdelghani, *Sens. Lett.* 7, 896 (2009).
- [2] M. B. Mejri, H. Baccar, E. Baldrich, F. J. Del Campo, S. Helali, T. Ktari, A. Simonian, M. Aouni, and A. Abdelghani, *Biosens Bioelectron.* 26, 1261 (2010).

Acknowledgments

This research is sponsored by NATO's Public Diplomacy Division in the Framework of "Science for Peace", project SFP 983115.

Biopolymer-degradation monitoring by chip-based impedance spectroscopy technique

S. Schusser^{1,2}, M. Leinhos¹, A. Poghosian^{1,2}, P. Wagner³, M.J. Schöning^{1,2*}

¹ Institute of Nano- and Biotechnologies, Aachen University of Applied Sciences, Campus Jülich, GERMANY

*Corresponding author : E-mail address : schusser@fh-aachen.de

² Peter Grünberg Institute (PGI-8, Bioelectronics), Research Centre Jülich GmbH, Jülich, GERMANY

³ Institute for Materials Research, Hasselt University, Diepenbeek, BELGIUM

Introduction: Biodegradable biopolymers are of distinct interest for patient treatment and care. Their field of application includes complex geometric structures like stents as well as simple woven structures for tissue engineering. But also coating techniques take advantage of these materials to guarantee a better biocompatibility.

One major question in this context is the degradation kinetic of the applied polymers. Unfortunately, adopting its kinetic to desired application is not a straight-forward procedure. Additionally, additives such as antibiotics, used for further enhancement of biocompatibility, also effect the degradation kinetic. As a consequence, degradation studies take a lot of time and effort to get all necessary information. Hence, online monitoring of the degradation procedure would be highly appreciated.

Methods: We fabricated thin platinum electrodes on a Si/SiO₂ structure, covered them with a biodegradable polymer and monitored its degradation by impedance spectroscopy. Due to the importance of poly(lactic acid) (PLA) in medical applications, we choose Resomer® R202H (Evonik Röhm GmbH, Germany) as a model polymer. The polymer layers were produced by spin coating using a solution of PLA solved in acetone.

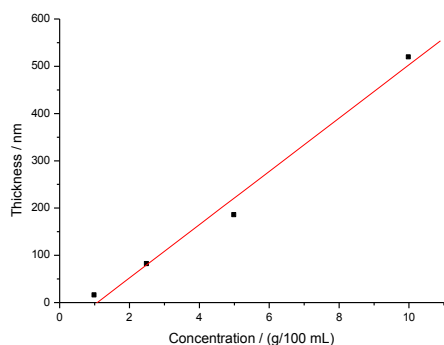


Figure 1: Thickness/concentration relation of spin-coated PLA layers.

The thickness of the polymer layer can be varied easily by adapting the polymer concentration in the solvent (Fig. 1). In a first run, we used layers made out of a concentration of 5% (w/v) (approx. 200 nm). We performed an accelerated degradation

test in two different pH values (buffer solution at pH 9 and pH 12).

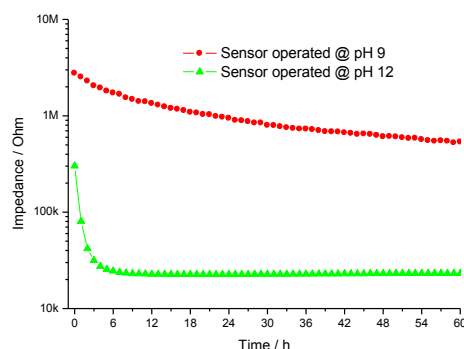


Figure 2: Impedance change during degradation process of PLA in pH 9 (dots) and pH 12 (triangles) at 10 Hz.

Results: The sensor signals of the degradation process are shown in Fig. 2. It is a well known fact, that the degradation kinetic of PLA is catalyzed by alkaline conditions. This fact is in good correlation with the achieved results. As expected, the impedance signal of the sensor that has been operated in a pH 12 analyte showed a faster response behaviour in terms of biodegradation (i.e., corrosion). Also visual control of the polymer layers after 60 hours verified these results. The layer of the sensor operated in pH 12 disappeared completely whereas the layer of the sensor in pH 9 analyte did not show any recognizable change.

References:

Amass, W., Amass, A. and Tighe, B. (1998) A review of biodegradable polymers: uses, current developments in the synthesis and characterization of biodegradable polyesters, blends of biodegradable polymers and recent advances in biodegradation studies *Polymer International*, 47, 89-144, 1998

Acknowledgements: This Programme is co-financed by the European Union (ERDF). The Commission, investing in your future.



Ministerium für Wirtschaft, Energie, Bauen, Wohnen und Verkehr des Landes Nordrhein-Westfalen



Improvement of a pesticide interdigitated microelectrodes immunosensor performance using oriented antibody immobilization

M. Marrakchi^{1*}, S. Helali³, N. J. Soto Camino², M. A. Gonzalez-Martinez², M. Hamdi¹, A. Abdelghani³

¹ Carthage University, Laboratoire d'Ecologie et Technologie Microbienne, INSAT, Centre Urbain Nord, BP676, 1080 Charguia Cedex, Tunisia

² Departamento de Quimica, Universidad Politecnica de Valencia, Camino de Vera s/n, 46022 Valencia, Spain

³ Carthage University, Nanotechnology Laboratory, INSAT, Centre Urbain Nord, 1080 Charguia Cedex, Tunisia

*Corresponding author: E-mail address: mounamarrakchi@yahoo.fr

Abstract:

Pesticides are nowadays considered as common environmental pollutants, although their use is necessary in order to satisfy the food demand of our society. The potential toxicity of pesticide residues in drinking water has meant a rigid regulation for the appearance of these pollutants in water destined for human consumption. Among the large number of different pesticide families, atrazine are one of the most widely used to protect from undesirable broadleaf weeds both in agricultural sites (as corn, sugarcane, sorghum...) and non-agriculture sites (as golf courses, rangeland, residential lawns, bermuda grass...). This fact, together with the high persistence of atrazines in the environment, their relative high solubility in water and their mobility, had led to the release of these compounds to ground and surface waters, and they have even reached at sea (Gascó et al. 1997). So, the United States Environmental Protection Agency (US EPA, 1992) allows a maximum level of 3 mg l⁻¹ for atrazine on drinking water, and the more strict regulations of European Union (EU directive, 1980) allow a maximum level of 0.1 mg l⁻¹ for any single pesticide. These rigid regulations imply the need of very sensitive analytical methods to monitor the presence of pesticides residues in surface waters, as biosensors.

In this work, we focused on the development of a sensitive immunosensor based on fast and simple immobilization technique. At first time, a physisorption of antibody on gold surface were used for the immobilization of goat anti-rabbit IgG. Second, rabbit anti-atrazine IgG are added and fixed on gold surface by the first layer of anti-rabbit antibodies. Thus, this immobilization method allows a fast and oriented fixation of anti-atrazine antibodies on gold surface to improve biosensor response.

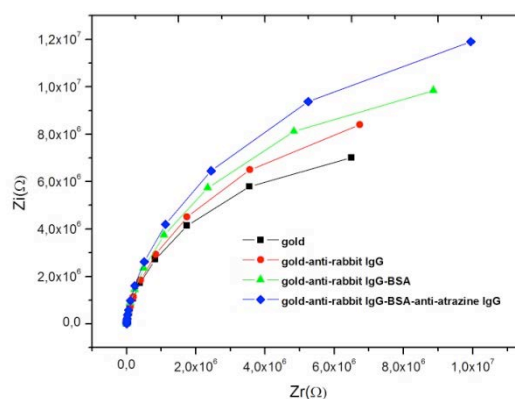


Figure 1: Nyquist diagram (Z_r vs. Z_i) for the impedance measurements corresponding to the different layers of the immunosensor: ■ Au-electrode; ● anti-rabbit IgG –Au electrode; ▲ BSA-anti-rabbit IgG – Au electrode; ◆ anti-atrazine - BSA-anti-rabbit IgG – Au electrode;

References:

- Gascón J., Salau J.S., Oubiña A, Barcelò D. in: *Immunochemical Technology for Environmental Applications* Edited by Aga D.S., Thurman E.M. (Eds.), ACS Symposium Series, vol. 657, American Chemical Society, Washington D.C., (1997), Chapter 20, pp. 254-260.
- US Environmental Protection Agency, National Survey of Pesticides in Drinking Water Walls, Phase II Report, EPA 570/9-91-020. National Technical Information Service, Springfield, VA, 1992.
- EU Directive 80/778/EEC, Commission of the European Union, 1980.

Photovoltaic response of InAs/InGaAs/GaAs quantum dots heterostructures intermediate-band solar cell

M. Ezzdini, B. Azeza, S. Rekaya, L. Sfaxi*, R. M'ghaieth, and H. Maaref

Laboratoire de Micro-Optoélectronique et Nanostructures

Faculté des Sciences de Monastir, Avenue de L'environnement, 5000 Monastir (Tunisie)

*E-mail: larbi.sfaxi@fsm.rnu.tn

Abstract: Recently low dimensional semiconductor quantum dots, (QDs) incorporated in the active region of a p-i-n junction solar cell (SC), have attracted intense research as a possible means of exploiting the sub-band-gap photons to generate an additional photocurrent beyond that corresponding to the band-to-band transition in a conventional single junction SC [1]. In quantum dots solar cells, the QDs should be uniform in size and periodically distributed in all three dimensions, which lead to the formation of an intermediate band or a mini-band rather than a multiplicity of discrete quantized levels in order to achieve the predicted high conversion efficiencies [2]. However, Stranski-Krastanov (S-K) growth in InAs/GaAs system usually results in a degradation of stacked QD structure and generation of misfit dislocation, as a result of accumulation of internal strain beyond the critical thickness [3]. For this reason, tensile strained barriers such as GaP, GaAsN and InGaAs have been studied to balance out or to compensate for the compressive strain induced in QD active region [4]. In this work, we have carried out basic studies on the characteristics of GaAs-based solar cell with and without 5 stacked InAs/InGaAs/GaAs QD heterostructures in the intrinsic region grown on GaAs (001) substrates. Epitaxial layers were grown on epitaxially n+-GaAs (100) substrate using solid-source molecular beam epitaxy (SS-MBE) with Riber MBE 32P system. Following oxide desorption at 600°C under As₄ ambient condition, we decrease the temperature to 520°C to start the growth of a 250 nm n+ doped GaAs buffer with a doping density of $2 \times 10^{18} \text{ cm}^{-3}$ followed by a 1000 nm n-doped GaAs base layer with a doping density $1 \times 10^{17} \text{ cm}^{-3}$. The substrate temperature is then lowered and stabilized to 500°C for the deposition of the active region. This later consists of 5 stacks InAs/In_{0.13}Ga_{0.87}As/GaAs QD heterostructures sandwiched by 80 nm intrinsic GaAs layer. At the end, a 500 nm p-doped GaAs emitter layer ($2 \times 10^{17} \text{ cm}^{-3}$) followed by a 100 nm GaAs p+ doped contact layer ($5 \times 10^{18} \text{ cm}^{-3}$) were grown on top of the structure. Silicon (Si) and Beryllium (Be) were used as n- and p-type dopants. A reference sample of the same p-i-n structure without QD was grown, with a 350 nm-thick i-layer. Figure 1 shows the spectral response measurements at room temperature for these solar cells. The QDs solar cell shows an extended response up to 1280 nm (figure 1) due to absorption from InAs QDs, wetting layer (WL) and InGaAs layer of the InAs/InGaAs/GaAs

QDs heterostructures, i.e., IB. Furthermore, the spectral response peak near $\lambda=1000 \text{ nm}$ is induced by the wetting layer (WL) [5] and the photo generated current between 880-1000 nm (1.24-1.42 eV) is due to the absorption from InGaAs layer [6], while that beyond 1000 nm (<1.24 eV) is due to InAs QDs absorption from both ground (GS) and excited state transition (ES) [7]. This implies that the incorporation of InAs/InGaAs QDs in the active region, although relatively weak compared with the GaAs solar cell response, is extended into the near infrared region of the solar spectrum.

The PL decay profiles for the QDs solar cell sample obtained by time resolved PL measurements. With increasing temperature the decay time was increased and then above 180K, drastically decreased. Furthermore the PL spectra for the QDs solar cell were measured by increasing every 20 K at the temperature range from 10 to 300K. The PL spectrum presents an asymmetric shape located in the high-energy side and which can be deconvoluted in two sub-bands.

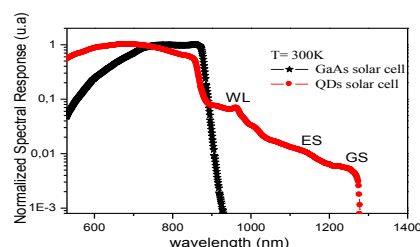


Figure 1: Spectral Response of the InAs/InGaAs QD solar cell and a GaAs reference cell.

References:

- [1] X.-J. Shang, J.F. He, M.F. Li, F. Zhan, H.Q. Ni, Z.C. Niu, H. Pettersson, and Y. Fu, *J. Appl. Phys. Letters* 99, 113514 (2011)
- [2] A. Luque and A. Marti, *Phys. Rev. Lett.* 78, 5014 (1997)
- [3] G. S. Solomon, J. A. Trezza, A. F. Marshall, and J. S. Harris, Jr., *Phys. Rev. Lett.* 76, 952 (1996)
- [4] S.M. Hubbard, C.D. Cress, C.G. Bailey, R.P. Raffaele, S.G. Bailey, D.M.Wilt, *Appl. Phys. Lett.* 92, 123512 (2008).
- [6] C.Y.Ngo, S.F.Yoon, W.K.Loek, T.K.Ng and S.J.Chua *Journal of Crystal Growth*, 311, 1885 (2009)
- [7] X.-J. Shang, J.F. He, M.F. Li, F. Zhan, H.Q. Ni, Z.C. Niu, H. Pettersson, and Y. Fu, *J. Appl. Phys. Letters* 99, 113514 (2011)

Energy of excitons and acceptor-exciton complexes to explain the origin of ultraviolet photoluminescence in ZnO quantum dots embedded SiO₂ matrix

L.Dallali^{1*}, S.Jaziri¹, J. Martínez- Pastor²

¹Département de Physique, Faculté des Sciences de Bizerte, 7021 Jarzouna, Bizerte, Tunisie.

*Corresponding author : E-mail adress : lobnadallali@hotmail.com

²Institut de Ciència dels Materials de la Universitat de Valencia (ICMUV), P.O. Box 2085, 46071-Valencia, Spain.

Abstract: Assuming finite depth and within the effective mass approximation, the energies of exciton states and of the acceptor–exciton complexes confined in spherical ZnO quantum dots (QDs) embedded in a SiO₂ matrix are calculated using a matrix procedure, including a three dimensional confinement of carrier in the QDs. This theoretical model has been designed to illustrate the two emission bands in the UV region observed in our experimental Photoluminescence spectrum (PL) with the first emission band observed at 3.04 eV and attributed to the bound ionized acceptor- exciton complexes, and the second one located at 3.5 eV, assigned to the free exciton. Our calculations have revealed a good agreement between the matrix element calculation method and the experimental results . The acceptor –exciton complexes binding energy of the acceptor-exciton complex as a function of the radius (or of the impurity position of the acceptor) and the normalized oscillator strength of the QDs have also been studied. Numerical results show that the binding energy of the acceptor- exciton complexes is particularly robust when the impurity position of the acceptor is in the centre of the ZnO QDs. It has been clearly shown from our calculations that these physical parameters are very sensitive to the quantum dot size. As a consequence, the optical and electronic properties of the dot can be controlled and also tuned through the nanoparticle size variation. These results could be particularly helpful, since they are closely related to experiments performed on such nanoparticles. This may allow us to improve the stability and efficiency of the semiconductor quantum dot luminescence which is considered critical.

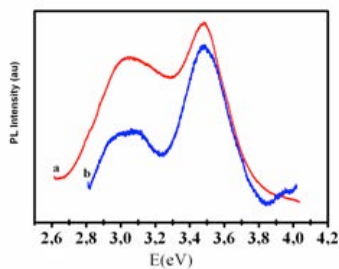


Figure1: PL Spectra for samples (a): Si/ Zn= 5, and (b): Si/ Zn= 10 measured at room temperature.

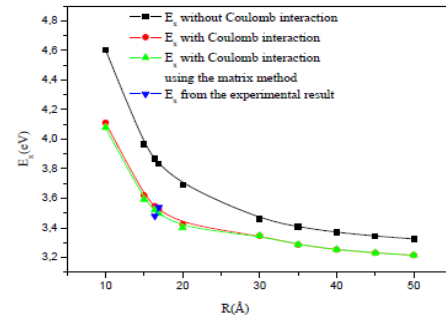


Figure2: Ground states exciton energy as a function of ZnO QDs radius.

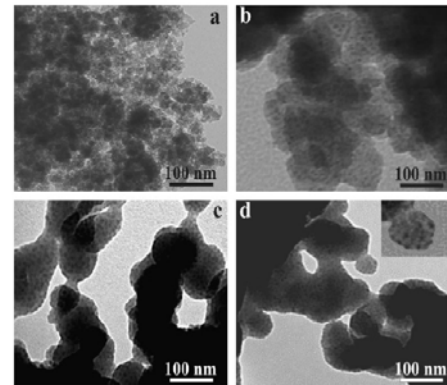


Figure 3: TEM images of ZnO-UVM-7 materials. a) UVM-7 (Si/Zn=∞), b) (Si/Zn=30), c) (Si/Zn=10), d) (Si/Zn=5).

References:

- L. Dallali, S. Jaziri, J. El Haskouri, P. Amorós (2009), Optical properties of exciton confinement in spherical ZnO quantum dots embedded in SiO₂ matrix, *Superlattices and Microstructures*, 46 (2009) 907-916.
- L. Dallali, S. Jaziri, J.M.Pastor.(2011) Optical properties of acceptor–exciton complexes in ZnO/SiO₂ quantum dots. *Solid State Communications* 151 (2011) 1355–1358.
- J. El Haskouri, L. Dallali, L. Fernández, N. Garro, S. Jaziri, J. Latorre, C. Guillem, A. Beltrán, D. Beltrán, P. Amorós. (2009) ZnO nanoparticles embedded in UVM-7-like mesoporous silica materials: Synthesis and characterization, *Physica E* 42 (2009) 25-31.

Relationship between the electronic and structural properties of n-GaAs layer grown on rough Si substrate by molecular beam epitaxy

B. Azeza, M. Ezzedini, Z. Zaaboub, R. M'ghaieth, L. Sfaxi , H. Maaref

Laboratoire Micro-Optoélectroniques et Nanostructures, Faculté des Sciences de Monastir, Université de Monastir. Avenue de l'environnement 5019 Monastir, Tunisie

Abstract

The relationship between the electronic and structural quality of n-GaAs layers grown on rough surface of silicon substrate (RSi) has been investigated respectively by time Resolved Photoluminescence TRPL (Fig.1) and High Resolution X-Ray Diffractometer HRXRD (Fig.2). The correlation between the electronic and structural properties of the n-GaAs layer as illustrated in table 1, showing that the defects density is a strong cause for trapping the minority carriers and show the effect of introducing intermediate rough silicon layer between silicon substrate and n-GaAs layer on the minority carrier lifetime. The results show that the structure grown on RSi involves higher lifetime than those grown on flat silicon substrate.

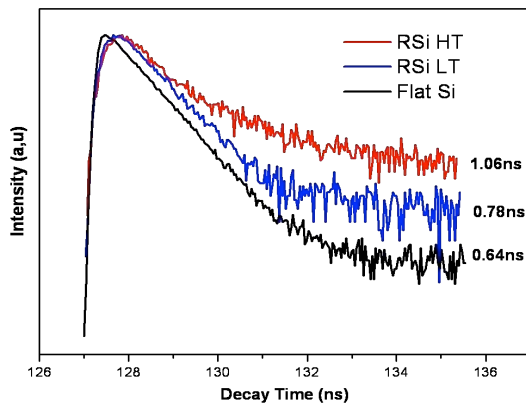


Fig.1. TRPL decay curves of GaAs grown on: (a) on RSi at T= 680°C, (b) on RSi at T= 570°C, (c) on flat Si substrate.

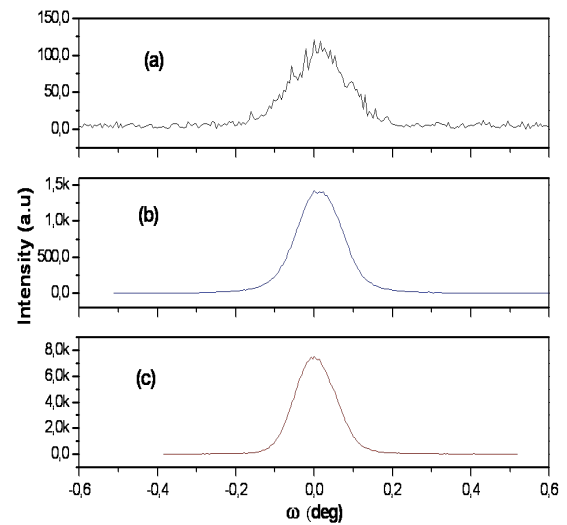


Figure 2: recording of ω -rocking curves of GaAs deposited on: (a) flat Si, (b) RSi at T=570°C, (c) RSi at T=680°C.

Samples	Δ_{GaAs} (arcsec)	Minority carrier lifetime (ns)
GaAs/ flat Si (T=570°C)	524	0,64
GaAs/RSi (T=570°C)	435	0.78
GaAs/RSi (T=680°C)	362	1.06

Table: Data of the recording ω -rocking curves and minority carrier lifetime for 2 μm thick of GaAs layer grown on flat silicon substrate and on RSi substrates.

Design of optical devices based on hybrid periodic/fibonacci photonic crystal in the visible and the near infrared domains

A. Mouldi*, M. kanzari

Photovoltaic and Semiconductor Materials Laboratory

Ecole Nationale d'Ingenieurs de Tunis, TUNISIA

*Corresponding author : E-mail adress : abir20052002@yahoo.fr

The photonic heterostructures are combinations between adjacent photonic crystals. This approach have been generally explored to design optical micro cavities (Escorcía-García and Mora-Ramos 2009) and to enlarge the Photonic Band Gap (PBG) (Srivastava et al. 2008). The heterostructure revealed in this work is the combination of periodic and Fibonacci structures. It is of the type Bragg mirror-(Fibonacci)^S-Bragg mirror and is exploited to design a micro cavity with strong mode localization in the visible range and to design a large omnidirectional PBG generating the optical telecommunication wavelengths 0.85, 1.3 and 1.55 μm . The system under consideration is a multiple of a Fibonacci multilayer $[F_1(m, n)]^S$ embedded between two periodic multilayer structures $(LH)^P$, that is, the structure is built according to the form $(LH)^P[F_1(m, n)]^S(LH)^P$. Here, H and L are defined as being two dielectric materials with H is the high refractive index material and L the low refractive index one. The theoretical simulation is done using the transfer matrix method.

In the visible range, the micro cavity was designed by stacking quarter wavelength layers with TiO₂ is the high refractive index material and the SiO₂ is the low one. It is obtained by optimizing the structure parameters such as the generation number l , the Fibonacci parameters m and n , the repetition number S , the period's number p and the reference wavelengths λ_0 of each block. With the structure $(LH)^8[F_3(1,1)]^8(LH)^8$ in which the reference wavelength in the two sidewall periodic stacks is chosen to be $\lambda_0 = 0.5 \mu\text{m}$, and that of the Fibonacci stacks is $\lambda_0 = 0.35 \mu\text{m}$, we achieved a transmission peak at $\lambda_0 = 0.5 \mu\text{m}$ of more than 99.5 % of transmission and with high quality factor $Q = 1000$. Figure 1 shows that the peak can be modulated by varying the reference wavelength of the Fibonacci blocks between 0.3 and 0.35 μm , outside of this interval, the microcavity becomes a weak transmission peak (Transmission of the peak is under 97%).

In the infrared range, the high refractive index material is the Si, that of the low refractive index is the SiO₂. We showed that the use of the hybrid structure $(LH)^8[F_3(1,1)]^7(LH)^8$ with 53 quarter wavelength layers permits to have an omnidirectional photonic band gap 4.3 times larger than that of the classic periodic structure. We must

also mention that the extended omnidirectional PBG covers all the optical telecommunication wavelengths which are 0.85 μm , 1.3 μm and 1.55 μm .

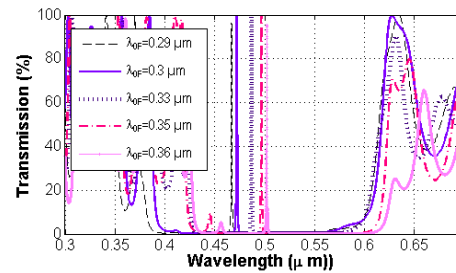


Figure 1: Modulation of the microcavity wavelength

Another work (Ben Abdelaziz et al. 2005) led to the broadening of the omnidirectional reflection band covering these optical telecommunication wavelengths using a deformed Fibonacci multilayer. This was achieved with the 15th generation of the deformed Fibonacci structure so with 610 layers. Thus, the realizing of this band is limited by the practical limitation to stacking many layers and to control layers thicknesses with a deformation law. Unlike this structure, the proposed design is simple to fabricate. Since different physical phenomena have their own relevant physical scales, we exploited the physical properties of the proposed structure in different wavelength domains to obtain different optical devices.

References:

- Ben Abdelaziz, K., Zaghdoudi, J., Kanzari M. and Rezig, B. (2005), A broad omnidirectional reflection band obtained from deformed Fibonacci quasi-periodic one dimensional photonic crystals, *Journal of Optics A: Pure and Applied Optics*, 7, 544–549.
- Escorcía-García, J. and Mora-Ramos, M.E. (2009) Study of Optical Propagation in Hybrid Periodic/Quasiregular Structures Based on Porous Silicon, *PIERS Online*, 5, 167-170.
- Srivastava, R., ShyamPati and Ojha, S.P. (2008) Enhancement of omnidirectional reflection in photonic crystal heterostructure, *PIER B*, 1, 197–208.

Perform SPRi binding measurement and MS identification on a single biochip: "biological model of the ligand fishing in human plasma"

Bellon Sophie¹, Boireau Wilfrid², Ducoroy Patrick³, Chiraz Frydman^{1*}

¹ HORIBA Scientific, France

² Institut FEMTO-ST, Université de Franche Comté, CLIPP, Besançon, France

³ IFR Santé STIC, CLIPP (Clinical-Innovation Proteomic Platform), Université de Bourgogne, Centre Hospitalier Universitaire de Dijon, France

*Corresponding author : E-mail adress : chiraz.frydman@horiba.com

Analysis of the affinity and the binding between bio-molecules and between molecule and cell tends more and more towards label-free approaches. Biosensors and Biochips are developed worldwide to propose new, fast, cheap, reliable and multiplexed tools to meet these demands. We present here the exploitation of the powerful approach of Surface Plasmon Resonance imaging and Mass Spectrometry coupling for protein fishing in biological fluids such as human plasma at the same sensitivity.

On one hand, multiplex format SPRi analysis allows direct visualization and thermodynamic analysis of molecular avidity, and is advantageously used for ligand-fishing of captured bio-molecules on multiple immobilized receptors on a SPRi-Biochip surface. On the other hand, MALDI mass spectrometry is a powerful tool for identification and characterization of molecules captured on specific surface. Therefore, the combination of SPRi and MS into one concerted procedure, using a unique dedicated surface, is of a great interest for functional and structural analysis at low femtomole level of bound molecules^{1,2}.

We have recently established a new strategy to detect and identify proteins of interest in ideal samples at low femtomole level combining SPR-MS directly onto the chip without elution step^{1, 2}.

To reach these goals, particular surface engineering has been engaged to maintain a high level of antibody grafting and reduce non-specific adsorption. Thus, various chemistries have been tested and validated towards biological fluids such plasma, keeping in mind the capacity of the in situ investigation by MS. Strategies of sample preparations have been carefully studied to push the limits in the ligand fishing. Finally, signal to noise ratio was magnified leading to the characterization of protein LAG3, a potential biomarker of breast cancer, in human plasma. As prospect in a clinical

view, these developments were transposed to arrays. They included the establishment of an automation procedure of on-a-chip treatments prior to mass spectrometry analysis and the development of an in situ MS interrogation. First trials of multiplexed analyses have been performed with the SPRi-PlexII apparatus (HORIBA Scientific) and the first results of biomolecular tracking in plasma provided by the "SuPRA-MS" platform will be presented

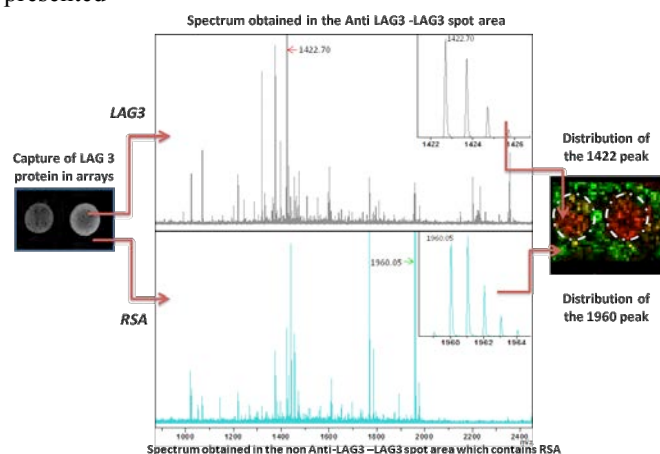


Figure 1: *On-a-chip detection, identification and imaging of LAG3 protein at 10nM in human plasma through the SuPRA-MS platform*

Multiplexed SPRi analysis provides rapid and high-throughput information in real time from up to several hundreds interactions in parallel. The technology is sensitive and does not require the use of labels. It can speed-up the workflow and reduce consumable costs during optimization processes. The coupling with MS analysis is straightforward and easier, which makes it a valuable tool for biomarker identification.

References.

- [1] W. Boireau et al. *Biosen Bioelec.* **2009**, 24, 1121–1127
- [2] S. Bellon et al. *Anal. Chem.* **2009**, 81, 7695-7702

Optical characterization of nanomaterials using spectroscopic ellipsometry

J-P Gaston¹, Celine Expert¹, Michel Stchakovsky

¹HORIBA Jobin Yvon SAS, Z.A de la vigne aux loups, 5 avenue Arago , 91380 CHILLY-MAZARIN, France

(*) Corresponding author: jean-paul.gaston@horiba.com

Introduction:

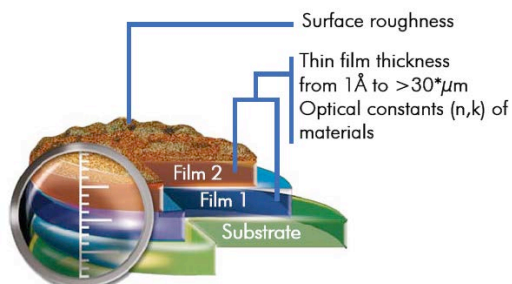
Nanomaterials are getting more and more attractive for industry thanks to their potential applications in different fields of technology like optoelectronics, displays, sensors, medical as well as solar cells.

Various analytical techniques are applied to understand the growth mechanisms, to monitor and control the optical properties and the composition, to measure the thickness of the layers during deposition, to profile the layers and see gradients.

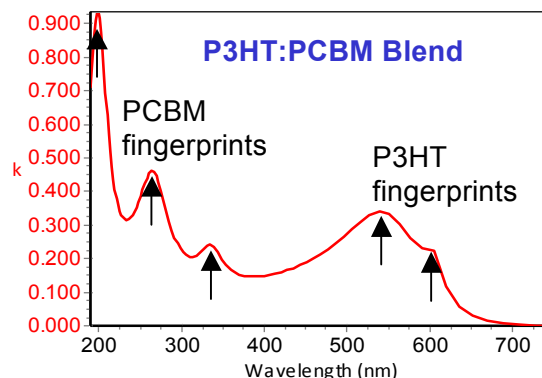
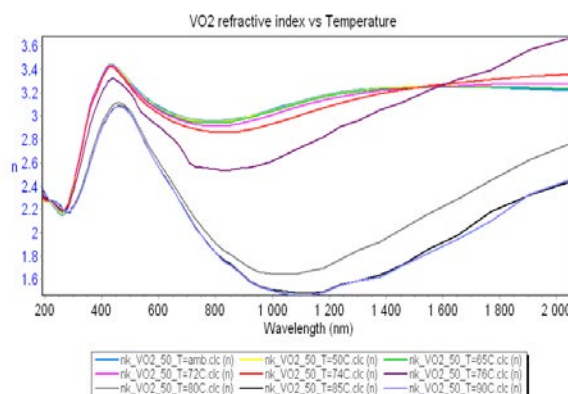
Spectroscopic Ellipsometry is a very powerful optical technique used to measure thin film thickness from 1 Å to tens of microns, optical constants, bandgap energy, surface and interface roughness, etc. It can be applied in situ or ex situ and it is ideally suited for the control of thin film structures.

In this presentation we will give a general introduction of spectroscopic ellipsometry [1,2], how it works, its main capabilities. Finally we will present results performed by HORIBA Jobin Yvon spectroscopic ellipsometers for several applications including characterization of vanadium dioxide VO₂ layers with the transition induced by a temperature change [3,4]

We will also describe how to characterise the optical properties of blends of poly(3-hexylthiophene)(P3HT) and [6,6]-phenyl C61-butyric acid methyl ester (PCBM)



Main properties determined by Spectroscopic Ellipsometry



References:

- [1] Tompkins, Harland G., and William A. McGahan, Spectroscopic Ellipsometry and Reflectometry, New York, NY: John Wiley&Sons, (1999).
- [2] Tompkins, Harland G., and Eugene A. Irene, Handbook of Ellipsometry, Norwich, NY: William Andrew Publishing, (2005).
- [3] H.W. Verleur, A.S. Barker, C.N. Berglund, Optical properties of VO₂ between 0.25 and 5 eV, Phys. Rev. 172,788-798 (1968).
- [4] J.C. Parker, U.W. Geiser, D.J. Lam, Y. Xu, W.Y. Ching, Optical properties of the Vanadium Oxides VO₂ and V₂O₅, Journal of the American Ceramic Society vol 73, issue 11, pages 3206-3208 (2009).

Design and prototyping of an electric city car in Tunisia

R. Rejeb^{1,2*}, C. Ben Salah³

¹Private University of Sousse, Tunisia

²Institute for Advanced Engineering and Research, Tunisia

³Faculty of Sciences, University of Gafsa, Tunisia

*Corresponding author: E-mail address: ridha.rejeb@ups.ens.tn

Introduction: Lack of fossil fuel supplies as well as greenhouse gases effect on the environment, have motivated car manufacturers to introduce new generations of cars in order to cope with fuel consumption and emissions issues. One of the most interesting structures that are introduced to the production lines belongs to hybrid electric vehicles.

Recently a lot of electric vehicles have been developed mainly to solve environmental and energy problems caused by the use of internal combustion engine vehicles. Some of them already have enough performance even in practical use. The environmental benefits from using electric vehicles promise to increase with time. That is because; electric generation continues getting cleaner as older, dirtier generating plants are taken out of service and replaced with newer, less polluting ones, and as pollution-free solar or wind generators come on-line.

A fundamental factor limiting series production of electric vehicles has been the lack of an appropriate batteries with a sufficiently large duration and capacity of energy, enabling the deployment of a satisfactory range and quick replenishment of energy.

The Institute for Advanced Engineering and Research (IAER) in Tunisia, as an innovative research institute in the area of Advanced Systems for Research and Development on Renewable Energy & Waste Recycling, is going to design and prototype an electric city car for tow-passenger as shown in Figure 1. This car is aimed primarily at the Tunisian domestic market with moderate cost.

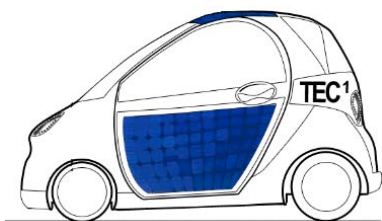


Figure 1: Prototype of a smart electric city Car

In this work we present the current state of development and future direction in the market for electric vehicles, with respect to the charging infrastructure. Specifically we discuss the electric vehicle network which is a proposed infrastructure system of publicly accessible charging stations, and battery swap stations to recharge electric vehicles.

A battery switch station is an infrastructure to swap a discharged battery or battery pack for a fully charged one, enabling fast charging and saving the delay of waiting for the vehicle's battery to charge.

As Tunisia is a country with more than 250 sunydays, it is reasonable to extend currently used filling stations by solar generators and battery-swapping equipments to build a balanced charging system for electric vehicles, support by renewable energy from distributed sources. Figure 2 shows a typical charging station using local renewable energy sources.

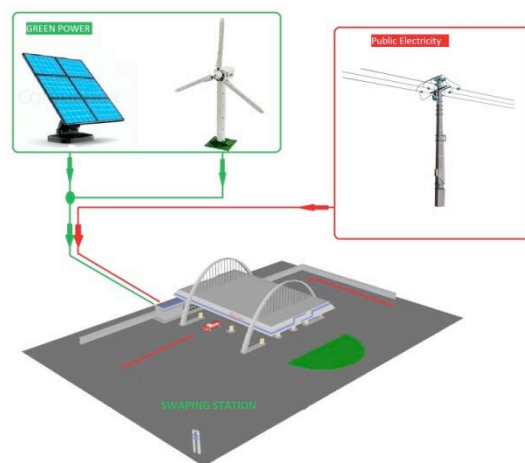


Figure 2: Renewable energy sources to supply electric vehicles charging terminals

References:

- Anthony, J and Il Yong, K. (2011) Design optimization of electric vehicle battery cooling plates for thermal performance, *Journal of Power Sources* 196 (2011) 10359– 10368.
- Benysek, G and Jarnut, M. (2011) Electric vehicle charging infrastructure in Poland, *Journal of Power Sources* 16 (2012) 320 – 328.
- Eberhard, M and Gerolf, R. (2005) The challenge to the automotive battery industry: the battery has to become an increasingly integrated component within the vehicle electric power system, *Journal of Power Sources* 144 (2005) 438–460.
- Pang-Chia Chen (2011) Configuration of solar-hydrogen mild hybrid fuel cell power systems for electric vehicles, *Journal of Power Sources* 201 (2012) 243– 252.

Synthesis, structural and electrical characterization of doped apatite-like silicates for fuel cell electrolyte

A.Madani^{1*}, A. Inoubli¹, A. M. Abbassi², R. Ternane² and J. Sanz³

¹ Laboratoire de physique des Matériaux .Faculté des Sciences de Bizerte, Université de Carthage . Tunisia

² Laboratoire de chimie des Matériaux .Faculté des Sciences de Bizerte, Université de Carthage. Tunisia

³ Instituto de Ciencia de materiales . CSIC. Cantoblanco . Madrid .Spain

*Corresponding author : E-mail adress : adelmadani2000@yahoo.com

Abstract

Apatite-type oxides of general formula $(Ln,M)_{10-x}(Si,M')_6O_{26+y}$ have been attracting considerable interest recently, because of their observed high oxide ion conductivity. In this paper, we report the effects on the conductivity of P and Al doping at the Si site. And the Ba and Ca doping in La site. The preparation of $La_{9.33-2x/3}Sr_x□_{0.67-x/3}Si_6O_{24}O_2$ ($0 \leq x \leq 2$) samples with different amounts of cation and anion vacancies is reported. Structure and unit cell parameters were deduced by Rietveld analysis of XRD patterns. Structural features that enhance oxygen conductivity in Sr doped apatites are discussed. Up to three components were detected in ²⁹Si MAS-NMR spectra which change with the amount and distribution of cation vacancies. For samples that are nominally stoichiometric in oxygen, $a_{9.33+x/3}Si_{6-x}Al_xO_{26}$ ($0 \leq x \leq 2$), we find that the oxide ion conductivity increases with Al content up to a maximum value ($\sigma_{700} = 1.3 \times 10^{-3} \text{ S cm}^{-1}$) for $x=0.5$, before decreasing with further Al incorporation. When we analyze the spectra of the series, no fast decay of conductivity was observed at low frequencies. This indicates that interfacial grain boundary and bulk contributions cannot be resolved in analyzed samples. In the higher frequency range, conductivity values were fitted to the equation (1):

$$\sigma_{ac} = \sigma_{dc} [1 + (\omega/\omega_p)^n] \quad (1)$$

The conductivity data is discussed in relation to results from other doping studies. X ray powder diffraction structural data collected for doped samples. In addition, the ²⁹Si and ²⁷Al HR-NMR spectroscopy showed a great dependence between Si chemical shift and Si second neighbor in Sr doped apatite, which is consistent with the higher conductivity of this sample. The improvement of conductivity is remarkable for low substitution rate not exceeding $x=0.5$ in Si sites. In the other hand, partial substitution of bivalent dopant ions (e.g. Ca, Ba, Sr,) onto the La site in the oxide ion conductor $La_{9.33}Si_6O_{26}$ has been reported to increase the conductivity [1]. In this paper, we report combined powder X-ray diffraction and refinement studies for low amount of doping rate with a view to explaining this enhancement. The X-ray diffraction studies show that, in agreement with

cation size expectations, an enlargement of the unit cell is observed on doped samples. In addition, the impedance study shows that a significant increase in conductivity. In general, oxygen conductivity increases with the amount of vacancies at La1 (6h) sites, passing through a maximum for $x=0.4$. In the case of activation energy, a minimum is detected near $x=1.2$, indicating that entropic and enthalpic change in different way. The presence of cation vacancies should enhance oxygen hopping along c-axis; however, the analysis of the frequency dependence of conductivity suggests that oxygen motions are produced along three axes. Structural reasons that enhance oxygen conductivity in Sr doped apatites have been discussed [2]. The analysis of ionic conductivity in $La_{9.33-2x/3}Sr_x□_{0.67-x/3}Si_6O_{24}(O_2)$ series showed that all vacancies created along c-axis participate into conduction processes, decreasing conductivity and increasing activation energies in samples with $x > 1.2$ (high Sr contents). In samples with cation vacancies, conductivity increases reaching a maximum near $x=1.2$ when the amount of Sr and unit cell volume increases. As a consequence of two opposite effects, conductivity values have been interpreted on the basis of two non related entropic and enthalpic terms.

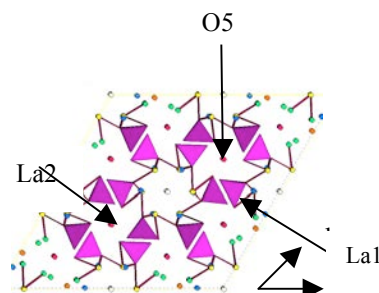


Figure 1: Structural features of the apatite $La_{9.33-0.67}(SiO_4)_6O_2$, illustrating Si tetrahedra and two La sites. Schematic view along the c axis.

References :

- [1] Sansom J E H, Richings D, Slater P R (2001) Solid State Ionics 139 : 205–210
- [2] Islam M S, Tolchard J R, Slater P R (2003) Chem. Commun. 1486-1487

Electrochemical behavior of Pt-Sn/C heat treated electrocatalysts for oxygen reduction reaction in direct methanol fuel cells

S. Knani^{1*}, L. Chirchi¹, S. Baranton², T.W.Napperon², J. M. Léger², A. Ghorbel¹

¹ Laboratoire de chimie des matériaux et catalyse, Département de chimie Faculté des Sciences de Tunis , 2092 Tunis, Tunisie

* Corresponding author: E-mail: sarraknani2@gmail.com

² Équipe électrocatalyse, Laboratoire de catalyse en chimie organique UMR CNRS 6503, 4, rue Michel Brunet B27, BP 633 86022 Poitiers France

As a consequence of the world large demand of the fossil energy limited sources, the development of renewable energy sources became essential. In this context, the Direct Methanol Fuel Cells (DMFCs) seems to be an efficient alternative. However, its commercialization is hindered by the slow reaction kinetics and especially kinetic of the oxygen reduction reaction, the high cost of the electrocatalysts based on precious metals and the methanol crossover through the membrane which affects the efficiency of the battery. For this purpose carbon supported platinum alloys are widely investigated as electrocatalysts in both anodic and cathodic sides of DMFCs.

Carbon supported platinum tin electrocatalysts was prepared by impregnation followed by borohydride reduction method. The bimetallic catalyst was heat treated under nitrogen at 500°C. The electrochemical activity of the as prepared electrocatalysts for oxygen reduction reaction in Direct Methanol Fuel Cell (DMFC) was investigated and compared to that of Pt/C. The structural and textural properties of catalysts were studied by X-ray diffraction (XRD) and N₂ adsorption-desorption at 77 K. X-ray diffractogram of Pt-Sn/C shows three main diffractions characteristic of fcc structure of platinum and heat treatment does not affect this crystallographic structure¹. The (111) diffraction peak measured on PtSn/C is slightly shifted to higher 2θ values with respect to that of pure platinum suggesting the alloy formation between platinum and tin. The N₂ adsorption-desorption revealed that all samples showed type III isotherms according to IUPAC classification², indicating the presence of macropores (>50 nm). The BET specific surface area of Pt/C is important and remains higher even after tin addition and heat treatment. From TEM images an heterogeneity of particle size was observed. The heat treated electrocatalysts show an increase of particle size due to agglomeration.

Catalytic activity of the materials was studied by cyclic and linear voltammetry in acidic medium. The electrochemical active surface area (EASA) estimated from cyclic voltammetry are represented in table. 1. It seems that Pt-Sn/C exhibits the higher EASA compared to Pt/C due to the formation of a Pt skin on platinum tin nanoparticle surface. However, the EASA drastically decreased with heat treatment at 500°C of Pt-Sn/C as expected from TEM images.

The electrochemical activity of samples toward oxygen reduction reaction (ORR) was studied using rotating ring disk electrode (RDE). The activity of electrocatalysts for ORR follow this order: Pt-Sn/C (500°C) > Pt-Sn/C > Pt/C. Furthermore, the number of exchanged electrons calculated using the Koutecky-Levich equation was found equal to four for all samples. This evidences that the oxygen reduction in acidic medium occurs with the production of water.

<i>samples</i>	<i>EASA (m². g⁻¹)</i>
Pt/C	27
Pt-Sn/C	33
PtSn/C (500°C)	11

Table 1: Electrochemical active surface area (EASA) for Pt/C, Pt-Sn/C and Pt-Sn/C (500°C)

References:

- [1] C .Jeyabharathi, P. Venkateshkumar, J. Mathiyarasu and K.L.N. Phani, *Electrochim. Acta* 54 (2008) 448–454.
- [2] K. S. W.Sing, D. H. Everett, R. A. Whaul, L. Moscou, R. A. Pierotti, J. Rouguérol and T. Siemieniowska, Reporting physisorption data for gas/solid systems, Physical chemistry division,(1984).

New biomaterials (PEK) from starch: characterization by MALDI-ToF and NMR

S.Chatti^{1*}, H. Abderrazak¹, H.R.Kricheldorf²

^{1*} Institut National de Recherche et d'Analyse Physico-chimique, Pole Technologique- Sidi Thabet-2020, Tunisia

^{1*}Corresponding author : E-mail address : saber.chatti@inrap.rnrt.tn

² Institut für Technische und Makromolekulare Chemie/Fachbereich Chemie TMC, Universität Hamburg, Bundesstr. 45, D-20146 Hamburg, Germany

Biomass constitutes a renewable source of natural products used as unfailing starting materials for access to less polluting new compounds able to substitute petroleum derivatives. Among the important by products of biomass are the dianhydrohexitols obtained in the sugar industry by the double dehydration of starch [1]. As an extension of the series of our studies on polymers syntheses based on renewable resources, novel PEKs containing isosorbide, isomannide or isoidide (**1a-c**) have been synthesized by polycondensation with various difluoro monomers (**2a-c**) by the aromatic nucleophilic substitution (Figure 1).

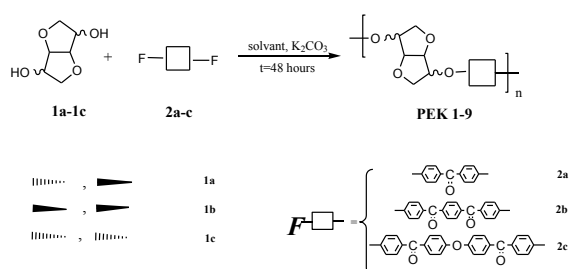


Figure 1: Synthesis of PEKs by polycondensation of diols (**1a-c**) with difluoro monomers (**2a-c**)

In order to find suitable conditions for these reactions, we have optimized reaction conditions by the polycondensation of isosorbide (**1a**) and 4,4'-difluorodiphenylketone (**2a**) (PEK1). We varied the nature of the couple solvent/co-solvent, excess of difluoro agent and temperature. However, we found that the inherent viscosities are strongly influenced by the nature of the difluoro agent. Compared to its isomers, isomannide gives the highest viscosity value (0.52dL/g) and glass transition temperature (209°C). The MALDI-ToF mass spectrum of PEK indicated the formation of a high molar fraction of cycles (Figure 2).

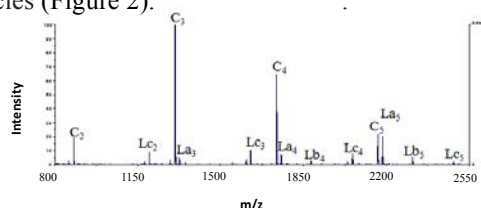


Figure 2: MALDI-TOF mass spectrum prepared from isomannide and monomer (**2b**)

Similar conditions were used for the polycondensation reaction of a stoichiometric mixture of isosorbide /bisphenol-A and three difluoro monomers (**2a-c**).

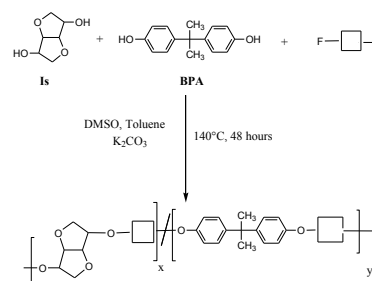


Figure 3: Synthesis of copo-PEKs by polycondensation of Is/BPA with difluoro monomers (**2a-c**)

These copolymers (Copo.PEK1-3) have high inherent viscosities (1.26 dL/g - 1.41 dL/g) and glass transition temperatures between 127 and 177°C. MALDI-ToF Mass spectrum of these copoly(ether-ketone)s revealed the presence of a majority of cyclic structures C_{ij} (Figure4).

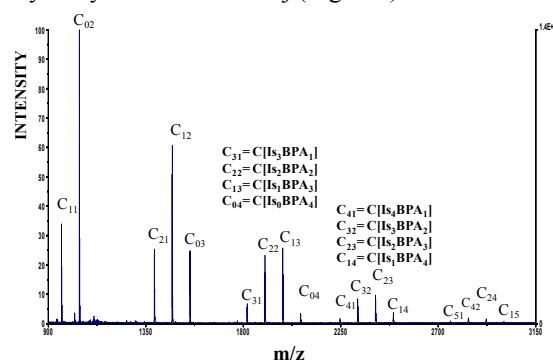


Figure 4: Maldi-ToF spectrum of Copo.PEK2 prepared from Is/BPA and monomer **2b**

[1] Fenouillot F., Rousseau A., Colomines G., Saint-Loup R., Pascault J.-P. (2010) Polymers from renewable 1,4:3,6-dianhydrohexitols (isosorbide, isomannide and isoidide): A review Progress in Polymer Science 35, 578–622.

New insights into organocatalysis

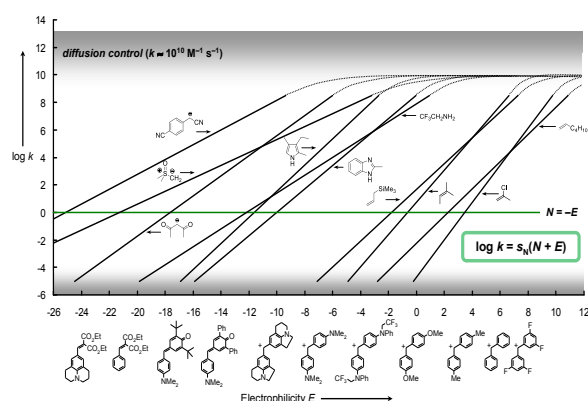
S. Lakhdar* and H. Mayr

Department Chemie der Ludwig-Maximilians-Universität München
Butenandtstr. 5-13, 81377 München, Germany
sami.lakhdar@cup.uni-muenchen.de

Extensive studies of the reactions of carbocations and Michael acceptors with n -, π -, and σ -nucleophiles have shown that the rates of these reactions can be described by eq. 1, where electrophiles are characterized by one parameter (E), while nucleophiles are characterized by the solvent-dependent nucleophilicity parameter N and slope-parameter s_N .¹

$$\lg k_{20^\circ\text{C}} = s_N (E+N) \quad (1)$$

Using reference electrophiles which cover more than 30 orders of magnitude we have been able to construct the most comprehensive nucleophilicity scale presently available.^{1b-d}



Scheme 1. Rate constants for the reactions of benzydrylium ions and structurally related Michael acceptors with diverse nucleophiles at 20 °C.

It will be reported, how N , s_N , and E -parameters can be employed to characterize organocatalysts² as

well as substrates³ and intermediates⁴ of iminium and enamine activated reactions.⁵

References:

- ¹⁾ a) H. Mayr, M. Patz, *Angew. Chem. Int. Ed. Engl.* 1994, 33, 938-957; b) H. Mayr, B. Kempf, A. R. Ofial, *Acc. Chem. Res.* 2003, 36, 66-77; c) H. Mayr, A. R. Ofial, *J. Phys. Org. Chem.* 2008, 21, 584-595. d) Database: www.cup.uni-muenchen.de/oc/mayr/reaktionsdatenbank/.
- ²⁾ a) N. De Rycke, G. Berionni, F. Couty, H. Mayr, R. Goumont, O. R. P. David, *Org. Lett.* 2011, 13, 530-533. b) M. Baidya, M. Horn, H. Zipse, H. Mayr, *J. Org. Chem.* 2009, 74, 7157-7164. c) M. Baidya, S. Kobayashi, F. Brotzel, U. Schmidhammer, E. Riedle, H. Mayr, *Angew. Chem. Int. Ed.* 2007, 46, 6176-6179.
- ³⁾ a) B. Maji, S. Lakhdar, H. Mayr, *Chem. Eur. J.*, accepted; b) S. Lakhdar, J. Ammer, H. Mayr, *Angew. Chem.* 2011, 123, 10127-10130; *Angew. Chem. Int. Ed.* 2011, 50, 9953-9956; c) S. Lakhdar, H. Mayr, *Chem. Commun.* 2011, 47, 1866-1868. d) T. Kanzian, H. Mayr, *Chem. Eur. J.* 2010, 16, 11670-11677. e) S. Lakhdar, R. Appel, H. Mayr, *Angew. Chem. Int. Ed.* 2009, 48, 5034-5037. ⁴⁾ a) T. Kanzian, S. Lakhdar, H. Mayr, *Angew. Chem. Int. Ed.* 2010, 49, 9526-9529. b) S. Lakhdar, T. Tokuyasu, H. Mayr, *Angew. Chem. Int. Ed.* 2008, 47, 8723-8726.
- ⁵⁾ Review: S. Lakhdar, A. R. Ofial, H. Mayr, *J. Phys. Org. Chem.* 2010, 23, 886-892.

Organic nanocomposites for OPV applications

A. Ltaief*, A. Bouazizi

¹Equipe: "Dispositifs Electroniques organiques et Photovoltaïque Moléculaire", Faculté de Sciences de Monastir, Boulevard de l'environnement, 5019, Monastir, Tunisie

*Corresponding author : E-mail adress : adnen_ltaief@yahoo.fr

Abstract

Organic semiconductors continue to receive considerable attention for their unique optoelectronic properties and compatibility with high-throughput processing. This attractive combination has led to the commercial application of these materials in displays, and the emergence of future markets for organic solid-state lighting, photovoltaic cells, and lasers. In an organic semiconductor, the molecular excited state is a tightly-bound, electron-hole pair known as an exciton. The excitonic character of these materials significantly impacts the design and physics of organic optoelectronic devices relative to those constructed using conventional inorganic semiconductor materials.

As an example, the generation of photocurrent in an organic photovoltaic cell (OPV) requires the use of a device architecture that permits the exciton to be dissociated into its component charge carriers. Often, this is accomplished using a heterojunction between electron donating and accepting materials. In this scheme, photocurrent generation occurs only at the donor-acceptor (D-A) interface, and exciton diffusion to the interface is hence a critical step in the photoconversion process.

Most organic semiconductors are characterized by exciton diffusion lengths (~10 nm) that are considerably smaller than the optical absorption length (~100 nm). While the short exciton diffusion length can be overcome through the use of thin active layers, the limited optical absorption of such structures limits the overall photoconversion efficiency. The implications of a short exciton diffusion length continue to drive materials and device design for the realization of high efficiency OPVs.

The focus of this talk will be on developing approaches and processing methods to optimize charge transfer and transport properties in organic photovoltaic cells. The effect of both used organic solvent and fillers concentrations in polymer matrix, on OPV performances, were discussed. We will present results reported using several bulk heterojunction active layers such as: MEH-PPV:C60, MEH-PPV:CNTs, MEH-PPV:CNPs (Carbon Nanopearls) (see figure 1), ...

We will also focus our work on CNTs and their applications in OPV and especially in flexible organic cells. Conductive CNTs coatings have recently become a prospective substitute based on

wide range of methods including spraying, spin coating, casting, layer-by-layer, and Langmuir-Blodgett deposition. The transfer from a filter membrane to the transparent support using a solvent or in the form of an adhesive film is another method for attaining flexible and optically transparent CNT films.

We have adopted the last method to prepare our flexible and transparent electrodes using the PET substrate, which is a practical method to obtain good optical transparency about 73%, as shown in figure 2.

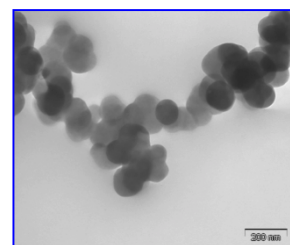


Figure 1: Carbon Nanopearls as acceptors in OPV cells

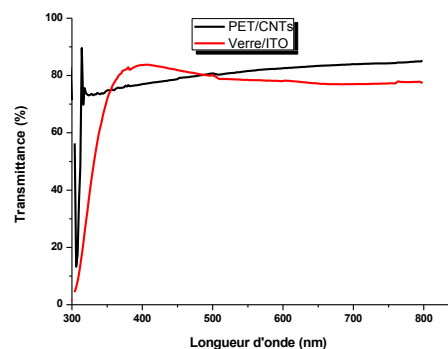


Figure 2: Optical transmittance of PET/CNTs flexible anodes compared to that of ITO classic anodes

References

- Davenas.J, Ltaief.A, Barlier.V, Boiteux.G, Bouazizi.A. (2008) Nanomaterials for photovoltaic conversion. *Materials Science and Engineering C*, 28, 744-750, 2008.
- Ltaief.A, Bouazizi. A, Davenas.J, Alcouffe.P. (2008) Influence of the processing conditions on charge transfer and transport properties in poly(2-methoxy-5-(2'-ethylhexyloxy)1-4-phenylenevinylene):C₆₀ composites for photovoltaics. *Thin Solid Films*, 516, 1578-1583, 2008.

Hydrothermal growth of ZnO nanorods by TiO₂ nanotubes template

S. Benkara^{1*}, S. Zerkout²

¹Larbi Ben M'Hidi University Oum El Bouaghi, Algeria.

*sali_benkara@yahoo.fr

²Ceramics laboratory, Mentouri University Constantine 25000, Algeria.

Introduction

One-dimensional (1D) nanostructures, including nanowires, nanotubes and nanorods have attracted significant interests owing to their unique geometries. [1]

As a kind of 1D oxide material, ZnO nanorod arrays are considered as important functional oxide nanostructures in a wide area of high-technology applications.

Various physical, chemical, or electrochemical methods [2–5] have been developed to prepare 1D ZnO. Among these fabrication methods, ZnO nanorods are most commonly grown by vapor phase methods like vapor–liquid–solid (VLS), chemical vapor transport, and thermal evaporation [3–7]. Compared with those techniques, chemical solution method is attractive to synthesize ZnO nanostructures because of the low cost equipments, lower growth temperatures, and controlled easily technology of growing high-density nanorods array [8]. A template-assisted approach has been proven to be effective for the growth of nanostructure oxides. Few efforts have been made on the study of the use of ZnO nanorods as a template [9–10]. A preparation of ZnO nanorods using TiO₂ nanotubes as templates remains largely unexplored although a few studies [11–12]. Therefore, in the present study we would like to present a detailed investigation on the preparation and characterization of ZnO/TiO₂ nanocomposite film. The ZnO/TiO₂ nanostructured composite film was prepared using two steps: (1) Formation of TiO₂ nanotube arrays in HF solution by anodization method, which is a simple technique to control the structure parameters of TiO₂ NTs. (2) Deposition of ZnO nanorods by hydrothermal process with ammonia and Zinc nitrate as inorganic precursors.

Experimental

Anodic oxidation method was adopted to prepare TiO₂ nanotubes TNTs. It is performed in 2 w % HF solution and distilled water with voltage of 20 Volts and annealed at 450 °C for 1 h. ZnO nanorod arrays have been fabricated on TiO₂ nanotube substrate via hydrothermal process, consisted at aqueous solution containing 0.02 M of Zn(NO₃)₂·6H₂O and (0.3-0.4) M of NH₃·H₂O, followed by heating at 80°C-100 °C-160 °C for 24h.

Results and discussions

The anatase crystal of Titania and the hexagonal wurtzite crystal of zinc oxide forms were identified by X-ray diffraction (XRD). XRD patterns show a disappearance of the peaks corresponding to titanium, at high temperature, the formation of ZnO increases with increasing of reaction rate into aqueous solution, and also the reaction rate between Ti and ZnO. No remarkable change in orientation of the films as the amount of ammonia was increased, but the intensity of the preferred crystalline orientation is influenced.

The SEM image reveals well ordered and uniform nanotubes array are formed. The diameters of these nanotubes range from 60 nm to 95 nm and their length is about 1.7 μm detected by pofilometry. The ZnO nanoparticles are deposited on the top of TiO₂ nanotube or entered into tube.

References

- [1] J.B.Chen, C.W.Wang, B.H.Ma, Y.Li, Thin Solide Films 517 (2009) 4390–4393.
- [2] Y. Zhang, N. Wang, S. Gao, R. He, S. Miao, J. Liu et al., Chem. Mater. 14 (2002), 3564–3568.
- [3] D. Banerjee, J.Y. Lao, D.Z. Wang, J.Y. Huang, Z.F. Ren, D. Steeves et al., Appl. Phys. Lett. 83 (2003), 2061–2063.
- [4] S.Y. Li, C.Y. Lee, T.Y. Tseng, J. Cryst. Growth 247 (2003), 357–362.
- [5] J.J. Wu, S.C. Liu, Adv. Mater. 14 (2002), 215–218.
- [6] P.C. Chang, Z. Fan, D. Wang, W.Y. Tseng, W.A. Chiou, J. Honget al., Chem. Mater. 16, 5133–5137 (2004).
- [7] M.J. Zheng, L.D. Zhang, G.H. Li, W.Z. Shen, Chem. Phys. Lett. 363 (2002), 123–128.
- [8] L.E. Greene, M. Law, J. Goldberger, F. Kim, J.C. Johnson, Y.Zhang et al., Chem. Int. Ed. 42 (2003), 3031–3034
- [9] J.Goldberger, R.He, S.Lee, Y.hang, H.Yan, H.Choi, P.Yang, Nature (2003) 422:599.
- [10] J.Hwang, B.Min, J.S.Lee, K.Keem, S.Kim, Adv Mater (2004) 16:422.
- [11] Z. Zhang, Y.Yuan, Li.Liang, Y.Cheng, Journal of Hazardous Materials 158 (2008) 517–522.
- [12] N.Wang, X.Li, Y.Wang, Y.Hou, X.Zou, G.Chen, Materials Letters 62 (2008) 3691–3693

Hybrid nanocomposites based on silicon nanowires and conducting polymer for photovoltaic application

N. Chehata^{1*}, A. Ltaief¹, B. Ilahi², T. Baron³, B. Salem³, A. Bouazizi¹ and H. Maaref²

¹Equipe Dispositifs Electroniques Organiques et Photovoltaïque Moléculaire, Faculté des Sciences de Monastir, Boulevard de l'Environnement, 5019, Monastir, TUNISIA

*Corresponding author : E-mail adress : chehata.nadia@yahoo.fr

²Laboratoire de Micro-Optoélectronique et Nanostructures, Faculté des Sciences, 5019, Monastir, TUNISIA

³Laboratoire des Technologies de la Microélectronique (LTM) -UMR 5129 CNRS-UJF, CEA Grenoble, 17 Rue des Martyrs, F-38054 Grenoble, FRANCE

Abstract

Hybrid nanocomposites based on a nanoscale combination of organic and inorganic semiconductors are a promising way to enhance the efficiency of solar cells through a higher aspect ratio of the interface and the good processability of polymers.

Nanocomposites are based on a heterojunction network between poly (2-methoxy-5-(2-ethylhexyloxy)-p-phenylenevinylene) (MEH-PPV) as an organic electron donor and silicon nanowires as an inorganic electron acceptor. Nanowires (NWs) seem to be a promising material for this purpose, as they provide a large surface area for contact with the polymer and a designated conducting pathway whilst their volume is low. In this paper, silicon nanowires are introduced by mixing them into the polymer matrix. Hybrid nanocomposites films were deposited onto ITO substrate by spin coating method. Optical properties and photocurrent response were investigated. The UV-Visible absorption measurements demonstrate that SiNWs broadened the absorption spectrum of the active layer, indicating that SiNWs participate at the absorption process and ameliorate the structure of nanocomposites. The photoluminescence quenching of MEH-PPV which is a convenient signature of the reduced radiative recombination of the generated charge pairs upon exciton dissociation (Figure 1). The photocurrent density of ITO/MEH-PPV:SiNWs/Al structures have been obtained by I-V characteristics. The J_{SC} value is about $2.11 \cdot 10^{-4} \text{ mA} \cdot \text{cm}^{-2}$ (Figure 2).

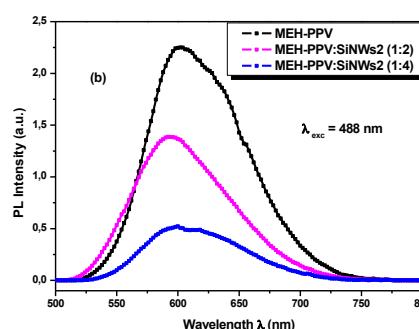


Figure 1: Photoluminescence spectra of MEH-PPV and MEH-PPV/SiNWs nanocomposites.

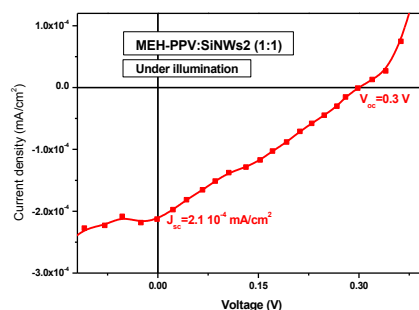


Figure 2: J-V curve of ITO/MEH-PPV:SiNWs/Al structure under illumination.

References:

- Eisenhawer. B, Sensfuss. S, Sivakov. V, Pietsch. M, Andrä. G and Falk. F (2011) Increasing the efficiency of polymer solar cells by silicon nanowires. *Nanotechnology*, 22, 315401-315408, 2011.
- Ltaief . A, Bouazizia. A, Davenas. J, Ben Chaâbane. R, Ben Ouadaa. H. (2004) Electrical and optical properties of thin films based on MEH-PPV/fullerene blends. *Synthetic Metals*, 147, 261–266, 2004.
- Yang. P, Zhou. X, Cao. G and Luscombe. C. (2010) P3HT:PCBM polymer solar cells with TiO₂

nanotube aggregates in the active layer. *J. Mater. Chem.* 20, 2612–2616, 2010.

Chem. 20, 2612–2616, 2010.

Effect of substrate type on CuInS₂ thin films properties sputtered from nanoparticles synthesised by solvothermal route

F. Ghribi¹, Z. Ben Ayadi¹, K. Djessas², A. Alyamani⁽³⁾, L. El Mir^{1,4,*}

¹Laboratoire de Physique des Matériaux et des Nanomatériaux appliquée à l'Environnement, Faculté des Sciences de Gabès, Cité Erriadh Manara Zrig, 6072 Gabès, Tunisie.

³Laboratoire de Procédés, Mathématiques et Energie Solaire (PROMES-CNRS), Université de Perpignan, Rambla de la thermodynamique, Technosud, 66100 Perpignan Cedex, France.

²National Nanotechnology Research Centre, KACST, Riyadh, Saudi Arabia.

⁴Al-Imam Muhammad Ibn Saud University, College of Sciences, Department of Physics, Riyadh 11623, Saudi Arabia.

* Corresponding author: E-mail adress: Lassaad.ELMir@fsg.rnu.tn

Abstract

Copper indium disulfide films were sputtered on various substrates. The target used in the sputtering was made from CuInS₂ nanoparticles synthesised by solvothermal route. The different substrates are : Glass, Molybdenum/Glass and Tin oxide/Glass. The effects of substrate on structural properties of the films were studied using X-ray diffraction (XRD), atomic force microscopy (AFM) and scanning electron microscopy (SEM). The optical transmittance, absorbance and reflectance of the powder and thin films in the UV to near infrared region (200 nm to 3000 nm) were investigated.

The obtained CuInS₂ films were polycrystalline textured, preferentially oriented with the (112) crystallographic direction. The (112) peak intensity change with substrate type. From AFM and SEM results the films deposited on molybdenum are promising for photovoltaic applications particularly as absorber layers in solar cells. From the optical study, the band gap of the CuInS₂ films were changing with substrate type, this is can be explained by the improvement of the crystallinity, which was also reported by other researchers [1, 2].

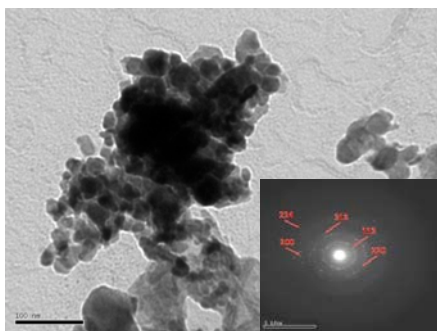


Figure 1: TEM micrographs of CuInS₂ powder.

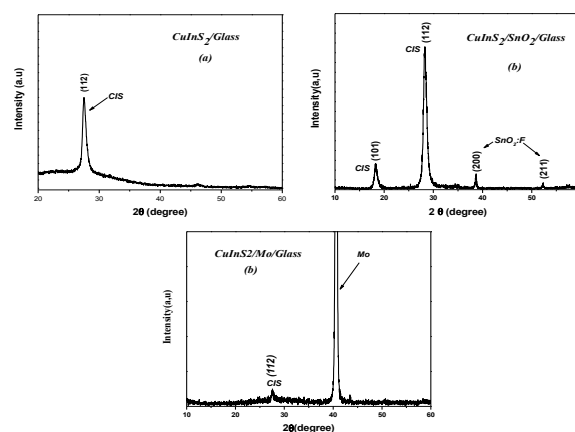


Figure 2: X-ray diffractions of CuInS₂ thin film sputtered on different substrate

References

- [1] Jebbari, N., Ouertanib, B., Ramonda, M., Guasch, C., Kamoun, N., Turki and Bennaceur, R., *Energy Procedia* 2 (2010) 79–89.
- [2] Peng, S., Cheng, F., Liang, J., Tao, Z., Chen, J., *Journal of Alloys and Compounds* 481 (2009) 786–791.

Scattering elastic wave by integrated nanostructure on mesoscopic system 2D

R. Tigrine^{(1,2)*}, B. Bourahla^(1,2), M. Boucherrab⁽¹⁾, S. Amoudache⁽¹⁾, A. Khater⁽²⁾

⁽¹⁾Laboratoire de Physique et Chimie quantique, Université Mouloud Mammeri, Tizi-Ouzou, Algérie

⁽²⁾Laboratoire PEC, Université du Maine, 72085 Le Mans, France

* Corresponding author e-mail: tigriner@yahoo.fr, tigrinerachid@mail.ummo.dz

Abstract

We investigate the scattering phenomena at the inhomogeneous boundary of an extended atomic integrated nanostructure in crystalline solid surfaces. The surfaces are considered as a semi-infinite slab of three coupled atomic layers, and the well as a double atomic chain. This simplified geometric configuration model of a slab atomic well in surface crystalline. The breakdown of translation symmetry in the direction normal to the surface and perpendicular to the extended nanowell gives rise to localized vibrational modes in its neighborhood. The formalism of matching method and Landauer-Büttiker theory are used in this work; to analyze the scattering vibration phenomena at the surface in homogeneities. Characteristic transmission and reflection modes, derived

from as elements of a Landauer-Büttiker type scattering matrix and phononic conductance are calculated for this system model. The evolutions of these spectra are presented as a function of the variation of the elastic parameters of the system. This illustrates the variation of the spectra for the bulk and at the inhomogeneous domain of the surface atomic well. The analysis of the spectra of the total transmission demonstrates the fluctuations, related to Fano resonances, due to the coherent coupling between travelling phonons and the localized vibration modes in the slab atomic well domain. The calculated spectra could yield, in comparison with experimental results to come, useful information concerning the cartography vibration fields at surface slab atomic well.

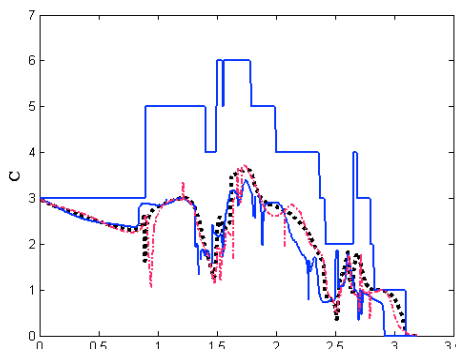


Fig.1 The curves of total conductance for the waveguide with the nanowell domain as function of the exciting dimensionless frequencies Ω and the parameters λ_1 and λ_2 respectively for softening (solid-line), homogenous (shaded-line) and hardening (dotted-line) cases.

References

- [1] M. Buttiker, Y. Imry, R. Landauer, S. Pinhas, Phys. Rev. B31, 6207 (1985)
- [2] R.Tigrine, A.Khater, O.Rafil, M.Belhadi and J.Hardy, Phys Stat Sol. (b) 239, 144 (2003)
- [3] H. Grimech and A. Khater, Surf. Sci. 323, 198 (1995)
- [4] M.Belhadi, A. Khater, J.Hardy and K.Maschke, Eur.Phys.J.Appl.Phys.35, 185 (2006)

AgInSe₂ ternary material synthesized by selenisation of nano-films of Ag and In elements obtained by thermal evaporation for photovoltaic application

A.Gantassi*, H.Essaïdi, S.Touihri, M.Amlouk

Unité de physique des dispositifs à semi-conducteurs

Université Tunis EL MANAR, 2092 Tunis, TUNISIE

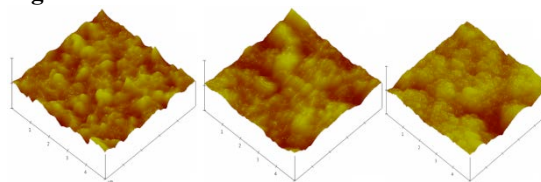
*Corresponding author : E-mail address : ganaymen@gmail.com

Introduction:

Solar cell technologies using I-III-VI₂ compounds have been extensively reported because of their interesting electrical and optical properties [6]. The I-III-VI₂ compounds are the ternary analogues of II-VI compounds [9]. They crystallize in the chalcopyrite structure, which is closely related to zinc blend structure. AgInSe₂ is a ternary analogue to CdSe, which has been used in several optoelectronic devices. Moreover, AgInSe₂ belongs especially to the chalcopyrite structure group with space group I $\bar{4}$ 2d. This ternary material was first prepared by Hahn et al. in 1953 [4] from the original binary compounds. It was also synthesized directly from the elements in sealed evacuated silica tubes [2]. In the same line thin films of AgInSe₂ have been prepared by the flash evaporation technique [7], co-evaporation [1], microwave [5], pulse laser vaporization [3], electrodeposited [10], Thermal evaporation [8] and RF magnetron sputtering [11].

AgInSe₂ thin films have been prepared on glass substrates by thermal evaporation of Ag and In element followed by a heat treatment in selenide atmosphere at various temperatures. X-ray diffraction analysis shows that the film annealed at T= 400°C is well crystallised in AgInSe₂ chalcopyrite phase with crystallinity preferentially oriented towards (112) direction. Moreover, the annealing treatment has effective role in the enhancement of the surface morphology by means of atomic force microscopy especially for films heated at 400°C. On the other hand, the optical transmittance and reflectance measurements reveals that the band gap energy E_g lies is 1.42 eV and the absorption coefficient in the range of 10⁴ cm⁻¹ was indeed obtained. In this work, AgInSe₂ thin film have been synthesized by solid state reaction under vapour selenide pressure at 350°C, 400°C and 450°C, during 6h, via a sequentially deposited silver and indium layers In/Ag/In...Ag/In/Ag. To date, this procedure to prepare this ternary compound has not been yet used.

Figures and Tables:



Surface topography 3D (AFM) of AgInSe₂ thin films (T=350°C, 400°C and 450°C).

heat treatment temperature (°C)	350	400	450
Roughness (nm)	101.97	89.90	110.37
Sizes of clusters (nm)	354.11	337.60	603
Average height (nm)	416.72	270.94	368.94

Table 1: Roughness, average height and sizes of clusters of AgInSe₂ thin films for various heat treatments.

References:

- [1] Arredondo, C.A., Clavijo, J.I. and Gordillo, G. (2009) 34th IEEE Photovoltaic Specialist Conference, Philadelphia – USA, (2009), 886 - 891.
- [2] Austin, L.G., Goodman, C.H.L., Pengelly, A.E. (1956) Nature 1956; 178:433.
- [3] Bodnar, I.V., Gremenok, V.F., (2000) J.Appl. Spectrosc. 67 (2000) 705.
- [4] Hahn, H., Frank, G., Klingler, W., Meyer, A.D., Str. orger G.Z Anorg (1956) Chem 1953; 271:153.
- [5] Lekse, J.W., Pischera, A.M., Aitken, J.A. (2007) Materials Research Bulletin 42, (2007), 395–403.
- [6] Pamplin, B.R., Kiyosawa, T., Masumoto, K. (1979) Prog Cryst Growth Charac 1979; pp. 1331.
- [7] Patel, S.M., Patel, A.D., (1984) Thin Solid Films, III, (1984), 53-58.
- [8] Santhosh Kumar, M.C., Pradeep, B., (2009) Applied Surface Science 255, (2009), 8324–8327.
- [9] Tell, B., Shay, J.T., Kasper, H.M. (1972) J Appl Phys 1972; 43:2469.
- [10] Ueno, Y., Kojima, Y., Sugiura, T., Minoura, H., (1990) Thin Solid Films 189 (1990) 91.
- [11] Weir, R.D., Jessop, P.E., Garside, B.K., (1987) Can. J. Phys. 1033 (1987) 65.

Skills requirements for today's embedded systems designs

I. Bennour

Ecole Nationale d'Ingénieurs de Sousse, TUNISIA, E-mail adress: imed.bennour@fss.rnu.tn

Introduction: An embedded system is a special purpose system in which the computer is encapsulated by the device it controls. Today it is hard to find an electronic system that does not contain an embedded controller. Such systems span all aspects of modern life: biomedical instrumentations (ECG recorder, patient monitor system), building systems (air conditioning, security camera), mobile devices (pager, cell phone), modern cars (brake system, diagnostics and security systems), peripheral controllers of a computer (printer controller, disk drive controller), manufacturing and control systems (automated factories, power stations, robots), network information appliances (modems, routers). The complexity of embedded systems is rapidly growing and their design is requiring a wide range of competencies varying from digital and analog electronic design, use of advanced platform FPGAs, multicore programming, software engineering, cryptography and wireless networking. In this work, we outline the skills requirements to develop the various categories of embedded systems, showing that they are more than programming microcontrollers.

Classification of embedded systems: Embedded systems are some combination of computer hardware (Hw) and software (Sw), developed for performing some predefined tasks. These systems can be classified into three categories based on their complexity: low, medium and high. Low complexity systems use a single 8 bit or 16 bit microcontroller, on-the-shelf hardware components (memory, led, LCD, etc). Medium complexity systems using one or few 32 bit microcontrollers, a microkernel OS basically providing real time scheduling services, one or few prototyping FPGAs. High complexity embedded systems have an enormous Sw and Hw complexity and often implement more than one application. Examples of these systems are home media systems, portable players, smart phones, embedded medical devices and automotive embedded systems.

Primary design skills: Development of low to medium complexity embedded systems requires a mixture of Sw competencies and Hw competencies. Sw competencies include not only assembly programming, embedded C programming, interrupt services routines development, DMA programming, low-level device drivers development, scheduling tasks using RTOS, memory management, use of Sw development chains (cross compiler, linker, Sw and Hw debug), but Sw competencies include also object oriented programming (C++, java ME), interfacing low-level device drivers to monolithic embedded OS kernel (as Linux, android),

networking programming (TCP/IP, http), etc. The Hw competencies include register transfer level (RTL) coding, FSM design and PFGA prototyping in addition to analog design. The essential considerations in the design of these systems are response time, cost, power, portability and fault-tolerance.

Skills for complex embedded designs: Embedded system technology has already moved from a system on a board (SoB) to a system on chip (SoC). A SoC is an integrated circuit that integrates all the various components of a computer and other electronic components onto a single chip. SoC design requires new competencies in system level design, Sw development and Hw development. System level design skills are about 1- system level modeling using concepts as transactional level modeling (TLM systemC), UML modeling (UML/MARTE), formal modeling (Khan process network, statechart, colored Petri net), 2- Hw/ Sw codesign and architecture exploration. Sw development skills are about 3- multicore systems programming (multithread, multiprocess, symmetric/asymmetric programming), 4- distributed systems programming (multi agent), 5- security/Encryption, and 6- internet-related technology (embedded web server, embedded browsers). Hw development skills include -7 designing with advanced programmable logic FPGAs that offer hundred of configurable analog/digital intellectual properties, 8- wireless sensors networking, and 9- interfacing to micro-electro-mechanical system (MEMS) devices and micro-opto (MOEMS) devices that combine optic, mechanic and electronic (Fig.1). In the near future we will talk more about embedded micro- and nanosystems (EMNS) rather than just embedded systems. However, the additional competencies requirements for designing these systems still not well defined because is not clear which technology for nanosystems will typically be used in future EMNS products.

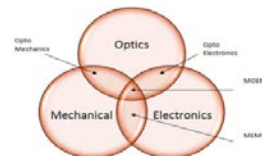


Fig. 1: MEMS

References:

- Peter Bertels et al. (2009) Teaching Skills and Concepts for Embedded Systems Design, Newsletter ACM SIGBED, vol. 6 Issue 1.
- Steffen Jaschke et al. (2010) Competence research: teaching embedded micro/nano systems, 6th Workshop on Embedded Systems Education.

On the coordinated path following control and trajectory tracking of multiple autonomous systems

J. Ghommam^{1,2}

¹Intelligent Control Design and Optimization of Complex Systems Unit,
Ecole Nationale d'Ingenieurs de Sfax, TUNISIA

² Institut National des Sciences Appliquées et de Technologies, TUNISIA

Introduction: One major overhead of autonomous systems' missions is the execution of tasks that sometimes may overlap its allocated mission's timing, to overcome such overhead this research that I led along with my cooperators from Canada and Spain exploited the path following approach for reason to consider the problem of coordinating a group of autonomous vehicles (mobile robots, UVS and AUVs) such that upon steering the motion of each vehicle, the group's overall motion is governed by a desired behavior. Thus, independent motion is coordinated as a formation according to the behavior decided by the designer. The talk will principally be focused on different challenging issues addressed to robustly cooperate a team of vehicles to seamlessly achieve a first level of distributed "intelligence" for navigation.

The impact of limited communication and time delays on the overall system performance is one of the major problems that arises in cooperative control implementation problems into digital platforms. Using quantized values in the cooperative controller is inevitable in some way or another. Considering the high nonlinearities in quantization functions, it is then very hard to obtain explicit solutions of a system involving quantized elements and the traditional methods for analyzing linear systems are not feasible anymore. In this presentation some key solutions for quantized cooperative controllers with and without time delay are presented .

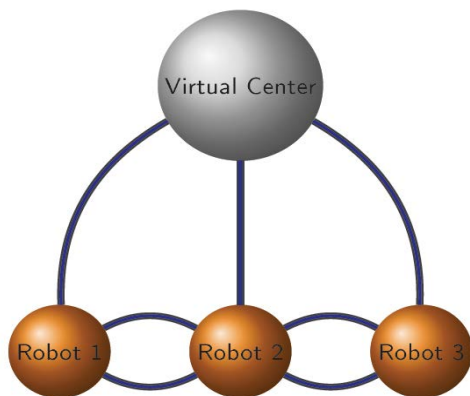


Figure 1: Underlying communication graph topology

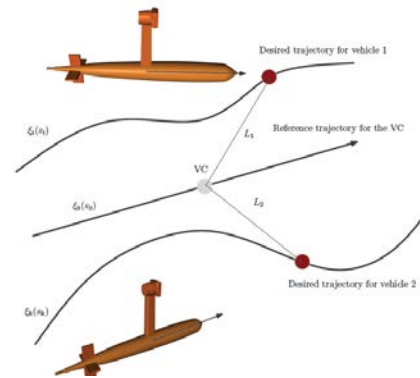


Figure 2: Formation of fleet of underwater vehicles

Cooperative control algorithms have been numerically tested through Matlab/Simulink software mainly applications that revolve around flocking of underwater and submarine vehicles. Some of the revamped algorithms for mobile robots have been successfully implemented on real apparatus. Most of the work that are about to be presented in this talk are published or underway of publishing and are given hereby

References:

- J. Ghommam, H. Mehrjerdi and M. Saad, Group Coordination Control of Multiple Mobile Robots with Communication Delay, *Transaction on System, Signals and Devices*, vol. 5, No. 1, pp. 1-20.
- J. Ghommam, H. Mehrjerdi and M. Saad, Adaptive Coordinated Path Following Control For Nonholonomic Mobile Robots with Quantized Communication, in *IET Control Theory and Applications*.
- J. Ghommam, H. Mehrjerdi, M. S. Mahmoud and M. Saad, Robust Cooperative Control for a Group of Mobile Robots with Quantized Information Exchange, submitted to *IEEE Trans on Control Systems Technology*, Oct, 2011.
- J. Ghommam, H. Mehrjerdi and M. Saad, Cascade Design for Formation Control of Nonholonomic Systems in Chained Form, *Journal of the Franklin Institute (Engineering and Applied Mathematics)*, vol. 348, no 6, p. 973-998.

Evaluation of a medical wireless sensors network at emergency cases

J. Khaskhoussi^{1*}, R. Ouni², A. Mtibaa¹

¹Ecole Nationale d'Ingenieurs de Monastir, TUNISIA

*Corresponding author : E-mail adress : jihed.khaskhoussi@tunisiatelecom.tn

² College of Computer and Information Sciences (CCIS)
King Saud University (KSU)

Abstract : While there are many areas where Wireless Sensor Networks (WSN) can be deployed to offer fast and low cost solutions for the monitoring, few real deployments can be found due to energy constraint. Medicine is one of the areas where we can deploy the WSN to monitor vital parameters like temperature, Electric Cardiogram (ECG) or blood Oxygen Saturation to allow urgent intervention.

Recently, the WSN-based telemedicine is considered as new paradigm for supporting remote clinical health care. It allows facilitating preliminary and periodically health diagnostics through a data base history of the patients. This paradigm was successfully employed in several pilot studies and commercial application.

The WSN for telemedicine is composed by many devices (nodes) scattered on the patient body as bracelets. These devices are equipped by physical sensors responsible for measuring target metric. They collaborate together to send data to one or multiple sinks (doctors and medical staff) for diagnostic and intervention if necessary.

In this paper, we analyze the behavior of a medical WSN where all nodes (or patient) are mobile (figure 1). We simulate multiple transmission scenarios to describe urgent situations.

- **Scenario 1:** 10% of patients needs intervention.
- **Scenario 2:** 50 % of patients needs intervention.
- **Scenario 3:** 100% of patients needs intervention.

For each scenario, we will evaluate a primitive network where all nodes have the right to diffuse received message and an organized network where the right of diffusion is limited to a special set of nodes. The protocols suggested for the organized networks are the multipoint relays (MPR) and the multipoint relays – Connected Dominate Set (MPR-CDS).

Simulation environnements are MATLAB and OPNET.

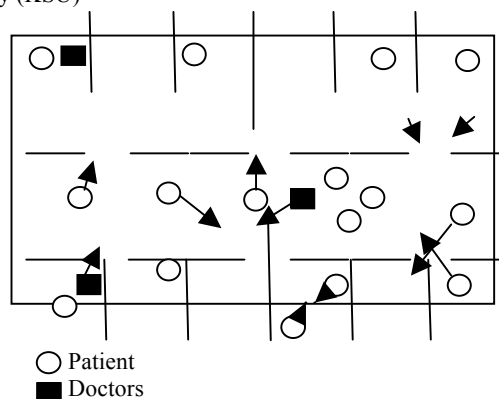


Figure 1: Simulation Scenario.

References:

- Beydoun, K. (2009) Conception d'un protocole de routage hiérarchique pour les réseaux de capteurs, PhD thesis, U.F.R DES SCIENCES ET TECHNIQUES.
- Crisostomo, S., Barros, J. and Bettstetter, C.,(2008) Flooding the network: Multipoint relays versus network coding,Circuits and Systems for Communications.
- Dessart , N., Fouchal , H., Hunel , P. and Rabat , C.(2010) Imulation of Large Scale WSN for Medical Care, Computers and Communications (ISCC)
- Furtado, H. and Trobec, R. (2011) Applications of wireless sensors in medicine , MIPRO 2011, Opatijia, Croatia.
- Geoffrey, G.M. and Ivars G.F. (2007) Traffic Models for Medical Wireless Sensor Networks, IEEE COMMUNICATIONS LETTERS, VOL.11, NO.1.
- Jie, W., Wei, L. and Fei, D.,(2006) Extended Multipoint relays to determine connected dominating sets in MANET's ,IEEE transaction on computer, vol. 55, NO. 3.
- Xiaoyu, S. (2011) Modeling and Simulation of WSN Routing Protocols, Communication Software and Networks (ICCSN).
- XIONG, S., WANG, L., WANG, X. and ZHAN, Y. (2009) Application of Wireless Sensor Networks to Remote Medical Treatment System, IT in Medicine & Education (ITIME '09).
- Yongsheng, F., Xinyu W., Wei, S. and Shanping, L.,(2008) Connectivity based greedy algorithm with multipoint relaying for mobile ad hoc networks, The 4th international conference on mobile ad-hoc ans sensor network.

Reinforcement learning based hierarchical dynamic power management

M. Triki^{1,2}, A. C Ammari^{2*}

*Maryam Triki : E-mail adress : maryam.triki@gmail.com

¹ Carthage University, INSAT Institute, MMA research laboratory
Institut National des Sciences Appliquées et de Technologies, TUNISIA

*Ahmad Chiheb Ammari : E-mail adress : chiheb.ammari@insat.rnu.tn

² Institut National des Sciences Appliquées et de Technologies, TUNISIA

Introduction: Dynamic power management (DPM), which refers to the selective shut-off or slow-down of system components that are idle or underutilized, has proven to be a particularly effective way of reducing power dissipation at system level [1]. The DPM methods proposed in the literature can be broadly classified into three categories: heuristic, stochastic, and learning based methods.

The heuristic methods are based on the idea of predicting whether the next idle period length is greater than the break-even time T_{be} .

The most widely used heuristic method is the time-out policy which assumes that after a device is idle for a time-out value τ , it will remain idle for at least T_{be} . The time-out policy is simple and easy to implement and has been adopted in many commercial products. However it does not take system performance into account and so does not achieve a good trade-off between performance and energy dissipation.

The stochastic approaches can take into account both power and performance and are able to derive provably optimal DPM policies by modeling the request arrival times and device service times as stationary stochastic processes such as Markov processes that satisfy certain probability distributions. Requiring an exact knowledge of the state transition probability function and the reward function of the MDP is the essential shortcoming of these method. The workload of a complex system is usually unpredictable and the workload variation has the most significant impact on the system speed and power consumption. Thus, a robust power management technique must consider the uncertainty and variability that emanates from the environment, hardware and application characteristics [2] and must be able to interact with environment to obtain information which can be processed to produce an optimal policy.

Reinforcement learning can simultaneously consider power and performance, and performs well under various workload when such a model is not known a priori.

Content: The proposed architecture decomposes the power management (PM) task into two layers: component-level and system -level. The component-level PM policy is pre-specified and fixed. We consider such a device as an uncontrollable or self power-managed component. Whereas the system-level PM employs temporal difference learning on semi-Markov decision process (SMDP) for model-free RL, and it is specifically optimized for a multi-type application framework., which is performing also application-level scheduling.

The contribution of this paper is twofold. First, we use reinforcement learning to optimize the power consumption at the system-level. the GPM possesses the following merits: model-free, independent of pre-designed policies, performing learning and power management in a continuous-time and event-driven manner, fast convergence rate and less reliance on the Markovian property. The second part of contribution is the development of a GPM, which performs effective application-level scheduling, thereby, performing an additional power saving . The fairness issues about distributing execution times among various software applications are also taken care of by the proposed GPM. Results of the experiments conducted in this regard establish that the proposed DPM scheme enhances power savings considerably.

References:

- L. Benini, A. Bogliolo, and G. De Micheli,(2000) A survey of design techniques for system level dynamic power management, IEEE Trans. on VLSI Systems, Vol. 8, Issue 3, 299-316, 2000.
- Y. Tan, W Liu, and Q. Qiu, Adaptive Power Management Using Reinforcement Learning, Department of Electrical and Computer Engineering
Binghamton University, State University of New York Binghamton, New York 13902, USA.

Posters Communications

P1 - Investigation of the band discontinuities effect in single and double a-Si:H/c-Si heterojunction solar cells using AMPS-1D simulations

A. Bensmain, H. Tayoub, B.Zebentout and Z.Benamara

Applied Microelectronic Laboratory, Faculty of Engineering, University of Sidi Bel Abbes (Algeria)

E-mail : bensmain.asmaa@gmail.com

Introduction: Thin film silicon technology is already mastered and become one of the most promising branches in present photovoltaic industry. The actual aim of researcher is focusing in performing of the efficiency of silicon solar cells based on amorphous materials. First concept was a-Si:H/c-Si heterojunction and especially when using a wide band gap layer by adding germanium (a-SiGe:H) or carbon (a-SiC:H) precursors to the gas flow for absorption of infrared light.

For any solar cell structure, it is necessary to optimize its parameters to get good performance. Usually, the optimized parameters are: the thickness of the cell, the levels and doping profiles, configuration contacts, and optical confinement. Of course, optimal parameter values depend on the structure of the solar cell and the quality of the substrate material (lifetime, mobility), quality of ohmic contacts, speed recombination at the surface (front and back) [1], etc...

In this work, the AMPS-1D [2](Analysis of Microelectronic and Photonic Structure) simulation program is used to study systematically the effect of band discontinuities on illuminated J-V characteristics and therefore the photovoltaic parameters (J_{SC} , η , V_{OC} and FF) in both cases of a-Si:H(p⁺)/c-Si(n) and a-Si:H(n⁺)/c-Si(p) heterojunctions solar cells.

The results of our simulations have shown that:

- The use of a P or N-type of a-Si:H leads to conversion efficiencies close to the discontinuities engineering.

- For a maximum of photons transmit in the base crystal, it should be to use an amorphous silicon layer with a wide band gap, highly doped and thin thickness.

- The best photovoltaic output are reached for an a-Si:H(P)/c-Si(N) heterojunction as those found experimentally.

- The establishment of the field back (BSF) based on a-Si: H is the crucial step to achieve the highest PV parameters.

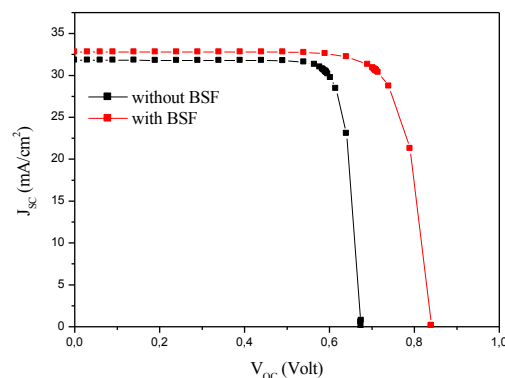


Figure 1: Influence of BSF on the characteristics J (V) for a heterojunction at the rear of the substrate N.

PV output	Values
J_{SC} (mA/cm ²)	32.809
V_{OC} (V)	0.840
η (%)	22.437

Table 1: The best of photovoltaic parameters of junction PN with BSF.

It appears from our simulations that the band structure related to N-type substrate is again more appropriate.

References:

AMPS 1D site web, Pennsylvania University: <http://www.emprl.psu.edu/amps>
 N. Oleksiy (2005) "Simulation, fabrication and analysis of solar cells interdigitated back contact" doct thesis, 2005.

P2 - Conception of an WDM optical transmission link at 4*10 Gbit/s

A.Benzina^{1*}, M.Hadjab¹, R.Naoum², H.Abid¹.

¹Applied Material Laboratory (AML), Department of Electronic,
Djillali Liabes University Sidi Bel Abes, Algeria
*benzina.amina@gmail.com

² Telecommunications and digital signals processing laboratory (LTNS), Department of Electronic,
Djillali Liabes University Sidi Bel Abes, Algeria

Abstract—The evolution of data transmission using optical fiber media has been accelerated since the advent of technical multiplexing wavelengths (WDM), which helps to achieve bitrates of a few Tb/s transported by a single fiber. In this context, we propose in this work, to make a simulation of a system WDM, at 4*10 GB/s with the COMSIS simulator system.

Introduction: Progress in the technologies laser and optical sources in the 1960s, the dream of the optical communications, drew the attention of the researchers more and more. One of the key issues to develop practical optical systems of communication was the lack of good middle of transmission. The field of optical communications is currently characterized by an increased demand in terms of capacity of transmission. We try to transmit more and more data and new applications are born. It persists however certain limitations, such as dispersive effects, which degrade the performances of the transmissions.

This request found at first an answer in the increase of the rate of TDM (Time Division Multiplexing). However, the limits of the electronic components of transmission, and those imposed by the problems inherent to optical fibers as the chromatic dispersal and the dispersal of polarization were quickly affected. Today, the maximal cadences are included between 2.5 and 10 Gbit/s-1. In the early 90 appeared the idea of transmitting information over several wavelengths instead of only within a single optical fiber. It is the multiplexing in wavelengths (Wavelength Division Multiplexing). This solution has the dual benefit of significantly increasing transmission rates, since they are multiplied by the number of channels, and can be implemented at low cost on the already installed optical fibers. For example, in 1999, the transmission systems used included 40 channels. Wavelengths separated by 0.8 nm, were situated in a spectral window of 1,53 μm in 1,56 μm , chosen for two main reasons related to the signal attenuation over long distances. On the one hand,

the absorption of silica is low around 1.55 μm . On the other hand, in the window, it is possible to use optical amplifiers Erbium-doped fiber. Amplifiers, installed at regular intervals along the route, make it possible to transmit over long distances.

Today, 40 channels are widely inadequate. To increase this number, two ways of research are explored: increasing the transmission window, and tighten channels (Dense Wavelength Division Multiplexing) optical transmission system to reduce the penalties resulting from the chromatic dispersion, the non-linearity of the fiber and to reduce the non-linear penalty had to inter channel. The simulator **COMSIS** (**COM**munication **S**ystem **I**nteractive **S**oftware) is developed by the company IPSIS. This software enables scientists and engineers to model, simulate, analyze and easily receive any signal processing module, from the simplest device to a complete system of communication. COMSIS is an interactive environment which allies digital tools to graphic features. It allows modeling of analog and digital systems described as block diagrams[1].

We propose in this work, to make a simulation of a WDM system, 4*10 Gbit/s, we are interested in non-linear effect precisely the Kerr effect.

References:

- The help of the COMSIS software (1992).
Aloisio, Paolo Branchini, Francesco Cevenini and Vincenzo Izzo. :“Transponders for Real Time DWDM Networks”. Journal of IEEE Indian institute of technology, kharagpur 721302(December 20-22,2004).
Alberto Aloisio, Francesco Cevenini, and Vincenzo Izzo.: “An Approach to DWDM for Real-Time Applications”. Journal of IEEE transactions on nuclear science, VOL. 51, N°. 3 p 526 - 531 (JUNE 2004).
A. Boyogu eno Bend e, M. A. Duguay, P. Fortier.: “ tude sur l’amplification en ligne des syst mes de communication optique” D partement de g nie  lectrique, Universit  Laval, Ste-Foy(Qu bec) Canada, G1K 7P4(2007).

P3 - Studying of endothelial cells adhesion onto fonctionalized substrates using surface plasmon resonance

A. Bouafsoun^{1*}, L. Mora².

¹Laboratoire de Nanotechnologie, Institut National de Sciences Appliqués et Technologie, Bp676, Centre Urbain Nord 1080 Charguia, Tunisia.

*Corresponding author : E-mail adress : amira.bouafsoun@yahoo.fr

²Laboratoire de Bio-Ingénierie des Polymères Cardiovasculaires (LBPC), INSERM U 698, Institut Galilée - Université Paris 13 Bât E, bureau 119, 99 Bvd Jean-Baptiste Clément 93 430 Villetaneuse, France.

Abstract

Surface Plasmon Resonance (SPR) is an established tool in the life-science sectors. It offers a new generation of label-free biomolecular analysis, providing information on kinetic processes (association and dissociation), binding affinity, analyte concentration and real-time molecule detection.

A large variety of bio-interactions can be monitored, such as antibody/antigen, peptide/antibody, DNA/DNA, antibody/bacteria etc.

A study concerning bovine serum albumin (BSA) adsorption by thiolated dextran layers present on metallic surfaces, monitored by SPR technique, was reported. Also, SPR sensors were used for kinetic studies of protein adsorption by polymeric surfaces and degradation of polymer surface. Papers describing SPR technique as a method of supplementing atomic force microscopy (AFM) in biomaterial studies have also been published.

The focus of this work will be on the endothelial cell monolayer immobilized adhesion onto fonctionalized substrates such as fibronectin/polystyrene/thiol/ gold electrodes, by surface plasmon resonance (SPR) spectroscopy and atomic force microscopy (AFM) (see figure 1).

The obtained results have been confirmed by impedance measurements and wettability studies.

Endothelial cells were obtained from a line (Eahy 926) and were grown in Medium 199 supplemented with 10% FBS, 2 mmol/l glutamine, 100 U/ml penicillin and 100 µg/ml streptomycin. Cultures were incubated at 37°C in a humidified atmosphere containing 5% CO₂. Replicated cultures were obtained by trypsinization and were used for passages < 5. The endothelial cell identification was confirmed by their polygonal morphology.

In the present study, we observed a suitable adhesion rate and an interesting cell proliferation on fibronectin which present a roughness rate about 47.2 nm.

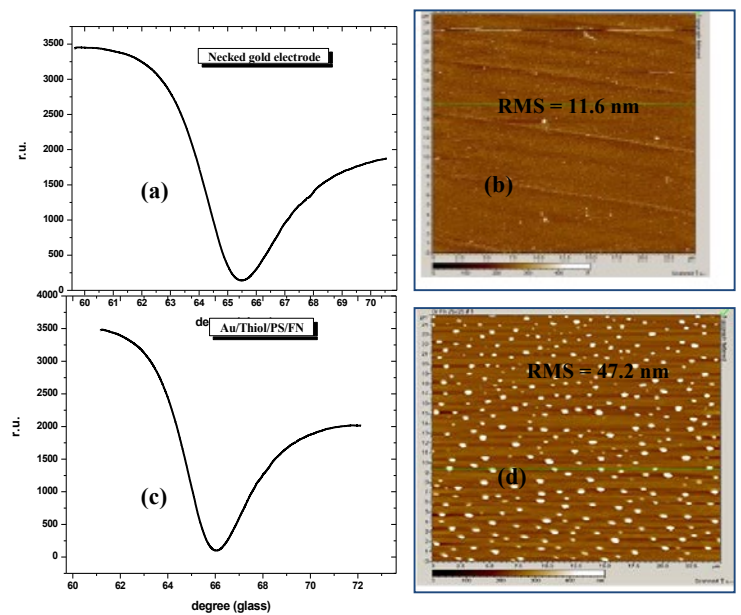


Figure 1: (a) SPR signal response of Necked gold electrode, (b) the corresponding AFM image, (c) SPR signal response of Au/Thiol/PS/FN fonctionnalised electrode and (d) the corresponding AFM image.

References

- Bouafsoun. A, Helali. S, Mebarek. S, Zeiller. C, Prigent. A.F, Othmane. A, Kerkeni. A, Jaffrézic-Renault. N, Ponsonnet. L. (2006), Electrical probing of endothelial cell behaviour on a fibronectin/polystyrene/thiol/gold electrode by Faradaic electrochemical impedance spectroscopy (EIS). *Bioelectrochemistry*, 71, 99-105, 2006.
- H. Hillebrandt, A. Abdelghani, C. Abdelghani-Jacquín, M. Aepfelbacher, E. Sackmann: Electrical and optical characterization of thrombin-induced permeability of cultured endothelial cell monolayers on semiconductor electrode arrays, *Appl Phys A* 73, 539-546.

P4 - QCM coated with plasma polymerized TEOS/O₂ for the detection of volatile organic compounds

A.Bougharouat¹, A.Bellel^{1,*}, S. Sahli², Y.Segui³, P.Raynaud³

¹ Laboratoire d'Etude de Matériaux Electronique pour Applications Médicales (LEMEAMED), Faculté des Sciences de l'Ingénieur, Université Mentouri de Constantine, Constantine 25000, Algeria

² Laboratoire de Microsystèmes et Instrumentation (LMI), Faculté des Science de l'Ingénieur, Université Mentouri de Constantine, Constantine 25000, Algeria

³ Laboratoire Plasma et Conversion de l'Energie (LAPLACE), CNRS, INPT, Université Paul Sabatier, 118 Route de Narbonne, 31062 Toulouse Cedex, France.

E-mail: azzedine.bellel@gmail.com

Abstract: The detection of volatile organic compounds (VOC) in environmental protection, health care and industrial processing has been a subject for research and development over the last decades. The exposure to some VOC for a long time may causes diseases or serious irreversible effect [1]. The development and construction of new chemical sensors, which are specific for particular chemical species, is an active area of research. For online detection, quartz crystal microbalance (QCM) is commonly used as transducer for chemical gas sensing. For this purpose, the surface of the quartz crystal electrode is coated with sensitive material capable of interacting with the analyte of interest. Polymers are widely used as chemically sensitive coating materials on QCM electrodes and are particularly suitable for detecting volatile organic compounds, because of the ability of the polymer to adsorb vapor reversibly [2]. In this work, plasma polymerization of Tetraethylorthosilicate (TEOS) and oxygen (O₂) was used for producing QCM chemical sensors. The sensor was exposed towards a wide range of VOC molecules such as ethanol, methanol, acetone and chloroform. We characterized the gas sensing properties of the elaborated gas sensor by monitoring the frequency shift (Δf) of the QCM due to additional mass loading.

To check the reproducibility and the reversibility of the VOC sensor, the responses signal of QCM electrode coated with 693 nm thick film (elaborated from the polymerization of pure vapor of TEOS) have been recorded. The measured isotherms on modified QCM electrode showed a good reproducibility and reversibility (figure1). It can be noted that the sensor attains the same Δf upon exposure to VOC vapor concentration at different times. In addition, the frequency of the crystal back shifted to its initial values indicates full desorption of analytes from the electrode surface, which indicated that the sensing interaction between polymer coating and VOC molecules is a physical absorption. Furthermore, the frequency shifts of the QCM were found to be linearly

correlated with the concentration of VOC vapor. In order to enable the coated QCM with large sorption capacity and specific selectivity to target analytes, chemical structures of the elaborated layer are modified by the use of suitable monomer and oxygen mixture proportion. Film elaborated from 50% of TEOS and 50% of O₂ was found to be significantly more sensitive than film deposited from high proportion of oxygen due to dense structure. Fourier transform infrared spectroscopy (FTIR) analysis suggests that the presence in the film structure of CH_n groups (which increase the free space in the film) and the OH groups (which provide a main source for hydrophylic capability to interact with foreign molecules) increase the gas sorption capacity of the elaborated layer. The stability performance test showed that the coated QCM electrode can be used over 6 month without any loss in sensitivity and performance.

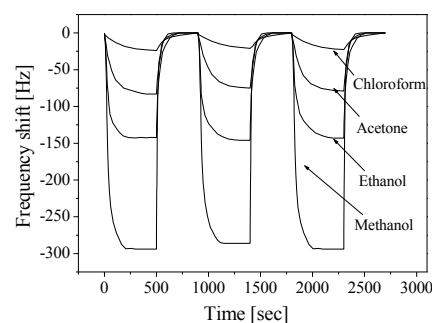


Figure1: Isotherms (for absorption and desorption cycle) of coated QCM electrode when exposed to VOC vapors.

References:

- [1] Chem, R., Semple, S., Dick, F. and Seaton, A. (2001) Nasal, eye, and skin irritation in dockyard painters, *Occupational and Environmental Medicine*, 58, 542-543.
- [2] Si, P., Mortensen, J., Komolov, A., Denborg, J. and Møller, P. J. (2007) Polymer coated quartz crystal microbalance sensors for detection of volatile organic compounds in gas mixtures *Analytica Chimica Acta*, 597, 223-230.

P5 - Theoretical study on interactions of β -Cyclodextrin with dimethylamino-4-benzal para-nitroaniline

A .Bouhadiba^{1,*}, N. Leila¹, H. Sakina¹, I, Djilani¹, F.Djebbloune¹

¹Laboratory of Computational Chemistry and nanostructure, Guelma University, BP: 401; Guelma, 24000, Algeria.

*E-mail: bouhadibaaziz@yahoo.fr

Abstract: Cyclodextrins (CDs) are cyclic oligosaccharides obtained by the enzymatic degradation of starch. They are formed by the association of six, seven or eight units of glycopyranose linked by α (1, 4) connections and named respectively α , β and γ CD. They bear hydrophobic cavities capable of forming inclusion complexes with a variety of organic molecules. In particular, β -CD has an internal cavity shaped like a truncated cone about 8 Å deep and 6.0–6.4 Å in diameter and this cavity possesses a relatively low polarity. These inclusion complexes do not contain any covalent bond between host and guest molecules and their stability depends on molecular size and shape complementation but also on the external medium and environmental conditions. Structural aspects of the complexation of dimethylamino-4-benzal para-nitroaniline with beta cyclodextrin (β -CD) were carried out using MM+, PM3, DFT and HF methods. Two orientations of the incoming dimethylamino-4-benzal para-nitroaniline inside β -CD were considered to determine the lowest energy complex, namely the A (NC_2H_6 group orientated to the centre of mass of β -CD) and B (NO_2 group orientated to the centre of mass of β -CD) orientations. The binding energy for both orientations considered in this research is reported. The calculations confirm that the A orientation is more favorable than the B one by 1.68 kcal/mol (PM3). Also an intermolecular hydrogen bond is established between host and guest molecules. This suggests that hydrophobic effect and hydrogen bond play an important role in the complexation process. Moreover, the statistical thermodynamic calculations at 1 atm and 298.15K demonstrate that 1:1 Dimethylamino-4-benzal para-nitroaniline / β -CD complexation is an exothermic process, enthalpically favorable in nature.

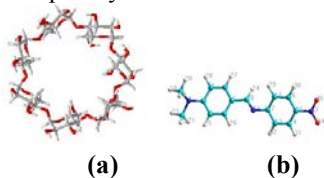


Figure 1: Molecular structures of β -Cyclodextrin (a) and B3LYP/6-31G* optimized structure of Dimethylamino-4-benzal para-nitroaniline (b).

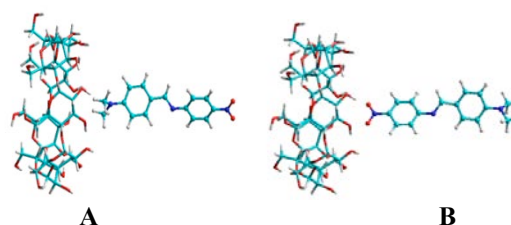


Figure 2: Coordinate systems used to define the process of complexation for: A and B orientations

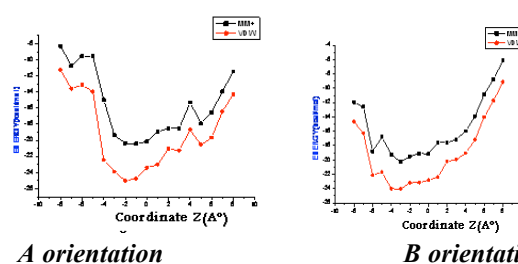


Figure 3: Binding energy of the inclusion complexation of dimethylamino-4-benzal para-nitroaniline into β -CD at different positions (Z) for both orientations.

References:

- Antonio C.S Lino, Yuji Takahata,2002, α - and β -cyclodextrin complexes with n-alkyl carboxylic acids and n-alkyl p-hydroxy benzoates. A molecular mechanics study of 1:1 and 1:2 associations, *J.Theochem* 207-213.
- Becke,1993, Density-functional thermochemistry. III. The role of exact exchange, *J. Chem. Phys.* 98 (1993) 5648-5652.
- Enric Cervelló, Carlos Jaime,1998. β -cyclodextrin bimodal complexes with n-alkylbenzenes and n-alkylcyclohexanes A molecular mechanics study, *J, Theochem*195-201.
- Fatiha, M., K. Djameleddine and L. Leila, 2009. Molecular modeling study of para amino benzoic acids recognition by B-cyclodextrin. *Orbital*, 1: 26-37.
- Frisch, M.J., G.W.Trucks, H.B. Schlegel, G.E. Scuseria and M.A. Robb, 2003. Gaussian 03, Revision B.05. Gaussian Inc., Pittsburgh PA.
- Jursic, B. S.; Zdravkovski, Z.; French, A. D., Molecular Modeling Methodology of β -Cyclodextrin Inclusion Complexes, *J. Mol. Struct. (Theochem)*, 1996, 366, 113-117.

P6 - Formation of porous amorphous silicon carbide thin films by electrochemical etching

A. Boukezzata^{1*}, A. Keffous¹, G. Nezzal², S. Merrazga³

*Corresponding author : E-mail address : assiab2006@yahoo.fr

¹Silicon Technology Development Unit, 02 Bd, Frantz FANON, B.P. 140, Algiers, Algeria

²Houari Boumediene University, (USTHB), Chemical Faculty, Algiers, Algeria

³Houari Boumediene University, (USTHB), Physical Faculty, Algiers, Algeria

Introduction: Silicon carbide (SiC) is a promising semiconducting material because of its excellent physical and electrical properties, such as the wide band gap, high electrical breakdown field, high thermal conductivity, high surface hardness, high saturated electron velocity and so on. These properties make SiC suitable for high power, high frequency, high temperature applications, surface coating, as well as corrosion-resistant coating. The porous silicon carbide (PSiC) has become the focus of considerable attention due to its excellent material properties, promising it for different applications.

Content: The amorphous porous silicon carbide (PASiC) was fabricated on a thin amorphous silicon carbide (a-SiC) films deposited on p-type Silicon substrate (a-Si_{1-x}C_x/Si(p)) by co-sputtering DC magnetron of Si and 6H-SiC as targets. The thickness of the elaborated a-Si_{1-x}C_x films was 1.4 μm. PASiC were made by electrochemical etching in HF/Ethylene Glycol solution (1:1 by volume) at an anodization constant current density (J) of 50 mA/cm² for 45 seconds. In experiment, the surface morphologies of porous amorphous Si_{1-x}C_x (PASiC) were characterized by scanning electron microscopy (SEM), infrared spectroscopy (FTIR) and photoluminescence (PL). The typical surface morphology of the PASiC obtained by SEM is shown in **Figure 1**, where a uniform deposit of the thin amorphous silicon carbide (a-SiC) film is observed, whereas the formation of a macroporous layer with a pore diameter around 80 to 150 nm is noticed on the etched (PASiC) surface (**Fig.1**).

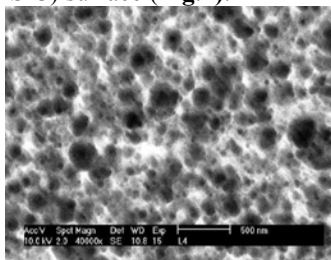


Figure 1. Plan view SEM image of PASiC sample

The Fourier Transform Infrared Spectroscopy (FT-IR) revealed several vibrations bands, the peaks located at 616 cm⁻¹ and 765 cm⁻¹ correspond to Si-C and Si-O-H bands (5), respectively their intensity

decreases after anodization. The absorption bands located at 680 cm⁻¹ and 1106 cm⁻¹ correspond to SiH₂ and Si-O₂ respectively, its intensity increases after anodization as reported by several authors (**Fig. 2**). We also noted the existence of a band centered at 2286 cm⁻¹ and 2396 cm⁻¹ corresponding to CO₂ (**Fig. 2**).

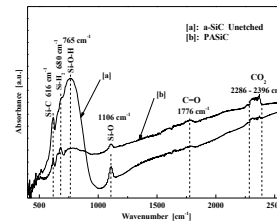


Figure 2. FT-IR spectra of unetched and PASiC sample..

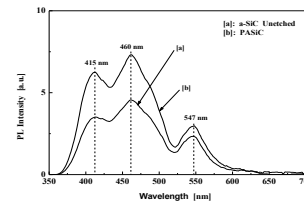


Figure 3. Photoluminescence spectra of unetched and PASiC sample.

Figure 3 shows the PL spectra of amorphous thin a-Si_{1-x}C_x films before and after anodization, which exhibit two bands: a blue one with two peaks centered at 415 nm and 460 nm and a green band centered at 542 nm, the PASiC sample exhibits a high PL intensity compared to the unetched sample, then after. Wang et al. found that the PL intensities are enhanced by UV irradiation 325 nm at room temperature and the luminescence center with peak 564 nm is induced by the UV light for the anodized porous-like SiC samples, they suggested that UV irradiation may induce metastable states as luminescence centers in the sample.

References:

Bayazitov, R.M., Khaibullin, I.B., Batalov, R.I., Nurutdinov, R.M., Antonova, L.Kh., Aksenov, V.P., (2003) Structure and photoluminescent properties of SiC layers on Si, synthesized by pulsed ion-beam treatment, Nuclear Instrum. Methods Phys. Res., **B** 206, 984-988, 2011.

P7 - Comparative study of optical properties of ZnO:In and ZnO:Yb sprayed thin films

A. Boukhachem*, B. Ouni, K. Boubaker, A. Amlouk and M. Amlouk

Unité de physique des dispositifs à semi-conducteurs, Faculté des sciences de Tunis, de Tunis El Manar

University, 2092 Tunis, Tunisia

Abstract:

ZnO thin films, which couple the property of being Conductive and transparent, (transparent conductive oxide, hereafter CTO), were deposited on glass substrates by a simple mini spray technique. Alternatively, some of the obtained films were doped with Indium (In) and Ytterbium (Yb) at the molar rates of: 1, 2 and 3 % (In) and 100, 200 and 300 ppm (Yb). The optical band gap calculated from transmittance and reflectance spectra [7] of the above samples show the effect of concentration on this energy. They equally show that these materials are characterized by the most direct gap absorption. Analysis of Urbach-Martienssen model parameters allows nano-scale explanations of the doping-related divergence of Urbach tailing evolution[2, 9, 10]. The refractive index and extinction coefficient of the differently doped ZnO thin films have been reached through their transmission and reflectance spectra on a wide range of wavelengths. By applying the model of single oscillator called Wemple-DiDomenico [6, 9], data analysis of refractive index gives values of the energy of the oscillator (E_0) and energy dispersive (E_d).

Finally, the refractive index and extinction coefficient are used to study the dielectric constants in terms of real and imaginary parts and then to estimate the plasma frequency ω_p , relaxation time τ and free carriers concentration-to-effective mass ratio [1, 3, 6, 8].

Figures and Tables:

Figure 1: Plots of $Ln(\alpha)$ versus $h\nu$.

Figure 2: Doping-related Urbach energy evolution

Table : The values of the main parameters

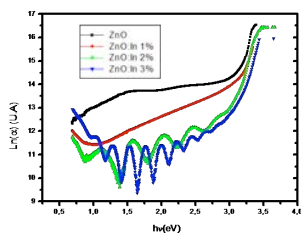


Fig 1.a

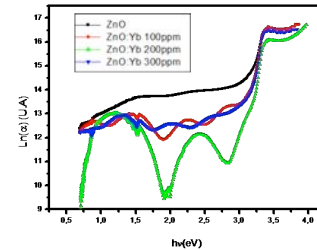


Fig 1.b

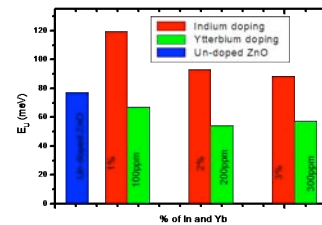


Fig 2

Sample	E_0 (eV)	E_0/E_g	E_d (eV)	λ_0 (nm)	$S_0(10^{-5}\text{nm}^2)$
Un-doped ZnO	3.849		8.825	322.486	2.204
ZnO:In1%	6.102	1.875	13.910	203.403	5.509
ZnO:In2%	6.396	1.957	14.975	194.059	6.217
ZnO:In3%	6.777	2.021	18.442	183.136	8.113
ZnO:Yb100ppm	5.252	1.597	8.740	236.300	2.980
ZnO:Yb200ppm	6.689	2.034	12.593	185.544	5.468
ZnO:Yb300ppm	6.499	1.981	13.343	190.963	5.629

Table

References:

- [1] A.K. Wolaton and T.S. Moss, Proc. R. Soc. A 81 (1963), 5091.
- [2] F. Urbach, Phys. Rev. 1953,92 1324.
- [3] F. Gervais, Materials Sciences and Engineering R 39 (2002), 29–92.
- [4] H.G. Tompkins and W.A. McGahan, Spectroscopic Ellipsometry and Reflectometry, John Wiley and Sons Inc., New York (1999).
- [5] J.I. Pankove, Optical Processes in Semiconductors, Prentice-Hall, New Jersey (1971) 92.
- [6] M. DiDomenico Jr., M. Eibschütz, H. J. Guggenheim, I. Camlibel, Solid State Comm., 7, Issue 16 (1969) 1119-1122.
- [7] M.t Caglar , Saliha Ilican, Yasemin Caglar , Thin Solid Films 517 (2009) 5023–5028
- [8] M. Sesha Reddy, K.T. Ramakrishna Reddy, B.S. Naidu, P.J. Reddy, Optical Materials 4 (1995) 787-790.
- [9] S. H. Wemple, Solid State Comm, 12, Issue 7(1973) 701-704.
- [10] W. Martienssen, J. Phys. Chem. Solids 1957, 2, 257

P8 - First principle study of electronics properties of Sb-doped SnO₂(110) surfaces

A.Boumeddiene⁽¹⁾, F. Bouamra⁽¹⁾, H.Belkhir⁽²⁾

⁽¹⁾ Physics Department, Surfaces, Interfaces and Thin Films Laboratory (LASICOM), Blida University, Algeria

⁽²⁾ Physics Department, LESIMS, Annaba University, Algeria

Introduction

Tin oxide film is a wide gap n-type semiconductor ($E_g = 3.6$ eV) having the rutile crystal structure. Dopants such antimony, indium, or fluorine are added to improve the electrical or sensing properties of tin oxide [1-4]. The aim of the present work is to use first-principles calculations to help in the interpretation of Sb-doped SnO₂ experimental result on the variation of the SnO₂ surface conductivity with respect to the atomic Sb/Sn ratio.

Computational details and geometric models

The computational density functional theory (DFT) applied here for periodic system is based on scf-lcao method and pseudopotential approximation using the hybridized B3LYP exchange-correlation functional. The Sn_{48-2n}O₉₆Sb_{2n} ($n = 2, 3, 4, 5$) supercells used in the calculation was generated by replacing 4, 6, 8 and 10 Sn ions in outermost in-plane by 4, 6, 8 and 10 Sb ions in the (4x2) 9L supercell of the stoichiometric (110) surface. The equilibrium structure was obtained after the supercell geometry were fully relaxed by minimizing the total energy.

Relaxed surface electronic structure: The band structure shows a qualitative change in the energy related to VB, CB, band gap, together with a shift of E_F towards CB, resulting in the appearance of new occupied surface states in band gap with increasing x from 9.09 to 26.31%. for $x=9.09\%$, the upper part of VB consists of O_{2c}-2p, O_{s2c}-2p, O_{3c}-2p and O_{v3c}-2p orbital while the lower part of CB is mainly formed from hybridized Sn_{5c}-5sp and O_{3c}-2p with significant mixture of Sn_{6c}-5s and Sb_{6c}-5sp orbital. For $x=14.28\%$, a number of change are noted in the lower part part of CB compared to that for $x=9.09\%$. An additional of three peaks associated to the news surface states appears in the band gap. With increasing x to 20%, there is no substantial change in the structure of these peaks. The lower part of CB mainly originates from hybridized Sn_{5c}-5sp mixed with O_{3c}-2p orbital are presents in the band gap. Again, the hybridized Sn_{5c}-5sp mixed with O_{3c}-2p orbital dominate the lower CB crossed by E_F . In progress from $x=20$ to 26.31%, the upper part of VB exhibits the same predominant orbital as for $x=9.09$ and 20%. The lower part of CB exhibits two surface bands as in stoichiometric (110) surface. The Calculated band gap between the VBM and the CBM are summarized in table 1. The band gap value decrease from 1.68 eV for stoichiometric (110) surface, i.e $x = 0$, to the minimum of 0.63 eV at $x =$

14.28% and then increase to 1.44 eV at $x = 26.31\%$. The oxidation states results shows that both Sb_{5c} and Sb_{6c} are a donor centers.

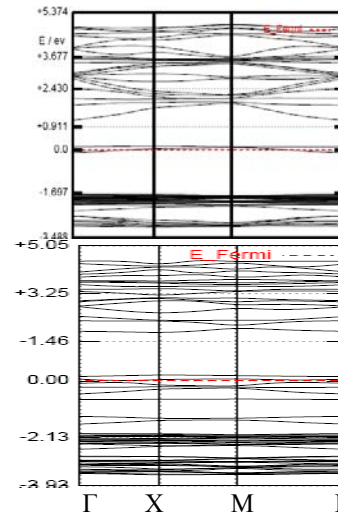


Fig.1: Band structure of stoichiometric

Table.1: Calculated Fermi Energy (E_F), VBM energy, CBM energy and optical band gap (eV)

Sb/Sn (%)	0	9.09	14.28	20	26.31
E_F	-6.56	-6.13	-6.16	-5.92	-6.09
VBM	-8.34	-8.05	-7.51	-7.85	-7.29
CBM	-6.66	-6.83	-6.88	-7.10	-5.85
gap _{op.}	1.68	1.22	0.63	0.74	1.44

Conclusions: As a result, the improved surface conductivity can be attributed to narrowing of the surface band gap coupled with the additional ingap surface states and the increase of the conduction electron concentration at the surface due to the symmetric and homogeneous distribution of Sb substituted for both Sn_{5c} and Sn_{6c} of the stoichiometric SnO₂(110) surface.

References

- [1] G. Korotcenkov, V. Brynzari, S. Dmitriev, Materials Science and Engineering B56 (1999) 195-204
- [2] G. Jimenez Cadena, J. Riu, F. X. Rius, Gas Sensors based on nanostructured Materials, Analyst 132(2007) 1083-1099
- [3] M. Batziel, U. Diedold, Prog. Surf. Sci. 79 (2005) 47
- [4] Y. Lee, K. Lee, D. Lee, Y. Jeong, H. S. Lee, Y. Choa, Curr. Appl. Phys. 9 (2009) 579.

P9 - Electrical properties of epoxy based nanocomposites

A. Bouzidi¹, H. Smaoui¹, H. GUERMAZI¹, L. EI MIR²

¹ Unit of Physics of insulators materials, IPEIS, Route Menzel Chaker, km 0.5, BP 1172, Sfax 3018, TUNISIA

²Physics Laboratory of Materials and Nanomaterials Applied to the Environment, Faculty of Sciences of Gabes, City Erriadh Zrig Manara, 6072 Gabes, TUNISIA

E-mail address : bouzidi.abdelfatteh@yahoo.fr

hichem.smaoui@fss.rnu.tn

hj.tounsi@ipeis.rnu.tn

Lassaad.ElMir@fsg.rnu.tn

Introduction: The material of this study is an epoxy polymer modified by the addition of conductive nanoparticles. Objective is to study the electrical properties of the composite and their evolution in function of the fraction added. Various experimental techniques were used in this study (Thermostimulated depolarisation currents (TSDC), dielectric relaxation spectroscopy (DRS) and thermal step method (TSM)).

Abstract: The material object of this study is an epoxy polymer modified by the addition of the ITO (Indium Oxide of Tin) conducting nanoparticles with different concentrations (in the range 0 – 2 wt. %). We were interested in this study to the electric properties of these nanocomposites. Different experimental complementary techniques were used: thermostimulated depolarisation currents (TSDC), dielectric relaxation spectroscopy (DRS) and thermal step method (TSM).

TSDC and TSM measurements have shown that heterogeneity induced by the incorporation of the ITO nanoparticles has increased the trapped space charges density. The quantity of dipolar relaxed charges during the TSDC measurements has also increased.

DRS measurements performed in the frequency range 1Hz – 10⁶Hz and at room temperature, have shown the existence of a dipolar relaxation around 10⁵ Hz which was influenced by the incorporation of the nanoparticles and confirms the TSDC and TSM results.

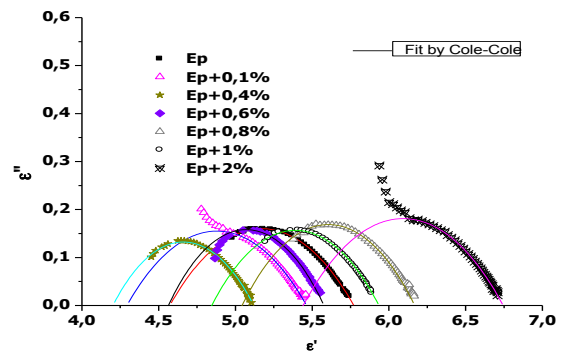
Key Words: Epoxy polymer, nanocomposites, space charges, dipolar relaxation.

Figures and Tables:

samples	α
pure Ep	0,667±0.001

Ep+0,1%	0,670±0.001
Ep+0,4%	0,643 ±0.003
Ep+0,6%	0,615±0.006
Ep+0,8%	0,628±0.003
Ep+1%	0,643±0.002
Ep+2%	0,655±0.004

Table 1: Values of the parameters fit of the experimental data by Cole – Cole model for the various samples



References:

- C. Bucci, R. Fieschi, G. Guidi, Ionic thermocurrents in dielectrics, Phys. Rev. 148 816-823, 1966.
- M. R. Neagu et al; "Evaluation of the dielectric parameters from TSDC spectra: application to polymeric systems"; Mat Res Innovat, 4: 115-125, Springer-Verlag, 2001.
- S. Hdiji, F. Namouchi, H.Medhioub, H.Guermazi, S.Guermazi, J.Castellon, S.Agnel, A.Tourelle: "Thermally Stimulated Depolarization Current analysis to the determination of polarization and relaxation parameters in aged PMMA", Materials Science and Engineering; 41, 2010.
- Tsangaris GM, Psarras GC, Kouloumbi N, «Electric modulus and interfacial polarization in composite polymeric systems », J Mater Sci; 33:2027-37, 1998.

P10 - Novel zwitterionic schiff base compound as corrosion inhibitor for mild steel in acidic media

A. Djedouani^{1,2*}, L. Hasniou², W. Merouani³, H. Boulemche³, S. Chafaa²

¹Laboratoire d'électrochimie des matériaux moléculaire et complexes
²Ecole Normale Supérieure de Constantine

*Corresponding author : E-mail address : djed_amelle@yahoo.fr

³Département de Chimie, Université Mentouri Constantine

The use of inhibitors is one of the most practical methods for protection against corrosion especially in acidic media [1]. Acid solutions are generally used in several industrial processes. HCl is widely used in pickling solutions. Because of their aggressiveness, the use of corrosion inhibitors is considered as the most effective method for the protection of many metals and alloys against such acid attack [2], reduces the dissolution rate of metals. Compounds containing functional groups with heteroatoms, which can donate one pair of electrons, are found to be very efficient as inhibitors against metal corrosion in many environments. Many heterocyclic compounds with polar groups and/or π electrons are efficient corrosion inhibitors in acidic solutions.

Organic molecules of this type can adsorb on the metal surface and form a bond between their N-electron pair and/or π electron cloud and the metal surface, thereby reducing the corrosion in acidic solutions [3]. Some Schiff bases inhibitors have been previously reported as effective corrosion inhibitors for various metals in acid media, such as Schiff bases containing oxygen substituents [4,5], and furoin thiosemicarbazone [6].

The aim of the present investigation is to examine the inhibitory action of ... (E)-6-methyl-2-oxo-3-[1-(p-tolyl-iminio)ethyl]-2H-pyran-4-olate Schiff bases containing nitrogen and oxygen heteroaromatic compound as substituents in its structure for the corrosion of mild steel in 1 M HCl solution, with and without addition of various concentrations of Schiff base at different concentration, using potentiodynamic and electrochemical impedance techniques. Polarisation curves reveal that the compound is mixed type (cathodic/anodic) inhibitor and inhibition efficiency (% IE) increases with increasing concentration of

compounds. The adsorption of Schiff bases on mild steel in 1 M HCl solution obeys Langmuir adsorption isotherm. The negative values of ΔG_{ads} show the spontaneity of the adsorption.

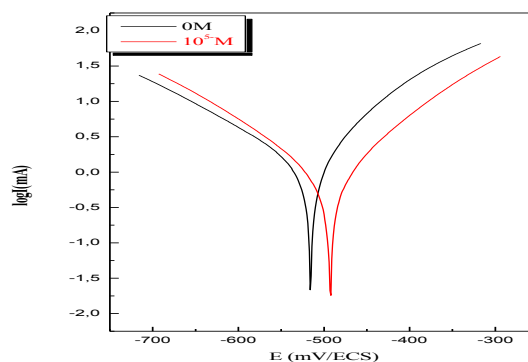


Figure 1 : Tafel polarisation curves for mild steel obtained at 25 °C in 1 M HCl containing different concentrations of Schiff base..

References :

- Bergmann, I.I. (1963) Corrosion Inhibitors, Macemillan, New York.
- Cruz, J R. Martinez, J. Genesca, E.G. Ochoa, J. Electroanal. Chem. (2004) 566 111–121.
- Ismail, K.M. (2007) Electrochim. Acta 52, 7811–7819, 2007.
- Behpour, M. Ghoreishi, S.M. Soltani, N. Salavati-Niasari, (2009) M. Corros. Sci 51, 1073–1082, 2009.
- Yurt, A. Balaban, A. Ustun Kandemir, S. Bereket, G. Erk, B. (2004) Mater. Chem. Phys. 85, 420–426, 2004.
- Stanly Jacob, K. Geetha Parameswaran, (2010) Corros. Sci. (2010) 52, 224–228, 2010.

P11 - Investigation of kink effect in indium doped silicon for sub 100 nm N channel MOSFET technology.

A.Fargi^{*1}, N. Hizem¹, A.Kalboussi¹, A. Souifi².

¹Laboratoire de Microélectronique et Instrumentation, Faculté des Sciences de Monastir, Université de Monastir, TUNISIA

*Corresponding author : E-mail adress : fargi.abdelaali@gmail.com

² Institut National des Sciences Appliquées de Lyon, France.

Abstract:

Low temperature operation of Silicon NMOS transistors is a promising way to improve the circuit performance. The temperature reduction allows the increase of the carrier mobility and saturation velocity, reduction in activated degradation processes, decrease of leakage current, reduced thermal noise, increased thermal conductivity, [C. Huang, E. Simoen and J. C. Woo]. For instance, the impurity freeze-out, kink phenomenon, series resistance effects, transient behavior, changes in mobility laws make it difficult the physical understanding and modeling of the MOS device operation at low temperature (77-300K).

In this paper, a brief review of the main physical properties of Indium doped Si NMOS devices operated at low temperature is presented. The influence of the impurity freeze out on the device operation via the kink effect is discussed. The effect of traps related to Indium in Si NMOS transistors is also investigated.

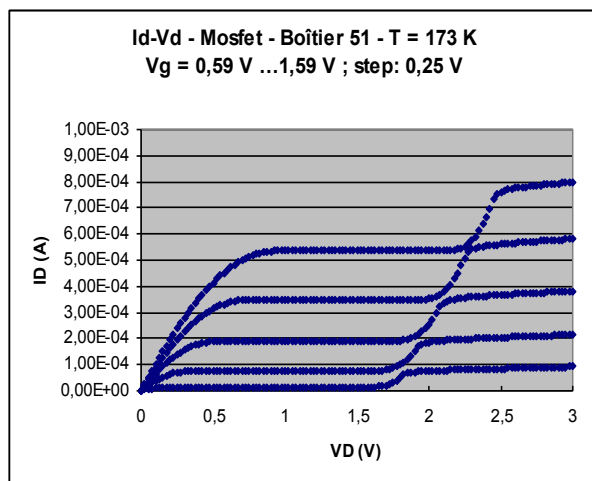


Figure 2: I_D - V_D Characteristics for different gate voltages showing the Kink Effect at $T=173$ K.

The main results show that traps related to Indium in Si could be responsible of the kink effect at low temperatures such as shown in Figure 1 and which can be confirmed by the substrate effect even at room temperature.

References:

- Aaron A. Prager, Hubert C. George, Alexei O. Orlov, and Gregory L. Snider, (2008) Cryogenic MOSFET kink effect abatement, Silicon Nanoelectronics Workshop IEEE, 15-16 June 2008, 1-2.
- Alexandre Siligaris, Gilles Dambrine and François Danneville, (2004) Non-Linear Modeling of the Kink Effect in Deep Sub-micron SOI MOSFET, Proceeding Of 12th European Gallium Arsenide and Other Compound Semiconductors Application Symposium (GaAs), Amsterdam, 47-50.
- C. Huang and S. Gildenblat, (1990) Measurements and modeling of the n-channel MOSFET inversion layer mobility and device characteristics in the temperature range 60-300 K. IEEE Transactions on Electron Devices, 37, 1289-1300.
- E. Simoen, B. Dierickx, L. Warmerdam, J. Vermeiren and C. Claeys, (1989) Freeze-out effects on NMOS transistor characteristics at 4.2 K. IEEE Transactions on Electron Devices, 36, 1155-1161.
- I.M. Hafez, G. Ghibaudo, F. Balestra, (1990) Analysis of the Kink Effect in MOS Transistors. IEEE Electron Device Letters, 11, 818-821.
- J.C. Woo and J.D. Plummer, (1986) Short-channel effects in MOSFET's at liquid-Nitrogen temperature. IEEE Transactions on Electron Devices, 33, 1012-1019.

P12 - AVHRR-NOAA and MODIS-Aqua/Terra data receiving and processing system

A.Hassini^{1,2*}, A.H. Belbachir²

¹Institut of Maintenance and Industrial Security –University of Oran Es-Senia, Oran, ALGERIA

*Corresponding author : E-mail address : hassini.abdelatif@univ-oran.dz

² Laboratory of Analysis and Application of Radiation, USTOMB , Oran, ALGERIA

Introduction: Meteorological satellite data provided by the geostationary and polar-orbital satellite are operationally received, pre-processed and archived at LAAR Lab. Meteorological products and geophysical parameters are derived and made available to the operational services like the vegetation coverage state and surface temperature images determination. LAAR Lab is equipped with a data acquisition system and a NOAA motorized system. In October 2011 a new AVHRR and MODIS Earth station was installed and is fully operational including data processing and archiving. The received images are calibrated to become significant physically. A mathematical function of the visible and infrared parts of the electromagnetic spectrum can be an indicator of the presence and condition of the vegetation. This leads us to the concept of Normalized Difference Vegetation Index (NDVI), which is an indication of the amount of green vegetation, the NDVI image was processed by combining the Channels 1 and 2, visible and near infrared, respectively, of AVHRR/3-HRPT satellite data. The Surface Temperature (TS) is a fundamental thermodynamic quantity in the energy exchange between the surface and the atmosphere and plays an important role in environmental studies. Many studies have proposed various algorithms, such as the split window method, for retrieving surface temperatures from two different thermal infrared bands of NOAA satellite data. Each algorithm is developed for a limited study area and application. Here, as part of the use of one split-window method in raw acquired data. A comparison of TS image result with the brightness temperature of each thermal infrared band is established to evaluate the performance of the used algorithm.

Acquisition System: Since September 2011 we archive AVHRR and MODIS data covering some area from terrestrial half disk, centred in North West of Africa. At the beginning of the reception period the station was not completely operational and we lost some passes due to maintenance of the receiving station as well as limited hardware and storage capacity. Since October 2011 we are in an operational status to receive all available NOAA passes per day. The amount of archived data exceeds the number of 200 NOAA-AVHRR images

takes from NOAA-17, NOAA-18, NOAA-19 and MODIS-7, respectively. Figure 1 shows a flowchart of the acquirement system. These data sets can be used for a variety of remote sensing applications, and daily captured with a feed horn motorized system and image processing equipment.

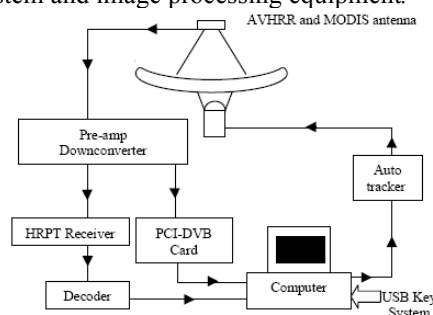


Figure. 1 Flow chart of Satellite images Realized Station

Pre-Processing: High Resolution Picture Transmission (HRPT) imagery was collected in real time from the National Oceanic and Atmospheric Administration's Satellites (NOAA). The visible channels (c1 and c2) were calibrated and converted to percent reflectance (Albedo) using our PCNOAA software and ENVI (The Environment for Visualizing Images, Research Systems, Inc., Boulder, USA) software with auxiliary parameters. The thermal IR channels (c4 and c5) were calibrated in brightness temperatures.

References:

- B. Katherine, N. Kidwell, NOAA Polar Orbiter Data Users Guide, NESDIS, USA November 2000.
- Coll, C., Casselles, V., Sobrino, J. A., and Valor, E., On the atmospheric dependence of the split-window equation for land surface temperature. International Journal of Remote Sensing, Vol. 15, n°11, 1994, pp. 105-122.
- G. Goodrum, K. B. Kidwell, W. Winston, "NOAA KLM user's guide with NOAA-N, -N' ", supplement, Appendix D.4, 2005.
- Sobrino, J. A., and Raissouni, N., Toward remote sensing methods for land cover dynamic monitoring: application to Morocco. International Journal of Remote Sensing, Vol. 21, No. 2, 2000, pp.353-366.

P13 - Hydrogen peroxide biosensor based on horseradish peroxidase immobilized on functionalized porous silicon

A. KERMAD^{1, 2*}, S. SAM¹, N. GHELLAI², N.E. GABOUZE¹.

¹Unité de développement de la Technologie du Silicium, UDTS, 02 Bd. Frantz-Fanon, B.P. 140, Alger-7 merveilles, Algiers, ALGERIA

²Unité de Recherche Matériaux et Energies Renouvelables, URMER, Département de Physique, Faculté des Sciences, Université Abou Baker Belkaid, B.P. 119, Tlemcen 13000, ALGERIA

*E-mail : amina_energetique@yahoo.fr

Tel/Fax: 043. 21. 58. 90 & 89

Introduction: In recent years, amperometric biosensors based on horseradish peroxidase (HRP) have been considered as the most effective measure for the determination of hydrogen peroxide (H₂O₂), which is of practical importance in many fields, including chemistry, biology, industry, clinical control and environmental protection, etc. Conventional H₂O₂ detection methods, such as titrimetry, chemiluminescence, fluorimetry, and spectrometry, are generally time-consuming and cumbersome for operation. Now electrochemical biosensors offer an attractive route because of their simplicity, high sensitivity and selectivity. The development of biosensors depends mainly of the coupling a biological entity with a suitable transducer. The excellent biocompatibility and capability of porous silicon to improve the electron transfer make it extremely attractive for applying to electrochemical biosensors. Moreover, the internal surface of porous silicon is hydrogen-terminated, which allows one to immobilize large quantities of biomolecules in a relatively small volume through bioconjugation.

Content: In the present work, it was reported the functionalization of porous silicon surface in order to immobilize HRP. Multistep strategy was used allowing maintaining the enzymatic activity. First, acid terminations were generated on porous silicon surface by thermal hydrosilylation of undecylenic acid. Then, the carboxyl-terminated monolayer was transformed to active ester (succinimidyle ester) using N-hydroxysuccinimide (NHS) in the presence of the coupling agent N-ethyl-N'-[3-(dimethylaminopropyl) carbodiimide (EDC). Subsequently, the enzyme was anchored on the surface via an amidation reaction. Infrared spectroscopy (FTIR) was used to investigate the different steps of functionalization. The direct electron transfer of immobilized HRP and its electrocatalytic response to the reduction of H₂O₂ were studied by cyclic voltammetry. Hydrogen peroxide concentration has been optimized. Figure (1) shows the FTIR spectra in transmission of the different stages of functionalization of the surface of porous silicon with immobilized HRP. The successive steps of functionalization of the

surface of SiP are illustrated by the changes undergone by the FTIR spectra at each stage.

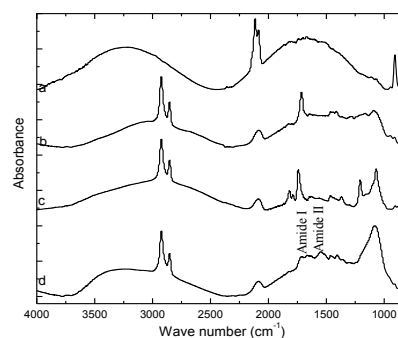


Figure 1: Transmission IR spectra of porous silicon layers: hydrogenated surface, after electrochemical fabrication (a); acid surface, after thermal grafting of undecylenic acid (b); after an activation treatment in an aqueous solution of EDC and NHS (c); after covalent immobilization of HRP (d).

The considerable decrease in intensity of the bands ν Si-Hx (between 2140 to 2085 cm^{-1}) (spectrum 1-a) and the appearance of ν C=O band (1715 cm^{-1}) confirms the grafting of acid (spectrum 1-b). The success of the activation step is verified by the disappearance of the band (spectrum 1-c) ν C=O of the acid and the appearance of the triple (between 1820 and 1745 cm^{-1}) corresponding to the succinimidyl ester. The presence of immobilized HRP enzyme on the functionalized surface of porous silicon was confirmed also by FT-IR spectra. Specter (1-d), showing the absence of the triplet characteristic of the succinimidyl ester and the appearance of the characteristic amide I band (1662 cm^{-1}) and amide II band (1550 cm^{-1}). The amide I band (1700–1600 cm^{-1}) is attributed to C=O stretching vibration of peptide linkages in the backbone of protein. The amide II band (1620–1500 cm^{-1}) results from the combination of N–H bending and C–N stretching.

References:

Archer. M and al. (2004) Biomed. Microdevices, 6, 211.

Canham. L. T. (1995) Adv. Mater, 7, 1033.

P14 - Spectroscopic ellipsometry and X-ray diffraction characterizations of the reactive sputtering powers effects on the physical properties of CuO thin film

A. Labidi¹, A. Bejaoui^{1,2}, J. Guérin², M. Maaref¹, K. Aguir²

¹URPSC (UR 99/13-18) Unité de Recherche de Physique des Semiconducteurs et Capteurs, IPEST, Université de Carthage, BP 51, La Marsa 2070, Tunis, Tunisia.

²IM2NP (UMR 6242 CNRS), Université Paul CEZANNE Aix-Marseille III, FST, Campus de St. Jérôme, Service 152 - 13397 Marseille Cedex 20, France.

Abstract

The cupric oxide (CuO) films were deposited on Si/SiO₂ substrates by reactive radio-frequency (RF) magnetron sputtering at different RF deposition powers of such as 40, 60, 80 and 120W. The effect of RF deposition powers on the structural, morphological and optical properties of the films was investigated using X-ray diffraction (XRD) and atomic force microscopy (AFM).

The films optical properties were studied by spectroscopic ellipsometry measurements (Figure.1), in order to determine the effects of RF deposition powers on the refractive index "n", extinction coefficient "k", thickness and the films band gaps "E_g". The investigations show that the prepared CuO thin films were a direct p-type semiconductor with a single phase orientation along the (020) direction. We note that the CuO thin film prepared at 80 W exhibits the best physical properties for further CuO based sensor applications.

These behaviors were attributed to the films morphological changes confirmed by AFM investigations (Figure.2). These variations were already could be explained by the Bruggman's effective medium theory [1], taking into account films growth conditions, morphology and structural variations [2].

References

[1] N.K. Sahoo, S. Thakur, R.B. Tokas, N.M. Kamble, Relative performances of effective medium formulations in interpreting specific composite thin films optical properties, Appl. Surf. Sci. 253 (2007) 6787–6799.

[2] C. Charton, M. Fahland, Optical properties of thin Ag films deposited by magnetron sputtering, Surf. Coat. Technol.;174 –175 (2003) 181–186.

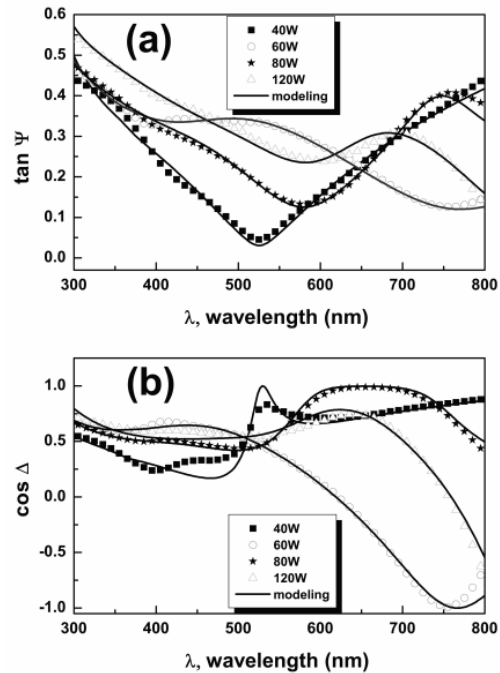


Figure 1: Ellipsometric measurements and modeling of CuO thin films: (a) Tan(Ψ) and (b) Cos(Δ).

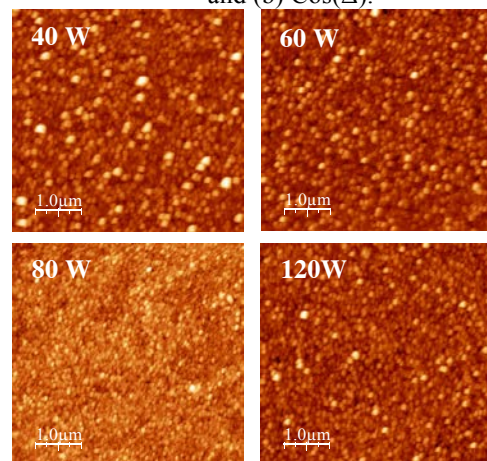


Figure 2: AFM microstructures of CuO thin films at different RF powers.

P15 - Study of vanadium doping effects on structural and optical properties of sprayed ZnO thin films

A. Mhamdi , A. Boukhachem, M. Madani, A. Amlouk* and M. Amlouk

Unité de physique des dispositifs à semi-conducteurs

Université Tunis EL MANAR, 2092 Tunis, TUNISIE

*Corresponding author : E-mail adress : Amel.Amlouk@fsg.rnu.tn

Introduction:

Zinc oxide ZnO represents hence an important basic material for the construction of nanoscale structures. Due to its low cost as well as its favorable opto-electronic and electro-luminescent properties, it has been satisfactorily involved in acoustic devices [8], fluid sensors [3], transparent electrodes [1], and solar cells [2, 4, 5, 6, 7].

Commonly, this oxide could be synthesized using several methods such as: reactive evaporation, electron beam evaporation (EBE), pulsed laser deposition (PLD), chemical vapor deposition (CVD), sol-gel coating, and chemical spray pyrolysis.

In this work, the sprayed pyrolysis technique was carried out to prepare Vanadium doped ZnO thin films with different controlled percentage (1-20%). Particularly, it has been demonstrated, through original conjoint morphological-structural and optical investigations some interesting physical properties. Indeed, X-ray diffraction (XRD) analysis show that the films with doping concentration less than 10 at.% have a wurtzite structure and grow mainly along the c-axis orientation. The surface morphology of the ZnO:V thin films was examined by AFM. On the other hand, the optical constants (refractive index, extinction coefficient, the dielectric constants ($\epsilon_1(\lambda)$ $\epsilon_2(\lambda)$) and the dielectric susceptibility χ_e) have been obtained by fitting the transmittance. The optical band gap energy changed from 3.12 to 3.72 eV as doping concentration increased from 1at.% to 20 at% mol. All the result have been discussed in terms of vanadium doping concentration.

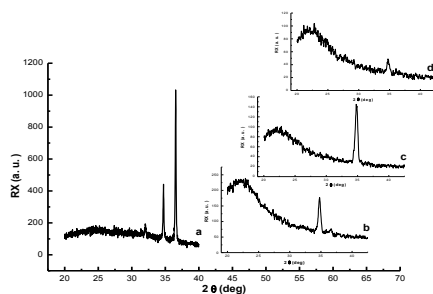


Figure 1: XRD patterns of ZnO thin films : (a) ZnO pur, (b) ZnO:V 1at.%, (c) ZnO:V 2at.%, (d) ZnO:V 3at.%.

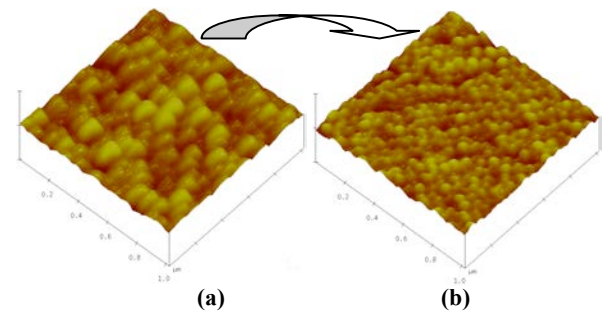


Figure 2: AFM (3D) micrographs of sprayed thin films: (a) ZnO:V 1at.%, (b) ZnO:V 3at.%.

References:

- [1] F. Michlotti, A. Belardini, A. Rousseau, A. Ratsimihety, G. Schoer, J. Mueller, J. Non-Cryst. Solids 352 (2006) 2339-2344.
- [2] J. Hupkes, B. Rech, O. Kluth, T. Repmann, B. Zwayagardt, J. Muller, R. Drese, M. Wutting, Sol. Energy Mater. Sol Cells, 90 (2006) 3054-3066.
- [3] M. Suche, S. Chiritoulakis, K. Moschovis, N. Katsarakis, G. Kiriakidis, ThinSolid Films 515 (2006) 551-566.
- [4] N. Phuangpornpitak, S. Kumar, Renew. & Sust. Energy Rev., 1, (2007) 1530-1543.
- [5] S. Nagae, M. Toda, M. Minemoto, H. Takakura, Y. Hamakawa, Sol. Energy Mater. Sol Cells, 90 (2006) 3568-3575
- [6] S. Rehman, I. M. El-Amin, F. Ahmad, S. M. Shaahid, A. M. Al-Shehri, J. M. Akhashwain, A. Shash, Renew. & Sust. Energy Rev., 11, (2007) 635-653
- [7] W. J. Jeong, S. K. Kim, G. C. Park, Thin Solid Films 506–507 (2006)180-199.
- [8] W. Water, S.-Y. Chu, Y.-D. Juang,S.-J. Wu, Mater. Lett., 57 (2002) 998-1004.

P16 - Optimization of the interface anode / organic materials in organic solar cells

⁽¹⁾A.Mohammed-Krarroubi, ⁽¹⁾L.Barkat, ⁽¹⁾FZ. Dahou, ^(*)J.C Bernede, ⁽¹⁾ A. Khelil.

(1) Physics laboratory of the Thin Layers and Materials for Electronics LPCMME, Department of Physics, University of Oran. Algeria.
Mohammed-krarroubi Asmaa E-mail: mk_asmaa@hotmail.fr

(*) Physics laboratory of the solids for Electronics
University of Nantes, BP92208, 44322 Nantes Cedex 3, France

Abstract:

The anodes and the nature of their contact with organic materials play a key role in obtaining efficient optoelectronic components

To maximize a good contact is required to submit to the anode surface treatment and / or using a buffer layer [1]. For optoelectronic component it is necessary that the anode is transparent, hence the use of a transparent conductive oxide (TCO) which is generally the ITO (indium oxide doped with tin). In fact, component properties depend strongly on the nature of the TCO. The ITO is the most efficient but it has several disadvantages: its properties, techniques for obtaining well the scarcity of indium plus indium is a too toxic. We propose to prepare a new TCO that has the same surface properties of ITO to replace a structure of multi-leaf type oxide / metal / oxide deposited by thermal evaporation under vacuum.

In the present work, we characterized the layers stacked oxide / metal / oxide prepared under thermal evaporation measurements by scanning electron microscopy, X-ray diffraction measurements as well as optical and electronic. As a result, the layers are conductive and transparent in the visible due to its characterization; we achieved organic photovoltaic cells using these layers as anode in these components. Provided it was shown that it is necessary to conduct a surface treatment of TCO obtained before deposition of organic materials. Among the various treatment options, we have shown that the introduction of a thin layer of gold and / or molybdenum oxide can optimize the performance of photovoltaic cells via the adaptation of the band structure at the interface and improving the growth of organic layers[2,3] Organic solar cells made for this application are composed of

active torque: the copper phthalocyanine (CuPc), the fullerene (C60), the cells are of type:

TCO/MoO₃ / Au/CuPc/C60 / BCP / Al / Se; the use of a thin layer of Au and / ou MoO₃ can increase the performance of the cell. This addition is well suited for the HOMO of the organic layer CuPc (work function of gold = 5.1 eV, work function of MoO₃ = 5.4eV) as it posted a return equal to 1.85%

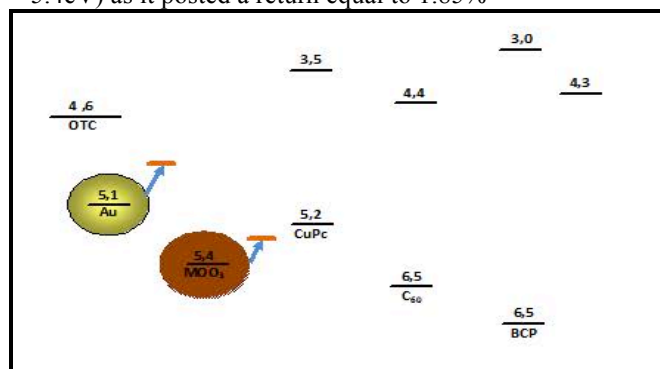


Fig 1: energy diagram

References :

- [1] J. C. Bernède, L. Cattin, M. Morsli, Y. Berredjem, Solar Energy Materials and Solar Cells, 92 (2008) 1508.
- [2] L. Cattin, F. Dahou, Y. Lare, M. Morsli, R. Tricot, S. Houari, A. Mokrani, K. Jondo, A. Khelil, K. Napo, J.C. Bernède, Investigation of low resistance transparent MoO₃/Ag/MoO₃ multilayer and application as anode in organic solar cells Journal of Applied Physics 105 (2009) 034507.
- [3] S.S. Braun, W.R. Salaneck, M. Fahlman, Adv. Mater., 21 (2009) 1450.

P17 - Theoretical investigation of the electronic properties of wurtzite $\text{In}_x\text{Ga}_{1-x}\text{N}$ alloys

A.Said¹, Y. Oussaifi¹, D.Ceresoli², and M. Said¹

¹Laboratoire de la Matière Condensée et des Nanosciences (LMCN), Département de Physique, Faculté des Sciences de Monastir, Avenue de l'Environnement, 5019 Monastir, Tunisie

²CNR-ISTM: Institute of Molecular Sciences and Technologies, Via Camillo Golgi, 19, 20133 Milano, Italy

*Corresponding author: Tel + 216-73500276, Fax: + 216-73500278, E-mail address: moncef_said@yahoo.fr

Abstract:

Heterostructures based on III-V nitrides gained in recent years considerable interest in the technology of light emitting diodes (LEDs) and lasers aimed to operate in a wide wave length spectrum ranging from visible to ultraviolet.

Since the III-nitride semiconductor devices are usually grown on the sapphire substrate, they all have wurtzite crystal structures.

Using the Empirical Pseudo potential Method (EPM) combined with an improved Virtual Crystal Approximation (VCA), where the effect of compositional disorder is included as an effective periodic potential, we have calculated the electronic properties of GaN and InN and their alloys $\text{In}_x\text{Ga}_{1-x}\text{N}$ in the wurtzite structure for the entire range of alloy concentrations.

The form factors were adjusted to reproduce band features which agree with recent experimental data.

Several researchers have investigated the band gap bowing parameters of these alloys.

However, the results are quite diverging. In this work we suggest that $\text{In}_x\text{Ga}_{1-x}\text{N}$ ($0 < x < 1$) alloys have a band gap bowing parameter of -2.388 eV. The agreement with experimental band gap $E_g^r = 2.966\text{eV}$ at indium fraction molar $x = 0.1$ [1] is reached for the value of $p = -0.458$.

The electron effective masses (a transverse and longitudinal masses) at the Γ point of $\text{In}_x\text{Ga}_{1-x}\text{N}$ alloys were also calculated as a function of indium molar fraction x .

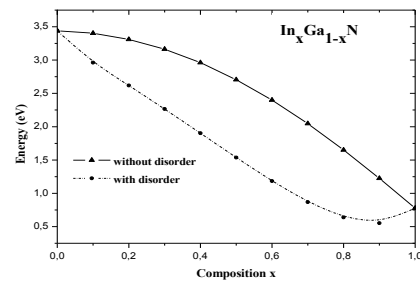


Figure 1: Energy gap as a function of x for wurtzite $\text{In}_x\text{Ga}_{1-x}\text{N}$ at Γ point calculated without disorder (standard VCA) and with compositional disorder (improved-VCA).

	<i>Without disorder</i>	<i>With disorder</i>
Bowing	-2.388	$0.257x + 3.951$

Table 1: Fundamental gap bowing parameters b (in eV) of InGaIn in the wurtzite structure

	<i>Without disorder</i>	<i>With disorder</i>
m^{\perp}	-0.234	$0.411x - 0.139$
m^{\parallel}	0.138	$-0.331x + 0.328$

Table 2: Bowing factors for electron effective masses of InGaIn calculated at conduction band minima

Reference:

- [1] M. D. McCluskey, C. G. Van de Walle, L. T. Romano, B. Krusor and N. M. Johnson. (2003) Effect of composition on the band gap of strained $\text{In}_x\text{Ga}_{1-x}\text{N}$ alloys. Journal of Applied Physics, 93, 4340.

P18 - Application of the near infra-red radiation in Medical imaging

A. Saouli¹, F. Mansour and K.Mansour

Laboratory of Electronic Materials Study for Medical Applications (LEMEAMED)

Electronic Department, Constantine University-ALGERIA

¹Abdou.zezou@yahoo.fr

Abstract:

Diffusive Optical Tomography (DOT) is a rapidly developing imaging technology for medical diagnoses and biomedical research. Breast cancer detection, brain function study, infant and fetus monitoring and arthritis diagnosis are among the numerous applications of DOT [Chen, N. G et al]. The advantages of the optical techniques in diagnostic modalities are significant and include the complete non-invasiveness, the use of harmless, non-ionising radiation and the prospects for revealing chemical contrast, which can represent valuable physiological information. The tomography imaging is an extension of the spectroscopy and the instrumentation used is common to both fields. Indeed, in Near-Infrared Spectroscopy (NIRS) of tissue, light attenuation is due to the absorption from chromophores of fixed concentration, the absorption from chromophores of variable concentration, and the light scatters [Delpy, D.T et al]. Therefore, the DOT is based on detection of a near InFra-Red Pulse (NIRP) called Time Pulse Spread Function (TPSF) on surface of the tissue sending by an optical source and simulation of propagation of this pulse source in our object. The combination between measured TPSF and simulated TPSF can be reconstructed an optical map of the optical properties of the study object. This optical map presents the image in DOT. Thus, the optical source has a significant role in reconstruction of the optical image [Saouli, A et al]; in this work we present the simulation of NIRP propagation in biological tissue and the influence of source frequency. This simulation is based on element finite method (FEM) programmed in COMSOL Multiphysics Software (Source pulse (Figure 3), maps intensity after 1.5×10^{-9} second times of simulation (Figure 2)).

Keywords: Diffusive optical tomography, near infra-red pulse, element finite method, source frequency.

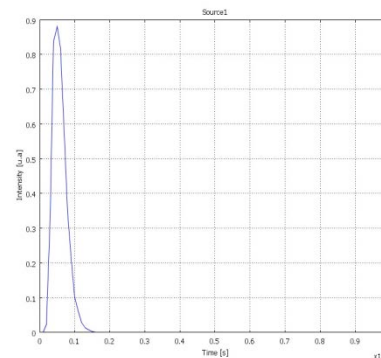


Figure 1: intensity source in time.

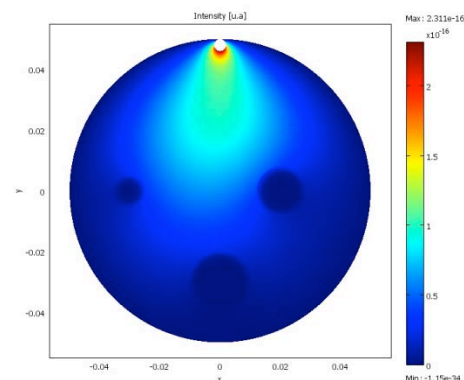


Figure 2 : maps intensity after 1.5×10^{-9} second.

References

- Chen, N. G., Zhu, Q. , Time-resolved diffusive optical imaging using pseudo-random bit sequences ,(2003), OPTICS EXPRESS, Vol. 11, No. 25 ,pp. 3445-3454.
- Delpy, D.T., Cope, M. (1997), Quantification in tissue near-infrared spectroscopy, Phil. Trans. Royal Society, vol. 352, pp. 649-659.
- Saouli, A., Mansour, K., Application of the finite elements method in optical medical imaging, IEEE conference proceeding (MMS) 2011 11th, pp 117–121.

P19 - Conception of single-electron memory with silicon nanowire using PSpice and Simon

A Soussou¹*, S Chatbouri¹, M Troudi¹, N Sghaier¹, A Kalboussi¹

¹Laboratoire de Microélectronique et Instrumentation
Faculté des Sciences de Monastir, Tunisia.

* Corresponding author: E-mail adress: soussou.asma.tt@gmail.com

Abstract:

To consolidate the synthesis of Nanowire Single-Electron Memory (NWSEM), we propose in this work a new theoretical model, which is suitable for efficient circuit simulation. The nanowire (NW) in our SNWSEM model is modeled by a series of seven islands separated by eight tunnel junctions (8TJs) to represent a semiconductor doped NW epitaxially grown from catalyst nanoparticles which is able to store electrons and can be named memory node[2]. The model is based on an equivalent circuit including a NW (for memorization) connected by the end (memory node) to the channel of Single Electron Transistor (SET for reading) between Drain and Source, a spacer capacitor for couplage, and a voltage source V_{Mem} combined with the first tunnel junction of NW for memorization commands (write/erase). We use the PSpice model SET published in [3] as a support. It is based on the orthodox theory of single-electron tunneling and determines the average current through the SET reader crossing the 8TJs as a function of the bias voltage, the gate voltage, the memorization voltage, and the temperature.

The PSpice simulation results represent a strong memory effect in the detector current while sweeping the writing voltage (Figure 4, Table 1). Finally we compared those results by others simulated in SIMON tool.

Figures and Tables

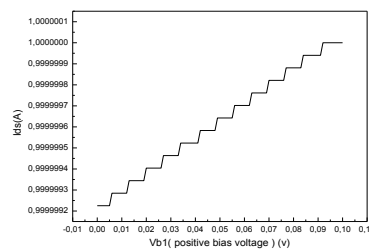


Figure 1: I(Vb2)_memorization process of SNWSEM

Vb1 (V)	I(Vb2) (A)
0	0.999999225139613
0.034	0.999999523162842
0.042	0.999999582767487
0.07	0.999999821186066
0.0920000000000001	1
0.1	1

Table 1: The corresponding table caption of SNWSEM memorization process

References:

- [1] Aïmen Boubaker, N. Sghaier, A. Souifi, and A. Kalboussi, (2010) Simulation and Modelling of the Write/Erase Kinetics and the Retention Time of Single Electron Memory at Room Temperature, Tunisia, France Journal of Semiconductor Technology And Science, vol.10, no.2 .
- [2] Claes Thelander, Henrik A. Nilsson, Linus E. Jensen, and Lars Samuelson, (2005) Nanowire Single-Electron Memory , Sweden, Nano Letters, vol.5, no.4, 635-638.
- [3] Günther Lientschnig, Irek Weymann and Peter Hadley, (2003) Simulating Hybrid Circuits of Single-Electron Transistors and Field-Effect Transistors, Netherlands, Japanese Journal of Applied Physics, Vol. 42 , pp. 6467–6472.

P20 - Effects of chemical modifications on optical, morphological, and electrical properties of three spin-coated PPV derivatives films

A. Touhami^{1*}, H. Hrichi¹, N. Jaballah², R. Ben Chaâbane¹, H. Ben Ouada¹, M. Majdoub²

¹ Laboratoire de Physique et Chimie des Interfaces (LPCI), Faculté des Sciences de Monastir, Bd. de l'Environnement, 5019 Monastir, Tunisia.

² Laboratoire des Polymères, Biopolymères et Matériaux Organiques (LPBMO), Faculté des Sciences de Monastir, Bd. de l'Environnement, 5019 Monastir, Tunisia.

*Corresponding author : E-mail adress : rafik.benchaabane@fsm.rnu.tn

Key words:

Poly (para-phenylene vinylene) derivatives, UV-Vis absorption, Morphology, Current-Voltage, Impedance spectroscopy.

Abstract:

Three organic diodes formed by sandwiching each new modified poly (para phénylènevinylène) layer between indium-thin oxide (ITO) and Aluminum (Al) contacts have been elaborated. The morphological, optical and electrical properties of spin-coated PPV derivatives thin films have been investigated. The energy band gap [5] of each thin film has been measured by UV-Vis absorption spectroscopy. Crystallinity and surface roughness [4] which is correlated with its hydrophobicity [1] have been determined by atomic force microscopy and by wettability test. The current-voltage (I-V) characteristics of ITO/PPV derivative/Al devices have been studied. The I-V dependence follows a

power law, $I \propto V^m$, which is typical of a space-charge-limited current (SCLC). Moreover, from the I-V measurements, we have estimated the effective hole mobility [2] in the PPV derivatives thin films. Using impedance spectroscopy in a frequency range between 100 Hz and 10 MHz for different bias voltage, it is found that the ac behavior of ITO/PPV derivative/Al devices shows several features. Therefore, the Cole-Cole plots were modeled as an equivalent circuit formed by a single parallel resistor and capacitor network placed in series with a resistance. Values of the electrical circuit parameters deduced from fitting experimental data to the model have given a dielectric relaxation time [3] in the millisecond range and an exponential trap distribution.

Figures:

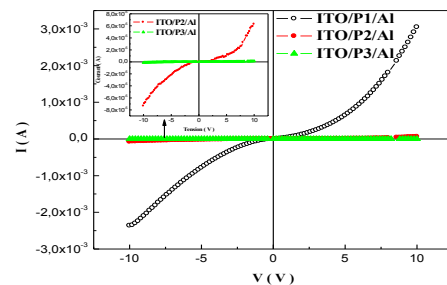


Figure 1: Current-voltage characteristics of ITO/P1/Al, ITO/P2/Al and ITO/P3/Al devices

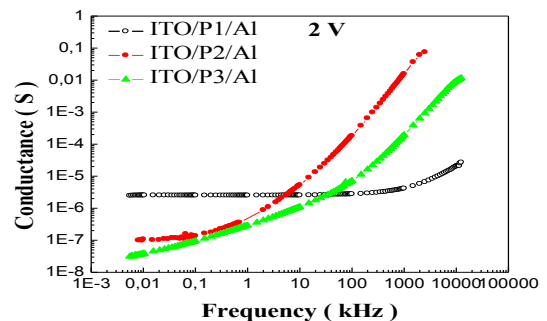


Figure 2: Variation of conductance versus frequency of the three devices at 2V.

References:

- [1] A. Abderrahmen, F.F. Romhane, H. B. Ouada and A. Gharbi, Science and technology of advanced materials, 9(2008)025001.
- [2] A. Moliton, W. Rammal and B. Lucas, Europhysics Letters, 72 (2005) 754.
- [3] A. N. Papathanassiou, I. Sakellis and J. Grammatikakis, Applied Physics Letters, 91(2007) 202103.
- [4] C.Dridi, R.B.Chaabane, J.Davenas, I.B.Dumazet and H.B.Ouada, Vacuum, 83(2009)883-888.
- [5] S.Decheveigne, J.Kelein, A.Leger, M.Belin and D.Defouneau, Phys. Rev. B, 15 (1977) 750.

P21 - Magnon scattering in ferromagnetic surface with atomic steps

B. Bourahla^{1,2*}, R. Rabhi¹, O. Nafa¹, A. Khater², R. Tigrine^{1,2}

¹Laboratoire de Physique et Chimie Quantique, université de Tizi Ouzou, BP 17 RP, 15000, Algérie

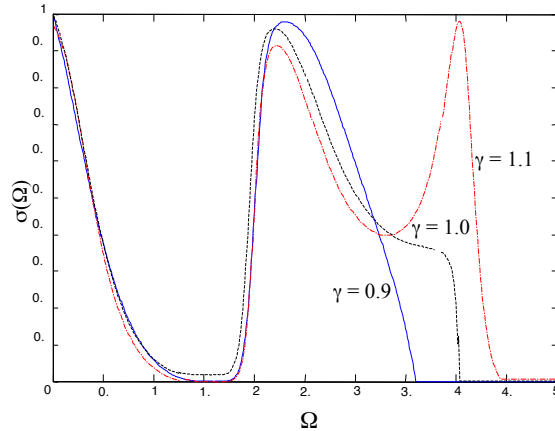
²Laboratoire de Physique de l'Etat Condensé UMR 6087, université du Maine, 72085 Le Mans, France

* Corresponding author: bourahla_boualem@yahoo.fr

Abstract

In this communication, we introduce a model to study the effect of the ferromagnetic steps on the propagation of the spinwaves at the atomic surface, whereby its magnetic properties can be analyzed via the total magnonic conductance. The model system consists of an atomic layer containing atomic steps with different heights. The matching method [1-2] is used to calculate the coherent magnon transmission and reflection scattering cross sections at the step boundary of the system. The spin dynamics are determined using the equations of motion for the spin precession displacements on the lattice sites.

This technique permits also the calculation of the localized magnon modes associated with the domain boundaries, and the spin spectra for the step atomic sites.

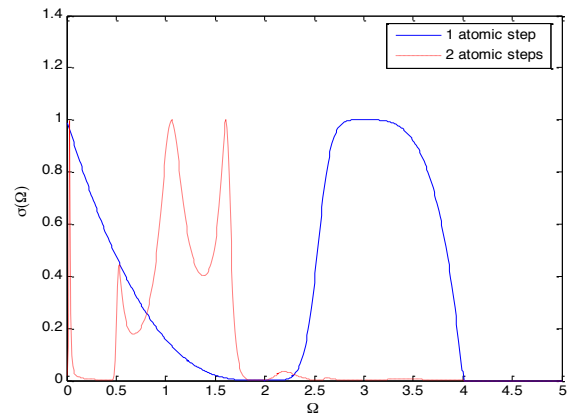


The surface observables are numerically calculated for different cases of magnetic hardening and softening, to investigate how the local dynamics can respond to changes in the microscopic environment on the atomic step. The calculations consider all magnon frequencies in the surface propagating bands, for arbitrary angles of incidence on the boundary, at low temperature. It is shown that the calculated spin spectra are sensitive and explicit signatures for the softening and hardening effects.

The analysis of the spectra, of the magnonic conductance, demonstrates the fluctuations related to Fano resonances [3], due to the coherent coupling between travelling magnons and the

localized spin modes in the step zone. In addition, it was observed that the transmission spectra intensity decreases gradually when the steps number increases.

Therefore, the intensity of the spectra can be used to identify the defect size. Finally, it is also interesting to note, in recent references concerning the magnetic break junctions [4], that some of their properties are driven by resonant states that are localized in the junction domain.



Keywords: Magnetic properties; Matching method; Atomic steps

PACS: 75.30.Ds; 75.40.Gb; 75.60.Cn; 75.75.-c

References

- [1] Bourahla, B. Khater, A. Tigrine, R. (2009) Calculations of the coherent transport properties of a symmetric spin nanocontact, *Thin Solid Films*, 517, 6857-6861
- [2] Khater, A. Bourahla, B. Abou Ghantous, M. Tigrine, R. and Chadli, R. (2011), Magnons coherent transmission and thermal conductivity at ultrathin insulating ferromagnetic nanojunctions, *Eur. Phys. J. B* 82, 53-61
- [3] Rau, A.R.P. (2004) Perspectives on the Fano Resonance Formula, *Physica Scripta* 69, 1.
- [4] Bolotin, K. I. Kuemmeth, F. Pasupathy, A. N. and Ralph, D. C. (2006) Magnetoresistance of single molecular junctions measured by a mechanically controllable break junction method, *Nano Lett.* 6, 123

P22 - Electrocatalytic activity of Pt nanoparticles deposited on TiO₂ anatase supports toward methanol oxidation

Bochra Abida ^{1*}, Lotfi Chirchi ¹, Stève Baranton ², Teko Wilhelmin Napporn ², Jean-Michel Léger ²
and Abdelhamid Ghorbel ¹

¹Laboratoire de Chimie des Matériaux et Catalyse, Faculté des Sciences de Tunis, Campus Universitaire El-Manar 2092, El-Manar, Tunis.

²Laboratoire de Catalyse en Chimie Organique, Equipe Electrocatalyse, UMR-CNRS 6503, Université de Poitiers, 40 avenue du Recteur Pineau, 86022 Poitiers Cedex, France

*Corresponding author : E-mail adress : abidabochohra@yahoo.fr

Introduction:

Direct methanol fuel cell (DMFC) has received extensive studies in the past decade because of the great application potential for a renewable power source. DMFCs can be operated at low temperatures, have a high energy density and a long life and are lightweight with a simple system design. Although DMFCs possess many merits as a power source, practical commercialization still faces several fundamental materials challenges. As far as the methanol oxidation reaction (MOR) is concerned, major challenges receiving particular attention are a higher electrocatalytic activity with a minimized Pt catalyst loading and a better resistance against the CO poisoning effect. The widely adopted method to improve the electrocatalytic mass activity of the precious Pt catalyst toward MOR is to disperse Pt nanoparticles on the catalyst support of large surface area. On the other hand, to improve the CO tolerance, considerable studies used Pt-based binary or ternary alloys as catalyst, in particular Pt–Ru, to enhance CO electro-oxidation via the bifunctional mechanism and the so-called electronic effect. Metal oxides, such as CeO₂, SnO₂ and RuO₂, can also effectively improve the CO tolerance of the Pt catalyst when used as a promoter or the catalyst support based on a similar principle [1, 2]. TiO₂ is one of the most important transition metal oxides with a wide range of industrial applications [3]. TiO₂ has intriguing photocatalytic properties and excellent chemical stability in both acidic and alkaline solutions, and has long been used as a catalyst or support in photo-electrochemical systems. Many recent studies on titania for DMFC applications prepared titania supports of high surface area for the Pt catalyst loading and found that the oxide supports could significantly enhance the electrocatalytic activity and the CO tolerance of the Pt catalyst. The better electrocatalytic properties of Pt/TiO₂ electrodes are usually attributed to the bifunctional mechanism and a strong metal–support interaction between the TiO₂ and the Pt catalyst.

Experimental:

In this study we synthesize, a new Pt base catalyst for direct methanol fuel cells using TiO₂ nanotubes obtained from anatase transformation as a new catalyst support. Pt nanoparticles are prepared by impregnation method and supported on TiO₂ nanotubes (TNTa) with excellent dispersion in comparison with anatase TiO₂. The structure and elemental composition of the anatase TiO₂ and Pt/TNTa catalyst are characterized by transmission electron microscopy (TEM), nitrogen physisorption and X-ray diffraction (XRD).

Results:

XRD analyses reveal that uniform anatase TiO₂ nanotubes were obtained. Furthermore, TEM shows that Pt/TNTa catalyst exhibits a homogeneous structure with small and uniform platinum particles well dispersed on TiO₂ nanotubes. The electrocatalytic properties of the Pt/TNTa catalyst for methanol and carbon monoxide electro-oxidation reactions are investigated by cyclic voltammetry (CV) in an acidic medium. Apparent electrocatalytic activity for methanol electro-oxidation reaction, high carbon monoxide tolerance and good stability are all observed for the Pt/TNTa catalyst. These may be attributed to the excellent dispersion of the Pt nanoparticles and the special properties of the TNTa support.

Conclusion

The Pt/TNTa is significantly more active for methanol oxidation. Furthermore, the onset potentials of Pt/TNTa are lower than those of Pt/TiO₂(Anatase) and Pt/C (XC72).

References

- [1] Rajalakshmi, N., Lakshmi, N., Dhathathreyan, K.S. (2008), International Journal of Hydrogen Energy, 33, 7521 – 7526.
- [2] Song, H., Qiu, X., Li, X., Li, F., Chen, W. (2007) Journal of Power Sources, 170, 50–54.
- [3] Yuana, H., Guo, D., Qiu, X., Zhu, W., Chen, L. (2009) Journal of Power Sources, 188, 8–13

P23 - The annealing effect on the nitride coatings properties obtained by magnetron sputtering

D. Dergham¹, C. Nouveau², L. Chekour¹, N. Tamacha³, A. Khelil³

¹Laboratoire Microstructures et Défauts dans les Matériaux, Université Mentouri, 25000 Constantine, Algérie

*Corresponding author : E-mail adress : Dergham.driss13@yahoo.fr

² LaboMaP, Arts et Métiers ParisTech de Cluny, France ;

³Laboratoire de Physique des Couches Minces et Matériaux (LPCM2E) Oran, Algérie.

Introduction: In this paper two kinds of films have been deposited by means of reactive magnetron sputtering then annealing.

In the case of the Cr_xN_y layers, the deposition conditions were a 80% Ar + 20% N₂ gas mixture, a working pressure of 0.2 Pa, a target bias voltage of -200V and two thicknesses (140 and 530 nm). In the case of the Ti_xN_y layers, we realized understoichiometric layers in view to anneal them under vacuum. The deposition conditions of these Ti_xN_y layers were a working pressure of 0.6 Pa, a deposition time of 1 h, 50% of N₂ in the plasma discharge and a target bias voltage of -500V. For both nitride layers, silicon substrates (100) were used (280 μm thick).

The first layers Cr_xN_y was annealed under an N₂ atmosphere (residual and working pressure of 1.33.10⁻³ Pa and 1000 Pa respectively), while the annealing of the Ti_xN_y layers was made under vacuum both from 600 to 1000°C during 1 h. The influence of the annealing on the structure of the deposited coatings are presented thanks to the DRX analysis the Ti_xN_y layer before annealing present a broad Ti₂N (004) diffraction peak and so, a bad crystallinity. Then, after an annealing under vacuum at a high temperature such as 1000°C, we obtained a well crystallized and stoichiometric cubic TiN layer from a bad crystallized Ti₂N layer only under the effect of the temperature. The residual stresses were determined with the Newton's rings method and the Stoney's equation. For Cr_xN_y layers the residual stresses were measured to be -12 GPa before annealing and then it decreases slightly to -3 GPa at 1000°C, while the Ti_xN_y layers obtained at 50 % have stresses from -1.5 to -2.5 GPa while the TiN layers are known to present stress in tension of around 0-0.5 GPa.

After heating Cr, Cr₂N layers under nitrogen and Ti₂N layers under vacuum the CrN, and TiN layers presents a cubic phase

The composition of the layers was determined by EDS analyses The Cr_xN_y layers were composed of 75% of Cr and 25% of N according to the EDS analysis

For Ti_xN_y according to the colour obtained we supposed that the layers were composed of a

mixture of Ti₂N (orange) and TiN (golden) phases. XRD analyses revealed that only the TiN (200) diffraction peak is present at 50% of nitrogen in the plasma discharge. Moreover, we observe that higher the thickness is, better the crystallization of the layers is the CrN layers are less sensitive to annealing than the TiN ones. [2]

Industrial CrN layers present a thermal stability until only 700°C. [1] Lee et al. [4] showed that from 700°C, Cr₂O₃ appeared into CrN layers and at 900°C, only the chromium oxide is present

Almer et al. [3] studied the evolution of CrN microstructures Laghrib et al. [5] studied TiN oxide thin layers obtained by vacuum evaporation of TiN and annealing under oxygen flow They observed that a longer annealing leads to an increase of the TiN dioxide proportion. Thicker Cr_xN_y layers are more thermally stable and less stressed than thinner ones. Besides, higher the thickness of the Ti_xN_y layers is, better their crystallization is. We obtained a well crystallized cubic TiN layer after annealing a bad crystallized Ti₂N coating at 1000°C.

Keywords: *thin films, nitrides, PVD, thermal properties, annealing*

References

- [1] B. Navinsek, P. Panjan, (59, 244.) (1993) oxidation resistance of PVD Cr, CrN, CrNO hard coating Surf. and Coat. Technol
- [2] E. Broszeit, C. Friedrich, G. Berg (115, 9) (1999) Deposition, properties and applications of PVD Cr_xN coatings Surf. and Coat. Technol..
- [3] J. Almer, M. Oden, L. Hultman, G. Hakansson, (volume 385 page 190-197) (avril 2001) Microstructure stress and mechanical properties of arc evaporated Cr-C-N Coatings thin solid films
- [4] S.C. Lee, W.Y. Ho, F.D. Lai, (43) (1996) Effect of substrate surface roughness on the characteristics of CrN hard film
- [5] S. Laghrib, H. Amardjia-Adnani, D. Abdi, J.-M. Pelletier, (82(8), 782) (2008) Tin oxide thin layers obtained by vacuum evaporation of tin and annealing under oxygen flow Vacuum

P24 - Theoretical study of inclusion complex ortho-anisidine with β - cyclodextrin

Djilani. Imene*, Nouar. Leila, Haiahem. Sakina, Bouhadiba. Abdelaziz, Madi. Fatiha, Khatmi. Djameleddine

Laboratory of Computational Chemistry and nanostructure,
Guelma University, BP: 401; Guelma, 24000, Algeria.

*E-mail: djilaniimene@hotmail.fr

Abstract: The formation of the inclusion complex of ortho-anisidine (O-AN) with β -CD has been studied theoretically using MM+ force field, PM3, B3LYP / 6-31G* theories. In this study we took into account only the stoichiometric 1:1 the penetration of ortho-anisidine in the cavity of the β -cyclodextrin can be done according to two orientations, A and B. In A orientation, the OCH₃ was introduced firstly however when it was introduced in the last the orientation is named, B. The results indicate that the complexation of ortho-anisidine / β -CD with the A orientation is significantly more favorable than that of the B orientation. The negative complexation energy calculated suggests that the inclusion complexes are stable.

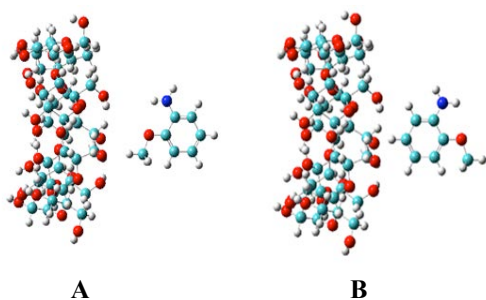


Figure 1: Two possible orientations of O-AN in β -CD.

Keywords: β -cyclodextrin, ortho-anisidine, MM+, PM3, B3LYP / 6-31G*

Result and discussion: The initial structures of O-AN were constructed by module builder of Hyperchem then optimized with B3LYP method at 6-31G level. The initial structure of β -CD is built with CS Chem3D Ultra (version 10, Cambridge software) from the crystal structure and fully optimized by PM3 method without imposing any symmetrical restrictions.

To quantify the interaction between host and guest in the optimized geometries, we have evaluated binding (ΔE binding) energy, which was calculated by subtracting the sum of the energy of individual free host and guest molecules to the energy of the inclusion complex (using the following formulae 1):

$$\Delta E_{\text{binding}} = E_{\text{complex}} - (E_{\text{CD}} + E_{\text{O-AN}})_{\text{isolated}} \quad (1)$$

Each derived complex was completely optimized without any restriction using the MM+ force field; considering the conjugate gradient Polak–Ribiere

algorithm with a Root Mean Square gradient of 0.01 Kcal/mol. The lowest binding complexes obtained by MM+ were re-optimized by PM3 semi empirical method under no constraints. We calculated the harmonic vibration frequencies at PM3 theory level to confirm that the PM3-optimized geometries correspond to a true minimum on the potential energy surfaces. The density functional theory (DFT) at the level of B3LYP/6-31G*, which considers the electron correlation and high precision of energy calculations is applied to calculate the single point energies of the inclusion complexes.

We remark that all binding energies are negative which demonstrate that the inclusion process of O-AN in β -CD is thermodynamically favorable.

To investigate the thermodynamics of the binding process, the statistical thermodynamic calculation were carried out at 1 atm and 298.15 K by PM3.

The complex reactions of O-AN with β -CD are exothermic judged from the negative enthalpy changes. And the negative enthalpy changes suggest that both the inclusion processes are enthalpically favorable in nature. In addition, it can be seen that the entropy change (ΔS) of A and B orientation are also both negative, this indicates that the formation of the complex becomes an enthalpy-driven process.

References:

- K. Srinivasan, J. Vaheethabanu, P. Manisankar, T. Stalin (2011) Study of inclusion complex of β -cyclodextrin and Ortho-Anisidine; photophysical and electrochemical behaviors K. Srinivasan et al., J. Mol. Struct., doi:10.1016/j.molstruc.2010.12.026.
- Nouar Leila, Haiahem Sakina, Abdelaziz Bouhadiba, Madi Fatiha, Largete Leila(2011) Molecular modeling investigation of para-nitrobenzoic acid interaction in β -cyclodextrin, Journal of Molecular Liquids, doi: 10.1016/j.molliq.2011.02.004
- S.K. Xing, C. Zhang, H.Q. Ai, Q. Zhao, Q. Zhang, D.Z. Sun, (2009) Theoretical study of the interactions of β -cyclodextrin with 2'-hydroxyl-5'-methoxyacetophenone and two of its isomers Journal of Molecular Liquids 146, 15–22
- Wenxiao Pan, Dongju Zhang, Jinhua Zhan (2011) Theoretical investigation on the inclusion of TCDD with β -cyclodextrin by performing QM calculations and MD simulations Journal of Hazardous Materials 192, 1780–1786

P25 - Improved electrical characteristics of porous germanium photodiode obtained by phosphorus ion implantation

E. Akkari^{1,*}, W. Touayar¹, F. J. del Campo², J. Mnotserrat²

¹Activités de recherche : Métrologie des Rayonnements, Institut National des Sciences Appliquées et de Technologie, INSAT, BP676, 1080 Tunis Cedex, Tunisie

²Instituto de Microelectrónica de Barcelona, IMN-CNM (CSIC), Campus de la Universidad Autónoma de Barcelona, 08193-Bellaterra, Barcelona, Spain.

Corresponding authors: E-mail adress : ak_emna@yahoo.fr,

In order to improve the characteristics of a germanium photodiode for an application in the field of IR, we introduced on the surface a porous layer. Starting substrates are P type, with (100) crystallographic orientation and resistivity $<1\Omega\cdot\text{cm}$. To form the junction, which will be the basis of the photodiode, we have doped the germanium with phosphorus using ion implantation with an energy of 150 keV and a dose of 1×10^{15} at/cm², in order to obtain an approximate doped thickness of 0.4 μm . The ohmic contacts are made by thermal evaporation, with gold covering the entire back side and indium on the front side of the photodiode.

To improve the performance of the photodiode, we introduced a porous layer on the front side to contain more absorbed optical radiation. The method used to produce the porous structure is based on an electrochemical anodization technique at usual room temperature. The electrochemical etching made on the front side (N-type germanium) requires the control and optimization of various parameters involved in the process such as the concentration of the solution, the etching time and the current density applied. To avoid damage to the junction, we opted for a small thickness of the porous layer that we succeeded in obtaining by using a hydrofluoric solution (HF / ethanol) having a concentration of 20%, a duration of 5 min., and a current density of 2.5 mA /cm².

Electrical characterization I-V shows the following characteristic parameters of the photodiodes:

	Germanium Photodiode	Porous Germanium Photodiode
Threshold voltage	$V_s = 0,422 \text{ V}$	$V_s = 0,452 \text{ V}$
Photonic current	$I_{ph} = -2 \cdot 10^{-8} \text{ A}$	$I_{ph} = -6 \text{ mA}$
Saturation current	$I_{sat} = 2 \cdot 10^{-3} \text{ A}$	$I_{sat} = 7,6 \cdot 10^{-4} \text{ A}$
Series resistance	$R_s = 6 \Omega$	$R_s = 10 \Omega$
Shunt resistance	$R_{sh} = 26 \Omega$	$R_{sh} = 123 \Omega$

The structural analysis of the porous layer with an AFM showed a pyramidal textured appearance allowing to trap, from the energy point of view the incident radiation (Figure 1). This structure contributes to reduce the reflectivity of the layer and to improve the performance of the photodiode.

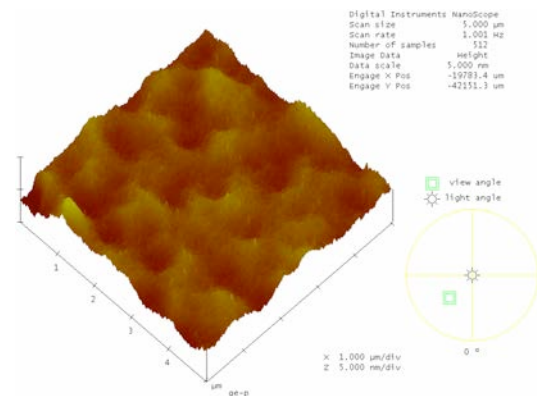


Figure 1: AFM 3D topographical image of the front face of the photodiode in porous germanium.

When the photodiode is provided with a porous germanium layer, we notice the improvement in the current response after the voltage change. The improvement in the I-V characteristic after introduction of the porous layer in the structure of the photodiode is due to the effect of passivation of hydrogen fluoride (HF) used as the electrolytic solution during electrochemical etching. Therefore, the introduction of the porous layer increases the threshold voltage, the shunt resistance and the series resistance of the photodiode.

References:

1. J. Vanhellefont and E. Simoen, Journal of the Electrochemical Society, 154 (7) H572-H583 (2007).
2. S. Koffel, P. Scheiblin, A. Claverie, V. Mazzocchi, Materials Science and Engineering B 154–155 (2008) 60–63.

P26 - DFT study of the Ni – (m-ZrO₂) interaction

E. Boudjennad^{1,2*}, N. Keghouche¹, C. Minot².

¹Laboratoire Microstructure et Défauts dans les Matériaux, route Ain El Bey Constantine.

*Corresponding author: E-mail address: thargua@hotmail.com

²Laboratoire de Chimie Théorique, Université Pierre et Marie Curie Paris France.

Introduction: Zirconium oxide is considered nowadays one of the most important ceramic materials in modern technology [1] ZrO₂ based materials are widely exploited in catalysis as well as in fuel cells, gas sensing, and other relevant technological devices [2]. In the last decade, together with hafnium, it has been proposed to substitute SiO₂ as a gate dielectric material in metal-oxide semiconductor devices [3].

Abstract : Periodic density functional theory (DFT) study was performed in order to investigate the Ni-*m*ZrO₂ interaction. First, the possibility of inserting atomic nickel in the bulk of ZrO₂ examined (figure 1). Second, the effects of both insertion and adsorption on the stable surfaces of ZrO₂ such as $(\bar{1}11)$ and $(\bar{1}01)$ are studied. It is shown that an increase amount of inserted nickel, from one Ni for 4Zr to an equivalent amount, enhances the insertion energy and makes insertion more exothermic. The later is accompanied by a lattice expansion ($\approx 26\%$) and by a reduction of symmetry. When the nickel is inserted in the bulk, the distance Ni-Zr is equal to 2.57 Å, in agreement with experimental value. Surface insertion and adsorption calculations show that the nickel atoms can penetrate inside the oxide much more easily across the surface $(\bar{1}01)$, than through the surface $(\bar{1}11)$ (Table 1).

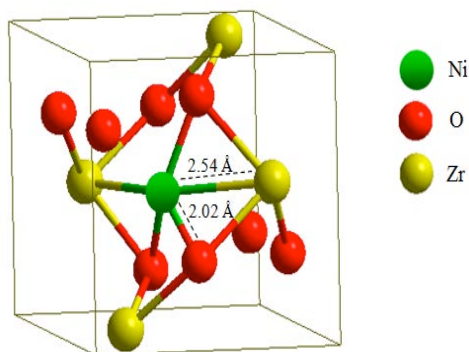


Figure 1: Nickel insertion: the optimized geometry for $\theta=1$ is shown.

Surface	$E_{\text{ins}}(\text{eV})$	$d_{\text{Ni-Zr}}(\text{Å})$	$d_{\text{Ni-O}}(\text{Å})$	Coordination
$(\bar{1}11)$	- 1.57	2.59	2.05	bound to 4 O
$(\bar{1}01)$	- 1.80	2.53	1.82 - 2.05	bound to 4 O and 2 Zr

Table 1: Nickel insertion energy in $(\bar{1}01)$ and $(\bar{1}11)$ surfaces of *m*-ZrO₂

References:

- [1] M. C. Munoz, S. Gallego, J.I. Beltran, J. Cerda, Surf. Sci. Rep. 61 (2006) 303-344
- [2] S. Heinbuch, F. Dong, J. J. Rocca, E. R. Bernstein, J. Opt. Soc. Am. B 25 (2008) B85-B91
- [3] V. Fiorentini, G. Gulleri, Phys. Rev. Lett. 89 (2002) 266101

P27 - Effects of Ce doping in (Bi,Pb)2212 phase

F. Benmaamar, M.-F. Mosbah, N. Kalkoul, S. Mahdjoub, F. Bouaïcha.

Laboratoire Couches Minces et Interfaces, Département de Physique,
 Université Mentouri Constantine, Route d'Ain El Bey, 25017Constantine – Algérie
 E-mail: fe_rialbe@yahoo.fr Tel/Fax: 213 31 61 47 11

Abstract:

The study of the effect of impurities on the physical and superconducting properties of high-Tc superconductors has long been recognized as being of great importance. For $\text{Bi}_2\text{Sr}_2\text{CaCu}_2\text{O}_{8+d}$ (Bi2212) there have been extensive studies on the cationic substitution of Ca and Sr by the rare earth elements to change the carrier density and to probe the underlying mechanism of superconductivity [1].

Doping by Ce in $(\text{Bi,Pb})_2\text{Sr}_2\text{CaCu}_2\text{O}_8$ (BPSCCO) should give interesting results because the CuO_2 superconducting planes are influenced. For that purpose, samples of $\text{Bi}_{1.6}\text{Pb}_{0.4}\text{Sr}_{2-x}\text{Ce}_x\text{CaCu}_2\text{O}_{8+d}$ ($0 < x < 0.025$) have been prepared from powders of carbonates and primary oxides (Bi_2O_3 , SrCO_3 , CaCO_3 , PbO , CuO and CeO_2) with the solid-state reaction technique.

The samples have been characterized by X-ray diffraction (XRD), scanning electron microscopy (SEM) and resistivity versus temperature measurements. Structural analysis shows that the crystalline lattice structure of the prepared samples belongs, mainly, to the superconductive tetragonal phase Bi(Pb)-2212. SEM Micrographics show the characteristic lamellar structure of high critical temperature superconductors.

After calcination, the XRD spectras show the obtaining of the Bi(Pb,Ce)2212 phase together with the Bi(Pb,Ce)2201 phase, with a fraction depending on the rate x of Ce and an intermediate phase Ca_2PbO_4 . The sintering has been made at a temperature of 840°C .

The XRD patterns show the obtaining of the Bi(Pb,Ce)2212 phase accompanied by the Bi(Pb,Ce)2201 and Ca_2PbO_4 phases. The figure 1 show the SEM micrograph of a doped sample ($x=0.010$). The characteristic lamellar structure of high critical temperature superconductors is revealed by this micrograph

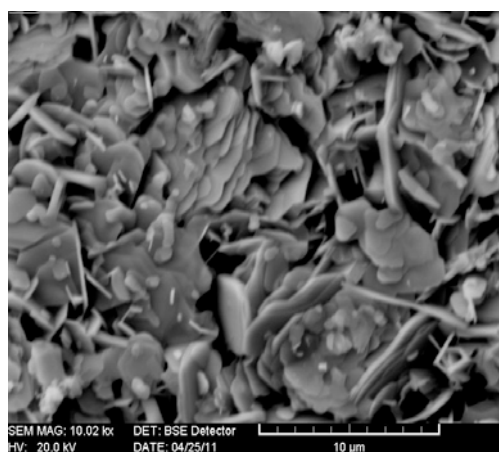


Figure1: SEM micrograph of a doped sample ($x=0.010$).

Reference:

[1] H. Salamati and P. Kameli and F. S. Razavi (2003), Effect of Pr doping on the superconductivity and interlayer coupling of the $\text{Bi}_2\text{Sr}_{2-x}\text{Pr}_x\text{CaCu}_2\text{O}_y$ system, *Supercond. Sci. Technol.* 16 pp 922-925, 2003.

P28 - Effects of doping by Ti on structural and electrical properties of Bi(Pb)-2212 superconducting ceramics.

F. Bouaïcha^{1,2*}, M.-F. Mosbah¹, N. Boussouf¹, A. Amira².

¹Faculty of Sciences Exactes and Natural Sciences and life, Department of Materials Sciences, University Larbi Ben M'hidi of Oum El-Bouaghi, BP 358, 04000 Oum El Bouaghi, Algeria.

²Laboratory of Thin Film and Interfaces, Department of Physique, University Mentouri Constantine, Campus de Chaab-Erassas 25000 Constantine, Algeria.

*Corresponding author: bou_faiza@yahoo.fr

³Laboratory of Non-Destructive Testing, Faculty of Sciences and Technology University of Jijel, BP 98 Ouled Aissa Jijel 18000, Algeria.

Abstract: In this work, the effect of doping by Ti on Cu site of the superconducting Bi(Pb)-2212 phase is presented. Samples with nominal composition of $\text{Bi}_{1.6}\text{Pb}_{0.4}\text{Sr}_2\text{CaCu}_{1-x}\text{M}_x\text{O}_8$ where $M = \text{Ti}$ and $x = 0-0.06$ are prepared by the solid state reaction method. The samples are characterized by X-ray diffraction (XRD), scanning electron microscopy (SEM) and resistivity measurements. The study shows that the crystalline lattice structure of the prepared samples belongs mainly to the tetragonal Bi(Pb)-2212 phase (Table). The obtained cell volume decreases progressively with x for the Ti doped one. For the undoped sample, the SEM micrographs show that the form and grain size have a random distribution. A quite different microstructure is obtained for the doped samples (Figure 1). The grains are more connected and have a flat shape which is characteristic of the Bi based superconductors. In the normal state, all samples exhibit a metallic like character. This resistivity decreases when x increases.

Keywords: Superconductivity, SHTC, Bi-Pb-Sr-Ca-Cu-O System, Substitution, Doping, Resistivity, Normal State.

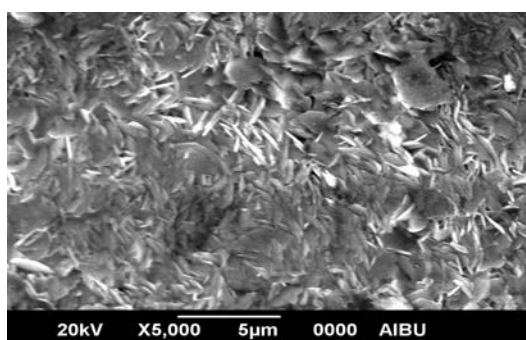


Figure 1: SEM Microphotographs of Sample (Bi,Pb)2212 doped with $y = 0.02$ of Ti.

Rat of Ti (y)	a (Å)	c (Å)	V (Å ³)
0	5.398	30.845	898.86
0.02	5.190	30.803	829.92
0.04	5.169	30.708	820.69
0.06	5.078	30.984	799.01

Table: Lattice parameters a and c of samples doped with titanium

References:

- [1] N. A. Hamid and R. Abd-Shukor, J. Mat. Sci. 35 2325 – 2329, (2000).
 [2] A. Boulouf, D. Louër, J. Appl. Crystallogr. 37, 724-731, (1991).

P29 - First-principle study of magnetic behavior of nano-clusters of Rh-doped SnO₂(110) surfaces

F. Bouamra ⁽¹⁾, A.Boumeddiene ⁽¹⁾, H.Belkhir ⁽²⁾

⁽¹⁾Physics Department, Surfaces, Interfaces and Thin Films Laboratory (LASICOM), Blida University, Algeria

⁽²⁾Physics Department, LESIMS, Annaba University, Algeria

Abstract: Tin dioxide is nominally a wide-band insulator ($E_g=3.6\text{eV}$) used widely as a component in microelectronic devices like gas sensor, varistor and catalyst [1,2]. Its properties depend on oxidation and reduction reactions at the oxide surface. The (110) surface is known to be the surface of lowest energy. First principle approach based on density functional theory calculations have been performed using the Becke' three parameters hybrid exchange functional together with the Lee-Yang-Parr correlation functional (B3LYP) to study the magnetic properties of Rh-doped SnO₂(110) surface with atomic Rh/Sn ratio over a range varying from 0% to 26.31%. Rh atoms are substituted with Sn_{5c} atoms of outer atomic plane composed from (Sn and O) atoms. Band structure and Density of states are reported and discussed with the increase of Rh concentration.

We have found that the Rh-doped SnO₂(110) surfaces are relaxed but not reconstructed as the stoichiometric SnO₂(110) surface. The calculated value of magnetic moment shows that the presence of Rh atoms in the supercell induces an important value of a magnetic moment. Several studies have focused on films and bulk samples of tin oxide SnO₂ doped with transition metal ions for their new area of spintronics application ferromagnetism in semiconductors and insulators is rare[3]. For this, we present in this paper an ab-initio investigation of Rh doped SnO₂(110) stoichiometric surfaces. Mulliken population analysis was used in this work to describe the charge distribution and overlap populations. The XCrysDen program was used to design band structure and density of state (DOS) diagrams.

The SnO₂(110) surface adopts a rectangular structure with lattice parameters $a=3.186\text{\AA}$ and $b=6.69\text{\AA}$. The unit cell contains 17 atoms, 6 metal atoms Tin (Sn) and 11 atoms Oxygen (O). Supercell corresponding to the specific rhodium concentration is built of $(4 \times 2) \times p$ unit cell. We have chosen the stoichiometric oxidized surface with 9 atomic layers (Fig. 1).

Sn and O centers have been described with pseudo-potential basis set of Durand and

Barthelat's, the Rh atoms are presented by Hay and Widt small core basis set. With corresponding configurations: Sn=[Kr]5s²5p², O=[He]2s²2p² and Rh=[Kr]5s¹4d⁸.

The main results are represented in table 1.

	μ (μ_B)	E_g (eV)	E_f (eV)	ΔE (eV)
0%		1.75	6.56	-
9.09%	4	2.68	6.44	1.96
14.28%	6	2.88	8.05	1.88
20%	4	1.66	7.40	0.21
26.31%	10	2.17	7.30	0.36

Tableau 1: magnetic moment μ (μ_B), Gap (E_g) and Fermi (E_f) energy and energy difference between FM and AFM spin-ordering $\Delta E=E(\text{FM})-E(\text{AFM})$.

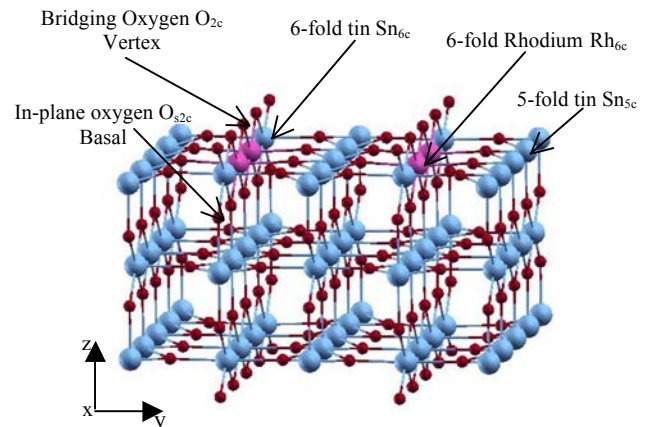


Fig1.: perspective view of SnO₂(110) doped Rh for Rh/Sn=9.09%.

References:

- [1] V.E. Henrich, P. A. Cox, the Surface Science of Metal Oxides, Cambridge University Press, Cambridge, 1966
- [2] F. J. Arlinghaus, J. Phys. Chem. Solids 35 (1974) 931
- [3] A. Sundaresan, R. Bhargavi, U. Siddesh, and C. N. R. Rao, Phys. Rev. B 74, 161306(R) (2006).
- [4] V.R. Saunders, R. Dovesi, C. Roetti, R. Orlando, et al. CRYSTAL03.
- [5] B. W. Licznarski, K. Nitsch, H. Teterycz, K. Wisniewski, Sensors and Actuators B 79(2001) 157-162.

P30 - Host-guest inclusion complex between β -cyclodextrin and paeonol: computational studies based on PM3 and ONIOM methods

Haiahem. Sakina*, Bouhadiba. Azize, Nouar. Leila,

*Corresponding author : E-mail adress : sakinahaihem@yahoo.fr

² Laboratory of Computational Chemistry and nanostructure, Guelma University, BP: 401; Guelma, 24000, Algeria.

Abstract

The inclusion interaction between paeonol and β -cyclodextrin (β -CD) binding site has been investigated, based on PM3 and ONIOM2 methods. The optimized geometric structures obtained from ONIOM2 calculations are used to perform natural bond orbital (NBO) analysis. Intermolecular hydrogen bonds between PAE and β -CD are investigated. The obtained results clearly indicate that the PAE entering into the cavity of β -CD from its wide side by OCH3 group (model 1) is energetic favorable. Moreover, Analyses regarding the complex structures suggest that one hydrogen bond between O of methoxy group OCH3 of PAE and H132 of β -CD is formed. This hydrogen bond interaction plays an important role in the bound PAE/ β -CD complex. The calculated results are in good agreement with the experimental results.

Keywords: Cyclodextrin, paeonol, inclusion complexes, PM3, DFT, HF, ONIOM2, NBO.

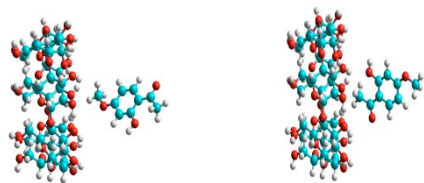


Figure 1 Coordinate systems used to define the process of complexation for: (a) model 1 and (b) model 2.

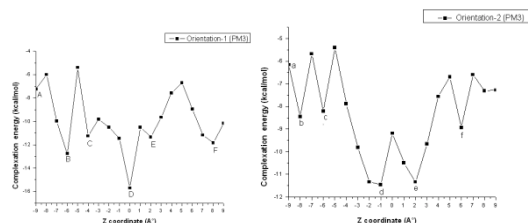


Figure 2 Stability energies of the inclusion complexation of PAE into β -CD at different positions (Z) and models: (a) model 1; (b) model 2. Point A, B, C, D, E, F

represent ZA=-9Å, ZB=-6 Å, ZC=-4 Å, ZD=0Å, ZE=2 Å, ZF=8 Å, respectively. Point a, b, c, d e, f represent Za= -9 Å, Zb=-8 Å, Zc=-6 Å, Zd= -1Å, Ze= 2Å, Zf= 6Å, respectively.

	PAE	β -CD	Orientation 1	Orientation 2
PM3				
E ^h (kcal/mol)	-98.26	-1457.10	-1571.05	-1566.81
ΔE^h (kcal/mol)			-15.96	-11.45
DEF (PAE)			2.16	2.10
DEF (β -CD)			1.66	0.79
E ^h _{HOMO} (eV)				
E ^h _{LUMO} (eV)	-9.18	-10.56	-9.61	-9.20
E _{HOMO} -E _{LUMO} (eV)	-0.89	1.09	-1.10	-1.19
μ (Debye)	-8.29	-11.65	-8.50	-8.01
	3.18	7.34	5.55	10.83
H(kcal/mol)				
ΔH^h (kcal/mol)	18.7	-667.31	-661.82	-657.82
G(kcal/mol)				
ΔG^h (kcal/mol)	-11.54	-784.46	-797.96	-796.54
ΔS^h (cal/molK)			-1.96	-0.54
			-50.90	-32.72
B3LYP/6-31G*				
E (kcal/mol)				
ΔE (kcal/mol)	-360623.19	-26811832.20	-27172507.57	-27172501.58
			-52.18	-46.19
HF/6-31G*				
E (kcal/mol)				
ΔE (kcal/mol)	-358292.53	-2666495.63	-3024748.09	-3024788.16
			-40.07	-31.22

Table 1: Thermodynamic parameters of the models1 and 2 calculated by PM3 method and the single point energies by B3LYP/6-31G* and HF/6.31G*.

References:

- S.K. Dordunoo, M. Burt., Int. J. Pharm. 133 (1996) 191.
 S.M.O. Lyng, M. Passos, D. Fontana, Process Biochem. 40 (2005) 865.
 S. Tommasini, D. Raneri, R. Ficarra, M.L. Calabro, R. Stancanelli, P. Ficarra, J. Pharm. Biomed. Anal. 35 (2004) 379.
 Nouar Leila, Haiahem Sakina, Abdelaziz Bouhadiba, Fatiha Madi J.Biol.Sci., 2011

P31 - Multiwall carbon nanotubes for chemical vapour sensor

H. Baccar¹, E. Llobelt², T. Ktari¹, A. Abdelghani^{1,*}

⁽¹⁾Nanotechnology Laboratory, INSAT, Centre Urbain Nord, Tunisia

⁽²⁾Research Centre on Engineering of Materials and micro/nanosystems, Universitat Rovira i Virgili, Tarragona, Spain

* Corresponding author e-mail: aabdelghan@yahoo.fr

Abstract

Interest in nanomaterials has been growing rapidly for the past several years. Especially, carbon nanotubes (CNTs) are promising as new materials for a variety of potential applications. Recently, CNT-based gas sensors [1–4] have received considerable attention because of their outstanding properties, such as faster response, higher sensitivity and wider variety of gases that may be detected compared with the other types of gas sensors. CNT based gas sensing utilizes a change in an electrical property due to adsorption of gas molecules as the output signal. We describe a new strategy for chemical vapor detection using sensor based on MWCNTs immobilized onto a gold electrode by Airbrushing.

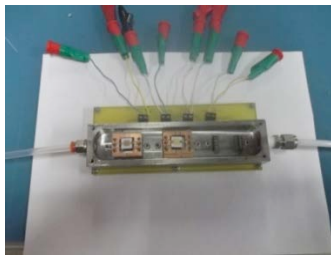


Figure 1. Multi- sensor vapour chamber



Figure 2. Experimental set-up

In first step the MWCNTs were dispersed in DMF (0,1mg of MWCNTs/1 ml of DMF). Then, the suspension is put in an ultra sonication bath during 30 min at 30 °C. Following that, the suspension is introduced inside a container connected to a spraying nozzle, and using a nitrogen gas flow, we get a spray of the suspension over the substrate. The substrate is kept heated to evaporate the solvent from the sample. To get a good adhesion and

homogeneous surface of MWCNTs onto the electrode, an annealing process is performed.

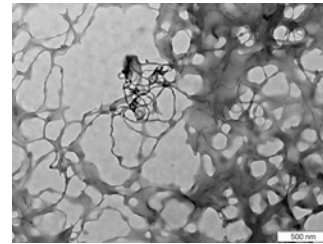


Figure 3. TEM images of MWCNTs deposited on interdigitated microelectrodes

The successful deposition of MWCNTs was verified by TEM. Impedance spectroscopy was performed before and after chemical vapor injections. The adsorption of ethanol vapor induces a decrease in the electrical conductivity of the multi-wall carbon nanotubes.

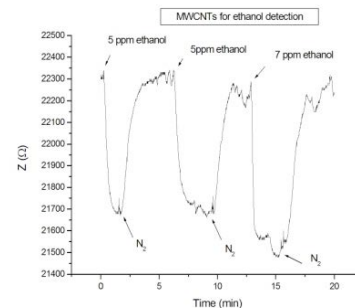


Figure 4: Impedance Z versus Time after different injection of ethanol concentrations

References:

- [1] Kong J, Franklin N R, Zhou C, Chapline M G, Peng S, Cho K and Dai H 2000 Science 287 622
- [2] Qi P, Vermesh O, Grecu M, Javey A, Wang Q, Dai H, Peng S and Cho K J 2003 Nano Lett. 3 347
- [3] Valentini L, Armentano I, Kenny J M, Cantalini C, Lozzi L and Santucci S 2003 Appl. Phys. Lett. 82 961
- [4] Valentini L, Lozzi L, Cantalini C, Armentano I, Kenny J M, Ottaviano L and Santucci S 2003 Thin Solid Films 436 95

P32 - Effect of silicon type on Si/PS/ZnO:In solar cell structure based on nanopowder synthesized by sol-gel method

H. Belaid¹, M. Nouri¹, A. Alaya¹, Z. Ben Ayady¹, K. Djessas², L. El Mir^{1,3*}

¹Laboratoire de Physique des Matériaux et des Nanomatériaux appliquée à l'Environnement, Faculté des Sciences de Gabès, TUNISIA

*Corresponding author : E-mail adress : Lassaad.ElMir@fsg.rnu.tn

²Laboratoire de Mathématiques et Physique des Systèmes (MEPS), France

³Al-Imam Muhammad Ibn Saud University, SAUDI ARABIA

Abstract:

We proposed in this study Si/PS/ZnO:In_{4%}/ITO as a new structure for solar cell application. ITO and ZnO layers were elaborated by sputtering using the correspondent nano-powder synthesized by sol-gel method. The obtained IZO film with a thickness of about 400 nm was polycrystalline with a hexagonal wurtzite structure and preferential orientation in the (002) crystallographic direction and a typical columnar structure and very smooth surface. Electric characterizations show a Schottky behavior with a depletion region developed through the PS layer. The structure exhibit photovoltaic effect and the p-type structure is more suitable for photovoltaic application.

Results:

The XRD pattern indicates the formation of hexagonal wurtzite phase of ZnO [El Mir].

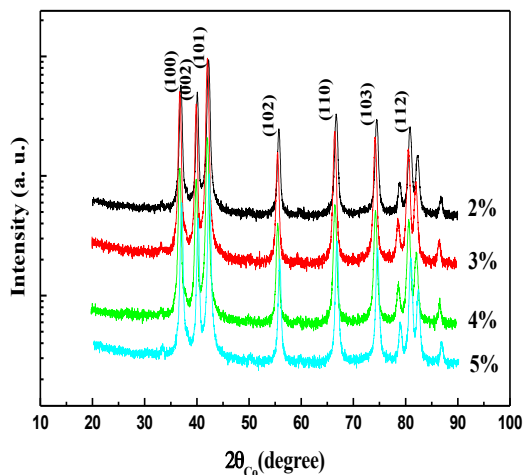


Figure 1. X-ray diffraction pattern of In-doped ZnO aerogel nanoparticles.

- The obtained ZnO:In_{4%} film shows a good morphology with a preferentially oriented along (0 0 2) direction perpendicular to the substrate.

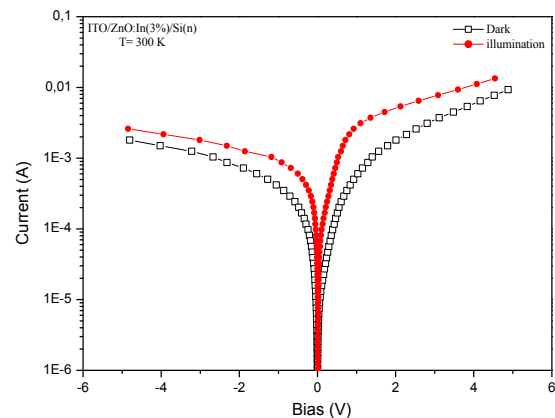


Figure. 2. The two structures exhibit a Schottky behavior indicating a well establishment of a p-n junction in the cell structure.

- CV measurements shows a well Schottky behavior with a net doping concentration of about 10^{16} Cm^{-3} ; which indicates that the depletion region is spatially in the PS layer
- We elaborate successfully a new structure Si/PS/IZO/ITO for solar cell application.

Reference:

El Mir, L., Ben Ayadi, Z., Rahmouni, H., El Ghoul, J., Djessas, K. and von Bardeleben, H. J., (2009) Elaboration and characterization of Co doped, conductive ZnO thin films deposited by radio-frequency magnetron sputtering at room temperature, *Journal of Thin Solid Films*, 517, 6007-6011.

P33 - Thermal decomposition study of AlGaN

H. Bouazizi*, N. Chaaben, A. Bchetnia, T. Boufaden and B. El Jani.

Unité de recherche sur les Hétéro-Epitaxies et Applications (URHEA)

Faculté des Sciences, Avenue de L'environnement ,5000 Monastir, TUNISIA.

E-mail corresponding author: bouazizihoda@gmail.com

Introduction:

Gallium nitride and AlGaN ternary alloy attracted much attention due to their large band gaps that make them potential candidates for their optoelectronic applications such as manufacturing in the blue emitters (LEDs, laser D) and detectors UV [1]. Although good thermal chemical and mechanical properties nitrides confer a wide range of applications, but for once they become sources of difficulties for the realization of devices [2]. Indeed, polishing, doping and the realization of ohmic contacts are operations often too complicated to achieve. In most cases, the post growth heat treatment can overcome these problems. So, it is important to determine the heat treatment conditions ensuring the thermal stability of the annealed material. In this work, we studied the influence of annealing conditions on the properties of AlGaN epilayer grown by metal organic vapor phase epitaxy (MOVPE).

Experimental:

The thermal decomposition was studied at temperature of 1200 °C under different atmosphere of N₂, H₂ and mixture of AlGaN/GaN heterostructures with low aluminum composition ($x_{Al} < 6\%$) grown on sapphire substrate by metal organic vapor phase epitaxy (MOVPE). The surface changes were observed in situ by laser reflectometry and ex situ by optical microscope (OM) and scanning electron microscopy (SEM). Photoluminescence (PL) and X-ray diffraction (XRD) measurements were also done after thermal treatments and compared to those given before annealing.

Results and Discussion:

Table (1) presents the aluminium composition of the Al_xGa_{1-x}N alloys determined from (PL) measurements. The samples were further annealed at a higher temperature of 1200 °C. It was found that AlGaN annealed in nitrogen atmosphere remained stable at 1200 °C for several minutes. However, the annealing at the same temperature under pure H₂ can leads to rapid decomposition of AlGaN. In addition, it was demonstrated by the optical microscopy that AlGaN after annealing had

a remarkable effect on the surface morphology. The room temperature Photoluminescence showed that optical property of Al_{0.056}Ga_{0.944}N does not significantly changes after partial decomposition (fig.2).

Figures and Tables:

Samples	Al composition (%)	T _g (°C)	heat treatment	Td (°C)
A	1.5	1120	Under N ₂	1200
B	6	1100	Under N ₂	1200
C	5.6	1100	Under (N ₂ +H ₂)	1200

Table1: Growing conditions and breakdowns AlGaN layers for the samples used in this study.

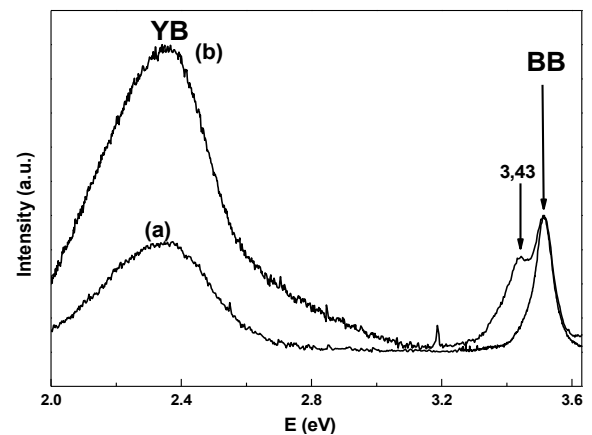


Figure 1: Photoluminescence spectrum at room temperature of the alloy Al_{0.056}Ga_{0.944}N before (a) and after (b) decomposition in H₂.

References:

- [1] Hadis Morkoc, Book Vol 3 (2009) "GaN-based Optical and Electronic Devices".
- [2] Tim Böttcher February, Book (2002) "Heteroepitaxy of group-III-Nitrides for the application in laser Diodes", University of Bremen.

P34 - Effect of acid treatment in silicon grain boundaries polycrystalline: Improving the performance of solar cells

H.Khemir*, W. Dimassi, M. Jbali, H. Ezzaouia,

Laboratoire de Photovoltaïque, Centre de Recherches et des Technologies de l'Énergie,
Technopole de Borj-Cedria, BP 95 Hammam-Lif 2050, Tunisia

*Corresponding author: E-mail adress: khemir.haikel@gmail.com

Introduction:

The main research activities in the photovoltaic are focusing on improving the conversion efficiency using a low-cost material development [3-7]. As a low-cost material, multicrystalline silicon (mc-Si) is the most used in solar cells fabrication [2]. However, the high presence of defects and grain boundaries (GBs) in mc-Si reduce the performances of solar cells [4]. Lim et al. developed a process to physically remove the GBs using the organic chemical Schimmel etchant of mc-Si [5].

The polycrystalline silicon has defects such as dislocations and grain boundaries that limit the performance of solar cells. So far the manufacturing process of photovoltaic cells has not only maintenance of the passivation of these defects that the final phase of the industrial process to cure these defects. In this work we study the effect of grain boundaries in polycrystalline silicon using a chemical etching (HFNO₃). With this treatment, the recombination at grain boundaries is reduced. Indeed, the grain boundary diffusion can deep phosphorus and metal contacts. Consequently the reflectivity is reduced causing an improvement in absorption as well as an improvement in LBIC current. With this technique LBIC we have measured the distribution of current circuit court in a cell subjected to illumination with monochromatic laser beam. For the result, the comparison is made between layers treated and untreated others.

To our study, six layers based polycrystalline silicon dimensions (2cm*2cm) are prepared, the first layer is cleaned by standard classical solution rich in nitric acid, formed by (64% HNO₃, 16% HF and 20% CH₃COOH) which allows for polished surfaces [6-7]. The other five layers were subjected to a pickling acid with a solution of HF/HNO₃ volume ration 4/1 that is to say low nitric acid during the following hard 10, 20, 30, 40, 50 second.

Figures:

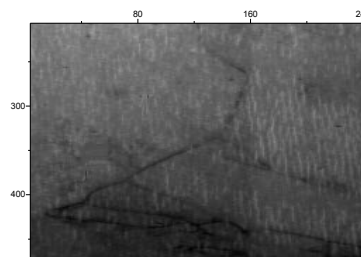


Figure1: LBIC image taken on a layer that has not suffered an acid burn.

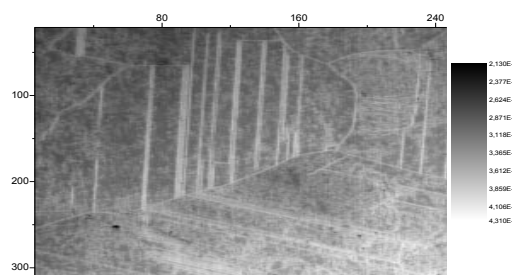


Figure2: LBIC image of a sample treated with low HF/HNO₃

References:

- [1] Ben Rabha, M., Thèse de doctorat, Faculté des Sciences de Tunis, 2004.
- [2] Goetzberger, A., Hebling, C., 2000. Photovoltaic materials, past, present, future. *Sol. Energy Mater. Sol. Cells* 62, 1.
- [3] Green, M.A., 2003. Crystalline and thin-film silicon solar cells: state of the art and future potential. *Sol. Energy* 74, 181.
- [4] Lim, D.G., Jang, D.M., Yi, J., 2002. A novel multicrystalline silicon solar cell using grain boundary etching treatment and transparent conducting oxide. *Sol. Energy Mater. Sol. Cells* 72, 571-578.
- [5] Schimmel, D.G., 1979. Defect etch for h1 0 0i silicon evaluation. *J. Electrochem. Soc.: Solid-State Sci. Technol.* 126, 479.
- [6] Skrotski, W., Wendt, H., Carter, C.B., and Kohlstedt, D.L., *Phil. Mag.*, a 57, (1988) 383.
- [7] Yamaguchi, M., Ohshita, Y., Arafune, K., Sai, H., Tachibana, M., 2006. Present status and future of crystalline silicon solar cells in Japan. *Sol. Energy* 80 (January), 104-110.

P35 - InP nanowires with InAs insertion grown by catalyst assisted molecular beam epitaxy on silicon substrates

H. Khmisi^{1a,2}, M. H. Hadj Alouane^{1b,2}, K. Naji^{1a}, N. Chauvin^{1b}, C. Bru-Chevallier^{1b}, B. Ilahi²,
H. Maaref², G. Patriarche³ and M. Gendry^{1a}

¹ Université de Lyon, Institut des Nanotechnologies de Lyon (INL)-UMR5270-CNRS,

^aEcole Centrale de Lyon, 36 avenue Guy de Collongue, 69134 Ecully, France

^b INSA-Lyon, 7 avenue Jean Capelle, 69621 Villeurbanne, France

² Université de Monastir, Laboratoire de Micro-Optoélectronique et Nanostructures (LMON),
Faculté des Sciences, Avenue de l'environnement, 5019 Monastir, Tunisia

³ Laboratoire de Photonique et de Nanostructures (LPN), UPR20-CNRS, route de Nozay, 91460 Marcoussis,
France

Introduction

The ability to realize radial and axial heterostructures of semiconductor nanowires (NWs) makes them ideal one-dimensional building blocks for potential applications in high performance nanoelectronics and optoelectronics. This work presents structural and optical properties of InP/InAs/InP NWs directly grown on silicon (Si) substrate by catalyst assisted molecular beam epitaxy [1-2]. We have optimized the growth conditions allowing NWs with purely wurtzite crystal structure, i.e. without any stacking faults. With these conditions both radial and axial growths occur simultaneously, leading to InAs quantum rods (QRs) and InAs radial quantum wells (rQWs), respectively. We show that the growth time of the InAs insertion could be adjusted to obtain rQWs emitting in the telecom wavelength range (1.3-1.5 μm).

Experimental details

InP/InAs/InP NWs were grown on Si(001) and Si(111) substrates by VLS- solid source molecular beam epitaxy (ssMBE) with gold-indium (Au-In) alloy as catalyst. First, the InP NW core is grown for 10 mn. Then, the InAs insertion is grown by a phosphorus/arsenic (P/As) flux switching for a growth time of 10, 20, 30 and 40 s for samples S1, S2, S3 and S4, respectively. The InAs growth is stopped by an arsenic/phosphorus (As/P) flux switching and the structure is completed with 10 min of InP growth. The morphology and crystal structure of the NWs were investigated by scanning electron microscopy (SEM) and by transmission electron microscopy (TEM). Photoluminescence (PL) experiments were performed to study the optical properties of the NWs

Results

The TEM image from Figure 1 shows the InAs QR and the InAs rQW which are grown simultaneously during the growth of the InAs insertion in the InP NW. We have shown that the PL is mainly due to emission coming from the InAs rQWs. In Figure 2, we clearly show a red shift of the room temperature

PL peak position when the InAs growth time increases. The growth time of the InAs insertion could be adjusted to obtain radial quantum well emitting in the 1.3-1.6 μm telecom band at room temperature.

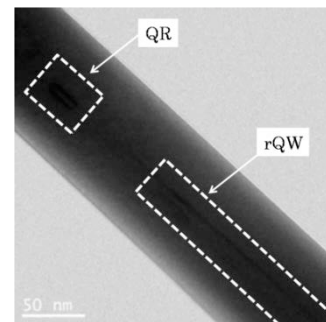


Figure 1: TEM image of a InP/InAs/InP NW grown on Si(111).

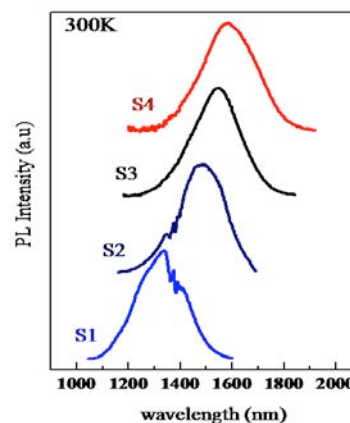


Figure 2: 300K PL spectra of InP/InAs/InP NWs for various InAs growth times: 10 s (sample S1), 20 s (S2), 30 s (S3), 40 s (S4).

References:

- [1] H. Khmisi, K. Naji, M. H. Hadj Alouane, N. Chauvin, C. Bru-Chevallier, B. Ilahi, G. Patriarche and M. Gendry. Journal of crystal Growth 2012.
- [2] M. H. Hadj Alouane, R. Anufriev, N. Chauvin, H. Khmisi, K. Naji, B. Ilahi, H. Maaref, G. Patriarche, M. Gendry and C. Bru-Chevallier, Nanotechnology, 22, 405702 (2011).

P36 - A combined HF and DFT study of the effects of implicit and explicit solvents on the conformations of lactulose and turanose molecules

H. M. Gafour^{1*}, M. Sekkal-Rahal¹, K. Sail¹
A. Sayede², M. Springborg³

¹L2MSM, Faculty of Sciences, University Djillali Liabes of Sidi-Bel-Abbès,
B.P. 89, Sidi Bel Abbas 22000, Algeria

*Corresponding author : E-mail address : gafour_chimiste@yahoo.fr

²UCCS, UMR CNRS 8181, Faculté des Sciences Jean Perrin, Université d'Artois, S.P. 18, rue
Jean Souvraz, Lens Cedex 62307, France

³Physical and Theoretical Chemistry, University of Saarland, Campus B2.2, 66123 Saarbrücken,
Germany

In this work, energetic properties of lactulose and turanose disaccharides have been calculated using HF/6-31G(d,p) level of theory both for the molecules in the gas phase and in a dielectric medium simulating the presence of water as solvent. Conformers corresponding to local minima are then identified and subsequently fully optimized using DFT method through B3LYP/6-31G(d,p) calculations. Four regions of low-energy conformers were identified for each compound. The inclusion of the implicit solvent does not lead to additional local minima in the potential energy surface for any of the two molecules, but changes only their relative energies. In order to study whether this conclusion is robust, further calculations were undertaken in which one, two, or three molecules of water were treated explicitly. Finally, we discuss the molecular flexibility based on the results on the conformational potential energy surface (PES).

At first, we performed HF calculations in order to obtain the iso-energetic maps (Figure 1 and 2). This approach is similar to what previously has been done to study anomeric effects in many sugar molecules¹⁻². In our calculations we used the B3LYP/6-31++G(d,p) level in order to carry out full optimizations of the obtained minima. This choice was made, because, according to Lii et al.³, B3LYP calculations give reasonable structures, but overestimates a stabilization by hydrogen bonds. These authors have also suggested that when using diffuse functions and larger basis [B3LYP/6-311++G(d,p)], most of the basis set superposition errors can be avoided. In an earlier work, Csonka et al.⁴ have demonstrated the importance of including diffuse functions to avoid errors in the calculated energy when electronic correlation is included.

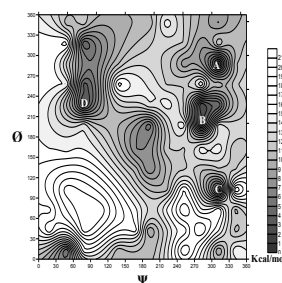


Figure 1: Relaxed isopotential maps at the HF/6-31G(d,p) level of lactulose in vacuum

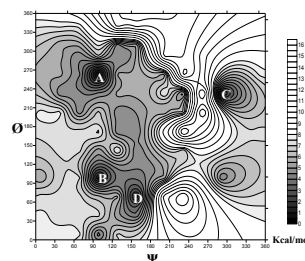


Figure 2: Relaxed isopotential maps at the HF/6-31G(d,p) level of turanose in vacuum

References:

- [1]da Silva, C. O.; Nascimento, M. A. C. (2004) *Theor. Chem. Acc*, 112, 342–348.
- [2]French, A. D.; Kelterer; A. M.; Johnson, G.P.; Dowd, M.K; Cramer, C. G. (2001) *J. Comput. Chem*, 22, 65–78.
- [3]Lii, J.-H.; Ma, B.; Allinger, N. L. (1999) *J. Comput. Chem*, 20, 1593–1603.
- [4]Csonka, G. I.; Elias, K.; Csizmadia, I. G. (1996) *Chem. Phys. Lett*, 257, 49–60.

P37 - A study on the photoluminescence properties of spray pyrolysis deposited crystalline nanostructured ZnO thin films.

H. Rahene¹, A. Zouaoui^{1*}

Laboratory of Semiconductors and Oxides Metallic
Faculté de Physique, USTHB, Bab Ezzouar- ALGERIA.

*Corresponding author : E-mail adress : amara_zouaoui@yahoo.fr

Abstract

This work is an experimental study of pure and doped zinc oxide films prepared by spray pyrolysis technique. The ZnO thin films doped with aluminum were deposited on glass substrates for different doping concentration, substrate temperature and time deposition .

The spectra of X-ray diffraction (XRD) allowed the structural identification of ZnO and determination of crystalline parameters such as lattice parameters $a = 3236 \text{ \AA}$, $c = 5183 \text{ \AA}$.and grain size

$D \approx 24 \text{ nm}$ (figure 1). The decrease in grain size for the high doping concentration can result in an increase in energy density due to surface segregation of Al atoms in the grain boundaries [1,2].

The characterization by transmission spectroscopy and reflection showed that our samples have a high transparency in the visible range ($T > 82\%$), a refractive index $1.84 \leq n \leq 1.96$ and optical gap $3.28 \text{ eV} < E_g < 3.30 \text{ eV}$. Analysis by Photoluminescence of pure and doped ZnO films allowed the identification of the various defects present in our samples, such as deficiencies in zinc (Vzn), zinc and oxygen interstitials (Zni , Oi) [3, 4] (Figure 2).

Figure 1 : Change in grain size as a function of doping layers of ZnO: Al deposited at 470 °C

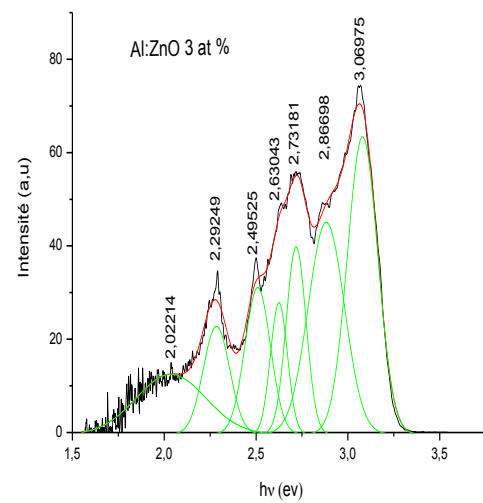
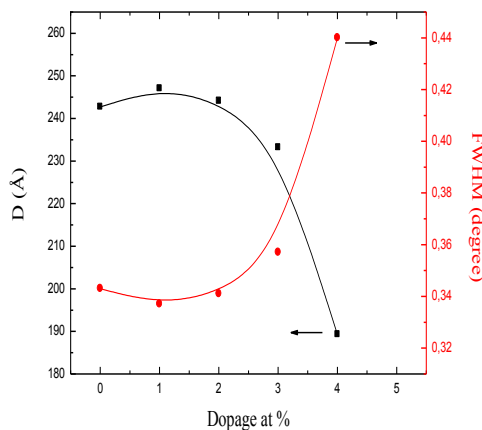


Figure 2 : Decomposition of the emission spectrum PL of ZnO doped with aluminum



References :

- 1 S.Venkatachalam, Y. Iida, Yoshinori Kanno, (2008) Superlattices and Microstructures, 44 127–135
- 2 Z.Ben Achour, T. Ktari, B.Ouertani, O.Touayar, B. Bessais, J. Ben brahim (2007), Sensors and Actuator A 134 447 451.
- 3 J.J. Ding, S.Y. Ma , H.X. Chen, X.F. Shi, T.T. Zhou, L.M. Mao, (2009) , Physica B 404 2439–2443
- 4 L.J. Li, H. Deng, L.P. Dai, J.J. Chen, Q.L. Yuan, (2008) Mater. Res. Bull. 43 1456.

P38 - Impact of the inhomogeneous structure of the active layer on the transfer characteristic of polysilicon TFT's

H. Tayoub, A. Bensmain, B. Zebentout and Z.Benamara

Applied Microelectronic Laboratory, Faculty of Engineering, University of Sidi Bel Abbes(Algeria)

Corresponding author : E-mail adress : : hadjira.tayoub@gmail.com

Introduction:

Poly-TFTs are made of a thin un-doped polycrystalline silicon film deposited on a glass substrate by the Low Pressure Chemical Vapor Deposition technique LPCVD; this choice limits the technological process to the temperature $< 600^{\circ}\text{C}$. The benefit of pc-Si is to make devices with large grain size. Unfortunately, according to the conditions during deposition, the pc-Si layers can consist of a random superposition of grains of different sizes, where it appears grains boundaries parallels and perpendiculars.

In this paper, the transfer characteristics $I_{\text{DS}}-V_{\text{GS}}$ are simulated by solving a set of two-dimensional (2D) drift-diffusion equations together with the usual density of states (DOS: exponential band tails and Gaussian distribution of dangling bonds) localized at the grains boundaries. The effect of thickness of active layer on the distribution of the electrostatic potential, the density of intergranular and interface traps states, band to band tunneling (BBT), thickness of active layer ,grain size and position of grain boundaries on the TFTs characteristics for a drain bias equal to 1V have been also investigated.

It has been found that:

The presence of grain boundaries in the structure creates heights potential barriers limiting the passage of free carriers of a crystallite to another, the sensitivity of the drain-source current is due to the application of the transverse voltage (-20V to 20V), the introduction of intergranular traps states or at the interface only increases the current or causes a shift of the characteristic. However, the reverse current tends to increase with V_{GS} , trap states behave in the blocking

state as states permit that will facilitate the transition of carriers from one band to another by creating through a gateway for the conduction. The introduction of intergranular traps states and the interface states increase just the off current.

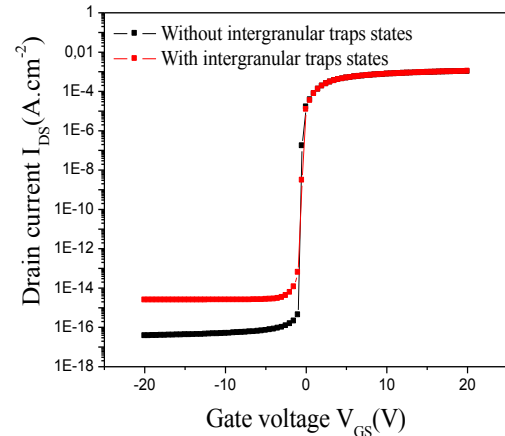


Figure 1: Simulated transfer characteristics $I_{\text{DS}}(V_{\text{GS}})$ with and without density of intergranular traps states in poly-Si TFT's.

Reference:

- [1] Brotherton, S.D., Ayres, J.R., Edwards M.J., Fisher C.A., Glaister C., Gowers J.P., McCulloch D., and Trainer M. (1999) Thin Solid Films 337,188.

P39 - Thermodynamic properties of Landau levels in semiconductor two-dimensional systems

I. Fezai, S.Jaziri

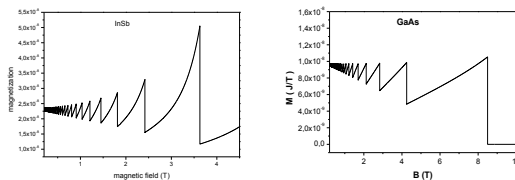
Laboratoire de Physique de matériaux, Faculté des Sciences de Bizerte
7021 Jarzouna, Tunisia
Email: sihem.jaziri@fsb.rnu.tn ; imen.fezai@hotmail.fr

Introduction: This work investigates the influence of low temperature, external magnetic field and broadened Landau levels on the thermodynamic properties of two dimensional electron systems (2DES). The interplay between these two physical parameters on the magnetic field dependence of the chemical potential and the magnetization is calculated. In the absence of a complete theory that explains the Landau level broadening, experimental and theoretical studies in literature perform different model calculations of this parameter. Here it is presented that different broadening parameter of Gaussian-shaped Landau levels cause width variation in their contribution to interlevel and intralevel excitations.

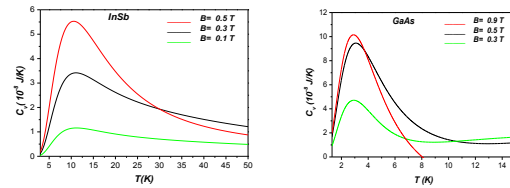
Motivation:

- 1) Two-dimensional electron systems (2DES) are widely investigated due to their intriguing non-bulk like properties and their possible applications [1].
- 2) One example of interest is the oscillating behavior of their thermodynamic properties with respect to a strong perpendicular magnetic field B at low temperature T [2, 3]. This general trend is attributed to the presence of Landau levels – the discretized energy spectrum of a 2DES subject to a strong magnetic field applied normal to the 2D plane [1].

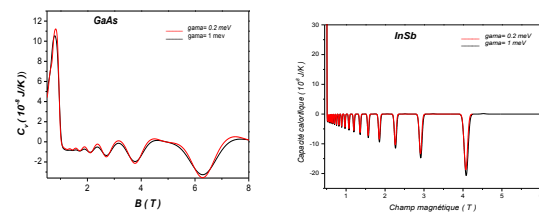
Figures and Tables:



The magnetization for $\Gamma = 0.2 \text{ meV}$ at $T = 0.3 \text{ K}$
In GaAs and InSb



The specific heat in this equation exhibits a single peak at low temperature region. The temperature T which C_v is a maximum can be obtained by taking $\partial C_v / \partial T = 0$.



The Heat Capacity for a Constant T

References:

- [1] T. Ando, A.B.Fowler, and F. Stern. Rev. Mod. Phys. , 54 (1982) 437-672.
- [2] M. A. Wilde, M. P. Schwarz, Ch. Heyn, D. Reuter, and A. D. Wieck. Phys. Rev. B, 73 (2006) 125325.
- [3] M. Zhu, A. Usher, A. Potts, M. Elliott, W. Herrenden-Harker, D. Ritchie, and M. Simmon. Phys. Rev. B, 67(2003) 155329.
- [4] Q. Li, X. C. Xie, and S. Das Sarma. Phys. Rev. B, 40 (1989) 1381-1384.
- [5] I. M. Lifshitz and A. M. Kosevich, Sov. Phys.JETP 2, 636 (1956).

P40 - Streptavidin-HRP immobilized on multiwall carbon nanotubes for biosensor application

I. Hafaiedh¹, H. Baccar¹, T. Ktari¹, A. Abdelghani^{1*}

¹Nanotechnology Laboratory, National Institute of Applied Science and Technology, centre Urbain Nord, Bp676, 1080 Charguia Cedex, Tunisia

*Corresponding author : E-mail adress : aabdelghan@yahoo.fr

Abstract:

The chemical and physical properties of carbon nanotubes (CNT) have paved the way to new and improved sensing devices, in general, and electrochemical biosensors, in particular [1]. CNT-based electrochemical transducers offer substantial improvements in the performance of amperometric enzyme electrodes, immunosensors and nucleic-acid sensing devices. CNT can be made by chemical vapor deposition, carbon arc methods, or laser evaporation and can be divided into single wall carbon-nanotubes (SWCNT) and multi-wall carbon nanotubes (MWCNT). SWCNT possess a cylindrical nanostructure (with a high aspect ratio), formed by rolling up a single graphite sheet into a tube.

In this work, we used gold labeled multiwall carbon nanotubes for peroxidase biosensor. The gold labeling on multiwall carbon nanotubes can be achieved with Pressure vapor Deposition (PVD) technique. The obtained carbon nanotubes can be immobilized on gold electrode with the airbrushing technique. The stability and the molecular structure of the labeled multiwall carbon nanotubes were characterized with cyclic voltammetry, impedance spectroscopy and Fourier Transform Infra-Red spectroscopy (FTIR). It shows a higher conductivity and a good stability in water interface. For streptavidin-HRP immobilization, the labeled gold nanotubes were activated over night with thiol-acid (16 carbons). An activation procedure was achieved with EDC/NHS for HRP-streptavidin immobilization (Figure 1).

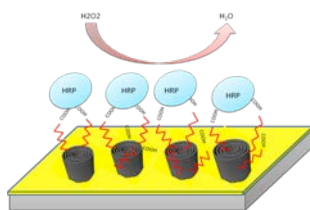


Figure 1: Representative scheme of the fabrication process of the multilayer biosensor based on multiwall carbon nanotubes

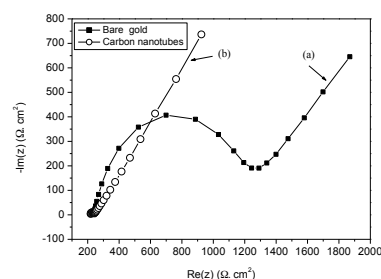


Figure 2: **(a)** Nyquist impedance plots for gold electrode with redox couple at 0V. **(b)** Nyquist impedance plots for gold electrode after MWCNTs deposition with redox couple at 0V

The development of biosensor for H_2O_2 detection was observed with the impedance spectroscopy and cyclic voltammetry techniques. This method could be used to determine total H_2O_2 concentration in the range 4–160 μM . The results show that the biosensor response depends on the conductivity and the large surface-to-volume ratio attained with multiwall carbon nanotubes. The response of the developed biosensors was reproducible with higher stability.

References:

- [1] Baughman R. H., Zakhidov A., de Heer W. A. (2002) Carbon Nanotubes: the Route Toward Applications, *Science* 2002, 297, pp.787-792.
- [2] Imene Hafaiedh, Adnane Abdelghani, Electrochemical Characterization of Streptavidin-HRP Immobilized on Multiwall Carbon Nanotubes for Biosensor Applications, *Jornal of Biomaterial and Nanobiotechnology*, in press, 2012.

P41 - Improvement of the polyimide films hydrophobic character by plasma deposited organosilicon nanolayers coating

I. Nouicer^{1*}, S.Sahli^{1**}, Z. Ziari¹.

¹Université Mentouri de Constantine, Laboratoire Microsystèmes et Instrumentation (LMI),
Faculté des Science de l'Ingénieur, Constantine 25017, Algeria

Corresponding author: E-mail address:

* ilyes.nouicer@gmail.com, ** sahli50@hotmail.com.

Abstract

Since a few decades, intense research works are focused on the study of polyimide films properties and their applications in several areas as biomedical, micro and nanoelectronics technologies [S.C.Cho et al.] [S.J. Park et al]. The great interest carried to this polymeric material is due to its many good properties as a high thermal resistance reaching 400°C, a low dielectric constant with a high electric strength and an appreciable mechanical strength with a good flexibility. In recent works, we have studied the potential decay phenomena at the surface of this material [Ziari et al. 2011] and the improvement of its wettability using SiO_x-like films deposited by plasmas [Ziari et al. 2008][Bellel et al]. Using AFM analysis, we have showed that this wettability is partially monitored by the surface nanostructure of that coated polyimide films.

The present paper work deals with the study of the hydrophilic or hydrophobic character of polyimide films coated by a plasma polymerized hexamethyldisiloxane (ppHMDSO) thin layer deposited using a capacitively coupled plasma reactor. The process parameters of this experiment are reported in Table 1.

<i>Parameters</i>	<i>Variation range</i>
Time deposition	30 – 900 s
HMDSO pressure	0.2 mbar
Power frequency	12.5 kHz
Discharge power	40 W

Table 1: Polymerization experiments operating conditions for plasma power electrical discharge.

Contact angle measurements have revealed an improvement of the hydrophobic character of the polyimide films surface coated with PPHMDSO nanolayers without modifying the external aspect and the bulk polyimide properties. Fourier transform infrared spectroscopy (FTIR) and FTIR-Attenuated Total Reflectance (FTIR-ATR) characterizations have been used to explain the modification of the polyimide surface wettability

properties. FTIR analysis shows that the chemical formula of the deposited thin layers are SiO_xC_yH_z – like (fig.1). On the other hand, the correlation between this analysis and the contact angle measurements revealed that dispersive groups have significant effect on the contact angle. The increase of the deposition time leads to an increase of the PPHMDSO thin layers thickness inducing a reduction in surface adhesion work.

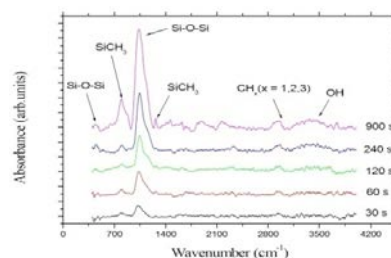


Figure 1 : FTIR spectra of plasma polymerization ppHMDSO-treated PI films at different time.

References:

- A. Bellel, S. Sahli, P. Raynaud, Y. Segui, Z. Ziari, D. Eschaich, G. Dennler, (2005) Improvement of the Polyimide Surface Wettability Using SiO_x Films Deposited in a DECR Reactor from HMDSO/O₂ Mixtures. *Plasma Process. Polym.*, 2, 586-594.
- S.C. Cho, Y.C. Hong, S.G. Cho, Y.Y. Ji, C.S. Han, H.S. Uhm, (2009) Surface modification of polyimide films, filter papers, and cotton clothes by HMDSO/toluene plasma at low pressure and its wettability. *Current Applied Physics*, 9, 1223-1226.
- S.J. Park, H.Y. Lee, (2005) Effect of atmospheric-pressure plasma on adhesion characteristics of polyimide film. *Journal of Colloid and Interface Science* 285, 267-272.
- Z.Ziari , S.Sahli , A. Bellel, Y. Segui, P. Raynaud (2011) Simulation of Surface Potential Decay of Corona Charged Polyimide. *IEEE Transactions on Dielectrics and Electrical Insulation*, 18(5), 1408-1415.
- Z. Ziari, A. Bellel, S. Sahli, Y. Segui , P. Raynaud, (2008) A comparative study on the effect of VUV radiation in plasma SiO_x coated polyimide and polypropylene films . *Progress in Organic Coatings*, 61, 326-332.

P42 - Influence of alkali substitution on the physical characteristics of alypbmg glass

I. Boudraa¹, H. Aallal¹, C. Benhamideche^{1,2}, S. E. Bouaoud¹ & M. Poulain³

¹Unité de recherche chimie de l'environnement moléculaire et structurale (URCHEMS), Université de Mentouri-Constantine, Route Ain El Bey, Constantine (25000)-Algérie.

²Département des sciences de la Matière, Université de Skikda, Route d'El-Hadaiek-Skikda.

³Lab. Matériaux Photoniques, Université de Rennes 1, Campus Beaulieu, F-35042 Rennes

issam.boudraa@gmail.com

Abstract:

Fluoroaluminate glasses have been reported as the earliest heavy metal fluoride glasses. By comparison with fluoroaluminates glasses, they offer a set of similar optical features, but also some differences in their mechanical and chemical properties. In practice they have been less developed because their stability against devitrification is smaller than that of the most stable fluorozirconates.

The purpose of this study was to investigate glass formation in systems $\text{AlF}_3\text{-YF}_3\text{-PbF}_2\text{-MgF}_2\text{-MF}_2$ (M= Li, Na, K). Synthesis was implemented at room atmosphere using the ammonium fluoride processing. After fining, the liquid was into a preheated brass mold, then annealed below the glass transition temperature for several hours. The samples were polished for optical measurements.

Glass formation has been investigated in a systematic way, using pseudo ternary systems in order to allow parameters to vary at the same time. We have chosen the most stable glass compositions for the determination of the physical properties. These properties including characteristic temperatures, density, micro hardness and proprieties mecanique.

Glass stability increases in multicomponent glasses. Bulk samples have been prepared for physical characterization. These glasses have a potential interest for passive optical fibers because they are less sensitive to water attack than ZBLAN glass, mechanically stronger. It is expected they could have a larger damage threshold for laser power transmission.

Glass stability was assessed using differential scanning calorimetry (DSC).Figure 1

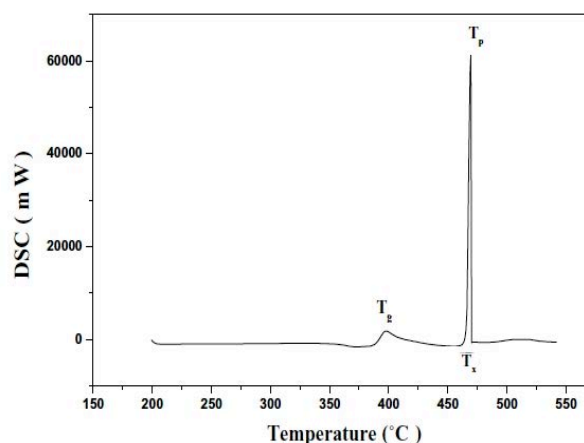


Figure 1: DSC curve of glass sample.

Key words:

Fluoride glass, aluminium fluoride, thermal properties, density, micro hardness, proprieties mecanique.

Reference:

K. H. Sun, and M. Huggins, Fluoride Glasses, US patent 2,551,224(1950).

P43 - Carrier relaxation mechanisms in CdS/ZnS core-shell quantum dots: Auger relaxation

I. Zgaren*, S.Jaziri

Laboratoire de Physique de matériaux, Faculté des Sciences de Bizerte 7021 Jarzouna, Tunisie

*Corresponding author : E-mail adress : ibtis10sem@yahoo.fr

Introduction:

The principal aim of our work is to investigate different Auger processes in CdS/ZnS Core-Shell quantum dots. Within the frame work of the effective mass approximation, we calculated the electron and hole energy levels and associated wave functions. Thereafter, we focused on Auger carrier relaxation inside the core.

Results:

First, we have numerically simulated the electron and the hole energy levels, and we have investigated the effect of the core and shell size on the energy levels.

Our results (fig.1.) show that energy levels depends on both core radius and shell thickness [1].

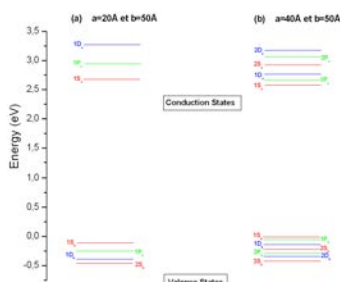


Fig.1. Electron and hole states for CdS/ZnS core-shell quantum dot for two different core radius and the shell thickness fixed equal 50 Å.

Second, We study the carrier Auger relaxation when the electron is inside the core. we consider as initial electron-hole state $|1P_e 1S_h\rangle$ that corresponds to the 1P electron state and the low-lying 1S hole state, and as final scattering states those that correspond to an electron occupying the 1S state and a hole in a deep state $k |1S_e k_h\rangle$.

We present in Fig.2. the thickness dependence of P→S Auger relaxation time τ_A for three different core radius, $a=18 \text{ \AA}$, $a=20 \text{ \AA}$ and $a=22 \text{ \AA}$. Our calculations show a great dependence of time relaxation on QDs size. It increases with shell thickness increasing; on the other hand it decreases

when core radius increases. However, time variation with shell thickness is clear as presented in Fig.2, but it is more important for smaller core radius. For 18 Å core radius, τ_A vary from 22 to 215ps corresponding to a shell thickness variation from 32 Å to 50 Å. This variation is smaller for greater radius; it is about 18ps for 22 Å core radius. This behaviour is observed by Wang et al. [2] for CdSe colloids. Auger mechanism requires the presence of a hole to be effective; this mechanism was challenged by Guyot-Sionnest et al [3] as an explanation of the observed P→S electron relaxation. Likewise, Califano [4] predict that the Auger mechanism can explain the experimentally observed intraband P→S relaxation time scale without the need to invoke any exotic relaxation.

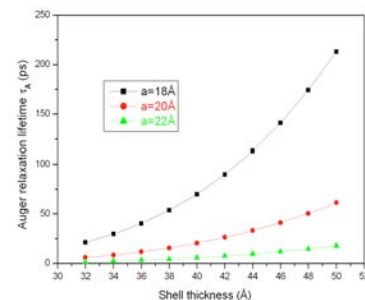


Fig.2. Auger relaxation lifetime in CdS/ZnS as functions of the nanocrystal Shell thickness for different Core radius “a”.

References:

- [1] Zgaren I., Sallemi K. and Jaziri S. (2009) Sensor Letters. Vol 7, 1-5.
- [2] Wang L.W., Califano M., Zunger A. and Franceschetti A. (2003) Phys. Rev. Lett. 91, 056404.
- [3] Guyot-Sionnest P., Wehrenberg B., and Yu D. (2005) J. Chem. Phys. 123, 074709.
- [4] An JM., Califano M., Franceschetti A., and Zunger A. (2008) Journal of Chemical Physics, vol 128 (16), 164720.

P44 - Modelling of biosensors for cancer monitoring

J. Chermiti^{1,2}, M. Ben Ali^{2,3}, C. Dridi¹, Y. Korpan⁴, N. Jaffrezic-Renault⁵

¹ University of Sousse ; Institut Supérieur des Sciences Appliquées et de Technologie de Sousse, Cité Taffala, 4003 Sousse, TUNISIA.

² University of Carthage, Unité de Recherche de Physique des Semi-conducteurs et Capteurs, IPEST, La Marsa, 2070 Tunis, TUNISIA

³ University of Carthage, Institut Préparatoire aux Etudes d'Ingénieur Nabeul - Nabeul – 8000, TUNISIA

⁴ Institute of Molecular Biology & Genetics NAS of Ukraine, 150 Zabolotnogo Street, 03680, Kyiv, UKRAINE

⁵ Laboratory LSA, UMR 5180, Université Claude Bernard Lyon 1, FRANCE

Current trends in health science and biomedical research indicate a continuous need for technologies that allow accurate measurements particularly for detection of biochemical species which is carried out in various areas: biomedical and environmental analyses. Indeed, in recent years, there has been an important development of biosensors of cancer-relating molecules, such as formaldehyde, amines and metal ions, because the early diagnostic of cancer and its real time monitoring is crucial for the successful treatment of disease. Moreover, we can notice that the scientific literature in the field of biosensors is very rich in terms of experimental results with a lack of theoretical analysis of the processes involved in these devices.

In this context, we designed and developed a numerical platform (which operating system is presented below) using the neural network in order to analyze cancer biosensors performances. This numerical tool allows the optimization of technological parameters of the devices and the extraction of intrinsic and extrinsic sensing characteristics such as sensitivity, detection limit, linear range, number of accessibility sites, complexation coefficient,...

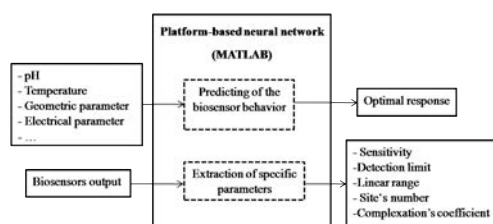


Fig 1: General aspect of the platform developed

The calculations are based on Mott-schottky equation (Eq.1) and the site binding model (J. Chermiti 2011).

$$\frac{1}{C_T^2} = \frac{2}{\epsilon_s q N_D} (V - V_{fb}) \quad (\text{Eq.1})$$

where N_D is the number of donors, V is the applied voltage, V_{fb} is the semiconductor flat band potential, k is Boltzmann's constant, q is the electronic charge, C_T represents the interfacial capacitance and ϵ_s is the semiconductor dielectric constant.

In this work, the site binding model was improved taking into account the buffer concentration effect on the biosensors responses (Eq.2).

$$P [X^{Z+}] = -\log [X^{Z+}] = \frac{Z q \psi_o}{2.3 K T} \quad \text{Eq (2)}$$

$$+ \log \left(\frac{q N_s}{C_{eq} \psi_o} - 1 \right) - pK + \alpha C^{-\beta}$$

where ψ_o is the potential of the functionalized insulator/electrolyte interface, N_s is the surface density of sites, pK is the complexation constant, C_{eq} is the equivalent capacitance, Z is the charge of the ionic species, C the buffer concentration, T the absolute temperature and α and β are parameters which depend on the buffer nature and the structure of the sensing layers, respectively.

The platform was used to characterize the formaldehyde and methylamine biosensors based on FDH and MAO-MAOX, respectively, as bio-recognition elements. The results of numerical study, by means of the electrochemical and fractal theories, are in good agreement with the ones observed in literature (M. Ben Ali 2007).

References:

- Chermiti, J., Ben Ali, M., Jaffrezic-Renault, N., (2011) Numerical modelling of electrical behaviour of semiconductor-based micro-sensors for copper ions detection, *Sensor Letters*, 9,1–4.
- Ben Ali, M., Gonchar, M., Gayda, G., Paryzhak, S., Maaref, M.A., Jaffrezic-Renault, N., Korpan, Y. (2007) Formaldehyde-sensitive sensor based on recombinant formaldehyde dehydrogenase using capacitance versus voltage measurements, *Biosensors and Bioelectronics*, 22, 2790–2795.

P45 - Reliability study of proton exchange membrane fuel cell by causal tree analysis

K. Brik¹, F. Ben Ammar^{1,2}, A. Djerdir³, A. Miraoui³

¹Unité de Recherche Matériaux Mesures et Applications,
²Institut National des Sciences Appliquées et de Technologie,
³FClab-UTBM, 13 rue Thierry Mieg, 9000 Belfort France,

Introduction: The integration of fuel cells in industrial applications is limited by the degradation phenomena which reduce the energy production. In fact the fuel cell loses its performances during the cycling by the deficiency of the membrane and the electrodes. Consequently, it seems important to study and evaluate the fuel cell reliability in order to ameliorate its life time. The authors present a reliability approach to analyze the degradation of proton exchange membrane fuel cell. This approach uses the reliability analysis tools such as the causal and fault trees to evaluate the fuel cell lifetime and exploits the experimental measurements to identify the used model parameters. The elaboration of causal tree offers powerful tools to a deductive analysis which consists on seeking the various combinations of events leading to the fuel cell degradation. The authors identify the maximum variation intervals according to each degradation mode. The proposed diagnostic system is applied to a useful fuel cell in order to evaluate its degradation degree.

Causal tree analysis of fuel cell: The performances of a fuel cell decrease during the cycles of use. This ageing is accompanied by the failure of one or more auxiliary elements in the system and the degradation of the various parts of the fuel cell: the electrodes and the membrane. The causal tree presents the combinations of events which lead to fuel cell system degradation.

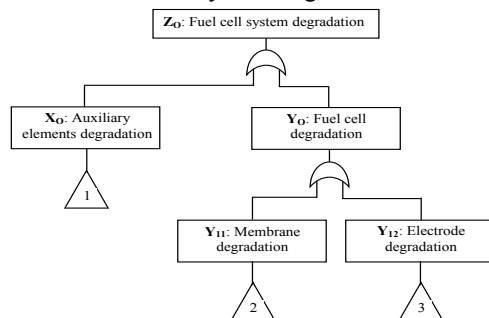


Figure 1: Causal tree of fuel cell system.

Fault tree analysis of fuel cell: The causality chain is completed by a fault tree analysis established starting from the elements of the fuel cell model. Therefore, it is determined to know which parameters well influence the starting of the degradation modes. The membrane degradation generates the variation of the area specific

resistance and the electrode degradation generates the variation of the charge transfer coefficient. The determination of upper limit of the fuel cell parameters model is particularly advantageous, since it helps to determine the depth of degradation. The lifetime of the fuel cell is achieved when its nominal voltage falls of 20 % for the nominal current.

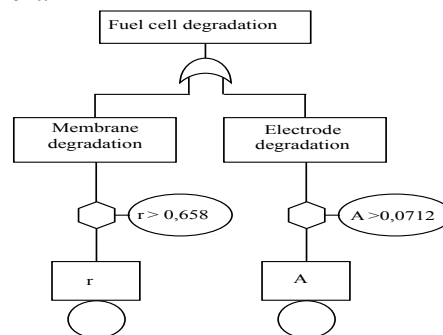


Figure 2: Fault tree analysis of the deficiency presenting the limiting values.

Failures detectability: The failures detectability is based on the comparison of the experimental output characteristic of a new fuel cell to the used fuel cell. This approach gives information about the lifetime and the degradation of the fuel cell. It consists to determining the impact of each degradation mode (membrane degradation and electrode degradation). Table 1 summarizes the several degrees of degradation relating to each failure mode. The sum $\alpha_1 + \alpha_2$ indicates the ageing of fuel cell, it is supposed degraded if the sum exceeds 100%.

α_1 : membrane degradation of %	48.24%
α_2 : electrode degradation of %	9.5%
Parameter variation of %	57.74%
Ageing of fuel cell	Non degraded

Table 1: Aging of fuel cell.

References:

Bia, W., Thomas, F. and Fullera, B. (2008) Temperature Effects on PEM Fuel Cells Pt Catalyst degradation Journal of The Electrochemical Society.
 Schmittinger, W. and Vahidi, A. (2008) A review of the main parameters influencing long-term performance and durability of PEM fuel cells Elsevier, Journal of Power Sources, Vol. 180.

P46 - Performance of modified SPEEK membrane by inorganic nanocomposite for fuel cell

K. charradi^{1*}, Z. Ahmed^{1,2,3} and R. Chtourou¹

¹Photovoltaic Laboratory, Centre for Research and Energy Technologies CRTEn, BP 95, Hammam Lif 2050 Tunisia

²National Centre for Research in Materials Science, Centre for Research and Energy Technologies B.P N°95-2050 Hammam Lif-Tunisia

³School of science and technology ESST hammam sousse- Tunisia

*Corresponding author: E-mail adress: charradi_kaled2000@yahoo.fr

Abstract: Among the best way to enhance fuel cell performances, is the improvement of the polymer electrolyte membrane. Over the last 10 years, there has been increasing interest in the polymers sulfonated polyetheretherketone (SPEEK). SPEEK is considered as a possible alternative to Nafion for proton exchange membrane fuel cell application, for his low cost, low fuel permeability, good proton conductivity and high thermal and chemical stability. Recently the organic-inorganic hybrid membranes have been prepared by addition of various inorganic compounds such as SiO₂, TiO₂ and clay. Nanocomposite of clay can be used to ameliorate the proprieties of the SPEEK membrane [Chang J. H, Jaafar J.]. Smectite is a 2/1 phyllosilicate composed of negatively charged layers. It has a high cation exchange, high surface area and high barrier properties. In order to understand the effect of this clay on the structure and the ionic conductivity of the SPEEK, a composite cast SPEEK membranes containing smectite powder were prepared and characterized. SPEEK was prepared using PEEK and concentrated sulfuric acid as sulfonation agent [Di Vona]. The degree of sulfonation was fixed at 70%. SPEEK was modified with various amounts (6, 5 or 4 wt%) of smectite. The synthesis was prepared in DMSO solution, stirred for 24h and heated at 80°C. The modified membrane was characterized by electrochemical impedance spectroscopy (EIS), field emission scanning electron microscopy (SEM) and thermogravimetric analysis (TG). The SPEEK-smectite membrane characterized concerning their water, ethanol and methanol solution uptake has amelioration of swelling behaviour (figure 1) and proton conductivity. The modification of polymer SPEEK permitted the amelioration of the

performance of membrane used as promising alternative proton exchange membrane (PEM) for Fuel Cell (FC) compared to SPEEK membrane.

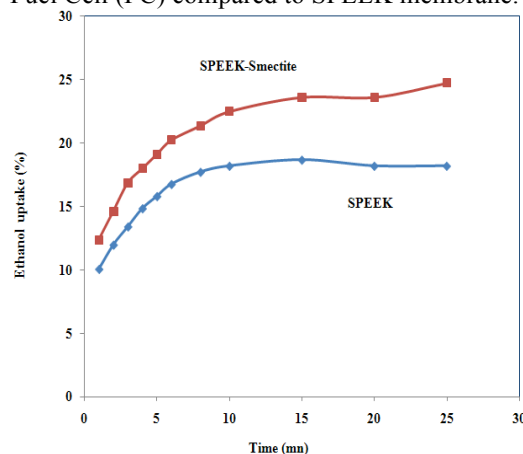


Figure 1: ethanol uptake of SPEEK and SPEEK-smectite membrane as function of time.

References:

- Chang, J. H., Park, J. H., Park, G.G., Kim C.S., Park O.O., (2003) Proton-conducting composite membranes derived from sulfonated hydrocarbon and inorganic materials, *Journal of power sources*, 124, 18-25.
- Di Vona, M. L., Marani, D., D'Epifano, A., Traversa, E., Trombetta, M., Licocchia, S., (2005) A covalent organic/inorganic hybrid proton exchange polymeric membrane: synthesis and characterization, *polymer*, 46, 1754-1758.
- Jaafar, J., Ismail, A.F., Matsoura, T., Nagai, K., (2011) Performance of SPEEK based polymer-nanoclay inorganic membrane for DMFC, *Journal of Membrane Science*, 382, 202-211

P47 - Effect of gamma irradiation and thermal annealing on the nanosize particles formation in silver ion-exchanged silicate glass

K. Farah^{1,2*}, F. Hosni¹, A. Mejri¹, B. Boizot³, A. H. Hamzaoui⁴

¹Unité de recherche : Maîtrise et développement des techniques nucléaires à caractère pacifique. Centre National des Sciences et Technologie Nucléaires. 2020, Sidi-Thabet. Tunisia.

²ISTLS, 12, rue Abdallah Ibn Zoubair, 4029, Université de Sousse. Tunisia.

³Laboratoire des Solides Irradiés, UMR 7642 CEA-CNRS-Ecole Polytechnique Ecole Polytechnique, Route de Saclay, 91128 Palaiseau CEDEX, France

⁴Laboratoire de valorisation des ressources naturelles et matériaux de récupération, Centre National de Recherche en Sciences des Matériaux, Borj Cedria, B.P. 95, Hammam-Lif 2050, Tunisia

*Corresponding author : E-mail adress : kafarah@gmail.com

Small silver particles embedded in glass matrix are widely studied because of their potential applications for glass colouration (Rao, 2002; Ageev et al., 2007; Bandyopadhyay, 2008), for ionizing radiation dosimetry (Schulman et al., 1951) and recently for fabricating optical devices (Bach and Neuroth, 1998). Ion exchange process with irradiation and thermal treatment is an important method for obtaining silver nanoclusters in glasses and provided an alternative way of forming metallic nanoclusters in glass to ion implantation. A microscope slide glasses have been subjected to ion exchange at 320°C in a molten mixture of AgNO₃ and NaNO₃ with molar ratio of 5:95 for 60 min. The ion exchange process was followed by annealing at the temperature of 550°C for different time periods ranging from 10 to 582 min. Optical properties of the ion exchanged glass are measured using UV-Vis absorption spectroscopy (figure 1). The gamma irradiation induced holes and electrons in the glass structure leading to the creation of a brown colour, and silver ions trapped electrons to form silver atoms. The silver atoms diffused and then aggregated to form nanoclusters after heating at 550°C. The surface plasmon absorption of silver nanoclusters in the glass indicated that the nanoclusters radius grew between 0.9 and 1.43 nm with increasing of annealing time from 10 to 242 min and then saturated. Usually, the growth of metallic clusters in glass is considered as a diffusion-limited process (Bartels et al., 1991; Rao and Doremus, 1996). We found that our data can be fitted by a first order formation kinetic function, which confirmed the diffusion-control process. The average cluster radius R of the clusters is calculated from the full width half maximum, $\Delta\lambda$ (FWHM) of the optical absorption peak using the formula:

$$R = \frac{V_f \lambda_m^2}{2\pi C \Delta\lambda}$$

Where V_f is the Fermi velocity of the electron in the bulk metal (silver=1.39×10⁸ cm/s), $\Delta\lambda$ is the full width at half maximum of the absorption band and

λ_m is the characteristic wavelength at which SPR occurs. The FWHM is determined by assuming the absorption peak as a Lorentzian distribution (Doremus, 1965). Both λ_m and $\Delta\lambda$ depend on the substrate and size of the metal nanoclusters forming the composites.

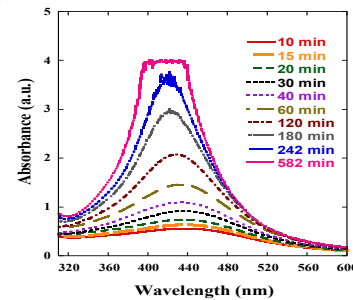


Figure 1: Absorption spectra of ion-exchanged silicate glass, irradiated with γ rays at 250 kGy and annealed at 550°C for the indicated times

References:

- Ageev, L. A., Miloslavskii V. K. and Makovetskiï, E. D. (2007) Coloring of silica glass with silver nanoparticles, *Optics and Spectroscopy* 102, 442–448.
- Bach, H., Neuroth, N. (1998) *The Properties of Optical Glass*, Springer, Berlin.
- Bandyopadhyay,, A. K. (2008) *Nano Materiels*, New Age International (P) Ltd., Publishers, Kolkata, India.P
- Bartels, J., Lembke, U., Pascova, R., Schmelzer, J., Gutzow, I. (1991) Evolution of cluster size distribution in nucleation and growth process. *J. Non-Cryst. Solids* 136, 181-197.
- Doremus, R. (1965) Optical properties of small silver particles, *J. Chem. Phys.* 42, 414-417.
- Rao, P., Doremus, R., (1996) Kinetics of growth of nanosized gold clusters in glass, *J. Non-Cryst. Solids* 203, 202-205.
- Rao, K. J. (2002) *Structural Chemistry of Glasses*, Elsevier Science & Technology Books.
- Schulman J. H., Ginther, R. J., C. C. Klick, R. S. Alger and Levy R. A. (1951) Dosimetry of X-rays and gamma rays by photoluminescence, *J. Appl. Phys.* 22, 1479-14871.

P48 - Elaboration and characterization of sol-gel

silica EPR dosimeters for high dose dosimetry

K. Marzougui ^{1*}, K. Farah ¹, A.H. Hamzaoui ², H. Ben Ouada ³

¹Centre National des Sciences et Technologie Nucléaires.Pôle Technologique de Sidi-Thabet, 2020. Tunisie

*Corresponding author : E-mail adress : kaouther.marzougui@topnet.tn

²Unité des Matériaux, Institut National de Recherche Scientifique et Technique.
BP 95, 2050 Hammam Lif. Tunisie

³Laboratoire des Interfaces et Matériaux Avancés.Faculté des Sciences de Monastir,
Avenue de l'environnement 5019 Monastir . Tunisie

Abstract

Silicate glass was considered as suitable material for dosimetric purposes (K.Farah et al, 2010), and the study of stable paramagnetic centers induced by radiation has proven its potential for radiation dosimetry (K.Farah et al, 2012). Despite its several advantages that make it especially attractive, silicate presents some disadvantages like heterogeneity of chemical composition and high melting temperature. These problems can be resolved by elaboration of silica glass at room temperature via sol-gel method, which was an excellent and economically process offering purity, homogeneity besides to control components and properties of this material (A.M.M.Santos and W.L.Vasconcelos,2000).

In this study, the sol gel process preparation starts from a solution containing tetraethoxysilane (TEOS) precursor and consist mainly on two steps, hydrolysis and polycondensation.

Hence, the sol to rigid glass conversion took place after loss of solvent, with drying gels at room temperatures and then gamma irradiated in order to induce paramagnetic centers. Therefore, we report in this study, the paramagnetic states induced after irradiation in iron doped and pure SiO₂ sol-gel glasses.

The aim of the present work is to investigate the EPR properties of sol-gel silica glass and to ascertain its possible use for high dose dosimetry.

The EPR spectra of unirradiated silica, recorded at room temperature and at 140 K exhibit a silent spectrum. However, major changes occur in the spectrums of gamma irradiated samples (Fig.1) are attributed to the formation of non-bridging oxygen hole centers and E' centers (G.Kordas, 1992).

The spectrum of iron doped silica recorded at 140 K consists of four resonances : g=4,3 attributed to ion Fe³⁺, g=8,27 and g=2,73 associated to presence of iron clusters in pores, finally g=1,99 may be due to defects of irradiation in sol-gel material.

The preliminary EPR analysis of radiation induced paramagnetic centers in sol-gel silica represents a relevant approach to dosimetry. According to the

current results, complementary AFM and FTIR studies are in progress.

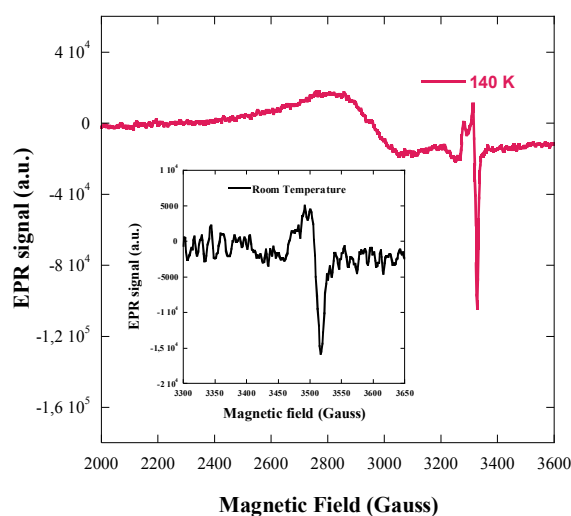


Figure 1: EPR spectrum of irradiated silica recorded respectively at room temperature and 140 K..

References

- Farah, K., Mejri, A., Hosni, F., Ben Ouada, H., Fuochi, P.G., Lavalle, M. and Kovacs, A. (2010) Characterization of a silicate glass as a high dose dosimeter. *Nuclear Instruments and Methods in Physics Research A*, 614, 137–144, 2010.
- Farah, K., Mejri, A., Hosni, F., Hamzaoui, A. H. and B. Boizot. (2012). Formation and Decay of Colour Centres in a Silicate Glasses Exposed to Gamma Radition: Application to High-Dose Dosimetry. *Ionizing Radiation Book 2*. 1-22.(In press).
- Santos, Ana Maria M. and Vasconcelos, Wander L. (2000). Properties of porous silica glasses prepared via sol-gel process. *Journal of Non-Crystalline Solids*, 273, 145-149, 2000.
- Kordas, G. (1992) EPR spectroscopy on sol-gel glasses . *Journal of Non-Crystalline Solids* 147&148,106-114, 1992.

P49 - Yellow emission in SiO₂/Zn₂SiO₄:Mn nanocomposite synthesized by sol-gel method combined with a furnace firing

K. Omri¹, H. Dahman¹, C. Barthou², L. El Mir^{1,3*}

¹Laboratoire de Physique des Matériaux et des Nanomatériaux appliquée à l'Environnement, Faculté des Sciences de Gabès, TUNISIA

*Corresponding author : E-mail adress : Lassaad.ElMir@fsg.rmu.tn

²Institut des NanoSciences de Paris (INSP), FRANCE

³Al-Imam Muhammad Ibn Saud University, SAUDI ARABIA

Abstract: The sol-gel method was used for the synthesis of the ZnO:Mn nanoparticles and SiO₂/ZnO:Mn nanocomposites. After the incorporation of ZnO:Mn nanoparticles in SiO₂ host matrix, heat treatment at 1500 °C for 2 hours was performed for the elaboration of SiO₂/Zn₂SiO₄:Mn nanocomposites. The structural, morphological and optical properties of these samples were investigated by X-ray diffraction (XRD), transmission electron microscopy (TEM), scanning electron microscopy (SEM) and photoluminescent (PL). The size of ZnO:Mn nanoparticles varies between 18-30 nm, however zincic willemite nanoparticles size varies between 75–84 nm. This phase (Zn₂SiO₄:Mn) in silica was obtained by solid reaction at high temperature, between silica and zinc oxide. The luminescence properties of the SiO₂/Zn₂SiO₄:Mn nanocomposite showed a broad yellow PL emission band centered at 575 nm. This yellow emission is originated from the ⁴T₁(⁴G)–⁶A₁(⁶S) internal transition of the Mn²⁺ ion in β-Zn₂SiO₄ phase.

Results:

The XRD pattern indicates the formation of hexagonal wurtzite phase of ZnO [El Mir]. The XRD pattern of the SiO₂/Zn₂SiO₄:Mn nanocomposite as shown in figure. 1, has confirmed the β-Zn₂SiO₄ as the main crystalline phase [Mai].

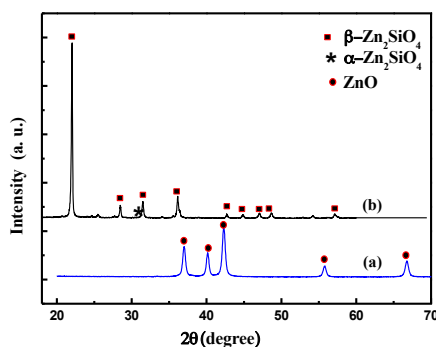


Figure 1. X-ray diffraction pattern of the (a): ZnO:Mn_{5%} nanopowder and (b): SiO₂/Zn₂SiO₄:Mn nanocomposite

Nanoparticles	Gap (eV)	Size (nm)
ZnO:Mn	3,35	28
β-Zn ₂ SiO ₄ :Mn	5,47	72

Table 1: Summary of experimental results of our samples.

The study of the photoluminescence spectrum shows that the strongest emission band was observed at about 575 nm under the excitation 255 nm [Yaqi].

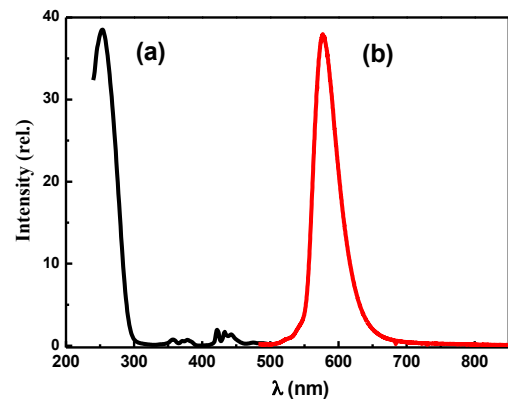


Figure. 2. PLE (a): (excitation=575nm) and PL (b): (λexcitation =255nm) spectrum of a typical SiO₂/Zn₂SiO₄:Mn²⁺ nanocomposite.

References:

- El Mir, L., Ben Ayadi, Z., Rahmouni, H., El Ghoul, J., Djessas, K. and von Bardeleben, H. J., (2009) Elaboration and characterization of Co doped, conductive ZnO thin films deposited by radio-frequency magnetron sputtering at room temperature, *Journal of Thin Solid Films*, 517, 6007-6011.
- Mai, M. and Feldmann, C., (2009) Two-color emission of Zn₂SiO₄:Mn from ionic liquid mediated synthesis, *Journal of Solid State Sciences*, 11, 528-532.
- Yaqi Jiang, Jie Chen, Zhaoxiong Xie and Lansun Zheng, (2010) Syntheses and optical properties of α- and β-Zn₂SiO₄: Mn nanoparticles by solvothermal method in ethylene glycol-water system, *Journal of Materials Chemistry and Physics*, 120, 313-318.

P50 - Electrochemical properties of spinel-type ZnM_2O_4 (M = Cr and Mn) electrodes for oxygen evolution in alkaline solutions

K. Rida^{1*}, L. Merabet¹, I. Kehal²

¹ Laboratoire Interactions Matériaux-Environnements (LIME), Université de Jijel-Algerie.

² Unité de Catalyse et de Chimie du Solide, Université Lille 1

*Corresponding author : E-mail address : rida_kamel2001@yahoo.fr

Introduction:

The oxygen electrode reaction is known to possess high activation overpotentials in aqueous solutions resulting in substantial energy losses. To decrease the oxygen overvoltage, numerous electrocatalysts have been investigated and extensively reviewed [1-2]. Among these, transition metal mixed oxides with spinellic as well as perovskite structures have been considered most promising and extensively studied [3-5].

In this paper, two spinel-type oxides ($ZnCr_2O_4$ and $ZnMn_2O_4$) were synthesized by sol-gel method at 800°C and investigated as electrodes for the O_2 evolution reaction (OER) in NaOH solutions. The physicochemical properties have been analyzed using TG-DTA, FTIR, XRD, SEM and BET surface area. From electrochemical measurement, it was found the Impedance spectroscopy and voltametric cyclic. The results show that the performance of the $ZnMn_2O_4$ electrode is observed to be better than the $ZnCr_2O_4$ towards the O_2 evolution reaction in 1M NaOH at 25°C.

2. Experimental

2.1. Preparation

A sol-gel (Pechini) method was employed to prepare $ZnCr_2O_4$ and $ZnMn_2O_4$ spinels.

2.2. Characterization

Thermogravimetric analysis and differential thermal analysis of the precursor decomposition were performed on a Perkin-Elmer TGA7 and a Perkin-Elmer DTA7.

Fourier Transform Infrared (FTIR) spectra were recorded in the 4000–400 cm^{-1} range with a Perkin-Elmer 1730 FT-IR, using the KBr pellet technique.

Powder XRD patterns were recorded in the 10–80° 2θ range in the scan mode (0.028 step size, 2 s counting time) using a D8-Advance de Bruker-AXS powder diffractometer employing Cu $K\alpha$ radiation.

The specific surface area of the samples was determined by applying the BET method to nitrogen adsorption isotherms recorded at -196°C, using a Micrometrics apparatus model ASAP-2000.

The general morphology of the ground samples was analysed by SEM using a Philips XL30 apparatus

2.3. Electrochemical properties

The electrochemical measurements are performed with an electrochemical cell connected to a potentiostat (PGZ Voltalab 301)

3. Results

$ZnMn_2O_4$ phase crystallizes in space group tetragonal system $I4_1$. $ZnCr_2O_4$ phase crystallizes in space group $Fd3m$ of cubic system

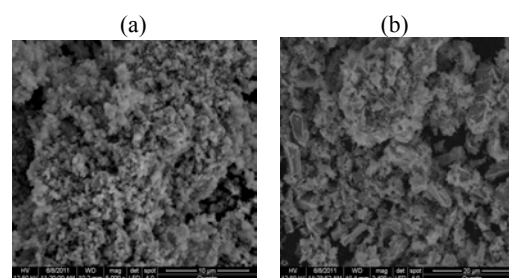


Figure 1: SEM of (a) $ZnCr_2O_4$ and (b) $ZnMn_2O_4$

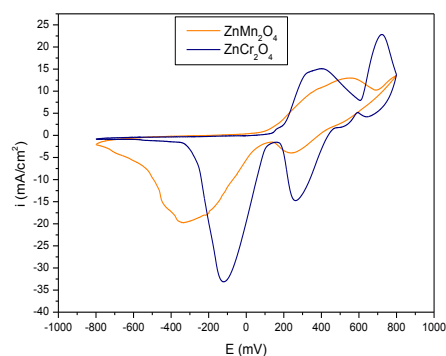


Figure 2: Curve of cyclic voltammetry in 1M NaOH

References:

- [1] Rajaram RR, Sermon A, J Chem Soc Faraday Trans 81 (1985) 2577.
- [2] Lahiri P, Sengupta SK, J Chem Soc Faraday Trans 91 (1995) 3489.
- [3] El Baydi M, Poillerat G, Rehspringer JL, J Solid State Chem 109 (1994) 281.
- [4] Singh JP, Singh RN, J New Mat Electrochem System 2 (2000) 137.
- [5] Bo Chi, Jianbao L, Xiaozhan Y, Hong L, Electrochim Acta 50 (2005) 2059.

P51 - Optimization of the detection in microanalysis X by sample treatment

¹K. Saïl1*, ¹M.H.Gafour, ¹G. Bassou, ¹M.Rahhal-Sekkal, ¹A.Kadoun

¹L2MSM, Faculty of Sciences, University Djillali Liabès of Sidi-Bel-Abbès,
B.P. 89, Sidi Bel Abbes 22000, Algeria

*Corresponding author: E-mail address: sailkari7@yahoo.com

Abstract

The Scanning Electron Microscope (SEM) is an essential tool for characterization in most scientific laboratories and particularly when it is equipped with an X-ray detector. The apparatus on which we carried out our investigations is a SX100, a Cameca mark SEM, coupled to four wavelength dispersion spectrometers. The sample studied in this paper is ores. It is calcic apatite would also contain oolites and coprolithes. Analyzes on these polished and non-polished samples were carried out in order to highlight the role of polishing

Metallographic preparation

The operation of polishing requires a preparation which consists in coating the ore powders some in an epoxy resin appearing itself as two liquids characterized by a very good fluidity as well as a very good hardness and a good chemical resistance to solvents and acids. After polymerization at a temperature about 80°C mechanical polishing is carried out in three stages as indicated on table 1

<i>Polishing</i>	<i>Pré-polishing</i>	<i>Fine</i>	<i>Finishing</i>
<i>Support</i>	Paper	Self-adhesive cloths, compressed, metal	Polyurethane cloths
<i>Abrasives, composition, size</i>	SiC	Diamond 45 to 0.25µm aerosol, suspension ou pâte	SiO ₂ 0.05µm
<i>Lubricating</i>	water	Alcohol Oily base	Water
<i>Speed Trs/mn</i>	300 and +	150 to 250	150 to 250

Table1: Polish stages

The last stage is the cleaning which is obtained by a washing with alcohol then with water plus liquid soap using an ultrasound tank and finally a rinsing and drying with the compressed air

Results

The comparison between spectra of the polished and no polished samples shows clearly the relative increase in x-emission in the case as of polished samples. Figures 1 represent the spectra of the ore respectively obtained by the spectrometers: CP1 (multi-layer crystal (W/Si)). It arises according to this qualitative analysis that the polished ore represents a relative increase in the intensity for each peak compared to the non-polished ore. The difference is about 1000 cps for crystal PC1.

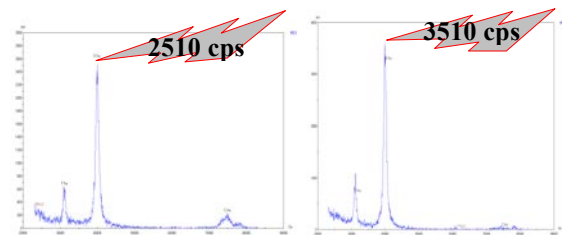


Figure 1: Ore spectra obtained with crystal PC1 (Polished at the right no polished at the left)

For the semi-quantitative analysis we note that the cartographies figure 2 represent an anomaly in the case of the non-polished ore.

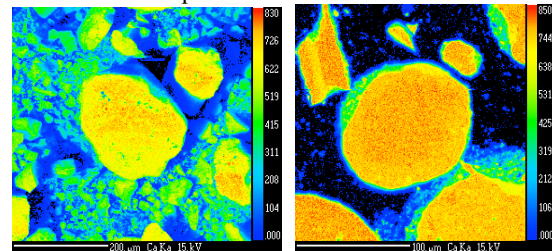


Figure 2: Cartography X of the Calcium distribution

(Polished at the right no polished at the left)

References

- J.L.Pouchou, (2008), Les méthodes de quantification en microanalyse X, Microscopie électronique à balayage et microanalyses. P 465-467.
- J.Ruste, (2008) la microanalyse quantitative en WDS des éléments très légers. Microscopie électronique à balayage et microanalyses. p 473-474.
- R. Wilmotte, J. Benezech " (1975), Pratique et Théorie des Traitement des Surfaces : tome 1 Décapage et Dégraissage", Editions B. P. J

P52 - Transparent conductive layers based multilayer MoO₃/Ag / MoO₃, application as an anode in organic optoelectronic devices

⁽¹⁾ L.Barkat, ⁽¹⁾ A.Mohammed-Krarroubi, ⁽¹⁾ FZ. Dahou, ^(*) J.C Bernede, ⁽¹⁾ A.Khelil.

(1) Physics laboratory of the Thin Layers and Materials for Electronics LPCMME, Department of Physics, University of Oran. Algeria.

Barkat Lamia E_mail:tissordz@yahoo.fr

(*) Physics laboratory of the solids for Electronics

University of Nantes,BP92208, 44322 Nantes Cedex 3, France

Abstract

The transparent conductive oxides (TCO) are used in many optoelectronic devices. These are generally OTC n-type ITO is currently the most efficient oxide and used. It is not without its drawbacks both in terms of its properties as its techniques for obtaining well the scarcity of indium. All this makes it necessary to seek an alternative material. Replacing ITO by another OTC, a multi-layers structure type oxide / metal / oxide, which appears as an original and promising opportunity [1], the application of these structures are varied as an anode in optoelectronic components [2], then. This is getting a thin conductive and transparent.

Thin films made of sheets stacked structure oxide (MoO₃) and metal (Ag) deposited by vacuum thermal evaporation on substrate at room temperature, are characterized by physical and chemical characterizations (micro analysis X.MEB.DRX. Transmission) and electrical measurements (4 points, van de Pauw). As a result, the layers are conductive and transparent in the visible, due to its characterization, we filed a Third-generation solar cells using these layers MoO₃/Ag/MoO₃ called "MAM" and also as the commercial ITO anode in these components. To obtain the organic cells more efficient, we introduce a buffer layer of cuprous iodide CuI between the anode and the organic material

Our organic solar cells of type: MAM/CuI/CuPc/C60/BCP/Al / Se and ITO/CuI/CuPc/C60/BCP/Al / Se, these cells are characterized by measurements of the JV characteristics in the dark and under illumination. Where the yield obtained approximately 0,15 % and 1, 37%, respectively. This shows the CuI buffer layer improves the performance of electronic devices.

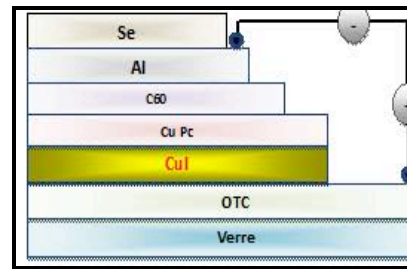
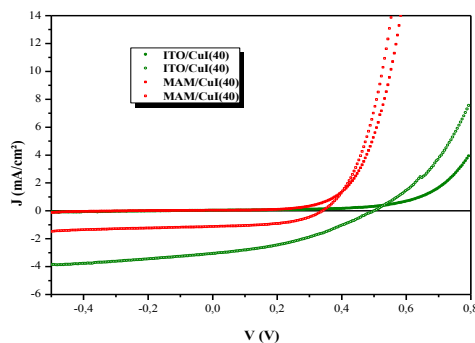


Fig1: structure organic photovoltaic cell



Anode	V _{oc} (V)	J _{sc} (mA/cm ²)	FF (%)	η (%)
ITO/CuI	0,55	03,26	37,20	0,61
MAM/CuI	0,37	0,85	50,10	0,15

Fig2: characteristic electric of the cells organic
Table1: proprieties electrical of the cells realize

References:

- [1]D.R.Sahu,S.Y.Lin,J.L.Huang.thin Solid Film 516(2008) 4728-4732
[2]K.H.Choi,H.J.Nam,A.Jeong,S.W.Cho.H.K.Kim. J.W.Kang,D.G.Kim,W.J.Cho,Appl.Phys.Lett.92(2008)223302.

P53 - Inactivation of E-coli bacteria by atmospheric dielectric barrier discharge

L.Benterrouche¹, S.Sahli^{1*}, F.Sebihi², A.Benhamouda¹

¹University of Constantine, Microsystems and Instrumentation Laboratory, Electronic Department, Engineering Faculty, Route de Ain El Bey – 25017 Constantine, Algeria

*Corresponding author: E-mail address: sahli50@hotmail.com

²University of Constantine, Nature and Life Sciences Faculty, Route de Ain El Bey – 25017 Constantine, Algeria

Abstract:

The introduction of polymers in almost all medical tools has raised the necessity of developing new sterilization processes for these heat sensitive materials. Because of their strength to generate at ambient temperature abundant chemical sterilizing species from many safety gases, great interests have been focused these last few years on plasmas discharges. Atmospheric pressure plasmas have attracted researcher's attention for biomedical applications and many research works in related with this area have recently been published [M. Laroussi et al.] [X.P. Lu et al.]. The main advantage of this type of electrical discharge is their use at ambient conditions (temperature, pressure and ambience) in a reliable way.

In this work, we have used an atmospheric dielectric barrier discharge (DBD) to inactivate *Escherichia coli* (E-coli) bacteria. The used plasma reactor consists of two plane- parallel metallic electrodes. The lower electrode was covered with a dielectric layer and spaced from the upper one of about 3 mm. The E-coli microorganisms were spread out on several glass plates. In each experiment, two contaminated glass plates were placed on the top of the lower electrode and exposed during different times (varying from 4 to 20 min) to an atmospheric plasma DBD created in air using a voltage of 10 kV. Once the plasma was turned off, samples were extracted from one of the two plasma treated glass plates and then seeded in culture medium that we placed in test tubes. The second treated contaminated glass plate was directly used for microscopy observations. On Table 1 is reported the variation of the optical density (measured at 660 nm using a Shimadzu UV120-02 spectrophotometer) of E-coli contaminated samples after their atmospheric plasma DBD treatments. An optical density reduction of more than 99% is observed for samples treated during 16 min. This high pronounced decrease of the optical density with the increase of the atmospheric plasma DBD treatment time

reveals a considerable increase of E-coli microorganisms' inactivation.

<i>Plasma time treatment (min)</i>	<i>Optical density</i>	<i>Optical density in %</i>
0 (control)	0,09	100
4	0,012	13,3
12	0,001	1,11
16	0,0008	< 1

Table 1: Variation of the optical density of the E-coli contaminated samples as function of their plasma treatment time.

The good efficiency of such plasma in bacteria sterilization has been found by many authors and have been explained by combined effects involving the UV radiation emission, the energy of the plasma species and the chemical reactivity of these species with the outer structures of bacterial cells [M. Laroussi et al.] [S.Moreau et al.]. As our microscopy observation has revealed a significant decrease of the bacteria cadaver concentration on the treated glass plate when the plasma time treatment increases, we suggest then that in our case, the reactive species created in the air by the plasma DBD have the dominant effect in the sterilization process.

References:

- M. Laroussi (2002) Nonthermal decontamination of biological media by atmospheric-pressure plasmas: review, analysis and prospects. IEEE Transactions on Plasma Science, 30(4), 1409- 1415.
- X.P. Lu, Z.H. Jiang, Q. Xiong, Z.Y. Tang, Y. Pan (2008) A single electrode room-temperature plasma jet device for biomedical applications. Appl. Phys. Letters 92 (15) 151504
- S.Moreau, M.Moisan, M.Tabrizian, J.Barbeau, J.Pelletier, A.Ricard, L.H.Yahia (2000). Using the flowing afterglow of plasma to inactivate *Bacillus subtilis* spores: influence of the operating conditions. J.Appl.Phys. 88(2) 1166-1174

P54 - Synthesis of carbon vulcan XC72 supported platinum/tin electrocatalyst and evaluation of its methanol tolerance for Direct Methanol Fuel Cells (DMFC)

Lotfi Chirchi^{1*}, Sarra Knani¹, Stève Baranton², Têko.W.Napperon², Jean Michel Léger², Abdelhamid Ghorbel¹

¹ Laboratoire de chimie des matériaux et catalyse, Département de chimie Faculté des Sciences de Tunis , 2092 Tunis, Tunisie

² Équipe électrocatalyse, Laboratoire de catalyse en chimie organique UMR CNRS 6503, 4, rue Michel Brunet B27, BP 633 86022 Poitiers France

* Corresponding author: E-mail: chirchilot@yahoo.fr

As a consequence of the world large demand of the fossil energy limited sources, the development of renewable energy sources became essential. In this context, the Direct Methanol Fuel Cells (DMFCs) seem to be an efficient alternative. However, its commercialization is hindered by the slow kinetic reactions and especially kinetic of the oxygen reduction reaction, the high cost of the electrocatalysts based on precious metals and the methanol crossover through the membrane which affects the efficiency of the battery. In this purpose carbon supported Platinum alloys are widely tested as electrocatalysts in both anodic and cathodic sides of DMFCs.

Carbon supported platinum tin electrocatalysts was prepared by impregnation followed by borohydride reduction method. The bimetallic catalyst was heat treated under nitrogen at 500°C. The electrochemical activity of the as prepared electrocatalysts for oxygen reduction reaction in Direct Methanol Fuel Cell (DMFC) was investigated and compared to that of Pt/C. The structural and textural properties of catalysts were studied by X- ray diffraction (XRD) and N₂ adsorption-desorption at 77 K. X-ray diffractogram of Pt-Sn/C shows three main reflections characteristic of fcc structure of platinum and heat treatment does not affect this crystallographic structure. The (111) reflection peak shifts slightly to higher 2θ values with respect to that of pure platinum suggesting the alloy formation between platinum and tin. All samples showed type III isotherms according to IUPAC classification, indicating the presence of macropores (>50 nm). The BET specific surface area of Pt/C is important and remains higher even after tin addition and heat treatment. From TEM images an heterogeneity of particles size was observed. The heat treated electrocatalysts show an increasing of particle size due to agglomeration.

Catalytic activity of the materials was studied by cyclic and linear voltammetry in acidic medium. The electrochemical active surface area (EASA) estimated from cyclic voltammetry are represented in table. 1. It seems that Pt-Sn/C exhibits the higher EASA compared to Pt/C due to the formation of a Pt skin on platinum tin nanoparticle surface. However, the EASA drastically decreased with Pt-Sn/C (500°C) result expected from TEM images.

The electrochemical activity of samples toward oxygen reduction reaction (ORR) was studied using rotating ring disk electrode (RDE). It seems that ORR electrocatalysts activities follow this order: Pt-Sn/C (500°C) > Pt-Sn/C > Pt/C. Furthermore, the number of exchanged electrons calculated using the Koutecky-Levich equation was found equal to four for all samples. This evidences that the oxygen reduction in acidic medium occurs with the production of water.

<i>samples</i>	<i>EASA (m2. g-1)</i>
Pt/C	27
Pt-Sn/C	33
PtSn/C (500°C)	11

Table 1: Electrochemical active surface area (EASA) for Pt/C, Pt-Sn/C and Pt-Sn/C (500°C)

References:

- C. Jeyabharathi, P. Venkateshkumar, J. Mathiyarasu and K.L.N. Phani, *Electrochim. Acta* 54 (2008) 448–454.
 K.S.W.Sing, D.H.Everett, R.A.Whaul, L.Moscou, R.A.Pierotti, J.Rouguérol and T.Sieminiowska, *Reporting physisorption data for gas/solid systems, Physical chemistry division*,(1984).

P55 - Photo-electrochemical cell from chalcopyrite Cu(In_{0.6}Ga_{0.4})₃Se₅ semiconductor

L. Djellal^{1*}, M. Trari²

¹ Laboratory of Solid Solutions, Faculty of Physic (USTHB), BP 32 16111 Algiers, Algeria .

*Corresponding author : E-mail adress : dlyakout@hotmail.com

² Laboratory of Storage and Valorization of Renewable Energies, Faculty of Chemistry (USTHB) BP 32 16111 Algiers, Algeria.

Introduction: During the last years, optically active semiconductor alloys in the ternary diagram Cu-In-Se receive a great deal of attention for photo-to-electrical and/or chemical energy conversions [Decock 2010]. Bulk quaternary Cu(In_{0.4}Ga_{0.6})₃Se₅, is prepared by the fusion technique in evacuated quartz ampoule from stoichiometric amounts of pure (Cu, In, Ga and Se).

Results: The compound is polycrystalline and the diffraction lines in the X-ray diffraction (XRD) pattern confirm the formation of the chalcopyrite phase (SG: 142C) [Decock 2010]. The diffuse reflectance spectrum gives a direct optical transition (E_g) at 1.42 eV in good agreement with literature. The electrical conductivity follows an Arrhenius-type law with activation energy (E_a) of 29 meV in conformity with small polarons hopping. This ordered vacancy compound (OVC) exhibits an excellent chemical stability over the whole pH range [Valderrama 2004]. The photoelectrochemical study, investigated for the first time on this material, confirms the *n* type behavior. The negative slope in the Mott Schottky plot $\{C^{-2} = - (2/\epsilon\epsilon_0 N_A)(V - V_{fb} - kT/e)\}$ confirms the *p*-type conductivity (Fig.1). The flat band potential (V_{fb} = -0.39 V_{SCE}) and the electron density (N_D = 7.8 · 10¹¹ cm⁻³) are also determined.

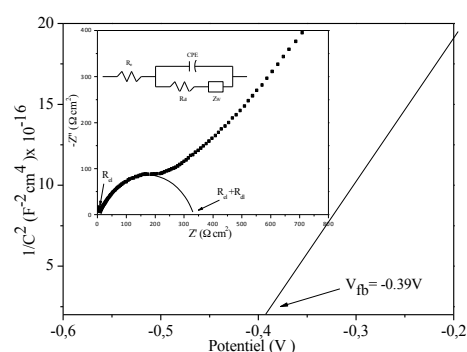


Figure 1: The Mott Schottky characteristic of Cu(In_{0.4}Ga_{0.6})₃Se₅ (frequency = 10 kHz). Inset: the Nyquist plot in KOH 0.5 M; scan rate 10 mV s⁻¹

The energy *P* of the valance band (VB) is given by : $P = e V_{fb} + E_a + 4.75$. The calculated value (5.75 ± 0.1 eV) is typical of materials in which VB is made up of selenium wave functions (Se-4*p* states with little admixture of Cu-3*d* orbital). Fig. 2

shows the energy diagram of Cu(In_{0.4}Ga_{0.6})₃Se₅/electrolyte junction. It shows the potentiality of this compound for the solar-to-chemical energy conversion.

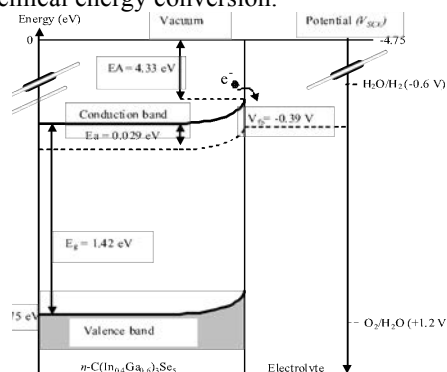


Figure 2: The energy band diagram of the system *n*-Cu(In_{0.4}Ga_{0.6})₃Se₅/KOH electrolyte.

The equivalent electric circuit of the photoelectrochemical cell (PEC) is deduced from the Nyquist plot i.e. the plot of the imaginary (*Z''*) vs the real (*Z'*) part of the complex impedance over a wide range of frequencies: $Z' = R_{el} + R_{sc}/(1 + \omega^2 C_{sc}^2 R_{sc}^2)$ and $Z'' = -\omega C_{sc} R_{sc}^2 / (1 + \omega^2 C_{sc}^2 R_{sc}^2)$. The Nyquist plot (Fig.1, insert) shows a semicircle at high frequencies corresponding to a faradic charge transfer and a slight offset near the origin indicating a low series resistance attributed to the electrolyte resistance *R_{el}* (4.8 Ω.cm²). The resistance (*R_{sc}* = 116.1 Ω.cm²) and the capacitance (*C_{sc}* = 342.6 μF/cm²) of the semiconductor can be evaluated at low frequencies. The straight line (frequencies > 10³ s⁻¹) is due to the diffusion process of electroactive species in solution known as the Warburg impedance (*Z_W*) where the ionic diffusion prevails.

References:

- Decock, K., Lauwaert, J. and Burgelman, M. (2010) Characterization of graded CIGS solar cells Energy, Procedia 2, 49–54, 2010
- Valderrama, R.C., Sebastián, P.J., Miranda-Hernandez, M., Pantoja Enriquez J. and Gamboa, S.A. (2004) Studies on the electrochemical stability of CIGS in H₂SO₄, Journal of Photochemistry and Photobiology A: Chemistry 168, 75–80, 2004

P56 - Electrochemical properties of metallic clusters nanoclusters

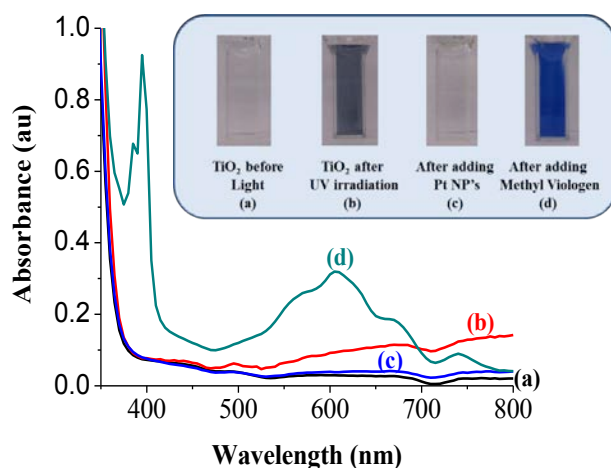
Liyana A Wajira Ariyadasa, Noah O Masika and Sherine O Obare*
 Department of Chemistry, Western Michigan University,
 1903 W. Michigan Avenue, Kalamazoo, Michigan, 49008-5413, USA
 *Corresponding author : E-mail address : sherine.obare@wmich.edu

Understanding charge transfer processes in nanoscale metallic particles is significant toward advancements in electronics, optics and catalysis applications. The ability to elucidate charge transfer on the nanoscale requires control of particle size and shape (Freemantle 2007, Ganesan 2007, Major 2009). Differential pulse voltammetry is a sensitive electrochemical technique and can be used to understand charge transfer in metallic nanoparticles. The technique also provides a method to determine particle size and dispersity of nanoparticles. Particles with diameters less than 5 nm have displayed unique electrochemical properties since within this size range the electronic properties transition from a bulk-like continuum of electronic states to molecular-like behavior. Thus, the particles have been found to display discrete electronic energy levels. Such properties have led us to investigate their charging and discharging at large band gap semiconductor interfaces (Freemantle 2007). We demonstrate the efficiency of the semiconductor/metal nanoparticle interfaces for electron and energy transfer applications. These results are paramount toward understanding and developing advanced materials.

Figure 1: UV-visible absorption spectra for demonstrating charging and discharging of metallic nanoparticles and the corresponding photographs indicating the associated changes in color observed.

References:

- Freemantle, R. G.; Guo, W.; Liu, M; Obare, S. O. (2007) One-Step Synthetic Procedures and Electrochemical Properties of Monodisperse 1-2 nm Metallic Nanoparticles. *ECS Transactions* 6, 93-99.
- Ganesan, M.; Freemantle, R.; Obare, S. O. (2007) Monodisperse Thioether Stabilized Palladium Nanoparticles: Synthesis, Characterization and Reactivity. *Chemistry of Materials* 19, 3464-3471.
- Lin, R.; Freemantle, R. G.; Kelly, N.M.; Obare, S.O.; Ofoli, R. Y. (2010) In-situ immobilization of palladium nanoparticles in microfluidic reactors and assessment of their catalytic reactivity. *Nanotechnology* 21, 325605.
- Major, K. J.; De, C.; Obare, S. O. (2009) Recent Advances in the Synthesis of Plasmonic Bimetallic Nanoparticles. *Plasmonics* 4, 61-78.



P57 - Molecular dynamics calculations of elastic constants in CoPt-L1₀ single crystal

L. Messad^{1*}, T. Bouzar¹, C. Goyhenex², H. Bouzar¹, V. Pierron-Bohnes²

¹Laboratoire de physique et chimie quantique, Université Mouloud Mammeri Tizi-ouzou, BP N° 17 RP, Tizi-ouzou, Algérie

²Institut de physique et chimie des matériaux de strasbourg, UMR7504, CNRS-UDS
23 rue du lœss, BP 43, Strasbourg CEDEX, France

*Corresponding author : E-mail address : messadleila@yahoo.fr

Introduction: Chemically L1₀-ordered CoPt alloys in bulk samples, thin films and particles are very interesting due to their possible applications as shape memory alloys, high density magnetic recording media because of their large magnetic anisotropy and catalytic properties due to the enhanced reactivity of Pt when associated to Co. Many properties of interest are related to their ability to form ordered phases almost in coherence with the disordered matrix. A good knowledge of ordering processes and dynamics is thus a necessary step in an extensive research on this system.

For the hetero-epitaxy of these alloys as films or nanoparticles or their preparation as core-shells, the interfacial strains can have a primordial role. The values and anisotropy of the elastic constants are interesting points in this frame.

Energy model: The atomic interactions are described by a tight binding Hamiltonian using an electronic density of state written in the second moment approximation. The energy of atom at site *i* is written as the sum of two terms, an attractive band energy and a repulsive pair interaction. Theoretical details can be found in the work of Rosato et al., The fitting procedure leading to potential parameter's values can be found in previous work of the authors given in references section.

Computational and results: The elastic constants of the CoPt L1₀ single crystal were calculated using the second moment approximation (SMA) of the tight-binding theory. The lattice parameters have been optimized to minimize the total energy leading to: $a = 0.3820$ nm and $c = 0.3650$ nm.

As expected the lattice is found to undergo a tetragonalization in agreement with experiments (c/a is found (0.955) in the calculation and (0.96) in the experimental determination).

We then based our calculations of the elastic constants on the numerical procedure described by Melh et al. Using an adequate strain tensor, the different elastic constants are deduced from the

variation of the final energy value within the corresponding deformations.

As the L1₀ lattice has six independent constants, we have to use six independent strains. Varying by small steps the values of the components of the strain and calculating each time the total energy, we obtain a parabolic variation of the energy around the equilibrium value (zero strain). Each of the six obtained curves (Figure 1) of $\Delta E/V$ is fitted to a second degree polynomial of the type Ax^2 , where x represents the strain and the coefficient A corresponds to a relation between different elastic constants depending on the chosen strain tensor the elements of which are expressed as a function of x

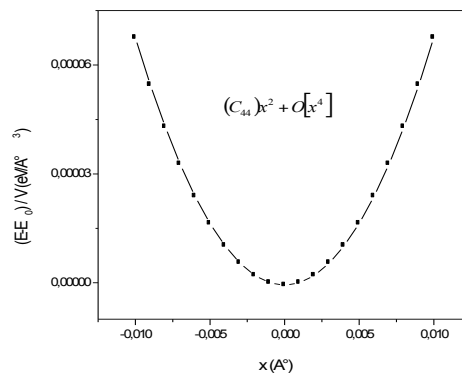


Figure 1: Variation of total energy within the corresponding deformation

From these elastic constants, we have deduced the bulk modulus B_V and the Young modulus E along all directions.

References:

- V. Rosato, B. Gillopie, and B. Legrand, *Philos. Mag.* A 59, 321 (1989); F.Cleri and V.Rosato, *Phys.Rev.* B 48,22 (1993).
- Michael J. Melh, Barry M. Klein, and Dimitri A. Papaconstantopoulos ; *Intermetallic Compounds : Principles and practice, Volume I :principles*, J. H. Westbrook and R. L. Fleischer, eds., John Wiley and Sons (London, 1995), Ch. 9 (pp. 1945-210).

P58 - Effect of the $\text{In}_x\text{Ga}_{(1-x)}\text{As}$ surrounding thickness and In compositions on electronic transitions of InAs DWELL structure grown on GaAs high index substrates

M.Bennour*, F.Saidi, L.Bouzaïene, L. Sfaxi and H.Maaref

¹Laboratoire de micro-optoelectronique et nanostructures,
Faculté des Sciences de Monastir, University of Monastir, TUNISIA

*Corresponding author : E-mail address : mbnnr@gmail.com

Introduction: Self-assembled semiconductor quantum dots (QDs) grown on the high index GaAs substrates have received considerable attention because of their large impact on the formation and optical properties of the confined structures. This is due to the significant piezo-electric field (PZ-field), surface polarity and the difference chemical potentials in surfaces. On the other hand, understanding theoretically the electronic states of the InAs Dot-in-a-well structures (DWELL), are important issues for the optoelectronic applications. By changing the quantum well thickness or In composition in the well, it is possible to change the response wavelength of the DWELL detectors [Barve et al. 2011].

Theoretical consideration: The optical transition energy as well as the wave function of the InAs DWELL structure were investigated by solving the Schrödinger equation using the finite-element method based on single-band effective mass approximation.

The model consisted on a single lens-shape QD with its wetting layer surrounding by InGaAs well or GaAs matrix and it is deposited on GaAs(11N)A surfaces, where $N=1$ to 9. For taken into account the effects of different substrate orientation, the coordinate system was rotating in such a way that one coordinate coincides with the growth direction [Mlinar et al.2007]. Furthermore, the strain and the PZ-field were taken into account.

Results: Figure 1 shows that the ground-state energy transition was red shifted with increasing the indium composition of the surrounding layer ($\text{In}_x\text{Ga}_{(1-x)}\text{As}$) and varying the substrate orientation from the (111)A to (119)A. We note that the conventional orientation (001) was obtained when $N=\infty$. These observations illustrate that the optical properties of QDs strongly affected by the substrate orientation and the surrounding layer composition. In fact, these effects is due to the reduction in Indium out diffusion and the reduction in hydrostatic strain and in PZ-field. On the other hand, by varying the wetting layer (WL) and InGaAs thickness we shall show that the degree of the influence substrate orientation is mainly influenced by the WL thickness when the QD is

smaller. In that situation, the carrier confinement was reduced, and the wave function was coupled by the 0D and 2D confinement.

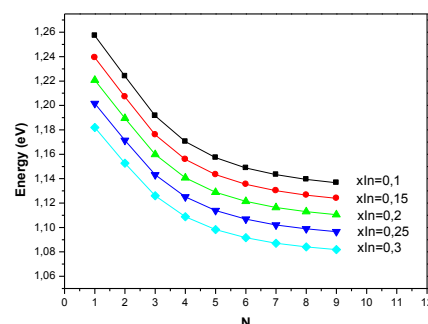


Figure 1: Calculated electron-heavy-hole transition energies in a lens-shape InAs DWELL as a function of the index N for different $\text{In}_x\text{Ga}_{(1-x)}\text{As}$ composition (0.1 to 0.3)

Conclusion: We have predicted the variation of the transition energies of InAs quantum dot embedded in GaAs and $\text{In}_x\text{Ga}_{(1-x)}\text{As}$ quantum well (DWELL) as a function of substrate orientation, $\text{In}_x\text{Ga}_{(1-x)}\text{As}$ surrounding compositions and WL thickness. By reducing the barrier height (increasing the In composition) and increasing the index N (decreasing the angle disorientation), the transition energy is red-shifted. We attributed this effect to the decreasing of the hydrostatic strain and the piezoelectric field which was presented in the high index substrates. The changing of the WL thickness qualitatively changes the transition energy dependence on the substrate orientation.

References:

- Barve, A.B., Sengupta, S., Kim, J.O., Sharma, Y.D., Adhikary, S., Rotter, T.J. Lee, S.J., Kim, Y.H. and Krishna, S. (2011) Confinement enhancing barriers for high performance quantum dots-in-a-well infrared detectors. *Applied Physics Letters*, 99, 191110-191112
- Mlinar, V., Peeters, F.M. (2007) A three-dimensional model for artificial atoms and molecules: influence of substrate orientation and magnetic field dependence. *Journal of Materials Chemistry*, 17, 3687-3695

P59 - Thermal annealing effects on structural and optical property of V-doped GaN films

M. Bouzidi*, M. Souissi, A. Bchetnia, Z. Chine, B. El Jani
 Unité de recherche sur les Hétéro-Epitaxies et Applications (URHEA)
 Faculté des Sciences, 5000 Monastir, Tunisia.

*Corresponding author e-mail: elbouzidimed16@yahoo.fr

Introduction: Thermal annealing is an important step in the process technology of semiconductor devices. It is used in particular to reach a more homogeneous distribution of a variety of electronic and optical properties. It is also necessary for the activation of doped ions [1]. In this work we report the annealing effect on the structural and optical property of V-doped GaN (GaN:V) films, in particular the effect of the thermal treatment in the blue band (BB) seen at room temperature (RT) photoluminescence (PL) spectra of our samples [2].

Experimental:

The growth of GaN:V films was performed by MOVPE using a vertical reactor on (0001) oriented sapphire substrates. Specific details of the growth conditions have been reported elsewhere [2]. After growth, the films were annealed at a temperature of 1075 °C for 30 min under nitrogen atmosphere (N₂). High resolution X-ray diffraction (HR-XRD) was used to examine the effect of the annealing in the structural quality. The optical properties of the samples were evaluated by means of optical absorption measurement and PL. PL was excited with a 15 mW HeCd laser working at 325 nm and was detected through a SpectraPro 275 monochromator.

Results and Discussion:

HR-XRD showed that the full width at half maximum (FWHM) of symmetric (0002) and asymmetric (10 $\bar{1}$ 5) rocking curves increase after annealing. This result indicates a reduction in the structural quality. Optical absorption measurement at 300 K revealed a red shift in the band gap energie position which means a strain relaxation [3]. Figure 1 shows the RT-PL spectra of unintentionally doped GaN and GaN:V before and after thermal treatment. After annealing, the BB exhibited a drastic reduction in integrated intensity. This observation was in good agreement with the results reported by different studies [3,4]. The reduction of BB is explained by vanadium diffusion or to the V-related complex dissociation [3]. At low temperature the PL spectra revealed a red shift in the donor bound exciton (D⁰X), as shown in Figure 2, confirming the observation by optical absorption measurement. In addition, we observed that the donor-acceptor (D-A) pair was strongly pronounced after annealing. This increase in the D-A intensity may be attributed to the increase of the nitrogen vacancies concentration

during annealing [5]. Taking account to these observations we propose that the V_{Ga}-V_N complex may be the possible origin of the BB.

Figures:

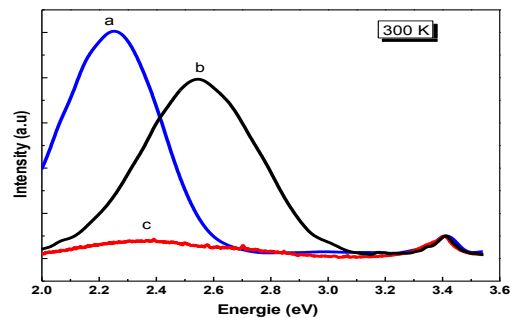


Figure 1: PL spectra obtained at room temperature from: a) unintentionally doped GaN, b) GaN:V and c) GaN:V and annealed for flow rate of VCl₄ = 4 sccm.

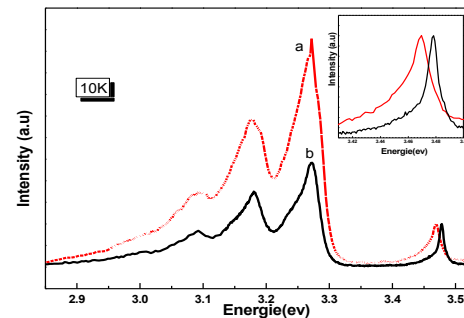


Figure 2: PL spectra obtained at 10 K from : b) GaN:V and c) GaN:V and annealed for flow rate of VCl₄ = 4 sccm.

References:

- [1] A Bchetnia, A Rebey, J L Fave, J C Bourgoin and B El Jani, (2006), Effects of thermal annealing on n-type GaAs:V grown by MOCVD, Tunisia, J. Phys. D: Appl. Phys. 39, 1337–1341.
- [2] M. Souissi, Z. Chine, A. Bchetnia, H. Touati, B. El Jani (2006) Photoluminescence of V-doped GaN thin films grown by MOVPE technique, Tunisia, Microelectronics Journal, 37, 1-4.
- [3] Abdul Majid, Akbar Ali (2009), Effect of isochronal annealing on photoluminescence properties of Mn-implanted GaN, Journal of Luminescence 129, 40–43.
- [4] C. Guarneros, V. Sánchez (2010) Materials Science and Engineering B 174, 263–265.
- [5] James A. Fellows, Y.K. Yeo, Mee-Yi Ryu, R.L. Hengehold, (2005), Optical study of implantation damage recovery from Si-implanted GaN, USA, Solid State Communications 133, 213–217

P60 - Theoretical investigation of kink effect and dependence between deep defects and temperature in AlGaIn/GaN HEMT's

M. Charfeddine^{1*}, M. Gassoumi¹, H. Belmabrouk², M.A. Zaidi¹ and H. Maaref¹

¹ Laboratoire des Micro-Optoélectroniques et Nanostructures, Département de Physique, Faculté des Sciences de Monastir, 5019 Monastir, Tunisia.

*Corresponding author : E-mail adress : charfeddine.manel@yahoo.fr

² Laboratoire d'Electronique et de Microélectronique, Département de Physique, Faculté des Sciences de Monastir, 5019 Monastir, Tunisia.

Introduction: A compact and accurate analytical model of Kink effect incorporating temperature and deep defects of AlGaIn/GaN high electron mobility transistors (HEMTs) with Silicon (Si) substrates is reported. The model takes into account the temperature dependencies of the carrier trapping effects. Both surface and substrate traps have incorporated in the model to calculate the observed current slump in the output characteristics' drain-source current voltage (I_{ds} - V_{ds} - T). The trapping/detrapping phenomenon of the deep defects which is explained that the capture and emission time constants of the traps are modified with the temperature resulting in a parasitic kink effect phenomena in the following, I-V trace. The detrapping of the captured electrons is initiated with increasing drain current and the electron concentration increases which are accelerated by increased thermal effects. As a result, the appearance of kink drain current is obtained when the quantity of traps is very significant.

Theoretical considerations: Drain-source current voltage (I_{ds} - V_{ds} - T) simulated as a function of gate voltage and temperature have been performed. Output characteristics registered at different temperatures show a parasitic effect such as kink effect phenomena, which may limit the performances of HEMT transistors expected on AlGaIn/GaN on silicon substrates. The kink effect is an abrupt increase in the drain current at a certain drain voltage that provokes an increase in the output conduction (g_{ds}).

Results: The result of this simulation is presented in figure1 and Figure2. Which shows the presence of a kink effect for $6V < V_{dsat} < 20V$. This effect is related to a sudden liberated of electrons, and it appears for high drain -to- source voltage V_{ds} increasingly when the channel opens up, thus, the liberate of electrons is due to a lateral electric field generated by the polarization gate-to-drain V_{gs} . This effect almost disappears when the gate-to-source bias is low, which implies a gradual release of electrons during the simulation. These results show that the characteristics' changes according to

the polarisation V_{gs} put forward the response of the traps.

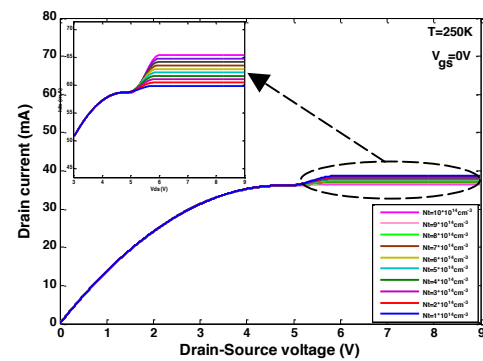


Figure 1: Theoretical spectra I_{ds} - V_{ds} characteristics at $T=250K$ as a function of concentration of defects are clearly shown in the kink effect.

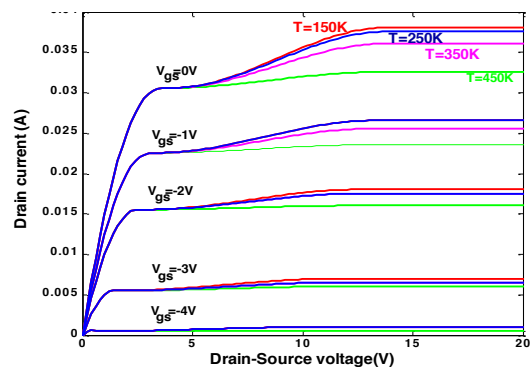


Figure 2: Theoretical spectra I_{ds} - V_{ds} , showing the variations of the Kink effect at $T= 150 K$, $T= 250 K$, $T= 350K$ and $T= 450 K$.

References:

- Arulkumaran, S., Liu, Z.H., Ng, G.I., Cheong, W.C., Zeng, R. J., Bu, Wang H. and Radhakrishnan, K., (2007) Temperature dependent microwave performance of AlGaIn/GaN high-electron-mobility transistors on high-resistivity silicon substrate. *Thin Solid Films*, 515, 4517-4521.
- Meneghesso, G., Zanon, F., Uren, M. J. and Zanoni, E. (2009) Anomalous Kink Effect in GaN High Electron Mobility Transistors, *journal IEEE Electron Device Letters*, 30, (2), 100-102.

P61 - Influence of heat treatment and indium concentration on structural and optical properties of ZnO thin films prepared spin-coating technique

M. Hajiri¹, F. Ghribi¹, L. El Mir^{1,2,*}

¹Laboratoire de Physique des Matériaux et des Nanomatériaux appliquée à l'Environnement, Faculté des Sciences de Gabès, TUNISIA

*Corresponding author : E-mail address : Lassaad.ELMir@fsg.rnu.tn

²Al-Imam Muhammad Ibn Saud University, SAUDI ARABIA

Abstract: Pure and indium doped zinc oxide were prepared on glass substrate by sol-gel spin coating method. Zinc acetate dehydrate, indium chloride, 2-methoxyethanol and monoethanolamine were used as a starting materials, dopant source, solvent and stabilizer, respectively. After coating, ZnO samples were annealed at 300, 400 and 500°C. However ZnO:In with indium concentration of 2 at. % was annealed only at 500°C. The effects of heat treatment and presence of In as doping element on the structural, electrical and optical properties were examined. Both pure and In doped ZnO samples are (002) preferentially oriented. The X-ray diffraction results indicate that the samples have polycrystalline nature and hexagonal wurtzite structure with average grain size varied from 26.5 to 38.7 nm. An increase in the heat treatment increases the crystallinity of the thin films. The optical transmittance spectra showed transmittance higher than 85 % within the visible wavelength region. The band gap energy is about 3.3 eV. Atomic force microscopy (AFM) was investigated to study the films morphology.

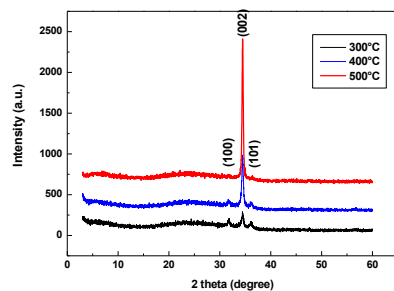


Fig.1: XRD pattern of the pure ZnO thin films annealed at 300, 400 and 500°C.

Fig.1 shows the X ray diffraction (XRD) pattern of pure ZnO thin films on glass substrates. It is found that the samples are polycrystalline and have hexagonal wurtzite structure with c-axis orientation. The (0 0 2) diffraction peak intensity had a tendency to increase with an increase of the annealing temperature in all films.

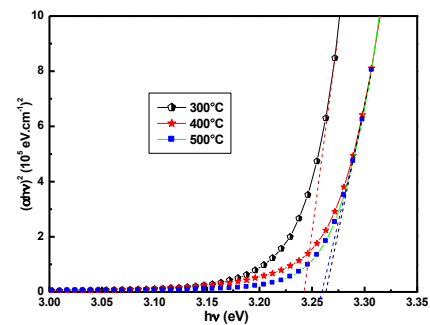


Fig.2: $(\alpha h\nu)^2$ vs. photon energy of the pure ZnO thin films.

Fig.2 shows plot of $(\alpha h\nu)^2$ vs. photon energy. The gap value increases with annealing temperature and reaches a maximum of about 3.263 eV for annealing temperature of 500°C.

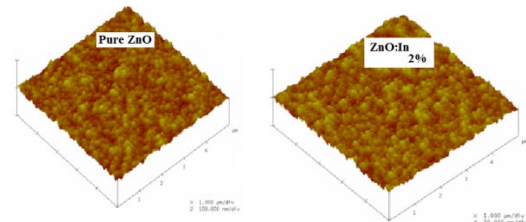


Fig.3: AFM images of pure and In (2%.at) doped ZnO thin films.

Fig.3 shows the 3D AFM micrographs of pure and In (2%.at) doped ZnO thin films. The images show granular and porous surfaces.

References

- Jong-Pil Kim, Sang-A Lee, Jong Seong Bae, Sung-Kyun Park, Ung-Chan Choi, Chae-Ryong Cho, Thin Solid Films 516 (2008) 5223.
- Powder Diffraction File 36-1451 for hexagonal Zinc Oxide (1997 JCPDS-International center for Diffraction data).
- Su-Shia Lin, Jow-Lay Huang, P. Sajgalik, Surf. Coat. Techn. 185 (2004) 254–263.

P62 - Effect of specific surface of Si substrates on TiO₂ nano-films on structural, optical and photocatalytic activity

M. Karyaoui¹, J. Ben Naceur¹, M. Ben Rabha¹, R. Chtourou¹ and M. Amlouk²

¹ Laboratoire de photovoltaïque, Centre de Recherches et des Technologies de l'Énergie, Technopole de Borj-Cédria BP 95, 2050 Hammam-Lif, Tunisia

² Unité de Physique des dispositifs à Semi-conducteurs UPDS, Faculté des Sciences de Tunis, Tunis El-Manar University 2092 Tunisia

karyaoui@yahoo.fr

Tel: +21679325160, Fax: +21679325934/+21679325825

Introduction:

Titanium dioxide (TiO₂) anatase phase is a large band gap semiconductor with many interesting physico-chemical applications especially as photocatalytic activity agent [1-2]. This oxide can be prepared by many techniques such as: the reactive sputtering pulsed laser deposition, chemical vapor deposition and so on. Among them the sol-gel technique [3], is characterized by its low processing cost, its simplicity and ability to produce thin and uniform films on large substrate area. The sol-gel process provides flexibility and a better control in the preparation of materials compared with solid state reactions [4].

In this paper we report the effect of the surface specific of some substrates on the structural, optical as well as photocatalytic activity of titanium dioxide (TiO₂) thin films prepared using sol-gel method. Used substrates are: Si, Porous silicon (PS) and nanowires silicon (NWS). The Microstructural properties of thin films were investigated by X-ray diffraction (XRD) and Spectroscopy IR. The surface morphology of the film was examined using Scanning Electron Microscope (SEM) and Atomic Force Microscopy (AFM) methods. On the other hand, the optical properties of TiO₂ thin films were characterized using UV-VIS and Spectroscopic ellipsometry techniques. The results showed a remarkable effect of the specific surface of substrates on the structural and optical properties of TiO₂ thin films, figure 1.

From this figure, it is not that NWS substrate exhibits a good catalytic activity owing to its large

specific surface. Further studies are in progress to improve this catalytic activity using appropriate doping of TiO₂ nano-films

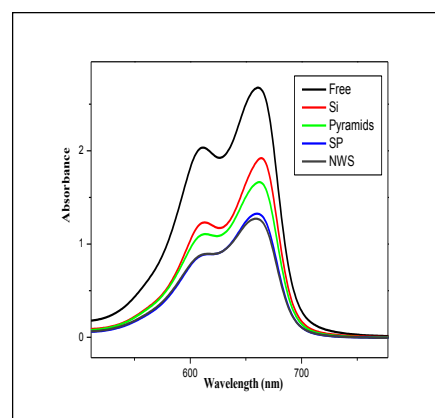


Figure1: Variation of the dye absorption spectra using TiO₂ nano-films deposited by sol-gel on various substrates on the photocatalytic activity.

References:

- [1] S. Janitabar-Darzi, A.R. Mahjoub, A. Nilchi, *Physica E* 42 (2009) 176e181.
- [2] Y. Zhang, J. Wan, Y. Ke, *J. Hazard. Mater.* 177 (2010) 750e754.
- [3] C.J. Brinker, M.S. Harrington, *Solar Energy Mater.* 5 (1981) 159e172.
- [4] J. Livage, M. Henry, C. Sanchez, *Solid State Chem.* 18 (1988) 259e341.

P63 - Relaxation effect in the nano-composites films deposited by plasma microwave from acetylene

M. Kihel^{1*}, R. Clergereaux², M. Calafat², S. Sahli^{1*}, P. Raynaud², Y. Segui², I. Nouicer¹

¹Université Mentouri de Constantine, Laboratoire de Microsystèmes et Instrumentation,

²Université de Toulouse, LAPLACE, CNRS, INPT, UPS, 118 route de Narbonne, bât. 3R3 31062 Toulouse

*Corresponding author : E-mail address : sahli50@hotmail.com, Kihel_mouloud@hotmail.com

Abstract:

In this work, hydrocarbon films a-C:H elaborated in microwave plasma reactor study has been reported. The pure acetylene precursor has been used to deposit hydrocarbon films for substrate temperature around 0° C. Whereas, the pressure and deposition power, has been kept constant at 200 W and 0.1 Pa, respectively. In previously study, hydrocarbon plasma shows the formation of nanoparticles during discharge plasma [M. Calafat]. It is revealed that nanoparticles are consist of carbon sp² cluster and/or metallic particles embedded in the amorphous carbon matrix, leading, to the formation of nanocomposition carbon-carbon films [M. Calafat]. In this investigation we have reported the nanoparticles effect on the electrical properties films. It has been found that the nanoparticles have significant effect on the dielectric losses. The figure 1 represente the response of the dielectric measurement in the dark (curve I0) and for different light intensity (I1-I3). The response of the dielectric measurement in the dark it's the same obtained elsewhere [M. Kihel] and no relaxation peak is observed. However, in the presence of the light we observed peak relaxation in the low frequency (around 1 kHz). This peak shifted to the high frequency according to the increase of the light intensity (see Figure 1). We suggest that the presence of nanoparticles in the carbon-carbon films matrix is responsible of relaxation phenomena and this is may be due to the generation-recombination phenomena of the electrons. Although, the shifte of the relaxation peak to the high frequency when the light intensity increase remained not fully understanding and need more investigations.

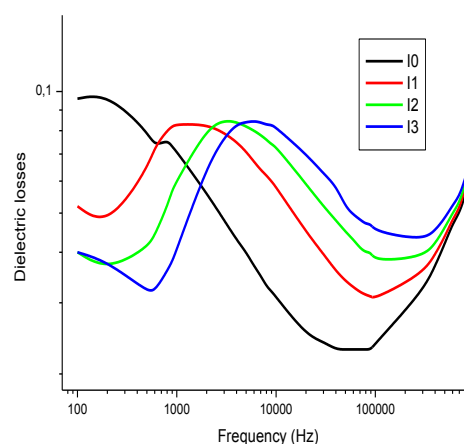


Figure 1: Dielectric losses response for dark (I0) and for different light intensity (I1 to I3).

References:

- M. Kihel, R. Clergereaux, D. Escaich, M. Calafat, P. Raynaud, S. Sahli and Y. Segui (2008) Investigations on electrical properties of a-C:H thinfilms deposited in a Microwave Multipolar Plasma reactor excited at Distributed Electron Cyclotron Resonance Diamond & Related Material, 17, 1710-1715.
- M. Calafat, D. Escaich, R. Clergereaux, P. Raynaud and Y. Segui, (2007) Particle formation in acetylene very low-pressure high density magnetized Plasmas Applied Physics Letter, 91, 181502.

P64 - Surface treatment of liquid crystal alignment: effect on electrical properties of nematic liquid crystal cell.

M. Sahraoui^{1*}, A. Abderrahmen¹, R. Ben Chaabane¹, H. Ben Ouada¹, A. Gharbi²

¹ Laboratoire des interfaces et matériaux avancés, Faculté des Sciences de Monastir

² Laboratoire de Physique de la Matière Molle, Faculté des Sciences de Tunis

* E-mail corresponding author: sahraoui.marwa@yahoo.fr

Introduction: Liquids crystals have shown in recent years many applications, they are used in the display cell LCD (Liquid Crystal Display).

The alignment of liquid crystal molecules in a predetermined management is the key to visual performance of LCD displays [1].

The work done was the surface treatment of alignment of liquid crystal molecules for construction of display cells.

Experimental:

The nematic liquid crystal (NLC) used in the experiment was 5CB which was introduced between two pieces of glass with transparent ITO electrodes on their surfaces. Calixarene is used as alignment layer; it was deposited by evaporation under high vacuum on transparent electrodes (ITO).

These alignment layers were characterized by the technique of wettability to analyze the hydrophobicity and their surface energy and the values of the polar and dispersive components.

The morphology of the alignment layer is of great consequence to the achievement of the desired orientation of the LC molecules so the morphology of these layers is performed by the atomic force microscopy (AFM). The effect of orientational treated surfaces was observed under an optical microscope polarizing.

The dielectric properties of nematic liquid crystal (5CB) cells were studied by impedance spectroscopy in a wide frequency range of 1mHz to 13MHZ.

Results and Discussion:

Table (1) presents the effect of orientational treated surfaces. The deposited alignment layers favour a planar orientation of the liquid crystals molecules [1].

For the dielectric properties, we studied in particular the conductance, admittance and impedance of the liquid crystal cell. In this work, the figure (1) presents the relaxation mechanism in the LC cell [2] and demonstrates the electrical effect of the alignment layer [3]. This study is followed by a model in terms of electrical equivalent circuit to the cell and to determine its components (figure (2)). This modeling was performed in order to better understand the dielectric phenomena that occur at different interfaces [2, 3].

Figures and Tables:

Samples	Alignment layer	Observed alignment
Cell 1	Calix[4]arene	Planar
Cell 2	Calix[6]arene	Planar
Cell 3	Calix[8]arene	Planar

Table 1: Observed alignment of 5CB on the calixarene films

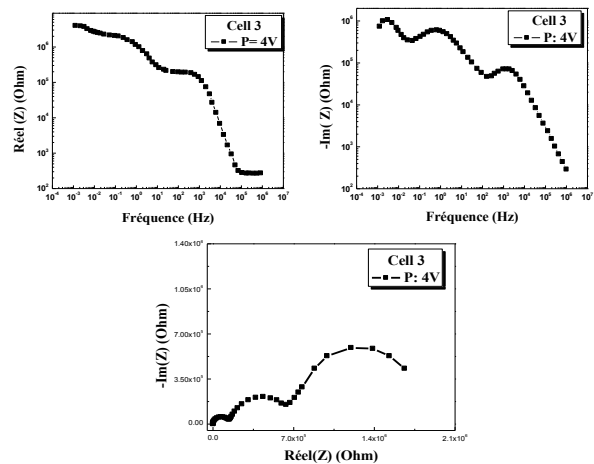


Figure 1: variation of the real impedance part with frequency, the imaginary impedance part with frequency and the cole-cole representation in the frequency ranges of 1 mHz- 1MHz

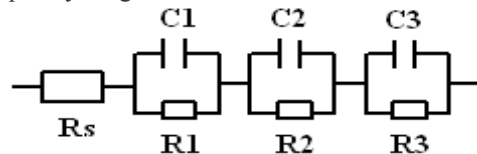


Figure 2: Schematic representation of the electrical equivalent circuit associated with the liquid crystal cell.

References:

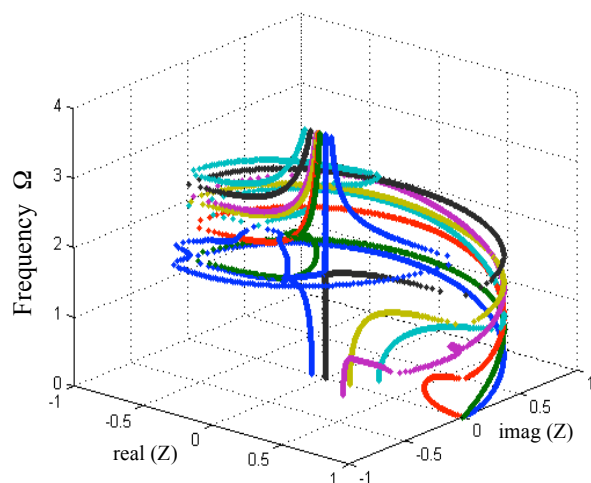
- [1] S.Peralta, F. Hapiot, Y. Barbaux and M. Wrentham, (2003) "Alignment of nematic crystal using substituted calixarène Langmuir-Blodgett films", *Liquid Crystal*, 30, 436-469.
- [2] S.Murakami, H. Iga and H. Naito (1996), *J. Appl. Phy*, 11 80.
- [3] A.Abderrahmen, F. Fekih Romdhane, H. Ben Ouada and A. Gharbi, (2008) *Science and Technology of Advanced materials*, 9, 025001.

P65 - Phonon scattering in a quantum nanowire: Application to substitution bulk defect

M. S. Rabia

Laboratoire de Mécanique des Structures et Energétique, Faculté du Génie de la construction, Université Mouloud Mammeri, Tizi-Ouzou 15000, ALGERIE
E-mail address: m2msr@yahoo.fr

In the present work we investigate the influence of substitution bulk defect on the elastic wave's propagation through a quantum nanowire modelled by four infinite monoatomic chains. The study is confined to the elastic scattering in the harmonic approximation framework. The problem is tackled from a classical point of view, using scattering boundary conditions and applying the matching formalism. This theoretical approach, based on Landauer principle, permits to determine the dynamics of the perfect waveguide (eigenmodes functional behaviours, polarizations, group velocities, etc.) and allows one to carry out the phonons localized induced states, the atoms displacements of the perturbed region, the transmission and reflection coefficients of the considered system.



Functional behaviours $\Omega(\mathbf{Z})$ of the vibrational modes characterizing the four atomic chains. Unit circles correspond to propagating modes whereas the evanescent modes are represented by the parts inside the unit circles.

We show that the mass defect fluctuations modify the transmission spectra. As expected, the influence of the defect is relatively small in the acoustical regime. However, for heavy defects, the oscillation amplitude of the transmission decreases considerably. This generalized behaviour is also observed when backscattering becomes more significant for wave vectors near the zone boundaries.

References:

- T. E. Feuchtwang, Dynamics of a Semi-Infinite Crystal Lattice in a Quasiharmonic Approximation. I. The Static Equilibrium Configuration of a Semi-Infinite Crystal Lattice, *Phys. Rev.* **155**, 731 (1967).
Imry Y (1997), Introduction to Mesoscopic Physics, (Oxford University Press, Oxford, 1997).
B. Kramer, Quantum Coherence in Mesoscopic Systems, (plenum, New York, 1991).
Landauer R. (1989), Conductance determined by transmission: probes and quantised constriction resistance, *J. Phys. Condens. Matter* **1**, 8099.
Pouthier V. and Girardet C. (2002), Electronic transmission through a metallic cluster attached to an adsorbed nanowire: creation of a nanoscale electronic on/off switch, *Surf. Sci.* **511**, 203-214.
Rabia M. S. (2006), Surface defects characterization in quantum wires by acoustical phonons scattering, *J. Mol. Struc-Theochem*, **777**, 131-138.
Rabia M. S. (2010), Coherent phonon scattering by geometric defects in a planar quantum waveguide, *J. Physica E* **42**, 1307-1318.
Szeftel J. and Khater A. (1987), *J. Phys.*, **C 20**, 4725
Tekman E. and Bagwell P. F. (1994), Fano resonances in quasi-one-dimensional electron waveguide, *Phys. Rev.*, **B 48**, 18 299.

P66 - Investigation of surface morphology and optoelectronic properties of monocrystalline silicon

N. Bachtouli¹, S .Aouida¹, B .Bessais¹

¹Photovoltaic Laboratory, Research and Technology Centre of Energy,
Borj-Cedria Science and Technology Park, BP 95, 2050 Hammam-Lif, Tunisia.
b.nesrine84@yahoo.com

Abstract:

The surface morphology of monocrystalline silicon (c-Si) has an enormous effect on the optoelectronics parameters of silicon cell. For this purpose we study three different types of surface structures: Porous silicon (PS), silicon nanowires (NWs) and pyramidal textures, these structures contribute to the decrease of the surface reflectivity and may be considered as antireflection coating. These surface treatments reduce the effective reflectivity less than 4%. Then we examine the evolution of the surface morphology of each structure, and correlate it with the progress of the Photoluminescence for a porous layer, and the photogenerated carriers' lifetime which improve with the etching time and the surface treatment. To approve our studies and our results we used two other techniques, the Fourier transform infrared spectroscopy (FTIR) and the X-Ray diffraction which can indicate the crystalline structures and the compounds of different samples.

Some figures:

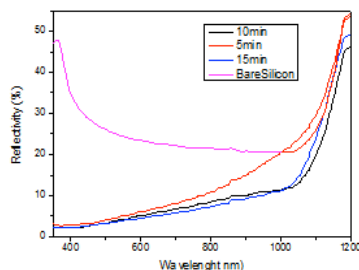


Figure 1: Reflectivity of c-Si surface with silicon nanowires for different etching times.

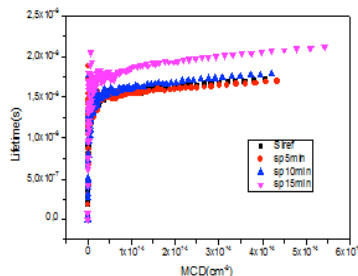


Figure 2: IDLS of porous silicon for different etching times.

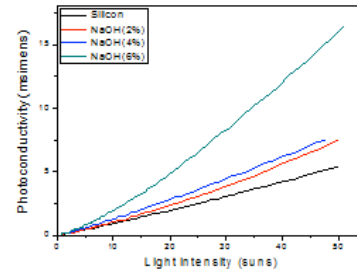


Figure 3: Photoconductivity variation of textured silicon sample during 30 minutes for different NaOH concentrations.

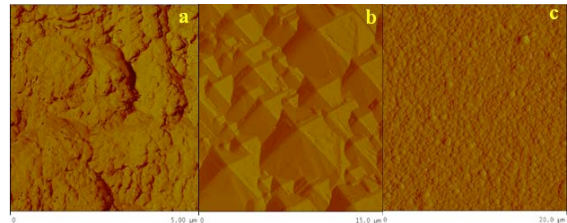


Figure 4: AFM top view of silicon surface with different surface treatment: (a) porous silicon (b) textured surface and (c) silicon nanowires.

References:

- Bomin Cho, Sunghoon Jin, Bo-Yeon Lee, Minwoo Hwang, Hee-Cheol Kim, Honglae Sohn(2012), Investigation of photoluminescence efficiency of n-type porous silicon by controlling of etching times and applied current densities, *Microelectronic Engineering* 89 (2012) 92–96.
- DaisyVerman, FirozKhan, S.N.Singh, P.K.Singh (2011), Correlation between reflectivity and photoluminescent properties of porous silicon films, *Solar Energy Materials & Solar Cells* 95 (2011) 30–33.
- Dinesh Kumar, SanjayK.Srivastava, P.K.Singh, M.Husain, VikramKumar(2011), Fabrication of silicon nanowire arrays based solar cell with improved performance, *Solar Energy Materials & Solar Cells* 95 (2011) 215–218.
- Khaldun A. Salman, Khalid Omar, Z.Hassan (2011), the effect of etching time of porous silicon on solar cell performance, *Superlattices and Microstructures* 50 (2011) 647–658.
- Jung M. Kim, Young K. Kim (2004), *Solar Energy Materials and Solar Cells* 81 (2004) 293-247.
- M.Saadoun, N.Mliki, K.Daoudi, B.Bessais, H.Ezzaouia, R.Bennaceur(2002), Vapour-etching-based porous silicon: a new approach, *Thin Solid Films* 405 (2002) 29–34.
- Sanjay K.Srivastava, DineshKumar, P.K.Singh, M.Kar, VikramKumar, M.Husain(2010), Excellent antireflection properties of vertical silicon nanowire arrays, *Solar Energy Materials & Solar Cells* 94 (2010) 1506–1511.

P67 - Electrical characterization of carbon-nickel nanocomposites prepared by sol-gel method

N. Ben Mansour¹, S. Gouadria¹, I. Najeh¹, M. Hajiri¹, H. Dahman¹ and L. El Mir^(1, 2, *)

(1) Laboratoire de Physique des Matériaux et des Nanomatériaux appliquée à l'Environnement, Faculté des Sciences de Gabès, Cité Erriadh Manara Zrig, 6072 Gabès, Tunisia.

(2) Al-Imam Muhammad Ibn Saud University, College of Sciences, Department of Physics, Riyadh 11623, Saudi Arabia.

E-mail : Lassaad.EMir@fsg.rnu.tn

Abstract: Carbon-nickel (C/Ni) nanocomposites were prepared by sol-gel method after the incorporation of nickel oxide (NiO) nanoparticles in organic matrix based on pyrogallol and formaldehyde (PF). These nanocomposites PF/Ni were heat treated under different pyrolysis temperature from 600 to 1000 °C. The increase of electrical conductivity with pyrolysis temperature is explained by the presence of the percolation phenomena. The direct current (dc) and alternating current (ac) electrical conductivities have been studied in the temperature range between 80 and 300 K and frequency range between 40 Hz and 110 MHz. The study of this samples present the dominated of 3D-VRH conduction model in direct current (dc) conductivity. ac conductance obeys the law of Jonscher's with the presence of hopping conduction mechanism in the nanocomposite treated at 650 °C which is confirmed by the proportionality between the dc conductance (G_{dc}) and relaxation frequency (ω_c). The as prepared nanocomposite is promising for electronic technological applications.

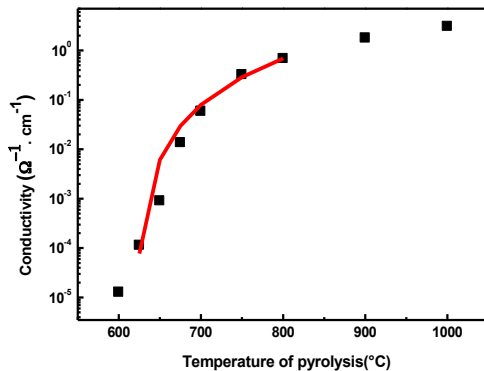


Fig.1: Electrical conductivity versus temperature of pyrolysis.

Figure 1 exhibits the evolution of conductivity as a function of pyrolysis temperature, the solid line is the theoretical fit with the equation of conductivity in the conduction percolation phenomenon.

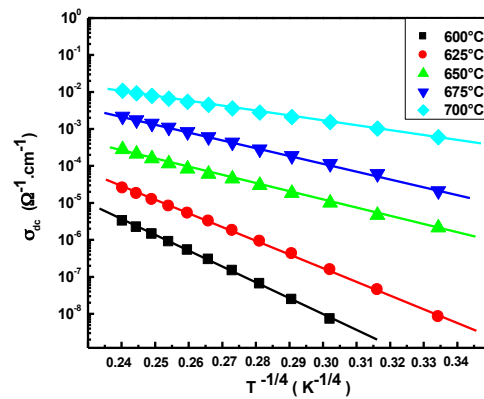


Fig.2 : dc conductivity versus $T^{-1/4}$.

Figure 2 shows the variation of conductivity as a function of measurement temperature for PF/Ni nanocomposites treated at different pyrolysis temperatures. The linear shape indicates the dominance of model 3D-VRH conduction.

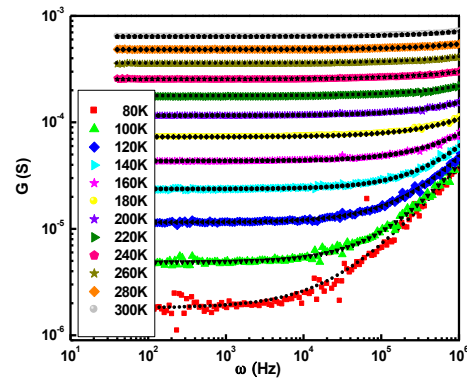


Fig.3 : Variation of ac conductance at different temperatures of measure for the sample PF/Ni-650 °C.

Figure 3 shows the frequency dependence of the ac conductance at different temperatures for PF/Ni-650 °C. The black lines is the theoretical fit with the equation of conductivity by Jonscher's.

P68 - Relaxed energetic maps of -2-O-sulphated 3,6 anhydro- α -D-galactose and ι -carrabiose : A DFT study

N. Berrekchi-Berrahma-Bestaoui^{1*}, M. Sekkal-Rahal¹, A. Sayede²
and N. Yousfi¹

¹ Faculté des Sciences, Laboratoire L2MSM, Université Djillali Liabes de Sidi Bel Abbès,
B.P.89, Sidi Bel Abbès, 22000, ALGERIA

*Corresponding author : E-mail address : nbesber@yahoo.fr

² Faculté des Sciences Jean Perrin, UCCS, UMR CNRS 8181, Université d'Artois,
S.P.18, rue Jean Souvraz, Lens Cedex 62307, FRANCE

Carrageenan found in the cell walls of numerous red seaweeds (Rhodophyta), are high-molecular-weight polysaccharides made up of repeating galactose units and 3,6-anhydro- α -D-galactose. The units are joined by alternating $\alpha(1\rightarrow3)$ and $\beta(1\rightarrow4)$ linkages. They have been abundantly used in the food industry as thickening, gelling and more recently in the pharmaceutical industry.

Carrageenan structures are based on linear chains of alternating 3-linked β -D-galactopyranosyl units, and 4-linked α -D-galactopyranosyl (or 3,6-anhydro- α -D-galactopyranosyl) units, usually sulfated in different positions.

The properties of these and other polysaccharides depend on their conformations and molecular flexibility, which is concentrated mostly on the glycosidic linkages.

In this work, we studied the structure and the energy of one of the unit 2-O-sulphated-3,6- α -D-anhydrogalactose, and the repeating disaccharide constituting neo-iota-carrabiose(4-O-sulphated3,6-anhydro- α -D-galactopyranosyl(1 \rightarrow 3)2-O-sulfated- β -D-galactopyranose).

DFT calculations using the B3LYP functional and the 6-31G(d) basis set were carried out on the two molecules, and performed with the Gaussian 03 program. The results have been explored using the Gaussview software. The maps have been plotted using the Surfer software. Relaxed iso-potential maps, often called Ramachandran plots, show where regions of low energy occur in the Φ and Ψ glycosidic bonds torsional space (θ and χ_1 for monosaccharide).

These energetic contour maps, performed in the gas phase (figure.1) and then by simulating the presence of water as solvent using the Onsager model, have been built as suggested by French and Dowd by interpolating a set of data comprising a total of 324 and 144 energy values for the mono and the disaccharide respectively. Once the set of the two specific values of Φ and Ψ angles fixed (θ and χ_1 for monosaccharide), they were kept frozen while optimizing all of the other geometrical parameters.

The lower energy conformers were then fully optimized using B3LYP and MP2 methods with several basis sets.

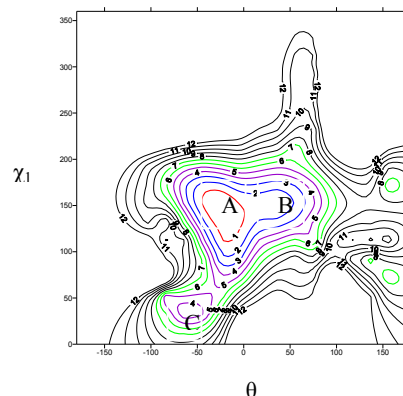


Figure 1: Relaxed iso-potential maps at the **B3LYP/6-31G(d)** level of monosaccharide in the gas phase. (ΔE in kcal/mol).

Conformer	Phase gas		water	
	ΔE	θ, χ_1	ΔE	θ, χ_1
A	0.00	-24, 152	0.00	-11, 133
B	2.10	56, 152	1.55	28, 173
C	3.36	-64, 32	3.19	9, -167

Table 1: θ and χ_1 (in degrees) and relative energies (Kcal/mol) in phase gas and in water for monosaccharide.

In the gas phase and in water for each case we have obtained three and two minima for the mono and disaccharide respectively, corresponding to the lower energy conformers. In water the molecule is more stable and the energy is lower. Intramolecular hydrogen bonding is formed and seems to contribute in the stability of the molecule.

References:

- Campo, V. L., Kawano. D. F., da Silva Jr. D. B., Carvalho. I. (2009) Carrageenans: Biological properties, chemical modifications and structural analysis-A review, *Carbohydr. Polymers.*, 77, 167-180.
French, A. D. and Dowd, M. K. (1993) Exploration of disaccharide conformations by molecular mechanics, *J. Mol. Struct.: THEOCHEM.* 286, 183-201.

P69 - The effect of SiO₂ addition on the microstructure and superconducting properties of Bi2212

N. Boussouf¹, M. -F. Mosbah¹, F. Bouaicha¹, Amira²

¹ Université Mentouri de Constantine, Laboratoire Couches Minces et Interfaces, Campus de Chaabet-Erressas- B.P. 325 Route d'Ain El Bey, 25017 Constantine. Algeria.

² Laboratoire des Essais Non Destructifs (LEND), Université de Jijel. B.P. 98, 18000 Jijel, Algeria.

Abstract SiO₂ particles were inserted (added) into Bi₂Sr₂CaCu₂O_{8+x} precursor powders in various weight fractions. The influence of Si addition to the Bi2212 system on its phase formation, microstructure and transport properties is investigated. Samples are characterized by means of X ray diffraction analysis (XRD), scanning electron microscopy (SEM/EDX), magnetic AC susceptibility and resistivity measurements. For 1% of added Si, the results showed an increase of the apparent superconducting volume fraction. All the samples doped with Si contained a majority fraction of the high T_C superconducting Bi2212 phase. SEM observation showed that the average grain size of the Si added samples increased more than that of the sample without Si. From resistivity measurement the T_c^{onset} was found to be increased

Keywords Superconductors, Bi2212, doping.

Doping (%Si)	0.0	1%	5%
a (Å)	5.3783	5.4276	5.6200
c(Å°)	30.931	30.80628	30.7213

Table.1: Results of of the lattice parameters

References:

A Biju, R P Aloysius and U Syamaprasad.(2005). Supercond. Sci. Technol. 18 .PP 1454–1459.
H.Sasakura Z.Y.O.Miura. Ito.(2001) Physica C 357-360. PP 216-221.

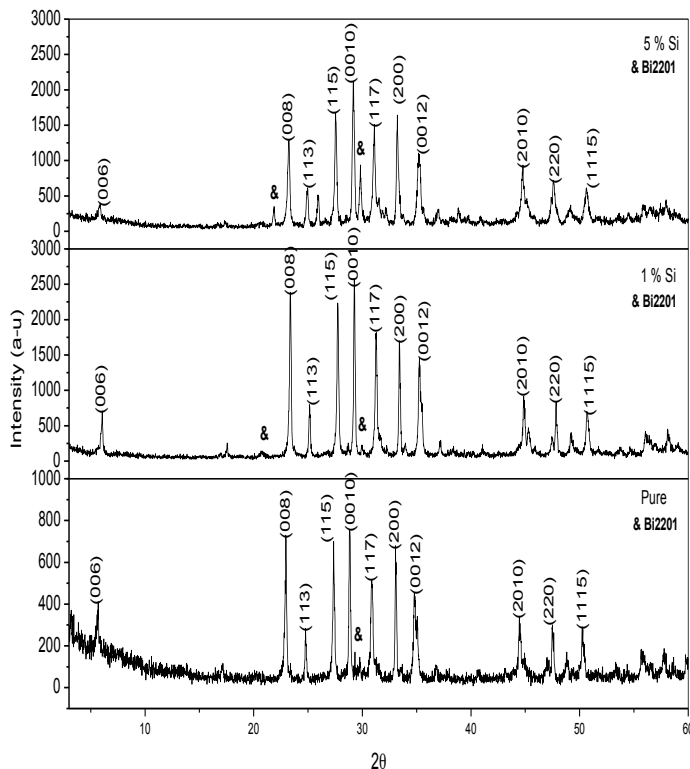


Fig.1. X-Ray powder diffraction patterns of samples pure and added with 1 % Si, 5% Si.

P70 - Induced phases transformation by mechanical alloying of the haematite/magnesium mixture

N. Boutabia^{1*}, B. Bouzabata¹

¹Laboratoire de Magnétisme et de Spectroscopie des Solides LM2S. Université Badji Mokhtar. Annaba. Algérie.

*Corresponding author : E-mail adress : boutabianedjoua@yahoo.fr

Introduction:

Since 1970 many materials scientists and metallurgists have been intrigued by the development of the mechanical alloying (MA) [Benjamin1970] method for preparing numerous advanced materials with unique properties and structures [Wright and al. 1974][Gessinger and al.1976]. Amorphous alloys, [Koch and al.1983][Sherif El-Eskandarany and al.1997][Sherif El-Eskandarany and al.1999][Sherif El-Eskandarany 1999] nanostructured metal nitrides [Sherif El-Eskandarany and al. 1998], metal hydrides [Sherif El-Eskandarany and al.1995], metal carbides [Sherif El-Eskandarany 1996], metastable materials [Sugiyama and al.2000][Matsui and al.2000][Ji and al.2000] and recently nanocomposite materials [Sherif El-Eskandarany and al.1998] are some typical examples of advanced engineering materials that are obtained by MA, using ball-milling and/or rod-milling [Sherif El-Eskandarany 1999] techniques.

The possibility of solid-state mechanochemical reduction of metal oxides by ball-milling technique in the presence of strong metallic reducing agents has been demonstrated by Schaffer and McCormick when they produced metallic Cu powder by milling cupric oxide (CuO) with Ca [Schaffer and al.1989] or Mg [Schaffer1990] using a method, the so-called mechanical solid-state reduction (MSSR).

It has been shown by Sherif El-Eskandarany [Sherif El-Eskandarany1995] that Cu₂O can be also reduced completely into metallic nanocrystalline Cu powders by milling a mixture of CuO₂ and elemental Ti powders in a low-energy rod mill. More recently, Yang and McCormick [Yang and al.1998] have reported the unique results for the reduction of NiO with graphite powders during ball milling at both ambient and elevated temperatures.

The present work shows the possibility of reducing haematite (α -Fe₂O₃) into metallic iron (bcc-Fe) powders by ball-milling a mixture of α -Fe₂O₃ and magnesium (hcp-Mg) powders.

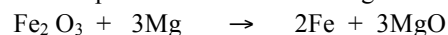
The mixture of haematite α - Fe₂ O₃ and magnesium Mg powders have been milled for various times using a ball mill type Fritsch P7, and all milling experiments were performed under argon atmosphere.

The as-milled powders were structurally characterized by X-ray diffraction using Origin and MAUD programs based on the rietveld method. The refinement of the X-rays diffraction patterns shows

the reactant powders at the initial stage of milling (0 hour) are polycrystalline mixture of α - Fe₂ O₃ (with rhombohedral structure) and hcp-Mg.

The reduction of haematite by the magnesium to forms α -Fe particles (cubic center structure with parameter cell $a_{Fe} = 2.8929 \text{ \AA}$) and the oxidation of magnesium by the haematite to forms MgO (cubic with $a_{MgO} = 4.2583 \text{ \AA}$) begins to appear just from one hour of milling.

The results show that the basic change that occurs during milling the reactants materials can be described as presented in the following reaction :



References:

- Benjamin J.S., Metall. Trans. A1 (1970) 2943.
 Gessinger, G.H. Metall. Trans. A 1 (1976) 203.
 Ji, Y. Kallio, M. Tiainen, T. Scripta Mater. 42 (2000)
 Koch, C.C. Cavin, O.B. McKamey, C.G. Scarborough, J.O. Appl. Phys. Lett. 43 (1983) 1017.
 Matsui, N. Yamada, T. Kobayashi, K. Sugiyama, A. Ozaki, K. J. Jpn. Soc. Powder Powder Metallurgy, JSPM 47 (2000) 332.
 Schaffer, G.B.. McCormick, P.G Appl. Phys. Lett. 55 (1989) 45.
 Schaffer, G.B. McCormick, P.G. Met. Trans. A 21 (1990) 2789.
 Sherif El-Eskandarany, M. Ahmed, H.A. Sumiyama, K. Suzuki, K. J. Alloys Comp. 218 (1995) 36.
 Sherif El-Eskandarany, M. Mater. Trans., JIM 36 (1995) 182.
 Sherif El-Eskandarany, M. Met. Trans. A. 27 (1996) 2374.
 Sherif El-Eskandarany, M. Aoki, K. Sumiyama, K. Suzuki, K. Appl. Phys. Lett. 70 (1997) 1679.
 Sherif El-Eskandarany, M. Omori, M. Konno, T.J. Sumiyama, K. Hirai, T. Suzuki, K. Met. Trans. A. 29 (1998) 1973.
 Sherif El-Eskandarany, M. Bahgat, A.A. Goma, N.S. Eissa, N.A. J. Alloys Comp. 290 (1999) 181.
 Sherif El-Eskandarany, M. J. Alloys Comp. 279 (1998) 263
 Sherif El-Eskandarany, M. J. Alloys Comp. 284 (1999) 295.
 Sugiyama, A. Kobayashi, K. Mstsumoto, A. Ozaki, K. Nishio, T. J. Jpn. Soc. Powder Powder Metallurgy, JSPM 47 (2000) 327.
 Wright, L.G Wilox, A. Metall. Trans. A5 (1974) 957.
 Yang, H. McCormick, P.G. Met. Trans. B 29 (1998) 449.

P71 - Optimization of properties of MEH-PPV/CNTs films for organic solar cells: effects of CNTs concentrations and thermal treatments

N. Chehata^{1*}, A.Ltaief¹, A. Farzi² and A. Bouazi¹

¹Equipe Dispositifs Electroniques Organiques et Photovoltaïque Moléculaire, Faculté des Sciences de Monastir, Boulevard de l'Environnement, 5019, Monastir, TUNISIA

*Corresponding author : E-mail address : chehata.nadia@yahoo.fr

²Department of Materials and Polymer Engineering, Faculty of Engineering, Sabzevar Tarbiat Moallem University, Sabzevar, IRAN

Abstract

The functionalization of carbon nanotubes (CNTs) is an effective way to prevent their aggregation and to improve their dispersion in polymer matrix. The interfacial adhesion could modify the interactions between the functional groups on the nanotubes and the conjugated polymer for optimal nanocomposites properties, including optical properties based on charge transfer efficiency.

Blends of MEH-PPV with two types of CNTs, multi-wall carbone nanotubes (MWCNTs) and multi-wall carbone nanotubes functionalized with polystyrene (PS:MWCNTs) are used as active layer in organic solar cells based on the bulk heterojunction concept. This work will be based on investigating both absorption and photoluminescence spectra of nanocomposites as function of composition of CNTs and thermal annealing treatment. The obtained curves will be analyzed by exploiting two tools: the quenching efficiency parameter (η) and the Stern-Volmer (SV) relation.

Photoluminescence (PL) measurements demonstrate that a photoinduced charge transfer has been occurred for the two investigated nanocomposites. Charge transfer efficiency was obtained for an acceptable concentration of PS:MWCNTs about 0.5 wt. % and at annealed temperature of about 80°C. Quenching efficiency studies prove that nanocomposites based on functionalized CNTs reveal a higher degree of PL quenching, reaching a value of $\eta = 76.9\%$.

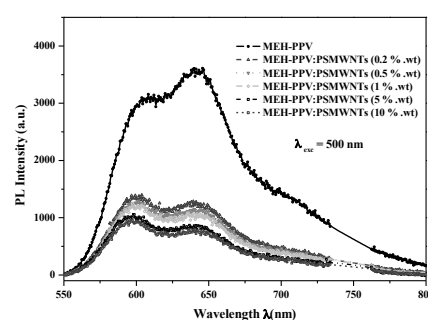


Figure 1: Photoluminescence spectra of MEH-PPV and MEH-PPV/PSMWCNTs nanocomposites.

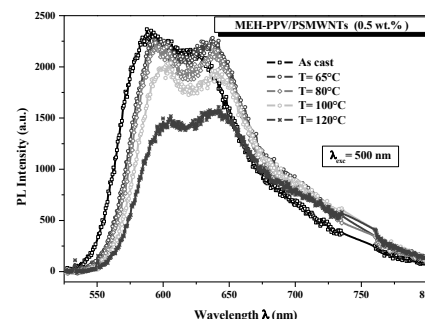


Figure 2: PL spectra of un-annealed and annealed nanocomposite films, for MEH-PPV/PSMWCNTs

References:

- Kymakis. E and Amaratunga. G.A.J. (2001) Single-Wall Carbon Nanotube/Conjugated Polymer Photovoltaic Devices, Applied Physics Letters, 80, 112-114, 2001.
- Sahoo. N. G, Ranab. S, Chob. J.W, Li. L and Chana. S. H. (2010), Polymer Nanocomposites Based on Functionalized Carbon Nanotubes, Progress in Polymer Science, 35, 837-867, 2010.

P72 - Nanocomposites based on boron-doped diamond for ammonia sensing

N.Chiboub^{1*}, K.Khalidi², N.Gabouze¹, R. Boukherroub³, S.Ghodbane⁴, S.Sam¹
¹ UDTS, 02, Bd. Frantz Fanon, B. P. 140 Alger-7 merveilles, 16200 Algiers, Algeria

*Corresponding author : E-mail address : chiboubn@yahoo.fr

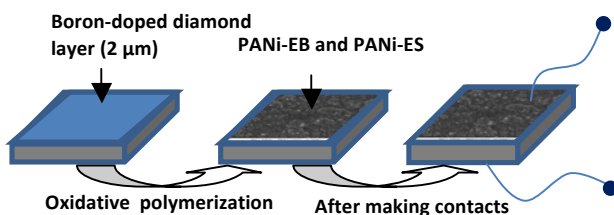
² Unité de Recherche des Matériaux et des Energies Renouvelables (URMER), Université Abou Bekr BELKAÏD

³ Institut de Recherche Interdisciplinaire (USR 3078) et Institut d'Electronique, de Microélectronique et de Nanotechnologie (UMR 8520), Avenue Poincaré – BP 60069, 59652 Villeneuve d'Ascq, France.

⁴ Rhobest coating Hartstoffbeschichtungs GmbH, Exlgasse 20a, 6020 Innsbruck, Austria.

Introduction: Planar boron-doped diamond (BDD) substrates have been identified as one of the most promising materials and sensing platforms due to the unique physical properties of the diamond film. The diamond interface is chemically stable. The electronic and chemical properties can be tuned by changing the surface termination of diamond [1]. BDD material have been consequently used for a wide range of electrochemical applications [2,3,4]. On the other hand, the polyaniline (PANi) is an intrinsically conducting ammonia vapor sensitive polymer. The responsive nature of PANi is highly dependent on the processing techniques employed.

Experimental setup: We report herein on the preparation of thin films of polyaniline (PANi) in the emeraldine base form obtained via the direct polymerization of the monomer on a BDD substrate. On the other hand, the PANi films were obtained in the emeraldine sel form. The PANi films adhere well to substrate materials. Elsewhere, the composite structures have been characterized by Scanning Electron Microscopy (SEM), Second Ion Mass Spectrometry (SIMS) and X ray Photoelectron Spectroscopy (XPS).



Results and discussion: The current-voltage curves were measured for ammonia vapors evaporated from different solution concentrations at 36°C and showed rectifying behavior due to a diode structure between the BDD substrate and the polymer (Figure.2).

A large current variation is observed for different ammonia concentrations. The maximum sensitivity occurs at low voltages, which is very advantageous for energy consumption.

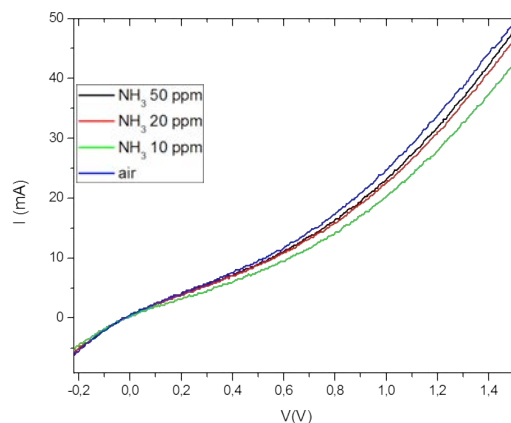


Figure.2: The current response was analyzed for - 0.4 to 1.5 V bias voltage against ammonia vapors.

Conclusion:

A direct deposition of polyaniline on boron doped diamond samples was performed during the oxidative polymerization of aniline in acidic bath using the ammonium persulfate as oxidant agent. The sensor has a high sensitivity for ammonia vapour and have a good response and recovery time and can operate at low voltages. The interaction between the conductive form of PANi, the emeraldine salt (ES), and the ammonia gas results in the change of the PANi doping state. The devices could be repeatedly used and tested in different atmospheres, proving that the adsorption and desorption processes on the sensor surface take place in a reversible and reproducible way.

References

- [1] S. Szunerits, R. Boukherroub, *J. Solid-State Electrochemistry*, 12, p.1205, 2008
- [2] R.L. McCreey, *Chemical Review*. 108, p.2646, 2008.
- [3] Y. Zhou, J. Zhi, Y.S. Zou, W.J. Zhang, S.T. Lee, *Analytical Chemistry*, 80, p.4141, (2008).
- [4] E. Fortin, J. Chane-Tune, P. Mailley, S. Szunerits, B. Marcus, J.-P. Petit, M. Mermoux, E. Vieil, *Bioelectrochemistry*, 63, 303–306, (2004).

P73 - Study kinetics of recrystallization, precipitation and texture development in cold rolled and annealed aluminium alloys

NEMOUR Hanéne , TRIKI Abdelhafid
 LM2S Laboratory, Physic's Department, University of Badji-Mokhtar Annaba, Algeria
 E-mail address: hanenenemour@yahoo.com

Abstract:

The aim of this present work is to study precipitation, recovery, recrystallization and texture phenomenon in a 86% cold-rolling 6060 alloy and aluminium pure. We have used several experimental techniques: DSC analysis, optique microscopy OM , X-ray diffraction and microhardness measurements H_v . This study allowed us to follow the recrystallization progression during an isothermal heat treatment at 340 °C, and the influence of the concurrent precipitation on the recrystallization. The Avrami's exponent value of 0,42 demonstrate that the recrystallization process is delayed. A qualitative study by X-ray diffraction shows a texture development of the principal exponent (110). This later was replaced after recrystallization treatment by another principal exponent (100), which is in agreement with the results obtained on the Al alloy severely deformed by cold rolling.

The chemical composition of 6060 alloy (wt %) and thermomechanical treatment:

Si	Mg	Fe	Cu	Mn	Cr	Zn	Ti	Al
0.45	0.5	0.2	0.1	0.05	0.05	0.08	0.05	reste

The homogenized alloys (6060 + Al pure) were deformed by cold rolling to reduction of 86 % , Samples were annealed at temperature 340° c for different times and then quenched in water.

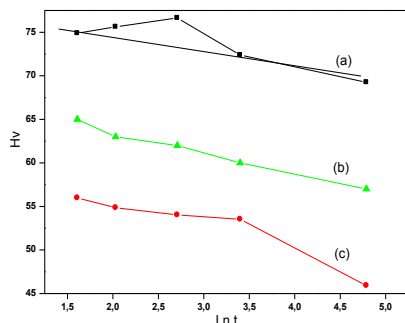


Figure 1 : Microhardness as a function of annealing time at T = 340° C (a) our alloy 6060 (b): drawn from the results of Lui et al [4]. (c) aluminium pure

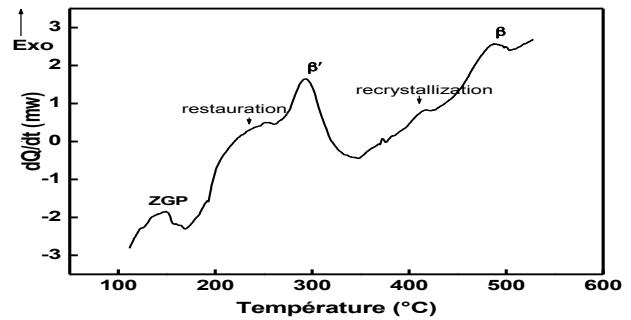


Figure 2 : DSC curve for 6060 alloy 86% cold rolled

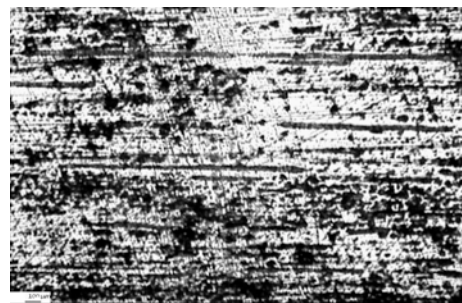


Figure 3: microstructural evolution of Aluminium pure during recrystallization at T = 340 °c

References

[1]A.N.Kolmogorov (1937): Akad. Nauk SSSR, Izv. Ser. Mat., , vol 1, pp.353-59.
 [2]J.Chem.Phys.(1940 , vol.8, pp. 212-24; J. Chem.Phys. 1941, vol.9, pp.177-84.
 [3] R.K. Roy, S.Kar, and K .Das, S.Das, (2006) "A study of precipitation and reristallization behavior of aluminum alloy AA1235", J. Mater .Sci.41 1039-1045.
 [4] W.C.Liu and J.G.Morris.(2005)"Evolution of Recrystallization and Recrystallisation Texture in continuous – cast AA 3015 aluminum alloy". Metallurgical and Materials Transactions A Vol. 36A, 2829.
 [5] W.F.Miao and D.E.Laughlin, ,(1999) Precipitation hardening in aluminum alloy 6022, Scripta Materialia, vol .40, No.7, pp. 873-878.

P74 - Capture of electrons in self-assembled InAs quantum dots

N Hamdaoui^{1*}, R Ajjel¹, B Salem², and M Gendry³

¹Laboratoire d'énergie et matériaux, Labem, Ecole supérieure des Sciences et de la Technologie Hammam Sousse, université de Sousse, 4011, Tunisia.

²Laboratoire des Technologies de la Microélectronique (LTM), UMR CNRS, CEA-Grenoble, 17 Rue des Martyrs, F-38054 Grenoble, France.

³Institut des Nanotechnologies de Lyon, INL-CNRS, Ecole Centrale de Lyon, 36 avenue Guy de Collongue, 69134 Ecully, France.

* E-mail address: hamdaoui_nejeh@yahoo.fr

Introduction: Considerable attention has recently been focused on the investigation of the dynamics of carrier capture, recombination and emission in self-organised quantum dots (QDs) by electrical methods [1]. Recently, the possibilities to design electronic memory devices using QD structures have attracted increasingly notable attention. Deep level transient spectroscopy was used to obtain the capture characteristics of InAs/InAlAs self-assembled quantum dots on InP substrate. The number of electrons captured by quantum dots can be controlled by varying the width of applied pulse voltage in the DLTS measurement. The Coulomb charging energy can be deduced

Experimental: The investigated sample was grown on a n^+ doped InP (001) substrate by solid source molecular beam epitaxy (SSMBE). It consists of a 0.4 μm -thick $\text{In}_{0.52}\text{Al}_{0.48}\text{As}$ (InAlAs) buffer followed by 0.9 nm of InAs. InAlAs buffer surface preparation and InAs growth conditions are adjusted to favour dot-like rather than wire-like islands.

Results and Discussions: An In a recent paper [2], DLTS of InAs/InAlAs QD sample was performed for various values of reverse bias, and filling pulse high. The DLTS investigation showed an InAs-related level (noted d) located at 76 meV below the InAlAs conduction band edge. In order to study the Coulomb charging effect, voltage pulse with different widths were applied for the DLTS measurements. Under the reverse bias of 1V, pulse voltage of 0 V, and different pulse widths, the DLTS spectra were measured and are shown in Fig.1. As the pulse width increases, the position of the peak shifts toward lower temperatures and the height of peak increases. The maximum amplitude of the DLTS signal also shows a feature of saturation for increasing t_p . Saturation is achieved at $t_p = 0.5$ ms. This is because the maximum amplitudes of the DLTS signal of $t_p = 0.5$ ms and 1 ms overlap, indicating that d level can be fully filled within 0.5 ms.. The activation energy for each spectrum can be calculated as shown in Figure 2. A phenomenological explanation can be provided for the capture kinetics of the QD. For long t_p , the

electron number in the d level is higher than that of the short (t_p) leading to the shift of the peak position to the lower temperature. Consequently, the d level shifts to lower activation energy and, the sequentially filled electrons will occupy different energy levels. The difference of these energy levels will be equal to the Coulomb charging energy. For shorter t_p values, a lower number of electrons is confined in the d level. Therefore, the activation energy is higher.

Figures:

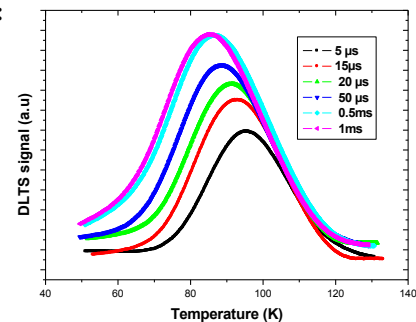


Figure.1. DLTS spectra with filling pulse widths varying from 5 μs to 1 ms

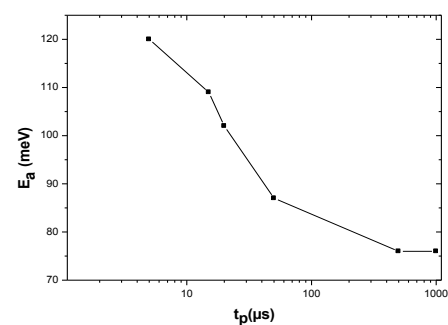


Figure.2. Dependence of the activation energy E_a on the duration of the filling pulses.

References:

- [1] A.Schramm, S.Schulz, T.Zander, Ch.Heyn, W.Hansen, Phys.Rev.B80(2009)155316.
- [2] N.Hamdaoui, R.Ajjel, H.Maaref, B.Salem, G.Bremond, M.Gendry, Semicond, Sci, Technol. 25 065011 (2010)

P75 - Effect of AlO₂ addition on the superconducting properties of Bi2212 superconductor

N. Kalkoul^{1*}, M. -F. Mosbah¹, F. Benmaamar¹, F. Bouaïcha¹.

¹Université Mentouri de Constantine, Laboratoire Couches Minces et Interfaces, campus de Chaabet-Erssas- B.P. 325 Route d'Ain El Bey, 25017 Constantine. Algeria

*Corresponding author : E-mail adress : nkalkoul@yahoo.fr

Abstract

The effect of AlO₂ addition on the superconducting properties of Bi2212 system was studied.

The samples were prepared by conventional solid state synthesis. The Al content was varied from $x = 0-0.05$ on a general stoichiometry of $\text{Bi}_2\text{Sr}_2\text{CaCu}_2\text{Al}_x\text{O}_{8+\delta}$. The samples have been characterized by X-ray diffraction (XRD), Scanning Electronic Microscopy (SEM), and measurements of resistivity versus temperature.

The results of DRX show the formation of $\text{Bi}_2\text{Sr}_2\text{CaCu}_2\text{O}_{8+\delta}$ compound and the second phase of Bi2201 is present with a fraction depending on the rate of doping. The c lattice parameter samples is slightly lower than in the non-doped sample showing the possibility of Al incorporating into the crystal structure of the Bi2212 phase.

The SEM micrographs show distinct variations in the grain morphology of the samples containing Al. And show the characteristic lamellar structure of high critical temperature superconductors.

The parts of the resistivity curves corresponding to the normal state show an influence of additions on the doping level (figure1).

The critical transition temperature (TC) is the most important superconducting that would be taken into account in technological applications. Bi-based

high TC superconductors are used in fabrication of wires and tapes because of their high TC [1].

On the other hand, the apparent superconducting volume fraction decreases when the rate of AlO₂ increases.

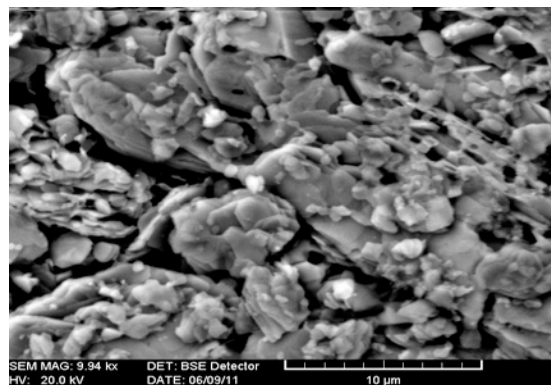


Figure1: SEM micrograph of a doped sample ($x=0.020$).

Keywords: Al addition; Bi-2212 superconductor; Critical temperature.

Reference:

[1] A. Biju, R.P. Aloysius, U. Syamaprasad (2006), Effect of Yb addition on the superconducting properties of (Bi,Pb)-2212 superconductor, Physica C 440 (2006) 52–58

P76 - Band structure calculations of $\text{Ge}_{1-x}\text{Sn}_x/\text{Si}_{1-x}\text{Sn}_x$ and $\text{Ge}_{1-x-y}\text{Si}_x\text{Sn}_y/\text{Ge}_{1-z}\text{Sn}_z$ alloys: achieving direct band gap materials

N. Yahyaoui¹, N. Sfina¹, J.-L. Lazzari², and M. Said¹

¹Laboratoire de la Matière Condensée et des Nanosciences (LMCN), Département de Physique, Faculté des Sciences de Monastir, Avenue de l'Environnement, 5019 Monastir, Tunisie

²Centre Interdisciplinaire de Nanoscience de Marseille (CINaM), UPR CNRS 3118 associée à Aix-Marseille Université, Case 913, Campus de Luminy, 13288 Marseille cedex 9, France

*Corresponding author: Tel + 216-73500276, Fax: + 216-73500278, E-mail address:

moncef_said@yahoo.fr

Abstract

Alloys of silicon (Si), germanium (Ge) and tin (Sn) are continuously attracting research attention as possible direct band gap semiconductors with prospective applications in optoelectronics. The direct band gap can be obtained for alloys relaxed or strained for well-defined compositions. The electronic structure of relaxed or strained $\text{Ge}_{1-x}\text{Sn}_x$ and $\text{Si}_{1-x}\text{Sn}_x$ alloys and of strained Ge grown on relaxed $\text{Ge}_{1-x-y}\text{Si}_x\text{Sn}_y$ was calculated using the empirical pseudo-potential method and the model-solid theory. Expressions are given for the direct and indirect band gaps in relaxed $\text{Ge}_{1-x}\text{Sn}_x$, strained Ge grown on relaxed $\text{Si}_x\text{Ge}_{1-x-y}\text{Sn}_y$ and strained $\text{Ge}_{1-x}\text{Sn}_x$ grown on a relaxed $\text{Ge}_{1-y}\text{Sn}_y$ substrate. The $\text{Ge}_{1-x}\text{Sn}_x$ bulk is a direct gap material for Sn content $>17\%$ with a gap values smaller than 0.2 eV. Against by the relaxed $\text{Sn}_x\text{Si}_{1-x}$ alloys have no direct gap for all x compositions. The binary GeSn and ternary SiGeSn alloys are considered to be very prospective materials for infrared detectors, as pointed by Soref and Perry [1], who used the linear interpolation scheme to calculate the electronic band structure and optical properties of $\text{Ge}_{1-x-y}\text{Si}_x\text{Sn}_y$ alloys and concluded that these will be tunable direct band gap semiconductors. The aim of this work is to theoretically explore the various possibilities of achieving tunable direct gap semiconductors based on group IV materials, and to investigate the composition dependence of their electronic and optical properties.

PACS. 73.21. Fg Quantum wells – 73.20.At Surface states, band structure, electron density of states– 71.20.Nr Semiconductor compounds

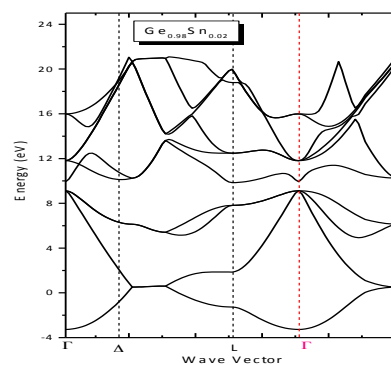


Figure 1 : Electronic band structure of $\text{Ge}_{0.98}\text{Sn}_{0.02}$.

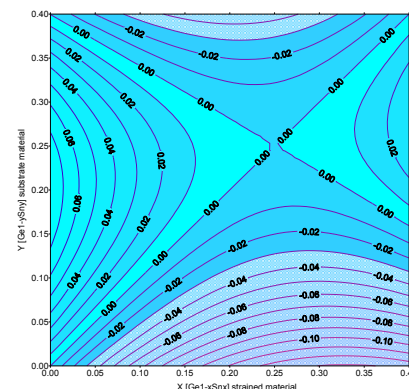


Figure 2 : Conduction-band offsets $E_c(x)-E_c(y)$ in minimum Γ , the $\text{Ge}_{1-x}\text{Sn}_x/\text{Ge}_{1-y}\text{Sn}_y$ heterointerface.

Reference:

[1] R. A. Soref and C. H. Perry *J. Appl. Phys.* **69**, 593, (1991)

P77 - Optical nonlinearities in asymmetric (CdS/ZnSe/BeTe)(ZnSe/ BeTe) quantum well

N. Zeiri¹, N. Sfina¹, S. Abdi-Ben Nasrallah^{1,*} and M. Said¹

¹Laboratoire de la Matière Condensée et des Nanosciences(LMCN)

Département de Physique, Faculté des Sciences de Monastir, 5019 Monastir, Tunisia

*Corresponding author : E-mail address : samiaabdi@myway.com

Abstract

The linear and nonlinear optical properties such as the second-harmonic generation susceptibility, the optical absorption and the refractive index change associated with intersubband transitions in (CdS/ZnSe/BeTe)(ZnSe/BeTe) quantum wells heterostructures have been investigated theoretically. The electronic states of these structures are calculated using both the envelope wave function approximation and the compact-density matrix formalism. The obtained results reveal that these properties strongly depend on the conduction-band states Γ and X as well as the doping concentration. It is found that the nonlinear optical behaviour of the modelled (CdS/ZnSe/BeTe)(ZnSe/BeTe) heterostructure is considerably improved in the X-BeTe conduction band minimum. Also, the incident optical intensity has a great effect on the total absorption coefficient and the refractive index.

These results suggest that the absorption process can be easily controlled by the structure parameters of an asymmetric rectangular quantum well. Thus, our results can be useful for electro-optical modulators and photodetectors in the infrared region.

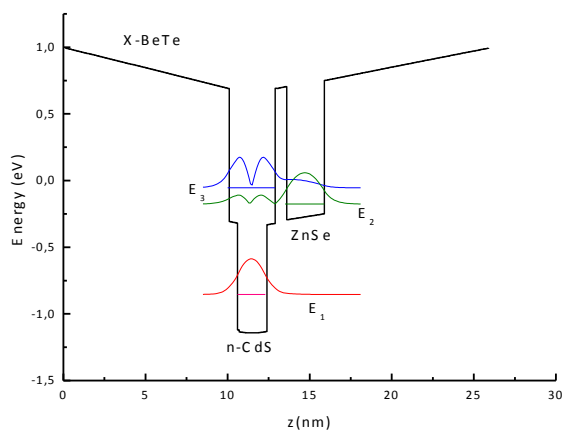


Figure 1 : The conduction band profile as well as intersubband transitions in the modeled structure

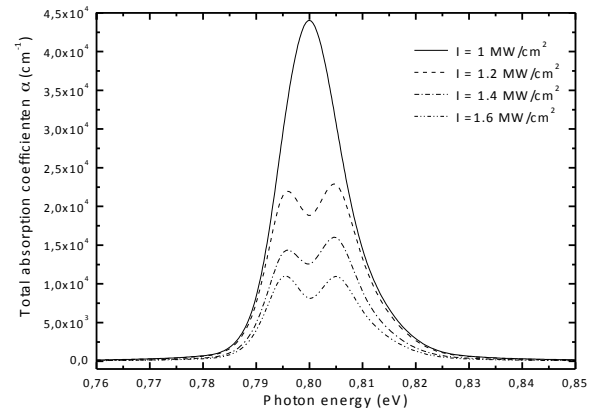


Figure 2 : The total absorption coefficient photon energy dependence $\alpha(\omega, I)$ (cm^{-1}) for the ISBT E_3-E_1 at different values of optical intensity I with fixed doping concentration $N_D=10^{19}\text{cm}^{-3}$.

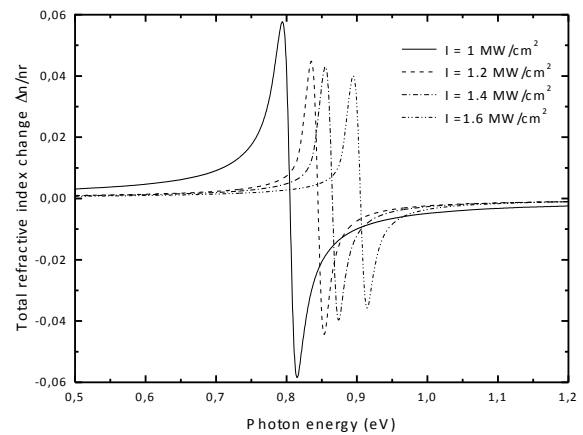


Figure 3 : The total refractive index change $\Delta n/n_r$ as a function of photon energy for different values of light intensity at $T=300\text{K}$ and doping concentration $N_D=10^{19}\text{cm}^{-3}$

P78 - First- principles calculation of magnetic properties of tetragonal $\text{BaTi}_{1-x}\text{TM}_x\text{O}_{3-\delta}$; TM=[Fe, Co, Cr, Mn,]

O. Benamara*, A. Boufelfel

¹Guelma physic laboratory (GPL), university 8 may 45 Guelma Algiers

*Corresponding author : E-mail adress : benamara_war@yahoo.fr

Abstract: The magnetic properties of TM-doped BaTiO_3 with TM= Fe,Co,Cr and Mn have been studied by means of a first-principles calculations base on density functional theory using the linear muffin-tin orbital method in the atomic sphere approximation with combined correction using the LSDA for exchange –correlation potentiel, we studied spin polarization induced by replacement of titanium atoms by an transition metal (TM) where TM= Fe,Cr, Mn, Co. in non magnetic tetragonal BaTiO_3 perovskit in a form of $\text{BaTi}_{0.9375}\text{TM}_{0.0625}\text{O}_{3-\delta}$. we first studied the magnetic moment in $\text{BaTi}_{0.9375}\text{TM}_{0.0625}\text{O}_3$ with spin orbital as perturbation

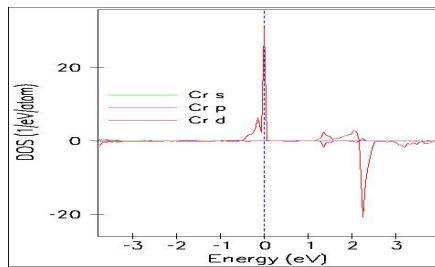


Figure 1: DOS of Cr with spin orbital

Secondary in the case of substitution of oxygen atoms forming the structure $\text{BaTi}_{0.95}\text{TM}_{0.06}\text{O}_{3-\delta}$ the result show that the spin orbital perturbation has a little effect in magnetic moment of Fe and Mn but a large increasing for Cr and Co, the contraire was observed for oxygen vacancies.

Magnetic moment	TM (μ_B)/atom	Theo/exp
$\text{BaTi}_{0.93}\text{Fe}_{0.06}\text{O}_3$	2.108	3.05/0.75
$\text{BaTi}_{0.93}\text{Cr}_{0.06}\text{O}_3$	2.528	-/-
$\text{BaTi}_{0.93}\text{Fe}_{0.06}\text{O}_{2.5}$	-0.017	-/-
$\text{BaTi}_{0.93}\text{Fe}_{0.06}\text{O}_{2.5}$	2.731	-/-

Table 1: magnetic moment studied with

Tetragonal symetrie

the data of this work was taken from (B,Xu et al) experimental work and compared with it and there theoretical prediction.

We find that with LSDA exchange correlation implemented in SPR-LMTO-ASA the magnetic moment of Fe are $2.10\mu_B$ less then the latter work and close to experimental one.

References:

- A. Perlov, A. Yaresko, and V. Antonov "PY-LMTO, A Spin-polarized Relativistic Linear Muffin-tin Orbitals Package for Electronic Structure Calculations", unpublished.
- B.Xu, K.B.Yin, Room-temperature ferromagnetism and ferroelectricity in Fe-doped BaTiO_3 . PHYSICAL REVIEW B 79, 134109(2009) .
- G.PING. Du et al ,Effects of niobium donor doping on the phase structures and magnetic properties of Fe-doped BaTiO_3 ceramics. Journal of Alloys and Compounds 492 (2010) L79–L81.
- H.Nakayama,H.Katayama-Yoshida, Theoretical Prediction of Magnetic Properties of $\text{Ba}(\text{Ti}_{1-x}\text{M}_x)\text{O}_3$ (M=Sc,V,Cr,Mn,Fe,Co,Ni,Cu), The Japan Society of Applied Physics. Vol. 40 (2001) pp. L 1355–L 1358.
- J.S. Lee, Magnetic properties of Co- and Mn-implanted BaTiO_3 , SrTiO_3 and KTaO_3 . Solid-State Electronics 47 (2003) 2225–2230.
- QIU Shen-yu, et al, Phase evolution and room temperature ferroelectric and magnetic properties of Fe-doped BaTiO_3 ceramics. Trans. Nonferrous Met. Soc. China 20(2010) 1911–1915.
- S. Ganopadhyay et al ,Understanding oxygen vacancy migration and clustering in barium strontium cobalt iron oxide. Solid State Ionics 181 (2010) 1067–1073
- Z. Chao, C. L. Wang, J. C. Li, and K. Yang, Chin. Phys. 16, 1422 (2007)

P79 - Optimization of electrical and dielectrical properties of ITO/MEH-PPV/Al structures by inserting of a thin gold interlayer

O.Dhibi¹, S. Zghal², A.Lateif¹, S.Jomni³, L. Beji¹ and A.Bouazizi¹

¹ Equipe Dispositifs Electroniques Organiques et Photovoltaïque Moléculaire, Faculté des Sciences de Monastir, Avenue de l'Environnement, 5019 Monastir, Tunisia.

*Corresponding author : E-mail adress : olfa_dhibi@yahoo.fr

² Ecole Supérieure des Sciences et de la Technologie de Hammam Sousse, 4011, Tunisia.

³ Laboratoire, Matériaux, Organisation et Propriétés, Faculté des Sciences de Tunis, Tunisia.

Abstract :

Indium tin oxide (ITO) coating on glass substrates are widely used as hole-injecting electrodes in polymer light emitting diodes. However, its chemical reactivity with organic molecules may form oxide related species, limiting therefore the performance of ITO/polymer base devices. In addition, its work function does not match well the highest occupied molecular orbital. As a solution limiting such interfacial problems is to introduce a buffer layer to modify the electronic behavior of adjacent materials.

In this work the effects of inserting a thin gold (Au) layer between the ITO electrode and the MEH-PPV organic material on the electrical and dielectrical proprieties of a ITO/MEH-PPV/Al devices are investigated through current-voltage $I(V)$ characteristics, surface morphology analysis, capacitance and conductance –frequency dependence (C-f) and G-f). The effect of Au layer thickness is also investigated.

The modified structures with ITO/Au anodes show improved current-voltage characteristics as compared with the device with ITO bare as anode. The $C(f)$ and $G(f)$ behaviors are typical of material with traps and exhibit a significant effect of series resistances at higher frequencies. The interface state densities and the relaxation times are evaluated using Schottky capacitance spectroscopy method. Low density and more homogenous distribution of interface states are observed in the modified structures with the addition of the Au layer.

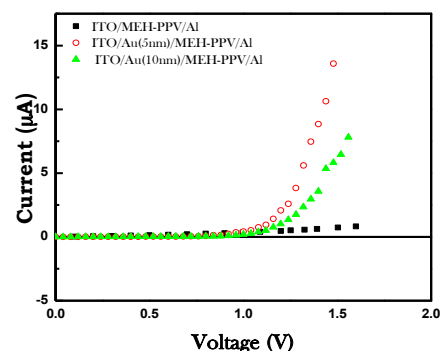


Figure 1: Current density-voltage characteristics of the structure with ITO bare, ITO/5nm-Au and ITO/10nm-Au as anodes.

References:

- Gu, G., Khalfin, V and Forrest, S.R. (1998) High-efficiency, low-drive-voltage, semitransparent stacked organic light-emitting device, *Applied Physics Letters*, 73, 2399-2402.
- Scott, J.C., Carter, S.A., Karg, S and Angelopoulos, M. (1997) Polymeric anodes for organic light-emitting diodes, *Synthetic Metals*, 85, 1197-1200.
- Scott, J.C., Kaufman, J.H., Brock, P.J., R. Salem, DiPietro, J. and Goitia, J.A., (1996) Degradation and failure of MEH-PPV light-emitting diodes, *Journal of Applied Physics*, 79, 2745-2752.
- Zacharias, N., Beltsios, K., Oikonomou, Ar., Karydas, A.G. and Bassiakos, Y. (2008) Thermally and optically stimulated luminescence properties of an archaeological glass collection from Thebes, Greece, *Journal of Non Crystalline Solids*, 354, 761-767.

P80 - Gold nanoparticle-nanobody complex: A comprehensive understanding of bio-functionalization

O. Msehli¹, I. Hmila¹, A. Mezni², I. Hafaiedh³, M. El Ayeb¹, L. Smiri², A. Mlayah⁴,
A. Abdelghani³ & B. Bouhaouala-Zahar^{1,5*}

¹Laboratoire des Venins et Toxines, Institut Pasteur de Tunis, 13 Place Pasteur, 1002, Tunis, TUNISIA

²Unité de recherche 991UR12-30, Département de chimie, Faculté des Sciences de Bizerte, TUNISIA

³Nanotechnology Laboratory, INSAT, Centre Urbain Nord, 1080 Charguia Cedex, TUNISIA

⁴Nanomaterials Spectroscopy, CEMES, 29 Rue Jeanne Marvig, 31055 Toulouse, FRANCE

⁵Faculté de Médecine de Tunis. Université de Tunis-EI Manar, TUNISIA

*Corresponding author : E-mail adress : balkiss.bouhaouala@pasteur.rns.tn

¹Institut Pasteur de Tunis, 13 Place Pasteur, 1002, Tunis, TUNISIA

Photothermal therapy is based on the functionalization of gold nanoparticles (AuNP) by specific ligands. Through irradiation, heated AuNP could destroy target cells. For effective antigen targeting, the size and nature of the ligand on AuNP surface have been herein considered.

In this work, gold nanoparticles are functionalized with nanobodies, the smallest antigen-binding fragments of camelid origin. We used the Nanobody NbF12-10, a highly specific recombinant nanobodies able of neutralizing toxicity of the *Androctonus australis Hector* scorpion venom.

Chemical and physical parameters for AuNP-NbF12-10 stable and functionally active conjugates have been determined.

UV-Visible spectrophotometer measurements show shifts in the refractive index and local λ_{max} of absorbance spectra. Interestingly, we noted the appearance of a SERS effect in Raman measurements, confirming the direct interaction of antibody fragments onto the surface of gold nanoparticles. The records of electrochemical impedance on the gold surface were used to determine the optimal NbF12-10 concentration for AuNP coupling.

Biological properties of washed AuNP-NbF12-10 conjugates were tested by ELISA. Specific binding to AaH1 toxin in dose dependent manner was registered. Indeed, 100% of mice survived to injection of washed AuNP-NbF12-10 Nanobody pre-incubated with lethal dose of AaH1 toxin. These results demonstrate that washed AuNP-NbF12-10 conjugates are effective and able to bind and neutralize their specific antigen.

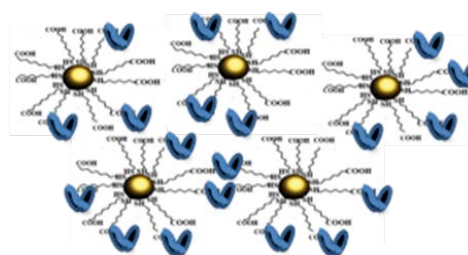


Figure 1: Representative scheme of AuNP-NbF12-10 conjugates. In blue, Nanobodies; In black, carboxyl branched domain. In yellow, 20nm gold particles

Electrochemical Impedance spectroscopy measurement were performed at room temperature in a conventional cell with a three electrode configuration using Autolab impedance analyzer (Ecochemie, Netherland). The gold electrode was used as working electrode, platinum (1 cm²) and Ag/AgCl electrodes were used as counter and reference electrodes respectively (Figure.2)



Figure 2: Impedance spectroscopy set-up

References:

- Hmila, I., Saerens, D., Ben Abderrazek R., Vincke, C., Abidi, N., Benlasfar, Z., Govaert, J., El Ayeb, M., Bouhaouala-Zahar, B. and Muyldermans, S. (2010) A bispecific Nanobody to provide full protection against lethal scorpion envenoming, *FASEB J.* 24, 3479-3489.
- Bouhaouala-Zahar B., Ben Abderrazek, R., Hmila, I., Abidi, N., Muyldermans, S. and El Ayeb, M. (2011) Immunological Aspects of Scorpion Toxins: Current Status and Perspectives, *Inflamm Allergy Drug Targets*, 10, 358-368.

P81 - Spin waves propagation through sandwich layers in ultrathin films

O.Nafa^{1*}, B.Bourahla^{1,2}, A.Khater²

¹ Laboratoire de Physique et Chimie Quantique, Université Mouloud Mammeri, 15000 Tizi-Ouzou, Algérie

*Corresponding author : E-mail address : ouahibanafa@yahoo.fr

² Laboratoire de Physique de l'Etat Condensé UMR 6087, Université du Maine, 72085 Le Mans, France

Abstract

In this work, we treated the behavior of spin waves through a nanojunction dividing two ferromagnetic ultrathin films. In particular, The model consists of a finite number of spin layers of lattice B joined two semi-infinite ultrthin films A having similar atomic layers. Each ultrthin film contain five atomic layers of a cubic lattice with magnetically ordered spins coupled by Heisenberg exchange as indicated schematically in Fig.1 where the gray area constitutes the effective nanojunction domain of B atomic sites. The model is treated as a simple cubic lattice with nearest neighbor magnetic interactions. J_A and S_A are the exchange interaction and the spin of the thin films A, J_B and S_B are the exchange interaction and the spin of the sandwiched layers B.

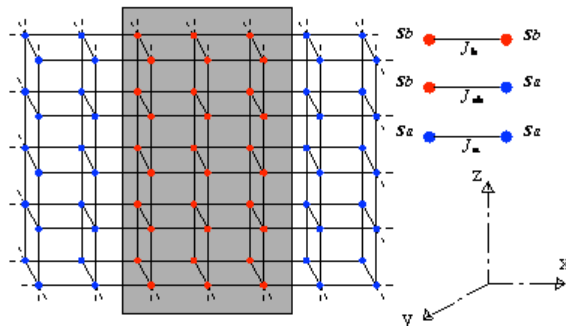


Figure.1: Schematic representation for a B layers sandwiched between two thin films of five parallel atomic layers.

The system is supported on a non-magnetic substrate and considered otherwise free from magnetic interactions. The spin dynamics of the ultrathin film is studied by the matching method. The total magnon transmission of the ultrathin ferromagnetic film, scattering coherently at the nanojunction zone, and the localized spin states in the boundary domain, are calculated and analyzed. The interatomic magnetic exchange is varied on the boundary domain specifically for three cases of magnetic exchange to investigate the consequences of magnetic softening and hardening for the calculated properties.

The results illustrate peaks in the conductance spectra caused by the interaction between the propagating magnon modes and localized spin precession states that are created by the nanojunction domain.

Our analysis can be traced back to the properties of interfaces in magnetic multilayer systems. It can also serve as a model for the study of other magnetic materials manufactured similarly to the system studied. The conductance spectra show that the nano-junction acts as a filter for magnons.

Keywords: Spin waves; Dynamic properties; Thin films

References

- [1] Abou Ghantous, M., Khater, A. (1999) Magnons localised on surface steps: a theoretical model Eur. Phys. J. B 12, 335
- [2] Barsukov, I., Römer, F.M., Meckenstock, and al. (2011) Frequency dependence of spin relaxation in periodic systems PhysRevB.84.140410(R)
- [3] Bourahla, B., Khater, A., and Tigrine, R. (2009). Dynamic properties of a symmetric spin nanocontact Eur. Phys. J. B 69, 343–349
- [4] Buczek, P., Ernst, A. and Sandratskii, L.M. (2011) Different dimensionality trends in the Landau damping of magnons in iron, cobalt, and nickel: Time-dependent density functional study PhysRevB.84.174418
- [5] Gagel F. and Maschke K. (1995) Finite-difference approach to edge-state transport in quantum wires and multiterminal devices Phys. Rev. B 52, 2013
- [6] Haupt, F., Novotny, T. and Belzig, W. (2009) Transport statistics of interacting double dot systems Phys. Rev. Lett. 103, 136601
- [7] Mercone, S., Perroni, C. A., and al (2005) Transport properties in manganite thin films, Phys. Rev. B 71, 064415
- [8] Niizeki, T., Mitani, S., Sukegawa, H., Kasai, S., and Inomata, K. (2011) Fully epitaxial Fe/MgO/Fe(001) junctions with nonmagnetic metal layer insertion, J. Appl. Phys. 109, 07C726

P82 - Annealing effect on the magnetic and structural properties of milled zinc ferrites ZnFe_2O_4 .

O. Ould Fella^{1*}, M. Tamine¹, N. Randrianantoandro² and J. M. Grenèche².

¹ : Laboratoire de Physique et Chimie Quantique, Département de Physique, Faculté des Sciences, Université de Tizi-Ouzou BP 17RP, 15000 Tizi-Ouzou, Algérie.

*Corresponding author: E-mail address : wlilidz@yahoo.fr

² : Laboratoire de Physique de l'Etat condensé, UPRESA, CNRS 6087, Université du Maine, Faculté des Sciences, 72085 Le Mans Cedex 9, France.

An increasing interest has been devoted to study magnetic properties of milled zinc ferrite $(\text{Zn}^{2+})[\text{Fe}^{3+}]_2\text{O}_4$ (Sun *et al.*). On the fundamental point of view, the motivation is to understand the dependence of the physical properties on the Zn^{2+} and Fe^{3+} distribution on the tetrahedral (A) and octahedral (B) positions of the FCC lattice formed by O^{2-} ions. In addition, the non-stoichiometry causes an imperfect cationic distribution and generates thus vacancies which disrupt the magnetic order.

Nanostructured zinc ferrite (ZnFe_2O_4) was milled at high energy for 12 hours. Portions of the powders were calcined at 400°C and 600°C for 24 hours, respectively. X ray diffractograms are recorded for all samples and are depicted in figure 1. The grain size increases with increasing annealing temperature. The inversion parameter increases with milling and decreases with increasing annealing temperature. Magnetic properties are studied using Mössbauer spectroscopy without and under magnetic field. The Mössbauer spectra recorded for all samples at 300 and 77K shown no evidence for the presence of the Fe^{2+} state confirming the perfect stoichiometry of all samples. At room temperature, only the sample milled at 12 hours is magnetically ordered whereas at 4.2K they reveal a magnetically blocked state. The Mössbauer spectra under external magnetic field ($B=6\text{T}$ and $B=8\text{T}$) parallel to the direction of gamma rays for sample milled at 12 hours shows the presence of ferrimagnetic ordering. Also, sample exhibits spin canting with a large canting, may be due to a spin glass or grain boundary (Chinnasamy *et al.*). The canting angle decreases with increasing external magnetic field.

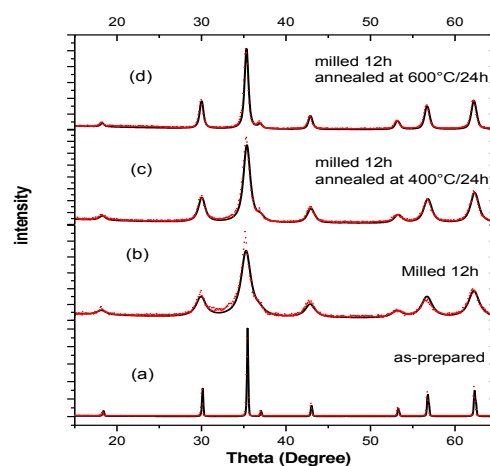


Figure 1: X-ray diffractograms of ZnFe_2O_4 .

References

- Chinnasamy, C.N., Narayanasamy, A., Ponpondian, N., Chattopadhyay, K., Guerault, H. and Grenèche, J.M. (2000) Magnetic properties of nanostructured ferrimagnetic zinc ferrite, *Journal of Physics: Condensed Matter*, 12, 7795-7805.
- Sun, S. and Murray, C. B. (1999) synthesis of monodisperses cobalt nanocrystals and their assembly into magnetic superlattices, *Journal of Applied Physics*, 85, 4325-4331.

P83 - Study of ion beam synthesized cobalt silicide layers in Si(111)

R. Ayache^{1*}, A. Bouabellou²

¹Pharmacy Department, University of Batna - 05000, ALGERIA

*Corresponding author : E-mail address : ayache_r@yahoo.fr

²Laboratoire Couches Minces et Interfaces, Campus Chaab Errassas, Université Mentouri de Constantine, Constantine, 25000, ALGERIA

Abstract: The study of transition metal silicides has attracted a great deal of interest for their applications as contact materials, gate electrodes, or interconnect materials in microelectronic devices. The fabrication of very thin CoSi_2 layers using ion beam synthesis (IBS) has attracted much interest recently. In IBS a compound layer is formed by the implantation of ions into a substrate, with subsequent high-temperature annealing to remove the residual radiation damage and to redistribute the implanted species.

The processes in the synthesis of a thin layer of CoSi_2 phase on a single-crystal Si(111) substrate by implantation of 195 keV Co ions with a dose of $2 \times 10^{17} \text{ Co}^+/ \text{cm}^2$ at room temperature (RT) followed by annealing in an N_2 atmosphere at different temperatures for 1h are investigated. The characterization of the as-implanted and annealed samples is performed using Rutherford backscattering spectrometry (RBS) and X-ray diffraction (XRD). Also the obtained samples have been characterized by means of infrared and Raman spectroscopies. The results show that the CoSi_2 phase is polycrystalline with a random crystallographic orientation.

Figure 1 shows the random RBS spectra for Si wafer implanted with high current density confirming the formation of the silicide, as the spectra show a clear step just behind the Si leading edge. It can be seen that by increasing the temperature treatment, the height of Co signal decreases whereas the energetic width increases, in the same time, the Si signal around, channel 520, corresponding to CoSi_2 layer is extended toward lower energy.

The first order Raman spectrum of crystalline Si is characterized by the presence of one peak corresponding to the only Raman active phonon that is allowed by the crystal symmetry. This peak has a Lorentzian shape, centred at a wavelength of

520 cm^{-1} with a full width at half maximum (FWHM) of about 3 cm^{-1} at room temperature.

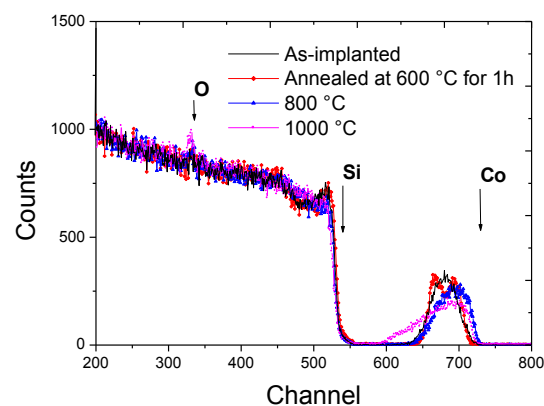


Figure 1: RBS spectra of a CoSi_2 structure before and after annealing for 1h.

References:

- Dekempeneer, E. H. A. J. Ottenheim, J. M. Zalm, Bulle, P. C. Lieuwma, C. W. T. Vandenhoutd, D. E. W. and Naburgh, E. P. (1991) *Appl. Phys. Lett.*, 58 2102.
- Jebasinski, R. Mantl, S. Dieker, Chr. and Vescan, L. (1991) *Appl. Surf. Sci.*, 53 264.
- Maex, Vanhellefont, K. J. Petersson, S. and Lauwers, A. (1991) *Appl. Surf. Sci.*, 53 273.
- Murarka, S.P. (1983) *Silicides for VLSI Applications*, Academic Press, New York.
- Nicolet, M.-A. Lau, S.S. in Einspruch, N.G. and Larrabee, G.B. (eds.) (1983) *VLSI Electronics Microstructure Science*, Vol. 6, Materials and Process Characterization, Academic Press, New York.
- Vantomme, Wu, A. M. Langouche, F. G. Maex, K. Vanderstraeten, H. and Bruynseraede, Y. (1991) *Nucl. Instrum. Methods Phys. Res. B*, 50 680.

P84 - Determination of epitope complementation groups of AahII toxin binders by surface plasmon resonance

R. Ben Abderrazek¹, I. Hmila¹, M. El Ayeb, S¹, Muyldermans^{2,3} and B. Bouhaouala-Zahar^{1,4*}

¹ Laboratoire des Venins et Toxines, Institut Pasteur de Tunis, 13 Place Pasteur, 1002, Tunis, TUNISIA

² Laboratory CMIM, Vrije Universiteit Brussel, Pleinlaan 2, 1050 Brussel, BELGIUM.

³ Department of Cellular and Molecular Interactions, VIB, Brussels, BELGIUM.

⁴ Faculté de Médecine de Tunis. Université de Tunis-El Manar, TUNISIA

*Corresponding author : E-mail address : balkiss.bouhaouala@pasteur.rns.tn

¹ Institut Pasteur de Tunis, 13 Place Pasteur, 1002, Tunis, TUNISIA

This work describe an approach used to determine the epitope complementation group(s) of scorpion toxin Nanobodies (Nbs) based on surface plasmon resonance (SPR) technique. To group the Nbs from the different CDR3 (complementing determining region 3) sequence clusters according to their targeted epitope, we coupled the specific AahII toxin covalently on the biosensor chip and after saturating the toxin with one Nb, we monitored the possible binding of a second Nb.

We injected an excess of a first Nb, after saturating the toxin on the sensor chip with this Nb and reaching equilibrium, we applied a second Nb in presence of this first Nb. No signal increase was observed if the second Nb binds to an epitope overlapping that of the first Nb.

In contrast, if the signal-increase upon addition of the second Nb equals the signal obtained with this Nb alone (in absence of the first Nb) then we conclude that these Nbs bind to non-overlapping epitopes.

This approach was applied for multiple pairs of Nbs in both directions, i.e. clone NbX followed by binding of clone NbY and vice versa. The interpretation of the sensorgrams might get complicated when the association of the first Nb induces a conformational shift on a distantly located area of the antigen that hinders the subsequent binding of the second Nb.

Our results show that all clones grouped within the same cluster (based on the CDR3 sequence length and homology) bind to the same epitope complementation group. Consequently, the CDR3 sequence that was used to define the clusters determines which epitope is targeted.

Some antigen binding sites are identical and have an extensive overlap. Other antigenic site of the Nbs have clearly an independent epitope.

Finally, clone NbAahII10 that was tested against binders of all other clusters attaches to a unique epitope since all other Nbs could bind equally well to the toxin, independent of the prior presence or absence of NbAahII10.

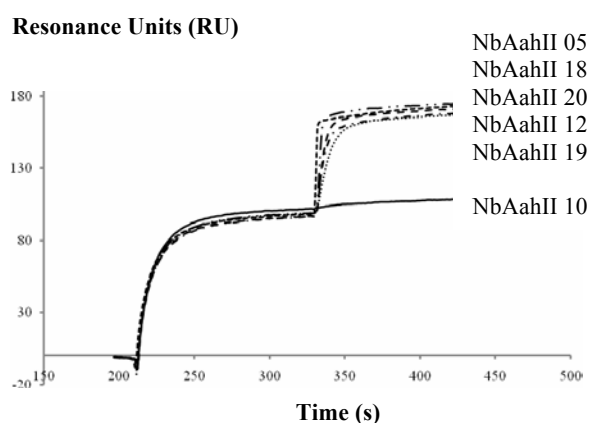


Figure : Epitope mapping whereby an excess of the NbAahII10 is first injected (at 215 s) to saturate its epitope, and from 330 s onwards a mixture of NbAahII10 with NbY (as indicated) is applied. A net signal increase is observed for all Nbs (except NbAahII10) indicating that they are binding to an epitope that is non-overlapping with the NbAahII10 epitope.

Reference:

Ben Abderrazek-Ben Abdallah, R., Hmila I., Vincke C., Benlasfar, Z., Dabbek H., El Ayeb M., Muyldermans S. and Bouhaouala-Zahar, B. (2009) Identification of potent Nanobodies neutralizing the most poisonous polypeptide from scorpion venom. *Biochem. J.*, 424, 263-272.

P85 - Effects of applied electric field, hydrostatic pressure and temperature on the second and the third harmonic generations in quantum dot

R. Ben Mahersia*, L. Bouzaienne, H. Maaref

Laboratoire de Micro-Optoélectronique et Nanostructures
 Departement de physique, Faculté des sciences de Monastir,
 Université de Monastir, Monastir 5000

*Corresponding autor : E-mail adress : mahrsia_r@yahoo.fr

Abstract:

The study of nonlinear optical properties due to intersubband transitions in low-dimensional semiconductor structures such as quantum wells, quantum wires and quantum dots (QDs) has been intensively carried out over the past two decades. The optical properties have the potential for promising device applications in the infrared region. With the advance of the technique fabrication, it is now possible to grow these structures with well-controlled dimensions and compositions. The experimental studies show that the semiconductor quantum dots have very large non linear optical susceptibilities as compared with those in bulk semiconductors. The effect of confinement on the electronic and optical properties increases from quantum wells to quantum dot. Large optical nonlinearities are also expected in theoretical studies in semiconductor quantum dots. In this work, the effects of applied electric field, hydrostatic pressure and temperature on the second and the third harmonic generations (SHG and THG coefficients) in quantum dot are studied under the density matrix formalism and the effective mass approximation.

The main findings for both SHG and THG coefficient can be summarized as follows:

- Intensity of the coefficient increases with the intensity of the applied electric field.
- Hydrostatic pressure causes a decrease in the peak height and a blue shift in peak position.
- Temperature increases the peak height and induces a red shift in peak position.

SHG and THG coefficients are affecting with external applied electric field, hydrostatic pressure and temperature. This study could be of utility in the application of devices based on SHG and THG in quantum dot.

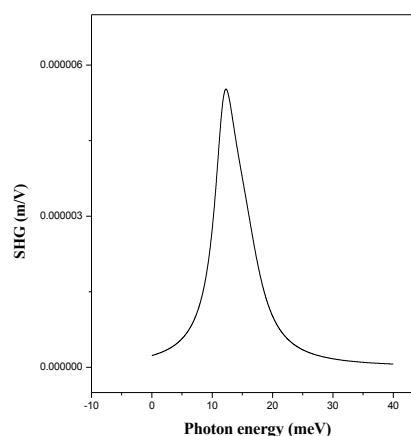


Figure 1: SHG coefficient in a GaAs parabolic QD as a function of incident photon energy with confinement frequency $\omega_0 = 10^{13} \text{ s}^{-1}$.

References:

- A Sivakami, M Mahendran (2010). Hydrostatic pressure and temperature dependence of correlation energy in a spherical quantum dot. *Superlattices and Microstructures*. 44, 530-537.
- Shuai Shao, Kang_Xian Guo, Zhi-Hai Zhang, Ning Li, Chao Peng (2010). Studies on the third-harmonic generations in cylindrical quantum dots with an applied electric field. *Superlatt and Microstructure*. 48, 541-549.
- Shuai Shao, Kang_Xian Guo, Zhi-Hai Zhang, Ning Li, Chao Peng (2011) Studies on the second-harmonic generations in cubical quantum dots with applied electric field. *Physica B*. 406, 393-396.

P86 - Structural and vibrational properties of Au(100)-c(2x2)-Pd ordered metallic surface alloy

R. Chadli^{1,2*}, A. Khater², R. Tigrine¹

¹ Laboratoire de Physique et Chimie Quantique, Université Mouloud Mammeri, B.P. N° 17, 15000 Tizi-Ouzou, ALGERIA

*Corresponding author: E-mail adress : rabah_abo@yahoo.fr

² Laboratoire de Physique de l'Etat Condensé (LPEC), Université du Maine, Av. Olivier Messiaen, 72085 Le Mans Cedex

09, France

Abstract

During the last two decade, the studies of the surface alloys systems have attracted a great deal of attention. Understanding the electronic, vibrational, magnetic, and catalytic properties of these system of surface alloys remains a major challenge in surface physics [1]. When a metal is deposited on the surface of another metal, there are several possible ways for it to react, depending on the species of the metals. The impurity atoms may reside in the surface layer or have a tendency to diffuse further into the bulk, and they may form separate islands or a pseudomorphic alloy.

Two classes of bimetallic surface alloys formed by the depositing B atoms onto a surface metal A can be distinguished. The first class corresponds to combinations of two metals that are immiscible in the bulk. In this situation, the alloy is restricted to the outermost layers of the A solid and this type of surface alloy represents a true equilibrium configuration [2]. Note that, the formation of this class of surface alloy depends on a series of considerations such as: temperature, type and concentration of elements, and the geometry of the surface. However, the second class of surface alloy contains those metals that exhibit bulk solubility, often forming a series of solid solutions over a wide compositional range. Single and multilayer surface alloys have been observed for both of these two classes [3, 4].

A deeper understanding of the physical and chemical phenomena associated with the creation of surface alloys appears to be essential in order to further progress in catalysis, where the electronic structure and geometric arrangement of the surface atoms strongly influences the surface reactions. In the present communication, we apply the matching theory to study the vibration properties of the Au(100) – c(2x2) – Pd ordered metallic surface alloy formed by depositing of Pd atoms onto the Au (100) surface substrate after annealing at a well determined temperature. Our results for the vibration modes at this ordered surface alloy, show the existence of new surface modes along the

directions of high symmetry directions $\overline{\Gamma X}$, \overline{XM} , and \overline{MT} of the two-dimensional Brillouin zone, in comparison with the clean surface Au(100) (see Figure 1 below).

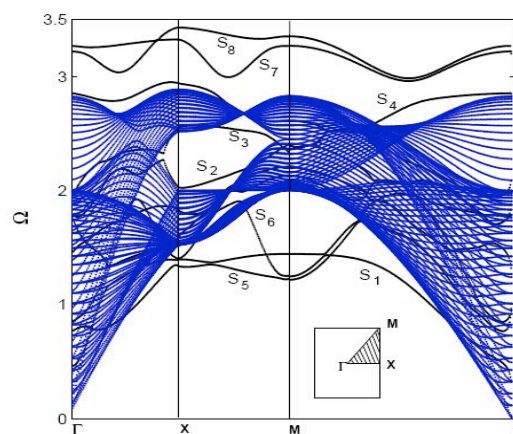


Figure 1: Calculated phonon dispersion curve for the Au(100)-c(2x2)-Pd ordered metallic surface alloy presented in the principal directions of the surface Brillouin zone. Surface states are indicated by the black curves. The blue lines represent the projected bulk phonon dispersions.

Keywords: Surface phonons; Surface alloy; LDOS

References

- [1] Woodruff, D. P. (ed.) (2002) Surface Alloys and Alloy Surfaces: The Chemical Physics of Solid Surfaces Vol 10, Elsevier Science B.V. Amsterdam, The Netherlands.
- [2] Woodruff, D. P. and Robinson, J., (2003) Some structural issues in surface alloys and alloy surfaces: rumpling, stacking faults and disorder, *Appl. Surf. Sci.*, 219, 1-10.
- [3] Bardi, U. (1994) The atomic structure of alloy surfaces and surface alloys, *Rep. Prog. Phys.*, 57, 939-987.
- [4] de Siervo, A., Soares, E. A., Landers, R., Fazan, T. A., Morais, J., Kleiman, G.G., (2002) Pd on Cu(111) studied by photoelectron diffraction, *Surf. Sci.*, 504, 215-222.

P87 - Hybrid polymer electrolytes Nafion-TiO₂ for PEMFCs: synthesis and characterization

R. Hammami¹, J. Ben Naceur¹, K. Charradi¹, I. Ben Assaker¹, A. Carbone², B. Auvity³
G. Squadrito², Z. Ahamed^{1*} and R. Chtourou¹

¹Photovoltaic Laboratory, Centre for Research and Energy Technologies CRTEn, BP 95, Hammam Lif 2050, Tunisia

*Corresponding author: E-mail address: zakarya_ahmed78@yahoo.fr

²Advanced Technologies for Energy Institute CNR-ITAE, Via Salita S. Lucia sopra Contesse, 5, 98126 Messina, Italy

³Polytech'Nantes, University of Nantes Rue C. Pauc, 44 000 -Nantes, France

Abstract - Many works was conducted to enhance the water retention and thermal stability of Nafion® and related membranes by incorporating transition metal oxide particles. Watanabe et al. [Watabe, M.] investigated silica and titania impregnated Nafion® composite membranes confirming the enhancement of performance of the composite membrane.

Room temperature synthesis (Nafion as a special polymer substrate for using in fuel cells need such low temperature in processing due to properties of Nafion) of nano particle titanium dioxide (TiO₂) using in-situ sol-gel technique on Nafion membrane is investigated in this work.

Titan tetraisopropoxide (TIP) is used as precursor and ethanol as the solvent (optimising precursor to solvent weight ratio) has been used for the synthesis of TiO₂ sol [Ben Naceur J.]. Nafion-TiO₂ were produced by impregnation of Nafion membrane in the TIP sol. Nafion membranes were previously dried at 100 °C for 24 h and immersed in absolute ethanol for 20 min. The membrane was then immersed in the TIP sol. The imbedded membrane was in the end treated in micro-wave for 10 min at room temperature.

The obtained membranes were characterized in term of morphologies by scanning electron microscopy (SEM) confirming the good dispersion of TiO₂ nano-particles (figure 1) and by infrared spectroscopy (IR); the IR spectrum of hybrid membranes Nafion-titanium dioxide confirm the presence of bonds Ti-O-Ti and Ti-OH which proves

that the hybridization of the membrane by sol-gel method is successful. This interaction between the organic and inorganic phase is favorable for the improvement of the thermal stability of the hybrids membrane. The nano-TiO₂ film as shown can be used to reduce the cross-over permeation of fuel through the PEM and increase electric power of the FC.

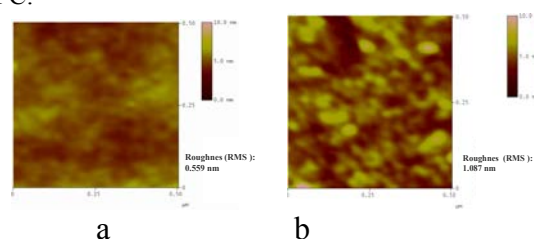


Figure 1: AFM surface morphology images of membranes: (a) pure nafion 212 membrane; (b) hybrid nafion membrane with TiO₂.

References:

- Ben Naceur, J., Mechiakh, R., Bousbih, F. And Chtourou, R., (2011), Influences of the iron ion (Fe⁺³)-doping on structural and optical properties of nanocrystalline TiO₂ thin films prepared by sol-gel spin coating, Applied surface science, 257, 24 10699– 10703.
- Watanabe, M., Uchida, H., Seki, Y., M. Emori, and P. Stonehart, (1996), self-humidifying polymer electrolyte membranes for fuel cell, Journal of Electrochemistry Society, 143 (12), 3847-3852

P88 - Room temperature synthesis of hybrid polymer electrolytes Nafion-TiO₂ for PEMFCs

R. Hammami¹, J. Ben Naceur¹, K. Charradi¹, A. Carbone², B. Auvity², I. ben assahe¹
G. Squadrito², Z. Ahamed¹, R. Chtourou¹

¹Photovoltaic Laboratory, Centre for Research and Energy Technologies CRTEn, BP 95, Hammam Lif 2050, Tunisia

*Corresponding author : E-mail address : hrafika40@yahoo.com

² Advanced Technologies for Energy Institute CNR-ITAE, Via Salita S. Lucia sopra Contesse, 5, 98126 Messina, Italy

Introduction: Many works was conducted to enhance the water retention and thermal stability of Nafion® and related membranes by incorporating transition metal oxide particles, such as SiO₂, obtaining promising results [1, 2]. Watanabe et al. [2] investigated silica and titania impregnated Nafion® composite membranes confirming the enhancement of performance of the composite membrane.

Room temperature synthesis (Nafion as a special polymer substrate for using in fuel cells need such low temperature in processing due to properties of Nafion) of nano particle titanium dioxide (TiO₂) using in-situ sol-gel technique on Nafion membrane is investigated in this work.

Titan tetraisopropoxide (TIP) is used as precursor and ethanol as the solvent (optimising precursor to solvent weight ratio) has been used for the synthesis of TiO₂ sol [3]. Nafion-TiO₂ were produced by impregnation of Nafion membrane in the TiO₂ sol. Nafion membranes were previously dried at 100 °C for 24 h and immersed in absolute ethanol for 20 min. The membrane was then immersed in the TiO₂ sol. The imbedded membrane was in the end treated in micro-wave for 7 h at room temperature.

A nanocomposite Nafion-TiO₂ membrane containing nano particle titanium dioxide (TiO₂) synthesized at room temperature using in-situ sol-gel technique on Nafion membrane is investigated. Nafion-TiO₂ membranes were produced by impregnation of Nafion membrane in TiO₂ sol with different percentage ([TiO₂]=0.6% and [TiO₂]=1.2%). The obtained membranes characterized by X-ray diffraction (XRD) show the crystallization of TiO₂ in anatase phase. The Infrared spectroscopy IR spectrum of hybrid membranes Nafion-titanium dioxide confirm the presence of bonds Ti-O-Ti and Ti-OH which proves that the hybridization of the membrane by sol-gel method is successful. Atomic Force Microscopy AFM confirmed the good dispersion of TiO₂ nanoparticles. This interaction between the organic and inorganic phase is favorable for the improvement of the thermal stability of the hybrid membrane. The nano-TiO₂ film can be used to reduce the cross-over

permeation of fuel through the PEM and increase electric power of the FC.

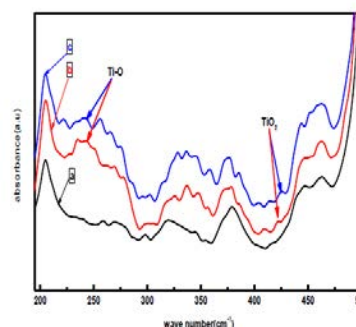


Fig. 1 : FT-IR ATR spectra of Nafion 212 membrane shown in the wave number range between 200 and 500 cm⁻¹ : (a) pure nafion 212 membrane; hybrid nafion membrane with TiO₂: (b) for [TiO₂]=0.6% and (c) for [TiO₂]=1.2%.

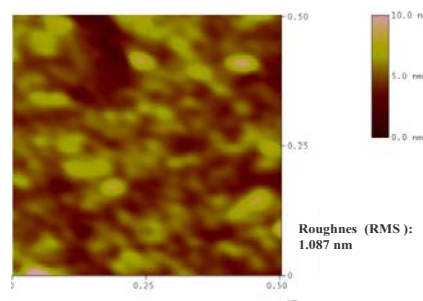


Fig. 2 : AFM surface morphology images of hybrid nafion membrane with TiO₂: for [TiO₂]=1.2%.

References:

- [1] P.L Antonucci, A.S Arico, P. Creti, E. Ramunni and V. Antonucci, Solid State Ionics 1999, 125 (1-4), 431-437.
- [2] M. Watanabe, H. Uchida, Y. Seki, M. Emori and P. Stonehart, J. Electrochem. Soc. 1996, 143 (12), 3847-3852.
- [3] J. Ben Naceur, R. Mechiakh, F. Bousbiha, R. Chtourou, Influences of the iron ion (Fe⁺³)-doping on structural and optical properties of nanocrystalline TiO₂ thin films prepared by sol-gel spin coating, Applied Surface Science 257 (2011) 10699– 10703.

P89 - Micro pressure sensor model validation by finite element method

R. Otmani^{1*}, N. Benmoussa²

^{1,2} Research Unit of Materials and Renewable Energy, University of Tlemcen, ALGERIA

*rad.otmani@yahoo.com

Abstract: In this paper, we propose to establish a mathematical model that describes the mechanical behavior of single crystal silicon micro membrane. The proposed model is based on the theory of thin plates and shell. It describes the deflection of the membrane and the stresses induced in by the effect of a homogeneous differential pressure applied to this membrane. Once the model is established (equation 1, 2 and 3) it constitutes a system of partial differential equations which will be solved by the semi-analytical method of Galerkin who is based on the theory of virtual work.

$$\frac{\partial^4 W(x,y)}{\partial x^4} + 2\alpha_{Si} \frac{\partial^4 W(x,y)}{\partial x^2 \partial y^2} + \frac{\partial^4 W(x,y)}{\partial y^4} = \frac{P}{D} \quad (1)$$

$$\begin{cases} W(x = \frac{a}{2}, y) = 0 \\ W(x, y = \frac{a}{2}) = 0 \end{cases} \quad (2)$$

$$\begin{cases} \frac{\partial W}{\partial x}(x = \frac{a}{2}, y) = 0 \\ \frac{\partial W}{\partial y}(x, y = \frac{a}{2}) = 0 \end{cases} \quad (3)$$

The resolution of this system allows us to calculate the displacement of the membrane (his deflection) and to know the stress distribution as a function of the applied pressure (Fig. 1).

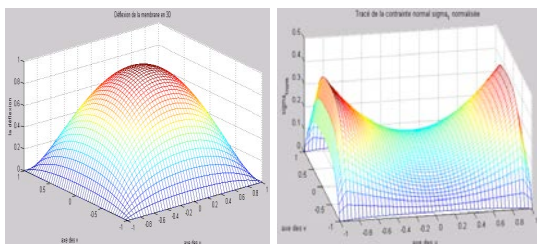


Figure 1: Deflection and stress distribution in the membrane obtained by semi-analytical method.

Then, in order to check the conformity of the semi-analytical method of Galerkin and validate the results obtained, we propose to solve the same model with an other method who is the finite element method which is known for its accuracy. The obtained results are given in Figure 2.

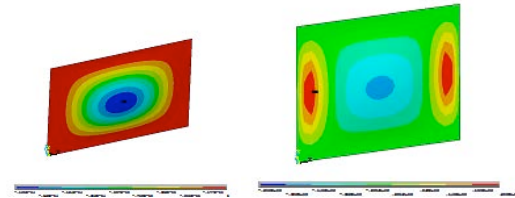


Figure 2: Deflection and stress distribution in the membrane obtained by finite element method.

comparison of results will allow us to know the benefits of semi-analytical method compared to the numerical one, but also to know the disadvantages and limitations of of Galerkin method.

After comparison, we remark that there is a convergence between the results obtained by both methods, which leads us to adopt the semi-analytical method which is much less expensive in terms of computation time. However, the semi-analytical model does not support multi-layered structures where the mechanical properties of those structure are not homogeneous.

References:

- Joseph C Doll, Sung-Jin Park and Beth L Pruitt. (2009) Design optimization of piezoresistive cantilevers for force sensing in air and water, *Journal of Applied Physics*.
- Lung-jieh Yang, Chen-chun Lai, Ching-liang Dai and Pei-zen Chang. (2005) A piezoresistive micro pressure sensor fabricated by commercial DPDM CMOS process, *Tamkang Journal Of Science And Engineering*.
- R. Otmani and N. Benmoussa. (2010) Modeling, Simulation and Optimization of the Mechanical Response of a Silicon Micro Membrane : Application to Piezoresistive Pressure Sensor, *International Review on Modelling and Simulation*, Vol. 3. n. 2, pp. 250-254.
- S. Aravamudhan and S. Bhansali. (2007) Reinforced piezoresistive pressure sensor for ocean depth measurements, *Science Direct, Sensor and Actuators*, 2007.
- Shuang Chen, Ming-quan Zhu, Bing-he Ma and Wei-zheng Yuan. (2008) Design and Optimization of a Micro Piezoresistive Pressure Sensor, pp. 351-356.

P90 - Vibrational-level spacings and evaluation of adiabatic correction for the six $1\Sigma^+$ states of LiK molecule

S. Bellayouni^{1*}, N. Mabrouk¹, and H. Berriche^{1,2}.

¹Laboratoire des interfaces et matériaux avancés, Département de Physique
Faculté des Sciences, Avenue de L'environnement ,5000 Monastir, TUNISIA.

²Physics Department, Faculty of Science, King Khalid University, P. O. Box 9004, Abha, Saudi Arabia

* E-mail corresponding author: belayounisaana@yahoo.com

Introduction: Potential energy curves of the first six $1\Sigma^+$ states calculated with the Born-Oppenheimer approximation which is generally a good one and is used in most molecular problems. However, it breaks down in many cases, since the neglected interactions in this approximation, which are responsible for many physical processes of interest e.g.; Predissociation, collisions or radiationless transition. It is still possible to use this approximation if we take into account the neglected terms. The first theoretical calculation of the adiabatic correction was performed for the H_2^+ molecule [1]. Our main purpose is to show especially the effect of this adiabatic correction in the zone of quantum well. To our Knowledge the vibrational level spacing with and without adiabatic correction for LiK are determined for the first time. This adiabatic corrections lead to a systematic overestimation of the full vibronic shift for the ground state and to an underestimation for the others states.

Method of calcul:

In our study the adiabatic correction is evaluated using the produced data in both adiabatic and diabatic representation. The vibrational energy levels have been calculated using the adiabatic and the corrected potential energy curves. These vibrational energy levels have been numerically obtained using the Numrov method.

Results and Discussion:

Table (1) presents the vibrational energy level spacing ($E_v - E_{v-1}$) which decrease respectively when the order of vibrational level increase. We notice that the number of level was related to the wide well. Figure (1) prove that the largest correction are located at short and intermediate distances close to the equilibrium distances, which affect all the vibrational energy levels. It's important to mention that the peaks positions of adiabatic correction, which shows the region where this correction is large, are shifted

to longer distances for higher excited states as the avoided crossings occur at larger internuclear distance.

Figures and Tables:

<i>vibrational level</i>	<i>Energy without correction</i>	<i>Energy with correction</i>
$v = 1$	209.372	209.629
$v = 2$	207.237	207.169
$v = 28$	130.297	130.267
$v = 29$	124.881	124.917
$v = 35$	92.981	93.13
$v = 36$	82.577	82.835
$v = 51$	0.087	0.089
$v = 52$	0	0

Table1: Vibrational energy level spacing ($E_v - E_{v-1}$) (in cm^{-1}) for the $X^1\Sigma^+$ electronic state of the LiK molecule.

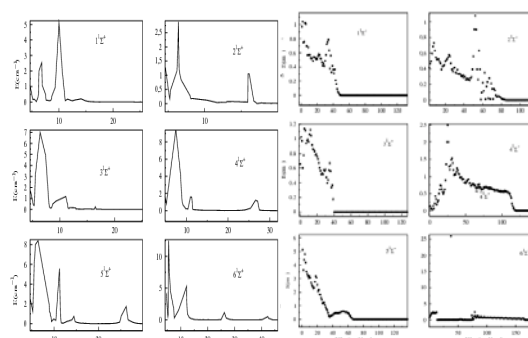


Figure1: the adiabatic correction and the vibrational shift for 1-6 $1\Sigma^+$ states of LiK

References:

[1]: Johnson VA (1941) Phys Rev 60:373

P91 - Structural and optical characterization of CdSe/TiO₂ nanocomposite

S. Ben Taieb, A. Bardaoui, I. Ben Assaker, R. Chtourou

Laboatoie de Photovoltaïque, Centre des Recherches et des Technologies de l'Énergie, Route touristique
Soliman B.P. 95, Hammam-Lif 2050, TUNISIA

*Corresponding author : E-mail adress : bentaieb.senda@gmail.com

Abstract: In this paper, CdSe was deposited on a titanium dioxide (TiO₂) films using the electrochemical deposition (ECD) method. Based on the physical appearance of the samples, the particles of CdSe seemed to penetrate the TiO₂ film. The film was confirmed to be a CdSe/TiO₂ composite via X-ray diffraction measurements. The optical and morphological properties have been investigated respectively by UV-vis spectroscopy and atomic force microscopy (AFM).

Introduction: Titanium dioxide (TiO₂), as an important IV–VI group semiconductor, has been widely applied in chemical [1], electronic [2,3], and cosmetic industries [4], as well as in environmental protection [5] and medical science. In its pure form it is an n-type semiconductor with indirect band gaps of 3.2 eV for the anatase phase.

Cadmium selenide (CdSe) is one of the most important II–VI group semiconductors. In fact, CdSe is a promising photovoltaic material thanks to its high absorption coefficient and nearly optimum band-gap energy (~1.7 eV) for the efficient absorption and conversion of solar energy [6].

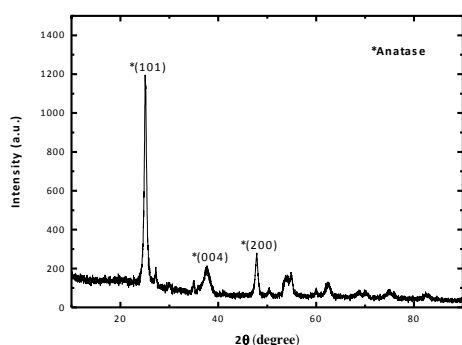


Fig. 1 – XRD patterns of TiO₂ particles (P-25) .

Experimental: TiO₂ films were prepared by the squeegee method using a 0.8 g/mL paste of TiO₂ powder (P25, Aldrich) with 0.5 mL of acetyl acetone. The paste was mixed and blended with 0.4 g of polyethylene glycol and 2.5 mL of triton X for about 5 min. Then, the TiO₂ films were heated and annealed at 100 °C and 400 °C for 30 min in air. The substrate used was (ITO) coated glass. The deposition of CdSe on the TiO₂/ITO substrate was accomplished by ECD.

References:

- [1] L. Caballero, KA. Whitehead, NS. Allen and J. Verran (2010). Photoinactivation of Escherichia coli on acrylic paint formulations using fluorescent light . *Dyes Pigm*2010;86: 56–62.
- [2] K. Hou, BZ. Tian, FY. Li, ZQ. Bian, DY. Zhao, CH. Huang. (2005). “Highly crystallized mesoporous TiO₂ films and their applications in dye sensitized solar cells”. *J Mater Chem*;15(24):2414–20.
- [3] UM. Khan Shahed, M. Al-Shahry, Jr B. William. Efficient photochemical water splitting by a chemically modified n-TiO₂. (2002). *Science* 297(5590):2243–5.
- [4] J. Labille ,J. Feng, C. Botta, D. Borschneck, M. Sammut, M. Cabie. (2010). Aging of TiO₂ nanocomposites used in sunscreen. Dispersion and fate of the degradation products in aqueous environment. *Environ Pollut*;158:3482–9.
- [5] A.V. Kokate, U.B. Suryavanshi, C.H. Bosale. (2006). *Solar Energy*. 80, 156.
- [6] Z. Xiaoshan, Y. Chang, Y. Chen. (2010). Toxicity and bioaccumulation of TiO₂ nanoparticle aggregates in *Daphnia magna*. *Chemospher* 78:209–15.

P92 - Study of the resistance to crack propagation in nano fine grained alumina by acoustic emission

S. Bouras, F. Gheldane, Y. Berriche

Laboratory of Advanced Materials, University of Annaba, B.P. 12, 23000 Annaba, Algeria

Corresponding author: bourasseddik@yahoo.fr

Introduction

The ceramic brittleness is due to pre-existent micro-cracks that become unstable under the effect of a stress and leads to the fracture of the specimen. However, alumina presents a crack growth resistance that translates stable crack propagation before the fracture. In this case, the material toughness is not constant but increases with the crack extension. It depends on the crack extension Δa from an initial crack size a . The curve representing the crack growth resistance variation R , or the stress intensity factor K_R , according to Δa is called R-curve or K_R -curve. The bridging by grains and the crack ramification are responsible for the crack propagation resistance [2].

Hertzian indentation

The hertzian indentation consists to load specimen surface using a spherical indenter. It requires the presence of an initial micro-crack that can be introduced by polishing. At a critical load P_c , this crack propagates on the surface as an entire circle around the ball and in depth as a cone. On materials presenting a resistance to crack propagation, we observe that the circular crack occurs progressively in several stages according to the loading. Critical load P_c is determined by the highest acoustic emission peak.

Acoustic emission

The interest of the acoustic emission is to obtain data on emissive events and to correlate them to mechanisms responsible for their generation. intervals (rate of numbering $N/\Delta t$: number of arks by unit of time).

Results

In hertzian indentation tests, the used monotonous loading leads to the progressively growth of circular cracks until the formation of a complete circle.

Figure 1 shows the result of loading followed by an unloading, and the recorded acoustic emission. The complete circle occurred at the fracture critical load $P_c = 900$ N identified by the peak of the highest amplitude. The loads below P_c provoke weak acoustic emissions translating a sub-critical crack propagation correlated to the resistance to crack propagation.

Figure 2 show that the arks numbering rate decreases first. That means that every time interval contains less acoustic events than the previous

interval. And it translates a resistance to cracks propagation. Close to the critical load, very fast growth of the arks numbering rate is obtained.

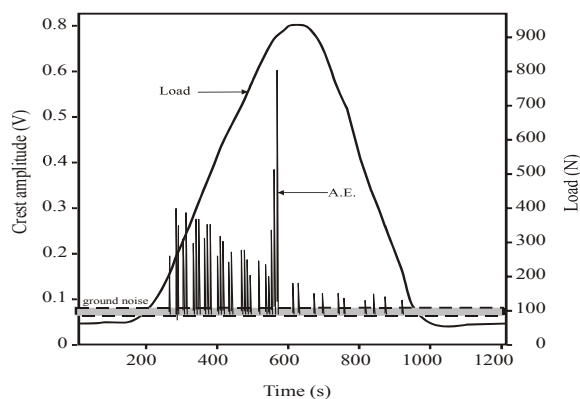


Figure 1. Acoustic emission and loading.

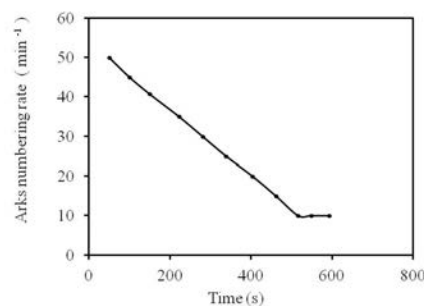


Figure 2. Arks numbering rate.

Conclusion

The decrease of the rate of the arks numbering variations obtained by acoustic emission indicates the resistance crack propagation for loads less than the critical load provoking the fracture

References:

- B.R. Lawn, "Indentation of Ceramics wit, Spheres: A Century after Hertz", J. Am. Ceram. Soc., Vol 81, (1998), p 1977-1994
- S. Bouras, and B. Bouzabata, "Study of Hertzian Indentation on a Transparent Vitroceramic and on an Alumina", Mat. Che. Phy., Vol.N°43, (1996), p.127-134

P93 - WS₂ binary material synthesized by sulfuration of nano-films of WO₃ obtained by spray for photovoltaic application

S. Dabbous*, A. Amlouk, K. Boubaker, M. Amlouk
 Unité de physique des dispositifs à semi-conducteurs
 Université Tunis EL MANAR, 2092 Tunis, TUNISIE

*Corresponding author : E-mail adress : Dabbous.sondes@gmail.com

Introduction:

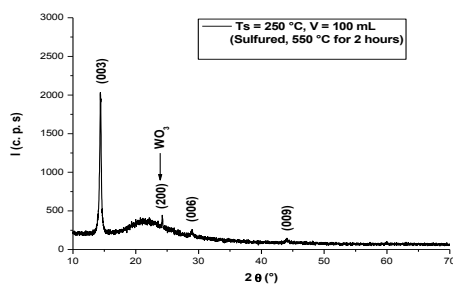
In the last four decades, layered-structure transition metal dichalcogenides, MX₂ (M=W, Mo, X= S, Se) have been widely investigated for their particular photovoltaic [1-3] and tribological [9] properties. Among these compounds, transition metal disulfides MS₂ (M=W, Mo...) have been of interest for several technological applications. They have been judged suitable for use as hydrogenation catalysts in high-energy density batteries, and their reported band gap (1.8 eV in the bulk solid and 1.32/1.4 eV in thin film form) is very near from the optimal value lying between 1 and 2 eV [4-7].

In 1992, Genut *et al.* [8] reported the existence of two major types of WS₂ single crystals: type-I, grown with c-axis parallel to the deposition surface and type-II with c-axis perpendicular to surface. This distinction became a major guide to recent studies on this oxide. The first attempts to synthesise WS₂ thin layers yielded randomly arranged crystals as admitted by Genut *et al.* [8] V. Buck [11] and P. A. Bertrand [9]. Recently, the type-II WS₂ layers have been synthesized by several methods, like electrodeposition [5] chemical vapour deposition (CVD) [6], Van der Waals rheotaxy [10], and reactive evaporation [2].

In this work, The obtained films were grown by the spray pyrolysis technique on Pyrex glass substrates using WCl₆ (10⁻²M) and thiourea SC(NH₂)₂ (2 10⁻²M) in a mixture of water and ethanol (1/2;1/2) at 250 °C. Second, an annealing process of these films in sulfur atmosphere during 2 hours at 550 °C under vacuum (10⁻²-10⁻³ Pa).

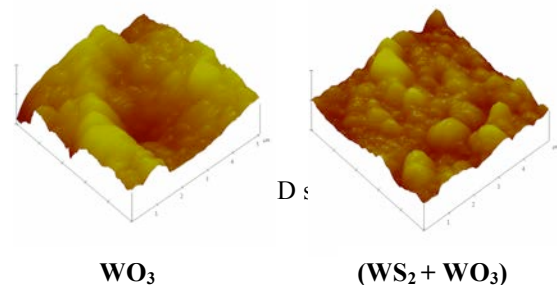
The sprayed deposited films were observed to be transparent, well adherent to the substrate, uniform, and pin-hole free whereas heated ones have dark colour.

Figures



XRD Diagrams of annealed of second sprayed thin film heated at T = 550 °C, during 2h

The mean surface roughness was estimated for the two materials. It was approximately 135.64 nm for WO₃ film and 58.920 nm for WS₂ one.



References:

- [1] A. Jager-Waldau, E. Bucher, Thin Solid Films, 200 (1991) 157.
- [2] A. Klein, S. Tiefenbacher, V. Eyert, C. Pettenkofer, W. Jaegermann, Phys. Rev. B, 64 (2001) 205416.
- [3] C. Donnet, A. Erdemir, Trib. Lett. 17 (2004) 389.
- [4] J. Cheon, J.E. Gozum, G.S. Girolami, Chem. Mater., 9 (1997) 1847.
- [5] J.J. Devadasan, C. Sanjeeviraja, M. Jayachandran, J. Cryst.Growth, 226 (2001) 67.
- [6] J.W. Chung, Z.R. Dai, F.S. Ohuchi, J. Cryst. Growth, 186 (1988)137.
- [7] K. Ellmer, C. Stock, K. Diesner, I. Sieber, J. Cryst. Growth, 182 (1997) 389.
- [8] M. Genut, L. Margulis, R. Tenne, G. Hodes, Thin Solid Films, 219 (1992) 30.
- [9] P. A. Bertrand, J. Mater. Res., 4 (1989) 180.
- [10] T. Tsirlina, S. Cohen, H. Cohen, L. Spair, M. Peisach, R. Tenne, A. Mattheaus, S. Tiefenbacher, W. Jaegermann, E.A. Ponomarev, C. Levy-Clement, Sol. Energy Materials and Solar Cells, 44 (1996) 457.
- [11] V. Buck, Thin Solid Films, 139 (1986) 157.

P94 - Controlling biological activity of coordination compounds at nanoparticle interfaces

Setare Tahmasebi Nick¹, Elizabeth L. Bejcek¹, Bruce E. Bejcek² and Sherine O.Obare^{1*}

¹Department of Chemistry and ²Department of Biological Sciences,
Western Michigan University, 1903 W. Michigan Avenue, Kalamazoo, MI 49008

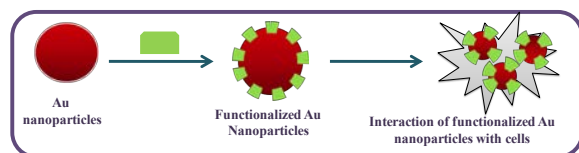
Synthetic procedures that produce nanoscale materials with controlled morphology are advantageous particularly when utilizing nanomaterials for biological applications. The attachment of molecular compounds at nanoparticle interfaces strongly influences their behaviour (Ciptadjaya 2009, Guo, 2008, Obare 2005). Electrochemical measurements of coordination compounds alone and when bound to nanoparticle surfaces were compared and found to be influenced by the surface morphology. In this regard, we have developed a strategy to fabricate well-controlled metallic and semiconductor nanoparticles (Freemantle 2007, Ganesan 2007, Lin 2010) and examined their toxicity toward brain tumor cells.

Non-toxic nanoparticles were used as scaffolds to conjugate coordination compounds derivatives. Neither the coordination compounds examined nor the metallic nanoparticles showed any activity on their own toward brain tumor cancer cells. However, when the coordination compounds were conjugated onto the nanoparticle surface, the resulting hybrid was highly effective in deactivating the cells. We attribute the effect to polyvalent interactions between the coordination compounds and the cells when bound to the nanoparticle surface, and changes in the electrochemical properties of the coordination compounds. Furthermore, we have investigated the effects of surface binding on the activity of molecular compounds and correlate surface morphology to activity. The presentation will focus on the synthesis and characterization of the nanoparticles, attachment of the coordination compounds and their interactions with brain tumor cells.

Figure 1. Gold nanoparticles functionalized with a coordination compound and then delivered to a brain tumor cell.

References:

- Ciptadjaya, C. G. E., Guo, W. and Obare, S. O. (2009) Controlling the Reactivity of Chlorinated Ethylenes with FMNH₂. *Environmental Science and Technology*, 43, 1591-1597.
- Freemantle, R. G., Guo, W., Liu, M., and Obare, S. O. (2007) One-Step Synthetic Procedures and Electrochemical Properties of Monodisperse 1-2 nm Metallic Nanoparticles. *ECS Transactions*, 6, 93-99.
- Guo, W., Ciptadjaya, C. G. E., Liu, M., Simms, C. M. and Obare, S. O. (2008) Modulating the Reactivity of Nanocrystalline TiO₂ for the Degradation of Organophosphorus Pesticides. *Journal of Advanced Oxidation Technology*, 11, 459-462.
- Ganesan, M., Freemantle, R., and Obare, S. O. (2007) Monodisperse Thioether Stabilized Palladium Nanoparticles: Synthesis, Characterization and Reactivity. *Chemistry of Materials*, 19, 3464-3471.
- Lin, R.; Freemantle, R. G., Kelly, N.M., Obare, S. O., and Ofoli, R. Y. (2010) In-situ immobilization of palladium nanoparticles in microfluidic reactors and assessment of their catalytic reactivity, *Nanotechnology*, 21, 325605.
- Obare, S. O., Ito, T., and Meyer, G. J. (2005) Controlling Reduction Potentials of Semiconductor-Supported Molecular Catalysts for Environmental Remediation of Organohalide Pollutants. *Environmental Science and Technology*, 39, 6266-6272.



P95 - Negative differential resistance in carbon-silica nanocomposites

S. Guadria¹, H. Dahman^{1,*}, K. Omri¹, L. El Mir^{1,2}

¹Laboratoire de Physique des Matériaux et des Nanomatériaux Appliquée à l'Environnement, Université de Gabès, Faculté des Sciences, Cité Erriadh Manara Zrig 6072 Gabès, Tunisie.

²Al-Imam Muhammad Ibn Saud University, College of Sciences, Department of Physics, Riyadh 11623, Saudi Arabia.

E-mail : h_dahman_2000@yahoo.com

Abstract: In this work, carbon-silica nanocomposites have been elaborated by sol-gel technique. SiO₂ nanoparticles were mixed with resorcinol-formaldehyde (RF) carbon precursor solution with concentration of 50%. The samples were dried by increasing temperature from ambient to 150 °C by step of 10 °C/day and then pyrolysed at several temperatures 675 °C (RF-SiO₂-675) and 700 °C (RF-SiO₂-700) under controlled argon atmosphere. The XRD investigations carried out on these samples outline that materials have amorphous phase for all pyrolysis temperatures. Current-Voltage characteristics exhibit non linear and symmetric behavior for all measurement temperatures between 80 and 300 K. Therefore a negative differential resistance (NDR) phase has been detected at ambient temperature for RF-SiO₂-675 sample. However, this non linear behavior appears for lower measurement temperatures when the pyrolysis temperature increases. The current threshold after each the NDR phase appears is found to increase with increasing sample temperature while the threshold voltage decreases. The $\sqrt{V_{th}}$ decreases linearly with measurement temperature, and the threshold power ($V_{th} \cdot I_{th}$) follows a Gaussian behavior. The found results will be discussed on the light of several phenomenons such as joule heating; charge density wave and quantum tunneling effects.

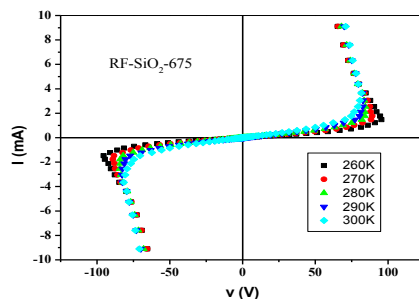


Figure 1: I-V characteristics at various temperatures for RF-SiO₂-675 sample.

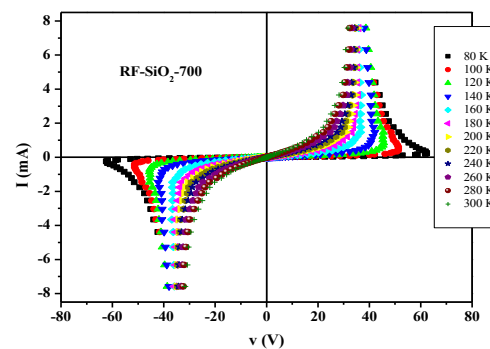


Figure 2: I-V characteristics at various temperatures for RF-SiO₂-700 sample.

Similar behavior has been observed in nano-carbon based on pyrogallol-formaldehyde xerogel and electrical conducting nanoporous carbon structures based on resorcinol formaldehyde. This non linear behavior makes these nanocomposites useful for electronic applications.

P96 - Effect of carbon black nanoparticle on the morphology rheology and thermal properties of immiscible polymer blends

S. Hammani^{1,3*}, N. Moulai-Mostefa², L. Benyahia³ J-F. Tassin³

¹LAFPC, Université Saad Dahlab, Route de Soumaa, 09000 Blida, ALGERIA

*Corresponding author : E-mail address : Hammani71@yahoo.fr

²Material and Environmental Laboratory, University of Medea, Ain d'Heb, 26001 Medea, ALGERIA

³Polymères, Colloïdes, Interfaces (PCI) UMR 6120. Université du Maine-CNRS, Avenue O. Messaien. 72085, Le Mans, FRANCE

Abstract:

In this study we investigated the effect of the rate of nanoparticle carbon black on the morphology of the emulsion polymer blends. The immiscible polymer blend PS90PP10 with and with out different content of carbon black nanoparticle has been prepared in twin screw mini extruder. The morphology of the blends were determined by scanning electron microscopy (SEM) and the thermorheological properties by dynamic scanning calorimetry (DCS) and rheometer dynamic analyser (RDAII), the thermal degradation of the blends has been studied by thermogravimetry (TG) and differential thermal analysis (DTG) over the whole rate of carbon black nanoparticle. The morphological results of blend with and without carbon black nanoparticle show a dispersion of circular particle in the matrix, the add of the carbon black nanoparticle increase significantly the size of the droplet of the dispersed phase and decrease the crystallization temperature. The melt and transition temperature remain less constant. The rheological properties of the blends are in between that the two components in weak content of carbon black nanoparticle, when this rate exceed critical values, the rheological properties increase significantly and exceed the properties of the two components.

The therogravimetry results show that the small quantities of carbon black nanoparticle does not influence the degradation of the blend but when we exceeds 4wt% of carbon black nanoparticle, we noticed a light increase in degradation temperature of the blends, all the thermograms representing the blend are in between those of the two polymers forming the blend. The DTG curves for blends show an intermediate behavior of rate maxima relative to component polymers.

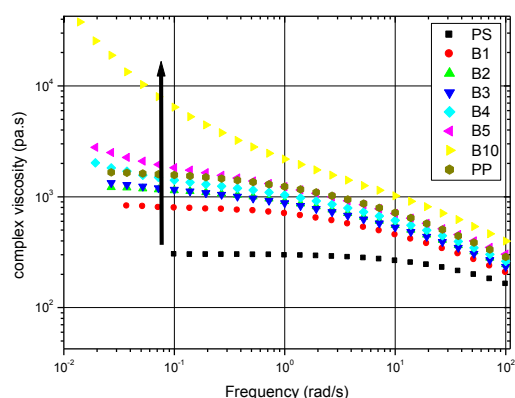


Figure 1: effect of nanoparticle carbon black content on the complex viscosity of the blend polymer

References:

- Baudouin, A.C. Auhl, D. Tao, F. Devaux, J. Bailly, C. (2011) Polymer blend emulsion stabilization using carbon nanotubes interfacial confinement, *Polymer*, 52, 149-156.
- Malkin, A.Y. (2009) The state of the Art in the Rheology of Polymers: Achievements and Challenges, *Polymer Science*, 51, 80-102.
- Segal, E. Tchoudakov, R. Narkis, M. Siegmann, A. (2004) Sensors for chemicals based on electrically conductive immiscible HIPS/TPU blends containing carbon black, *Journal of Materials Science*, 39, 5673- 5682.
- Wu, G. Li, B. Jiang, J. (2010) Carbon black self-networking induced co-continuity of immiscible polymer blends, *Polymer*, 51, 2077-2083.

P97 - Thermal oxidation of heavily boron-doped thin films of polycrystalline silicon

S. Merabet¹, A. Bounar¹, M. Boukezzata², D. Bielle-Daspet³, G. Sarrabayrouse³

¹Electronic Department, Faculty of Science engineering, University of Jijel, Cité Ouled-Aissa B. P. 98 Jijel, 18 000 Jijel, Algeria

*Corresponding author : E-mail address: msouad03@yahoo.fr, s_merabet@umc.edu.dz

²Electronic Department, Faculty of Science engineering, University of Mentouri, way of Ain El-bey, 25 000 Constantine, Algeria

³LAAS du CNRS, 7, Avenue du Colonel Roche, 31077 Toulouse cedex 4, France.

Abstract

The thermal oxidation of polycrystalline-silicon films deposited by low pressure chemical vapor deposition and doped heavily in situ boron-doped with concentration level of around $2 \times 10^{20} \text{ cm}^{-3}$ has been studied. Their properties are analyzed using electrical and structural characterization means by four points probe resistivity measurements and X-ray diffraction spectra. The thermal-oxidation process are performed on sub-micron layers of 200nm/c-Si and 200nm/SiO₂ deposited at temperatures $T_d = 520^\circ\text{C}$ and thermally-oxidized in dry oxygen ambient at 945°C . The variation of the oxide thickness as function of oxidation time t_{ox} , and oxidation temperature T_{ox} are analyzed in terms of a linear-parabolic oxidation law. The experimental data are simulated using our own computer program based on some theoretical models, particularly, we have interest in the Deal and Grove and Han and Helms models. First, we note that the oxide thickness varies proportionally with the variation of the time oxidation. Second, it appears that the results of the Han-Helms model is always smaller than the Deal-Grove model, to explain this specific behavior we refer to the linear-parabolic model, where the linear constant is correlated with the reaction between the silicon and oxidant. While the parabolic rate constant, is related to the diffusion of the oxidant through the SiO₂ film, it is predicted that at

$T_{ox} < 1000^\circ\text{C}$, where boron depletion maximally, the depletion of boron from the surface should yield a minimal effect of linear constant.

Compared to the as-grown resistivity with silicon wafers is known to be in the following sequence $\langle \rho_{200\text{nm}/\text{c-Si}} \rangle < \langle \rho_{200\text{nm}/\text{SiO}_2} \rangle$. The measure X-ray spectra is shown, that the Bragg peaks are marked according to the crystal orientation.

References

- H. Morikawa, Y. Kawama, Y. Matsuno, S. Hamamoto, K. Ishihara, K. Kojima, T. Ogama (2001) Development of high-efficiency thin-film Si solar cells using zone-melting recrystallization, Soc. Energy Mater. Sol. Cells 65 261-268.
- E. D. Readinger, S. D. Wolter, D. L. Waltermeyer, J. M. Delucca, S. E. Mohnney, B. I. Prenitzer, L. A. Giannuzzi, and R. J. Molnar (1999) J. Electron. Mater. **28**, 257.
- B. E. Deal, A.S. Grove (1965) J. Appl. 132 2815.
- C.J. Han, C.R. Helms (1987) J. Electrochem. Soc. 134 (3) 1297.
- M. Boukezzata (1988) Doctorate Thesis, Université Paul Sabatier of Toulouse, France, N°. 353.
- E.A. Irene, D.W. Dong (1978) J. Electrochem. Soc. 125 (7) 1146.
- M. Boukezzata, B. Birouk, D.B. Daspet (1998) Thin Solid Films 335 70-79.
- A. Y. Messaoud, E. Scheid, G. Sarrabayrouse (1993) Jpn. Appl. Phys. 32 (1, 12A) 5805.

P98 - Effect of hydrogen on the optical and structural properties of amorphous silicon carbide films

S.Merazga¹, A. Brighet², A. Keffous³, K. Mirouh¹, M. Kechouane²

¹Mentouri University, Physics Faculty, Constantine, Algeria

²Houari Boumediene University (U.S.T.H.B), Physics Faculty, Algiers, Algeria

³Silicon Technology Development Unit, 02 Bd, Frantz FANON, B.P. 140, Algiers, Algeria

*Corresponding author : E-mail address : merazgasal@yahoo.fr

Introduction: Because of their excellent properties such as an excellent resistance to high temperature, abrasion and radiation ;hydrogenated amorphous silicon carbide thin films have attracted great interest in recent years for various applications of microelectronic and optoelectronic devices, such as sensors, photodiodes and solar cells.

Content: hydrogenated amorphous silicon carbide thin films (a-SiC:H) were elaborated by dc magnetron sputtering technique by using 6H-SiC as target. The a-SiC:H films of 0.9 – 1.5 μm thicknesses were deposited on p-type Si(100) and corning glass 9075 substrates, which were cleaned with ethanol and 2% hydrofluoric acid before deposition. The pressure in sputtering chamber before deposition was 1×10^{-5} mbar. A mixture of hydrogen and argon gases with a flow rates of 3.4 and 5 sccm, respectively, and a plasma power of 130 W have been used. The substrates have been maintained at different temperature

temperature 250, 350, 450 and 550°C. The deposited films (a-SiC:H) were investigated by infrared spectroscopy (FTIR), spectrophotometry (UV-visible-NIR), Raman spectroscopy, secondary ion mass spectrometry (SIMS), photoluminescence spectroscopy and electrical measurements.

Finally, The preliminary results of optical characterization namely measurements of transmission and reflexion of the worked out layers, show that when the temperature increases the thickness of the layer increases by 1.4 μm to 1.5 μm , then at the temperature of 450°C the thickness of the layers geos decreased by 1.2 μm , 0.9 μm ; just as the optical gap ($E_{g, \text{opt}}$) 1.91 eV to 2.08 eV to temérature of 450°C it decreased to 2.06 eV, this is due to the desorption of H_2 as the temperature decreases , then it decreased at temperature up 550°C and becomes 2.10 eV due to the temperature effect who is more dominate (Figure.1). The characterization by FTIR reveals the existence of a band located at 775 cm^{-1} which corresponds to Si-C stretching of SiC amorphous whereas the Si-C bonds of SiC crystalline is around 810 cm^{-1} . Using The SIMS depth profile (^{28}Si Signal/ ^{12}C Signal) was obtained as 1.73, this value is higher and due

essentially to H present into the layer that influence the stoichiometry of the film. In addition, the elaborated films a-SiC:H exhibit a blue luminescence, and the their intensity decreases with the thickness's film(Figure.2).

Figures:

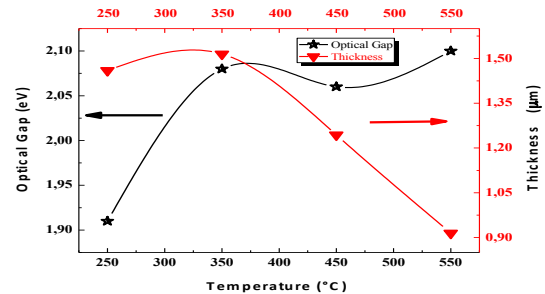


Figure 1: variation of optical gap, thickness of the films of a-SiC:H a function of temperature substrate.

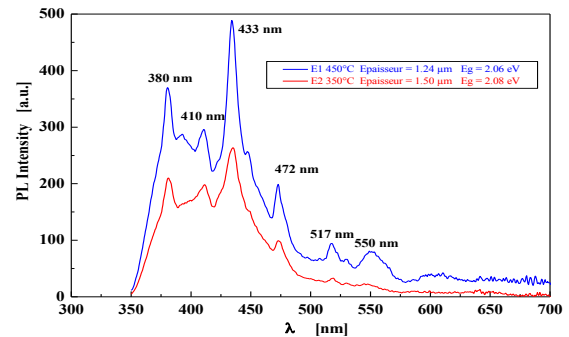


Figure 2: PL spectra of a-SiC:H sample deposited at two substrate temperature (350°C, 450°C).

References:

- Dengyuan Song, Eun-Chel Cho, Gavin Conibeer, Chris Flynn, Yidan Huang, Martin A. Green.(2008) Structural, electrical and photovoltaic characterization of Si nanocrystals embedded SiC matrix and Si nanocrystals/c-Si heterojunction devices, Australia, Journal of Solar Energy Materials & Solar Cells 92,474–481
- J. Huran , I. Hotovy, J. Pezoldt , N.I. Balalykin , A.P. Kobzev. (2006)Effect of deposition temperature on the properties of amorphous silicon carbide thin films, Journal of Thin Solid Films 515, 651 – 653.
- Matthias Künle , Thomas Kaltenbach , Philipp Löper , Andreas Hartel , Stefan Janz , Oliver Eibl , Klaus-Georg Nickel.(2010) Si-rich a-SiC:H thin films: Structural and optical transformations during thermal annealing,Germany, Thin Solid Films 519,151–157.

P99 - Molecular dynamics simulations of atomic migration in ordered CoPt L1₀ Alloys

T. Bouzar^{1*}, L. Messad¹, C. Goyhenex², H. Bouzar¹, V. Pierron-Bohnes²

¹Laboratoire de physique et chimie quantique, Université Mouloud Mammeri Tizi-ouzou, BP N° 17 RP, Tizi-ouzou, Algérie

²Institut de physique et chimie des matériaux de strasbourg, UMR7504, CNRS-UDS 23 rue du lœss, BP 43, Strasbourg CEDEX, France

*Corresponding author : E-mail address : bouzartounsia@mail.ummo.dz

Introduction: Equiatomic L1₀ CoPt alloys exhibit high magnetic anisotropy, resulting from the chemical order anisotropy. These alloys are extensively studied in view of ultra-high density magnetic storage applications. Molecular dynamics simulations of vacancy migration in CoPt L1₀ alloy were performed in the frame of the second moment approximation of the tight binding model (TB-SMA). A statistical approach exploring the probability of a 6 jump cycle (6JC) mechanism was carried out in the temperature range of 900-1000K. This cycle, first suggested for B2 alloys by S. Divinski, allows vacancy migration without long range order change.

Energy model: The atomic interactions are described by a tight binding Hamiltonian using an electronic density of state written in the second moment approximation. The energy of atom at site *i* is written as the sum of two terms, an attractive band energy and a repulsive pair interaction. Theoretical details can be found in the work of Rosato et al., The fitting procedure leading to potential parameter's values can be found in previous work of the authors, given in references section.

Computational details: We have used a standard Fortran molecular dynamics code, implementing the Verlet algorithm. The simulation box consisted of 10x10x10 unit cells with one vacancy (1999 atoms) and used periodic boundary conditions. The simulations were started from equilibrium positions with randomly set atomic velocities which were then re-normalized so as to get the desired temperature, below the order-disorder temperature (1100K) but high enough to have reasonable computational time. For each molecular dynamics step (taken equal to 2 femtosecond) the displacements of the 12 atoms surrounding the vacancy were monitored and the simulation ended when *n* atomic jumps were recorded. The numbers of jumps recorded in a simulation was varied in order to study a possible correlation effect between successive jumps.

Results: The starting configurations used in this work are the steps of the 6JC in which a vacancy (V) is initially placed as shown in figure 1.

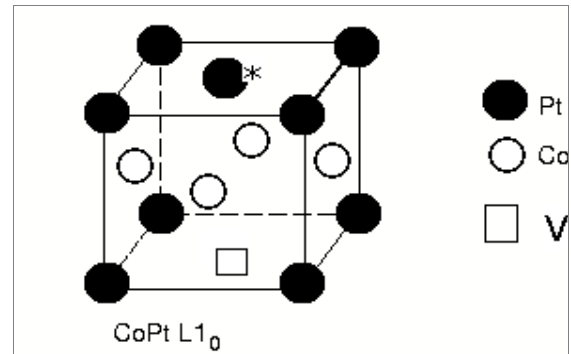


Figure1: The 6JC consists of 6 nearest-neighbors atom-vacancy exchanges in a plane perpendicular to Pt (Co) atomic layers and leads to a V-Pt* exchange. The first 3 jumps are disordering, followed by 3 ordering jumps.

For each starting configuration, 100 simulation runs were made, and those showing jumps consistent with the 6JC were counted. The statistical analysis of our results shows that the 6JC has a non negligible probability of occurring and can be used to explain order conserving vacancy migration observed in CoPt bilayers. Our results are consistent with published total energy calculation (Orsen). An interesting fact observed in our simulations is the absence of vacancy migration in the Pt or Co planes at the studied temperatures. This is consistent with long range order conservation.

References:

- Davinsky S. et al, *Intermetallics* 8 (2000) 1357
 Goyhenex C., Bulou H., Deville J.-P., Trégliat G., *Phys. Rev.B* 60 (1999) 2781.
 V. Rosato, B. Guillope, and B. Legrand, *Philos. Mag. A* 59, 321 (1989); F.Cleri and V.Rosato, *Phys.Rev. B* 48,22 (1993)
 O. Ersen, C. Goyhenex, V. Pierron-Bohnes *Phys. Rev. B* 78, 035429 (2008)

P100 - PET/CNTs flexible electrodes for organic solar cells devices

W. Aloui¹, A. Ltaief¹, H. Majdoub², A. Farzi³, A. Bouazizi¹

¹Equipe: “Dispositifs Electroniques organiques et Photovoltaïque Moléculaire”, Laboratoire de Physique et Chimie des Interfaces, Faculté de Sciences de Monastir, Boulevard de l’environnement, 5019, Monastir, Tunisie

²Laboratoire de Matériaux Polymères et Biopolymères, Faculté de Sciences de Monastir, Boulevard de l’environnement, 5019, Monastir, Tunisie

³Department of Materials and Polymer Engineering, Faculty of Engineering, Sabzevar Tarbiat Moallem University, Sabzevar, Iran

Abstract:

ITO is currently the most popular material used for the transparent electrodes in OPV devices; however, it has a number of deficiencies. For one, it is not very compatible with polymeric substrates due to its high deposition temperature of around 600 °C. Traditional ITO also has unfavorable mechanical properties such as being relatively fragile. In addition, the combination of costly layer deposition in vacuum and a limited supply of indium results in high quality ITO transparent electrodes being very expensive. Therefore, developing and commercializing a replacement for ITO is a major focus of OPV research and development.

Conductive CNT coatings have recently become a prospective substitute based on wide range of methods including spraying, spin coating, casting, layer-by-layer, and Langmuir–Blodgett deposition. The transfer from a filter membrane to the transparent support using a solvent or in the form of an adhesive film is another method for attaining flexible and optically transparent CNT films.

We have adopted the last method to prepare our flexible and transparent electrodes using the PET substrate, which is a practical method to obtain good optical transperance about 73%.

In the visible and infrared range, the performance characteristics of fabricated films are comparable to those of indium tin oxide ITO. The light transmittance and electrical conductivity varied according to the concentration of the MWCNTs dispersion. Good optimal transparency and electrical properties were obtained when the electrically conductive transparent network was fabricated from a 0.07 wt. % aqueous MWCNTs dispersion. PET / CNTs could be used as anode for optoelectronic devices such as organic diodes. We have deposited a layer of MEH-PPV by spin coating on the PET / CNTs structures, in order to elaborate a flexible organic diode. As shown in figure 1, we have obtained a rectified behavior typical for organic diodes.

This study represents an important step for the integration of CNTs in opto-electronics devices as an anode in flexible organic solar cells.

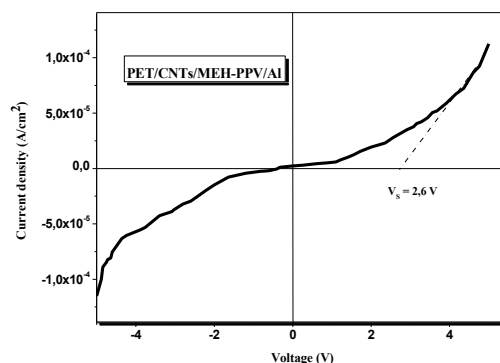


Figure I: J-V characteristic, in the dark, of the PET/CNTs / MEH-PPV / Al flexible organic diode

P101 - Exctonic behavior in self-assembled InGaAs/GaAs quantum rings in low magnetic fields

W.Ouerghi^{1*}, R.Naouri¹, M.A.Maaref¹, C.Testelin², F, Bernadot²

¹Unité de recherché de Physique des Semiconducteurs et Capteurs, Institut Préparatoire aux Etudes Scientifiques et Techniques, La Marsa, Université de Carthage, Tunis, Tunisia.

²Institut des nanosciences de Paris, UPCM, Univ paris 06, CNRS UMR 7588, 4 Place Jussieu, 75252 Paris cedex 05, France.

*Corresponding Author: E-mail adress: ouerghuiwalid@yahoo.fr

Abstract:

The fine structure of excitons is studied by polarization-resolved photoluminescence spectroscopy of self-assembled quantum rings InGaAs/GaAs in magnetic field up to 3.2T. These studies allow us to develop a comprehensive picture of the exciton fine structure. We Show that the exciton energy levels are nonequidistant and split up in only two levels in magnetic field, reflecting the ring like geometry. Finally, we measure the bright exciton exchange energy as a function of interband emission, we measure an increase from 110 to 160 μeV . This behavior is explained by the fact that the splitting is essentially due to the anisotropic shape in this quantum ring.

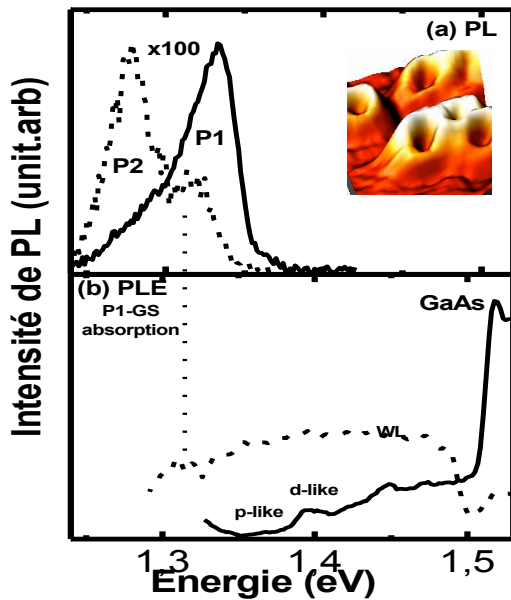
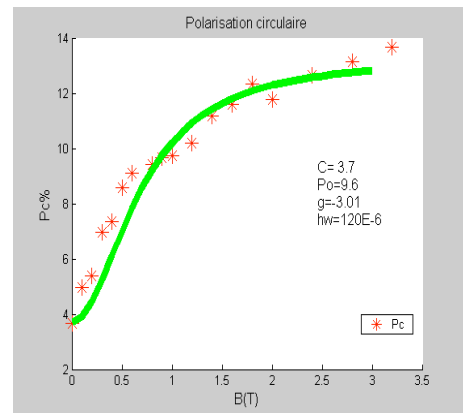


Figure 1. (a) Spectre de PL sous une excitation résonante (trait discontinu) et non- résonante (ligne continue); (b) Spectre de PLE.

Figure 2 : Longitudinal-magnetic-field dependence of the circular polarisation.

The solid line is the best fit obtained with:

$$P_C = P_c^0 \frac{\Omega_p^2}{\omega^2 + \Omega_p^2}$$

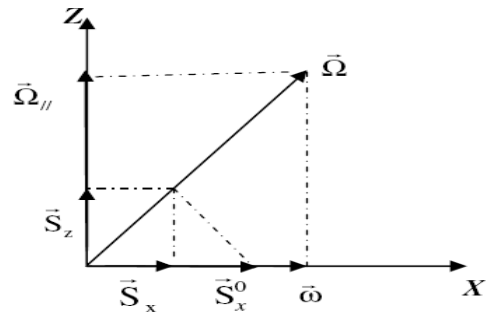


Figure 3: Schematic representation of the exciton pseudo spins projections. S_x^0 is the initial pseudo spin vector under [110] linearly polarized excitation; S_x and S_z are the components of the average pseudo spin.

P102 - Preparations and characterizations of organic-inorganic hybrid perovskite multiple quantum well structure embedded in porous anodic alumina

W. Zaghdoudi^{1*}, A. Bardaoui¹, Y. Abid², H. Houichet³, and R. Chtourou¹

¹Photovoltaic Laboratory Research and Technology Centre of Energy, Borj-Cedria Science and Technology Park, BP 95, 2050 Hammam-Lif, Tunisia.

*Corresponding author : E-mail address : walid_inrst@yahoo.fr

²Laboratoire *Laboratory of Applied Physics*(LPA), Faculty of Science of Sfax, 3018, BP802, Tunisia.

³Department of *Physics*, Faculty of Science of Tunis, Campus ElManar 2092, Tunisia .

Introduction:

Porous anodic aluminum oxide (PAA) has long been considered a viable material for template growth of nanomaterials for electronic, magnetic and optical applications due to the ability to form self-organized, high aspect-ratio nanochannels [1]. More recently these porous materials have been incorporated with fluorescent molecules to create a template for nanostructured materials [2–3]. However, there has been no investigation into how pore growth is affected by confining the pre-anodized aluminum dimensions to the nanometer scale. The photoluminescence (PL) from organic-inorganic perovskite quantum well called $C_{12}PbI_4$ embedded in the pores of anodic alumina thin films on glass and aluminum substrates was investigated in detail. It was found that the PL was strongly dependent on the diameter and depth of the pores.

Experimental:

The porous anodic alumina was fabricated on aluminum substrate and on evaporated aluminum on glass substrate. The surface morphology of the $C_{12}PbI_4$ films deposited on porous alumina is investigated using atomic force microscopy (AFM). A photoluminescence blue shift with a maximum value of 30 nm was observed when the fluorenes were embedded into 40 nm pores of the alumina film compared to the corresponding spectrum on glass substrate. The results have shown the penetration of the molecules into the pores.

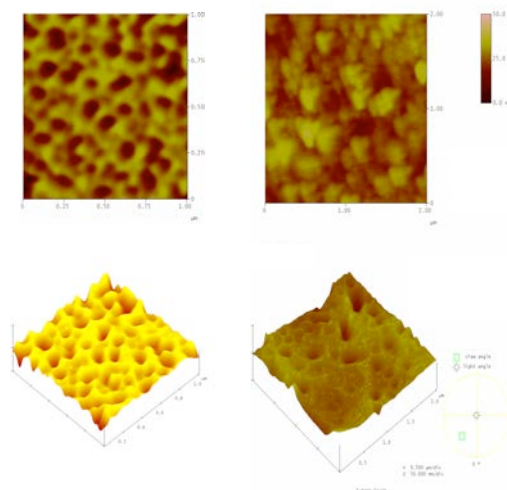


Figure 1: OSL vs. administered dose for the studied aliquots.

References:

- [1] Yuxiang Li, Min Guo, Mei Zhang, Xidong Wang. *Materials Research Bulletin* 44 (2009) 1232–1237.
- [2] G. Schmid, *J. Mater. Chem.* 12 (2002) 1231
- [3] T.L. Wade, J.E. Wegrowe, *Eur. Phys. J., Appl. Phys.* 290 (2005) 3.

P103 - Modified gold electrode with proteus mirabilis bacteria for urea biosensor development

Y. Braham¹, H. Barhoumi¹, A. Maaref¹ and A. Bakhrouf²

¹Laboratoire de Physique et Chimie des Interfaces Fac des Sciences, Monastir 5000, Tunisia.

*Corresponding author : E-mail adress : braham.yosra@yahoo.fr

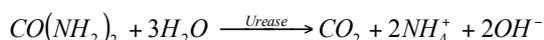
²Laboratoire d'analyse, de traitement et de valorisation des polluants de l'environnement et des produits, Faculté de pharmacie, Monastir

Introduction: The development of biosensors is an expanding research area. Indeed, biosensors are rapid, selective and cost-effective analytical tools which find applications in various fields (environment, health, food,...). They are constituted of a sensitive biological element (antibody, enzyme, microorganism, DNA...), which can selectively recognize one analyte or a group of analytes, associated to an electrochemical, optical or thermal transducer.

In this work, we developed a biosensor based on bacteria immobilised onto gold electrode. For this reason we immobilize the bacteria, *Proteus mirabilis* who product urease enzyme which able to urea catalysis (S. Da Silva, L. Grosjean, N. Ternanc, P. Mailley, T. Livacheb, S. Cosnie...). For that, an original route, including the functionalisation of the transducer with a self-assembled-monolayer method using diazonium salt and nanobeads was investigated for the bacteria immobilisation (Pankhurst QA, Connolly J, Jones SK, Dobson J...).

Theoretical considerations: The measurements were performed in a 11 mM solution of PBS buffer at pH 7.4 A potential range of -0.3 to 0.6 V was applied with a scan rate of 200 mV/s. The bare gold electrode has a reversible voltammogram indicating the oxidation-reduction peaks of the redox couple ($\text{Fe}(\text{CN})_6^{3-/4-}$). Figure (1) shows the cyclic voltammograms of the bare and modified gold surface by the bacteria. Figure (2) presents the Nyquist spectra corresponding to different urea concentrations.

Results: The figure (1) shows a variation of the current as a function of the potential before and after the bacteria immobilisation. The figure (2) shows an interfacial impedance change when urea concentration increase. The hydrolysis of urea by the immobilized proteus mirabilis urease biomolecules, generates ammoniac and carbon dioxide, leading to a change in the conductivity at the electrolyte/urease-modified gold interface (Eq. (1)).



We can conclude that bacteria-substrate interaction can be evaluate by impedimetric measurements.

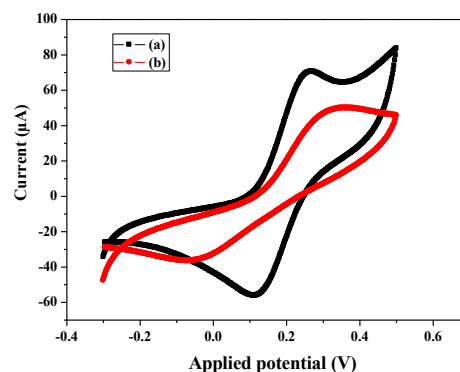


Figure 1: Cyclic voltammograms of bare (a) and (b) modified gold electrode with bacteria.

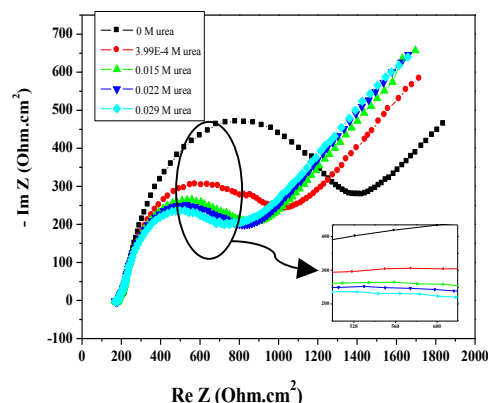


Figure 2: Impedance spectra of Urease/Bacteria/Au biosensor for different urea concentrations in a phosphate buffer solution, pH 7.4 at room temperature.

References:

- Pankhurst QA, Connolly J, Jones SK, Dobson J. (2003) Applications of magnetic nanoparticles in biomedicine. *J Phys D Appl Phys* 36, 167.
- S. Da Silva, L. Grosjean, N. Ternanc, P. Mailley, T. Livacheb, S. Cosnie. (2004) Biotinylated polypyrrole films: an easy electrochemical approach for the reagentless immobilization of bacteria on electrode surfaces. *Bioelectrochemistry* 63, 297– 301.

P104 - Optical properties of the compound FeN

Y. Cheballah¹, A. Ziane¹

¹Laboratoire de Physique et Chimie Quantique, Faculté des sciences,
Université Mouloud Mammeri, 15000 Tizi-Ouzou, ALGERIA

*Corresponding author: E-mail adress: Yamina_Cheballah@yahoo.fr

Introduction: The theoretical aspect of the optical response of nitrides has attracted much attention these last years in order to interpret the growing amount of experimental results. Chen and al, have studied the electronic and the optical properties of rock-salt gallium nitride [1]. However, the optical properties of rock-salt (NaCl) and zinc-blend (ZnS) iron transition-metal nitride (FeN) have been investigated using the LMTO-ASA method (Linear Muffin-Tin Orbital within the Atomic Sphere Approximation) [2] which is ab initio density functional calculation [3, 4]. For the exchange-correlation functional, the generalized gradient approximation (GGA) was adopted [5]. Our results show that the imaginary part of the dielectric function exhibits dominant peaks. We show that all peaks have their origin in inter-band and intra-band transitions and all these transitions are identified by the atomic sites involved in the process and their orbital symmetries.

Figure 1: Dielectric function to the rock-salt structure type of the FeN nitride.

For confirmation of the validity of the present calculation method, the lattice constant of zinc-blend FeN is calculated which is 4.25 \AA , almost the same as the experimental value of 4.307 \AA [6]. The lattice constant of the rock-salt FeN is determined to be 4.40 \AA , which is also very close to the experimental value of 4.50 \AA [7]. We note that the calculated values are underestimated compared to the experimental data; it is common to have an underestimated value when GGA approximation is used. The calculated bulk modulus of the rock-salt FeN is 389 GPa. This value is higher than the bulk modulus of the zinc-blend structure 226 GPa.

References:

- [1] Chen, Z. W., Lv, M. Y., Li, L. X., Wang, Q., Zhang, X. Y. and Liu, R. P. (2006) Theoretical investigation on electronic and optical properties of rock-salt gallium nitride, *Thin Solid Films*, 515, 2433-2436.
- [2] Andersen, O. K. (1975) Linear methods in band theory, *Physical Revue B*, 12, 3060-3083.
- [3] Hohenberg, P. and Khon, W. (1964) Inhomogeneous Electron Gas, *Physical Revue B*, 136, 864-871.
- [4] Khon, W. and Sham, L. J. (1965) Self-Consistent Equations Including Exchange and Correlation Effects, *Physical Revue A*, 140, 1133-1138.
- [5] Hu, C. D. and Langreth, D. C. (1985) A Spin Dependent Version of the Langreth-Mehl Exchange-Correlation Functional, *Physical Scripta*, 32, 391-396.
- [6] Lukashev, P. and Lambrecht, W. R. L. (2004) First-principles study of the preference for zinc-blend or rocksalt structures in FeN and CoN, *Physical Revue B*, 70, 245205-1, 8.
- [7] Kong, Y. (2000) Electronic and magnetism of equiatomic FeN, *Condensed Matter*, 12, 4161-4173.

Figure 2: Dielectric function to the zinc-blend structure type of the FeN nitride.

P105 - Synthesis and characterisations of organophile montmorillonite –copolymer (St-THF) nanocomposite

Y. Hattab^{1*}, N. Benharrats¹

¹ LPPMCA, Department of Chemistry, Faculty of Science, University of Science and Technology of Oran, PB 1505 al M'naouer .Oran 31000 Algeria.

*Corresponding author : E-mail address :Hattab_Youcef@yahoo.fr

Introduction: Nanocomposites, are mixed materials synthesized from one or many polymers blended in optimized percentages and organophilic clay. The objective of this study is to use the organophilic clay (Montmorillonite) in the presence of tow monomers to obtain a copolytetrahydrofuran- styrene nanocomposite by in situ polymerization.

Organophilic montmorillonite (O-MMT) was prepared by ion exchange between Na^+ ions in the clay hexadecyltrimethylammonium bromide cations in an aqueous medium. The organophilic MMT particles were easily dispersed and swollen in styrene (St) and tetrahydrofuran (THF) monomer. To make the clay compatible with the polymers, the sodium ions in clay (such as sodium montmorillonite) are usually ion-exchanged with an organic ammonium or phosphonium salt to convert this material into a hydrophobic ammonium or phosphonium treated clay.

The result is an important soft segment for producing thermoplastic elastomers such as polyester and polyurethane material, In these applications, Nanocomposites is valued as a precursor leading to products with outstanding hydrolytic stability at elevated temperatures, high fungal resistance, superior abrasion resistance, excellent resiliency, and attractive dynamic properties.

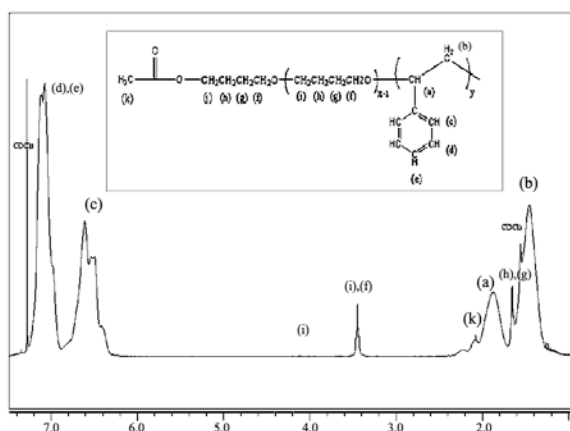


Fig. 1: RMN¹H spectrum (300 MHz) of copolymer: poly(THF-co-St), solvent CDCl₃.

The structure of obtained modifier was investigated by proton nuclear magnetic resonance (RMN¹H), Fourier-transform infrared (FT-IR) spectroscopy. The exfoliating structure of nanocomposite was probed by X-ray diffraction (XRD) and transmission electron microscopy (TEM).

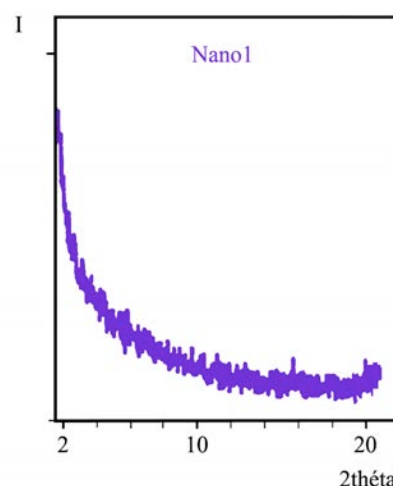


Fig. 2: XRD patterns for the poly(THF-co-St)/O-MMT nanocomposite

The Thermal stability were also investigated with thermogravimetric analyzer (TGA), comparing with pure polystyrene, the nanocomposite showed much higher decomposition temperature.

References:

- Belbachir, M., Bensaoula, A. (2001) U.S. Patent, 6, B1, 274-527.
- Celik, M., Onal, M. (2007) J Polym Res, 14, 4, 313.
- Chavarria, F., Shah, R.,K., Hunter, D.,L., Paul, D.,R., (2007) Polym Eng Sci, 47, 1847.
- Ouis, N., Benharrats, N., Belbachir, M. (2004) C. R. Chimie, 7, 955-962.
- Ray, S.,S., Okamoto, M. (2003) Prog Polym Sci, 28, 1539.
- Uthirakumar, P., Hahn, YB., Nahm, KS., Lee, YS. , (2005) Eur Polym J, 41, 1582.
- Yenice, Z., Tasdelen, M., A., Oral, A., Guler, C., Yagci, Y. (2009) J. Polymer Science Part A: Polym. Chem. 47, 8, 2190–2197.

P106 - Electrochemical properties study of high-frequency magnetic induction melting Al- 4 to 50 wt.% Mg alloys

Y. Souilah*, S. Boulkheissaim, M. Draissia, M.Y. Debili

LM2S, Physics Departement, Faculty of Science, Badji-Mokhtar University, PB 12 Annaba, 23000, Algeria

*Corresponding author : E-mail adress : souilahyamina@yahoo.fr

Abstract: The Al-Mg alloys are widely used in a variety of industrial applications, in automotive structures due to their mechanical and electrochemical properties such as high strength, good formability and corrosion resistance. In general they offer the best combination of strength and corrosion resistance of all Al alloys.

In this article, the electrochemical properties of the binary Al-Mg alloys system have been investigated .A set of Al-4 to 50 wt.%Mg alloys samples were made by the high frequency (HF) magnetic induction melting (300kHz). The corrosion potential measurements of the as melted Al-Mg alloys were carried out with a voltalab (PGZ 301) apparatus and conducted by computer and voltmaster4 software in a neutral aerated 3%NaCl solution at 25°C. It was found that the corrosion potentials with Mg contents between are between -800mv and -1000mv. Compared with the Al-Cr, Al-Fe and Al-Cu systems, the Al-Mg alloys are anodic and can be used as sacrificial protection.

Figure 1. curves the tafel $I=f(E_{corr})$ curve of (HF) Al-40 wt% Mg alloy.

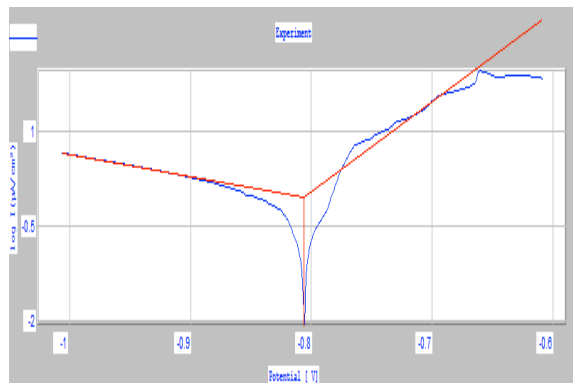


Figure 2. curve stabilization of the corrosion potential versus time for Al-40 wt % Mg alloy

References:

- Debili, M.Y., Tran, H.L., Frantz, C., Y(1998) Caractérisation chimique et structurale de dépôts métastables aluminium-fer obtenus par pulvérisation cathodique magnéton, *Revue de Métallurgie-CIT/Science et Génie des Matériaux*, décembre 1998, 1501-1509.
- Draissia, M., Debili, M.Y., Millet, J.P., Y(2005), Comportement à la corrosion du système de films minces aluminium-cuivre, *Journal of New Materials for Electrochemical Systems*, 8, 229-233.
- Milijana, P., Endre, R., Y(2002) Stress corrosion cracking susceptibility of Al-Mg alloy sheet with high Mg content, *Journal of Materialas Processing Technology*, 125-126, 275-280.
- Souilah, Y., Boulkheissai, S., Draissia, M., Debili, M.Y., Y(2011) Experimental analysis of the dendritic growth in Al-Mg alloys, *ICONEM'11*, 03 to 05 May 2011 Annaba University.

P107 - Electrical and dielectrical behaviours of CdS layers grown on GaAs and porous GaAs substrates

Z. Harrabi^{1,2}, A. Ltaief¹, L.Béji³ and A. Bouazizi¹

¹Equipe Dispositifs Electroniques Organiques et Photovoltaïque Moléculaire, Faculté des Sciences de Monastir, Avenue de l'Environnement, 5019 Monastir, Tunisia.

²Institut Supérieur de Biologie Appliquée de Médnine, Route El Jorf, 4119, Médnine, Tunisie.

³Institut Supérieur d'Informatique et des Technologies de communication, 4011, Hammam Sousse, Tunisia.

Abstract :

CdS/ GaAs and CdS/ porous GaAs heterostructures are an interesting systems for optoelectronic devices technology and particularly for the elaboration of solar cells[1,2].

In this work, we elaborate p-n junctions using n-type CdS deposited either on p-type GaAs or on p-type porous GaAs by vacuum evaporation technique. The electrical and dielectrical characteristics of such structures were investigated under ambient conditions.

Theses heterojunctions show a rectifying behaviour. The current-voltage plots show typical diode characteristics, theoretically expected for n-p heterojunctions between two semiconductors. The current of the heterojunctions, which is essentially a thermoionic emission of charges carriers, has a Schottky diode's behaviour. Electrical parameters such as zero bias barrier height, ideality factor and the saturation current have been investigated. The mechanisms of conduction of these heterojunctions devices have been also studied; current-voltage characteristics indicated a space charge limited current conduction mechanism.

Capacitance-voltage data at different frequencies determines the doping concentration and built-in-potential of depletion region (Figure1).

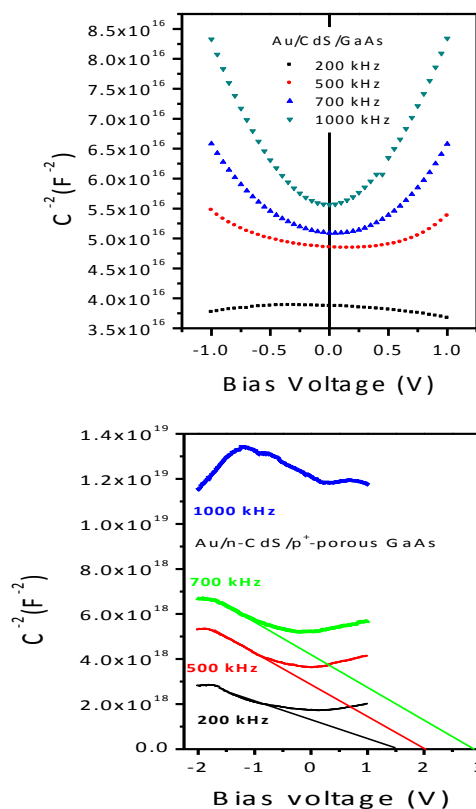


Figure.1

References:

- [1] P. Schmuki, D. J. Lockwood, H. J. Labbé, and J. W. Fraser, Appl. Phys. Lett. 69, 1620, 1996
- [2] M. Rojas-López, M. A. Vidal, H. Navarro-Contreras, J. M. Gracia-Jiménez, E. Gómez, R. Silva-González, J. Appl. Phys. **87** (2000) 1270

P108 - Detection of human apolipoprotein E genotypes by a DNA electrochemical biosensor

Z. Mazouz^{1,3}, A. Omezzine², R. Kalfat³, A. Othmane¹

¹ Laboratoire de Biophysique, Faculté de Médecine de Monastir, Monastir, Tunisie

² Service de Biochimie, Hôpital universitaire Sahloul, Sousse, Tunisie

³ Laboratoire Méthodes et Techniques d'Analyse (LMTA), Sidi Thabet - Tunisie

The apolipoprotein E (ApoE) is a protein which plays an essential role in the lipids metabolism. The ApoE gene is affected by a polymorphism 112/158 leading to 3 isoforms and 6 genotypes implied in several pathologies, neurodegenerative, metabolic etc (Marrazza et al., 2000). The ApoE genotyping is thus very useful to predict these diseases risk. Traditional methods, like the fluorescence method, chemiluminescence (Ma et al., 2000), spectrofluorimetric and resonance light scattering (RLS) methods (Wang et al., 2005) ... are generally complex and expensive and need a lot of time for samples preparations. A DNA electrochemical sensor for genetic polymorphisms detection of (ApoE) in human blood samples, has thus been developed and will be presented in this work. Polymerase chain reaction (PCR) was used to amplify and extract DNA from human blood.

We have utilized a classical three-electrode system connected to a Voltalab 40 impedance analyzer: a chemically modified silicon nitride matrix (Si/SiO₂/Si₃N₄) was used as a working electrode; Platinum plate and saturated calomel electrode (SCE) were used as counter and reference electrodes, respectively. All experiments were performed at room temperature. Electrochemical measurements consisted to record impedance variations and to deduce the capacitive data. They were carried out in a potential range from -1000mV to 4000mV at an optimized frequency of 10KHz.

In order to detect the ApoE polymorphism, two specific DNA probes were covalently immobilized on the modified silicon nitride substrate and the hybridization tests were first performed with four known oligonucleotides, and second with the DNA of six patients. Results have shown that whatever is the DNA type, the relative capacitance ΔC increases linearly with DNA concentration before reaching saturation, suggesting that ΔC was the result of the large-scale molecular structure changes, such as the DNA conformational changes during hybridization, from single strand DNA (ssDNA) to double strand DNA (dsDNA) (Figure. 1).

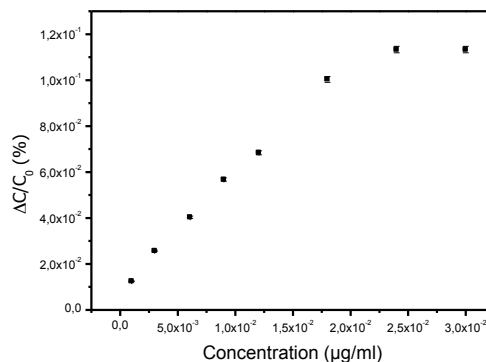


Figure1 : Capacitance change versus the concentration of the DNA (for completely complementary DNA) .

We have also investigated the possibility of detecting DNA molecules presenting a single-base mismatch. We have demonstrated that we are able to differentiate them from the 100% complementary targets and the non complementary ones.

All these results were in concordance with those obtained by conventional clinical method namely Restriction Fragment Length Polymorphism (PCR-RFLP).

References

- Ma, Y., Zhou, M., Jin, X., Zhang, Z., Teng, X. and Chen, H., 2004. *Analytica . Chimica. Acta*, 501 (1), 25–30
- Marrazza, G., Chiti, G., Mascini, M. and Anichini, Mario.(2000). Detection of Human Apolipoprotein E Genotypes by DNA Electrochemical Biosensor Coupled with PCR, *Clinical Chemistry* ,46:1, 31–37.
- Wang, R.-Y., Gao, X.and Lu, Y.-T., (2005). *Analytica . Chimica. Act.*, 538 (1–2), 151–158.

Impressum

Proceedings of the 2nd Humboldt Kolleg, Hammamet, Tunisia

Organizer: Alexander von Humboldt Stiftung, Germany

Print: 150 Exemplars

Picture credits:

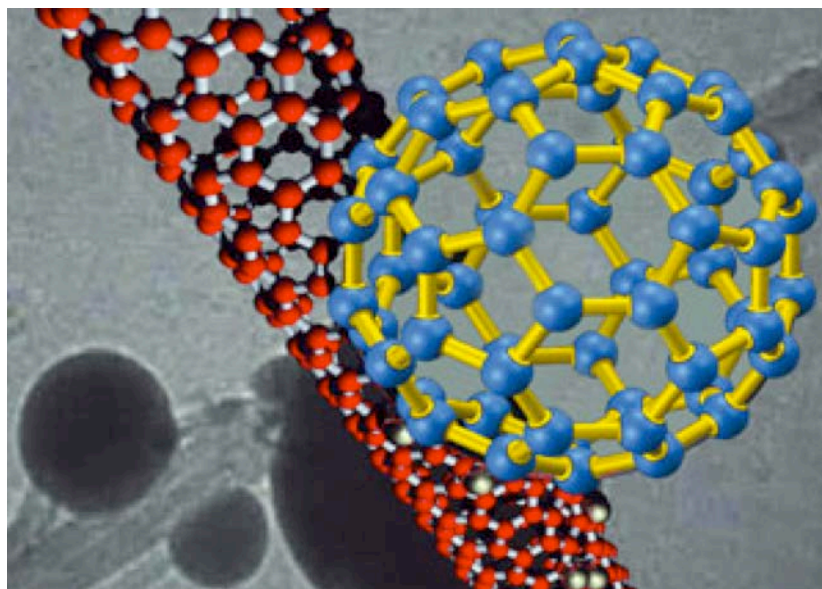
<http://biology-official.blogspot.com/> Bacteriophage viruses

<http://www.epmm.group.shef.ac.uk/research/snom.php>

<http://www.exponent.com/files/Uploads/Images/electrical/semiconductor%20photo.jpg>

Acknowledgement

The organizing committee gratefully thanks all sponsors of this conference, especially the « Alexander von Humboldt Stiftung, Bonn, Germany ».



The Ministry of Higher Education and Scientific Research as well as the National Institute of Applied Science and Technology is acknowledged for supporting the 2nd Humboldt Kolleg in Tunisia.

